METEOROLOGICAL CONDITIONS AND TRANSPORT OF AIR POLLUTANTS AT BACHOK MARINE RESEARCH STATION (BMRS) IN PENINSULAR MALAYSIA

NORAINI BINTI MOHYEDDIN

INSTITUTE FOR ADVANCED STUDIES
UNIVERSITY OF MALAYA
KUALA LUMPUR

2020

METEOROLOGICAL CONDITIONS AND TRANSPORT OF AIR POLLUTANTS AT BACHOK MARINE RESEARCH STATION (BMRS) IN PENINSULAR MALAYSIA

NORAINI BINTI MOHYEDDIN

DISSERTATION SUBMITTED IN FULFILMENT OF THE REQUIREMENTS FOR THE DEGREE OF MASTER OF PHILOSOPHY

INSTITUTE FOR ADVANCED STUDIES
UNIVERSITY OF MALAYA
KUALA LUMPUR

2020

UNIVERSITY OF MALAYA

ORIGINAL LITERARY WORK DECLARATION

Name of Candidate: **Noraini Binti Mohyeddin**

Matric No: **HGT150005**

Name of Degree: **Master of Philosophy**

Title of Dissertation ("this Work"): **Meteorological conditions and transport of air pollutants at Bachok Marine Research Station (BMRS) in Peninsular Malaysia**

Field of Study: **Earth Science**

I do solemnly and sincerely declare that:

(1) I am the sole author of this Work;
(2) This Work is original;
(3) Any use of any work in which copyright exists was done by way of fair dealing and for permitted purposes and any excerpt or extract from, or reference to or reproduction of any copyright work has been disclosed expressly and sufficiently and the title of the Work and its authorship have been acknowledged in this Work;
(4) I do not have any actual knowledge nor do I ought reasonably to know that the making of this work constitutes an infringement of any copyright work;
(5) I hereby assign all and every rights in the copyright to this Work to the University of Malaya ("UM"), who henceforth shall be owner of the copyright in this Work and that any reproduction or use in any form or by any means whatsoever is prohibited without the written consent of UM having been first had and obtained;
(6) I am fully aware that if in the course of making this Work I have infringed any copyright whether intentionally or otherwise, I may be subject to legal action or any other action as may be determined by UM.

Candidate's Signature Date: **14 September 2020**

Subscribed and solemnly declared before,

Witness's Signature Date: **14 September 2020**

Name:

Designation:

METEOROLOGICAL CONDITIONS AND TRANSPORT OF AIR POLLUTANTS AT BACHOK MARINE RESEARCH STATION (BMRS) IN PENINSULAR MALAYSIA

ABSTRACT

This study is focused at relatively new regional Global Atmospheric Watch (GAW) station at Peninsular Malaysia – Bachok Marine Research Station (BMRS) using the observational and remote sensing data. The study consists of three main objectives. Firstly, to investigate the meteorological conditions during two major Southeast Asia monsoon – NE and SW monsoon. Secondly, to determine the potential sources of air pollution at BMRS during the monsoon periods. Thirdly, to examine the relations of carbon dioxide (CO_2), methane (CH_4) and particulate matters (PM_{10}, and $PM_{2.5}$) with the meteorological conditions during intensive case study periods. The first case study (CS1) was conducted from 25 to 27 January 2016 while the second one (CS2) was conducted from 3 to 5 June 2016.

The results of this study are divided into two parts. In the first part, the meteorological conditions, variations and transport of air pollutants during the Northeast (NE) and Southwest (SW) monsoons from 2014 – 2016 were determined. Data analysis shows BMRS is influenced by both synoptic flows and land-sea breeze events during the NE monsoon. However, BMRS dominated by land-sea breeze events during the SW monsoon. BMRS is associated with dominant flows of onshore winds, no diurnal effect and low level of air pollutants during strong synoptic influence in the NE monsoon. This period is also associated with transboundary sources originated from the continental region of China, East China Sea (ECS) and South China Sea (SCS) using Hybrid-Single Particle Lagrangian Integrated Trajectory (HYSPLIT) model and CWT analysis.

In the second part, the meteorological conditions, relations and transport of air pollutants during CS1 and CS2 were shown extensively. CS1 and CS2 represent a strong synoptic and local meteorological conditions in the NE and SW monsoon respectively. During CS1, BMRS was influenced by strong easterly winds that penetrated 60 km inland and prevailed within 2500 m height with high relative humidity (>80%). This caused a weakened vertical thermal gradient hence suppressed the typical land-sea breeze event over BMRS. Conditional Probability Function Polar (CPFP) plots and HYSPLIT-CWT analysis incorporated with hotspots data shows there are influence of long-range transport of CO_2 and CH_4 from the continental region of China and coastal area of Vietnam which are mainly attributed to the industrial emissions and biomass burnings. Contrarily, BMRS was associated with clear vertical thermal gradient within 1000 m, strong diurnal effect and daily occurrence of land sea breeze event during CS2. The sea breeze event able to penetrate within 30 to 90 km inland in the late afternoon and prevails within 1000 m height over BMRS. The variations of air pollutants are strongly influenced by the land sea breeze event i.e. sea breeze reduces while land breeze increases the level of air pollutants significantly. BMRS is mainly influenced by local and regional sources of emissions during this period. Overall, the site at BMRS presents a valuable opportunity to study the influence of regional and local atmospheric flows to the variabilities of air pollutants, thus enabling better understanding and providing a key reference to formulate effective pollution abatement strategies.

Keywords: Coastal station, Northeast monsoon, synoptic, land sea breeze, air pollution, greenhouse gases, atmospheric aerosols

[KEADAAN METEOROLOGI DAN PENGANGKUTAN BAHAN PENCEMAR UDARA DI STESEN PENYELIDIKAN MARIN BACHOK (BMRS) DALAM SEMENANJUNG MALAYSIA]

ABSTRAK

Kajian ini difokuskan di stesen baru serantau di bawah Pemantau Atmosfera Global (GAW) yang terletak di Semenanjung Malaysia – Stesen Penyelidikan Marin Bachok (BMRS) menggunakan data pemerhatian dan pemantauan jarak jauh (remote sensing). Kajian ini terbahagi kepada tiga objektif. Pertama, menyiasat keadaan meteorologi semasa dua musim monsun utama – monsun timur laut (NE) dan barat daya (SW). Kedua, untuk menentukan sumber-sumber yang berpotensi untuk menyebabkan pencemaran alam di BMRS semasa monsun-monsun tersebut. Ketiga, mengkaji hubungan antara karbon dioksida (CO_2), metana (CH_4) dan bahan partikel-partikel (PM_{10} dan $PM_{2.5}$) dengan keadaan meteorologi semasa kajian intensif dilakukan. Kajian pertama (CS1) telah dijalankan dari 25 sehingga 27 Januari 2016 manakala yang kedua (CS2) telah dijalankan dari 3 hingga 5 Jun 2016.

Hasil kajian ini terbahagi kepada dua bahagian. Pada bahagian pertama, keadaan meteorologi, variasi-variasi dan transportasi bahan-bahan pencemar udara semasa monsun NE dan SW dari 2014-2016 telah ditunjukkan. Analisis data menunjukkan BMRS dipengaruhi oleh aliran-aliran sinoptik dan fenomena bayu darat-laut semasa monsun NE. Walaubagaimanapun, BMRS didominasi oleh bayu darat-laut semasa monsun SW. BMRS dikaitkan dengan aliran angin dari laut yang dominan, tiada kesan diurnal dan tahap bahan-bahan pencemar udara yang rendah di bawah pengaruh sinoptik yang kuat. Keadaan ini juga dipengaruhi oleh sumber rentas sempadan yang berasal dari wilayah benua China, Laut China Timur (ECS) dan Laut China Selatan (SCS) menggunakan model Hybrid-Single Particle Lagrangian Integrated Trajectory (HYSPLIT) dan analisis CWT.

Pada bahagian kedua, keadaan meteorologi, hugungkait serta transportasi bahan-bahan pencemar udara semasa CS1 dan CS2 ditunjukkan dengan lebih terperinci. CS1 dan CS2 masing-masing mewakili keadaan meteorologi sinoptik yang kuat dan tempatan ketika monsun NE dan SW. Semasa CS1, BMRS dipengaruhi oleh angin timur yang kuat menembusi sehingga 60 km ke daratan dan ia berlaku dalam ketinggian 2500 m dengan kelembapan yang tinggi (>80%). Ini melemahkan kecerunan termal menegak sehingga menekan fenomena bayu darat-laut yang biasa berlaku di BMRS. Plot-plot CPFP dan analisis HYSPLIT-CWT yang disatukan dengan data titik panas menunjukkan CO_2 dan CH_4 dipengaruhi oleh transportasi jarak jauh iaitu dari wilayah benua China dan kawasan pesisir pantai Vietnam yang mana ianya disebabkan oleh emisi industri dan pembakaran-pembakaran biojisim. Sebaliknya, BMRS menunjukkan kecerunan termal menegak yang jelas sehingga 1000 m, kesan diurnal yang kuat dan fenomena bayu darat-laut terjadi setiap hari semasa CS2. Kejadian bayu laut di BMRS mampu menembusi dari 30 sehingga 90 km ke daratan pada lewat tengahari dan ianya terjadi sehingga ketinggian 1000 m. Variasi bahan-bahan pencemar udara sangat dipengaruhi oleh fenomena bayu darat-laut yang mana kejadian bayu laut mengurangkan manakala bayu darat meningkatkan kandungan bahan-bahan pencemar udara tersebut dengan ketara. BMRS sangat dipengaruhi oleh sumber emisi tempatan dan setempat dalam tempoh ini

Kesuluruhannya, stesen BMRS menunjukkan peluang yang berharga untuk mengkaji aliran atmosfera serantau dan tempatan kepada bahan-bahan pencemar udara. Oleh itu, ianya membolehkan pemahaman lebih baik dan menyediakan rujukan utama untuk memformulasikan strategi pengurangan pencemaran udara yang efektif.

Kata kunci: Stesen pesisir pantai, monsun timur laut, sinoptik, bayu laut dan darat, pencemaran udara, gas rumah hijau, aerosol atmosfera

ACKNOWLEDGEMENTS

I would like to thank my supervisors, Professor Dato' Dr. Azizan bin Hj Abu Samah and Dr. Sheeba Nettukandy Chenoli for the guidance and support given to me, for all the time taken and patience in teaching and dealing with. I wish to express my gratitude to Mr. Ooi See Hai for the help and advice given in the scripting analysis. I also would like to thank Dr. Matthew J. Ashfold, Dr. Mohammed Iqbal Mead, Dr. David Oram, Dr. Grant Forster, Prof. Talib Latif, Dr, Sivaprasad Patissery, Dr. Mohd Fadzil Firdzaus Mohd Nor, Dr. Mohd Shahrul Mohd Nadzir and Dr. Wee Cheah for the discussions related to this study. Anonymous reviewers from Meteorology and Atmospheric Physic (MAAP) Journal are also thanked for the careful review on the manuscript and valuable suggestions to improve the quality of the paper which leads to further improvement of this dissertation.

This research was supported by the Higher Institution Centre of Excellence (HICoE) Research programme 1.1 (Air-Land Interactions) – IOES-2014A. The greenhouse gas measurements were partly funded by the UK Natural Environment Research Council (International Opportunities Fund, NE/J016012/1 and NE/J016047/1). I would like to thank the Department of Environment (DOE) and the Malaysian Meteorological Department for providing the air quality observational data. Special thanks are also due to my colleagues in the National Antarctic Research Center (NARC) and the Institute of Ocean and Earth Sciences (IOES) for their insights and expertise that greatly help in this research study.

Finally, I would like to express most thank to my family for their supports and encouragements throughout this study.

TABLE OF CONTENTS

LIST OF FIGURES

LIST OF TABLES

LIST OF SYMBOLS AND ABBREVIATIONS

NOAA	:	National Oceania and Atmospheric Administration
WHO	:	World Health Organization
SEA	:	Southeast Asia
ABCs	:	Atmospheric Brown Clouds
CO_2	:	Carbon Dioxide
CH_4	:	Methane
NE	:	Northeast
SW	:	Southwest
BMRS	:	Bachok Marine Research Station
FIO	:	First Institute of Oceanography
GAW	:	Global Atmospheric Watch
WMO	:	World Meteorological Organization
CS1	:	Case Study 1
CS2	:	Case Study 2
PM_{10}	:	Particulate matter with aerodynamic diameter less than 10 μm
$PM_{2.5}$	:	Particulate matter with aerodynamic diameter less than 2.5 μm
DOE	:	Department of Environment
H_2O	:	Water vapor
O_3	:	Ozone
g-to-p	:	Gas to particles
Cl-VSLS	:	Chlorinated very short-lived substances
ABL	:	Atmospheric Boundary Layer
FT	:	Free troposphere
SL	:	Surface layer

ML	:	Mixed layer
EZ	:	Entrainment zone
SBL	:	Stable Boundary Layer
NBL	:	Nocturnal Boundary Layer
CI	:	Capping Inversion
RL	:	Residual Layer
API	:	Air Pollution Index
TTL	:	Tropical Tropopause Layer
WRF	:	Weather Research Forecasting
WRF-Chem	:	WRF-Chemistry
HYSPLIT	:	Hybrid Single Particle Lagrangian Integrated Trajectory
GDAS	:	Global Data Assimilation System
CWT	:	Concentration Weighted Trajectory
PSCF	:	Potential Source Contribution Function
(i,j)	:	Indices of grid
$m_{i,j}$	:	Number of times that pollutant was high when the trajectories passed through the cell (i,j)
n_{ij}	:	Number of trajectories passed through cell (i,j)
k	:	Index of trajectory
N	:	Total number of trajectories for study
C_k	:	Concentration of pollutant at receptor site (upon arrival of trajectory k)
τ_{ijk}	:	Residence time of trajectory k in grid cell (i,j)
$\bar{C}_{ij}$	:	Mean concentration of pollutant in grid cell (i,j)
CFP	:	Conditional Probability Function

LIST OF APPENDICES

CHAPTER 1: INTRODUCTION

1.1 Introduction

Air pollution and climate change are critical environmental issues at present and also for the coming decades (IPCC, 2014). According to World Health Organization (WHO) report, an estimated of 7 million deaths is responsible for air pollution annually and it contribute to one in eight premature deaths every year (World Health Organization, 2018). This makes it the world's largest environmental health risk which is comparable with other health risks such as smoking, high cholesterol, high blood sugar and obesity (D'Amato et al., 2014; De Sario et al., 2013; McMichael et al., 2006). Global studies of composition, characteristic and transport of air pollutants are rising with the availability of monitoring technologies and global in-situ and reanalysis data (Akimoto, 2003; Liu et al., 2003; Newell & Evans, 2000). Economic outlook for China, India and Southeast Asia shows continuous growth for 2019 to 2020 (OECD, 2019). The rising challenges these regions faced with rapid growth of urban areas are managing their levels of air pollution, and encouraging policy makers are encouraged to coordinate across various levels of government to reduce emissions in a targeted way (OECD, 2019). Air pollution is generally defined as the contamination of the indoor or outdoor environment by any chemical, physical or biological substances that modify the natural characteristics of nature (World Health Organization, 2016). Air pollution can be transported locally as well as across continents and oceans basins by large-scale weather conditions (Akimoto, 2003) or due to quick transboundary transport resulted from trans-continental and trans-oceanic plumes of atmospheric brown clouds (ABCs) containing atmospheric aerosols (Ramanathan & Feng, 2009).

Extreme air quality episodes are linked with changing weather patterns such as heat waves with stagnation episode (García-Herrera et al., 2010) and transboundary haze

events with the presence of El Niño (Huijnen et al., 2016). Variabilities in the exposures to air pollution can also be largely due to different scales of meteorological phenomena (Beaver & Palazoglu, 2009; Elminir, 2005). There are 65 Continuous Air Quality Monitoring Stations (CAQMS) in Malaysia as of 2018 (Department Of Environment). Malaysia particularly experiences two major monsoon periods namely the Northeast (NE) and the Southwest (SW) monsoons. Air pollution episodes in Malaysia mainly experienced during the SW monsoon (Juneng et al., 2011; Razali et al., 2015; Toh et al., 2013) due to transboundary air pollutants (haze) resulting from the biomass burning in Indonesia, in addition to the drier-than-normal condition due to the presence of El-Nino and stable atmospheric condition (low wind speed) (Afroz et al., 2003; Latif et al., 2018; Tangang et al., 2017).

The focus of air pollution study during the NE monsoon is less because of the complexity of meteorological conditions that are able to wash out of (some) pollutants by the heavy downpours. NE monsoon is usually associated with synoptic-scale features such as the presence of transient disturbances known as northeasterly and easterly surges. Recent studies noted that during the NE monsoon, ozone (Ashfold et al., 2017) and short-lived anthropogenic chlorocarbons (Oram et al., 2017) can be transported to Malaysia through cold surge events. Trajectory computation analysis reveals that the polluted air masses are transported southwards and further lifted to the tropical upper troposphere through intense convective processes (Ashfold et al., 2015; Oram et al., 2017) in the northeastern fringe of the near-equatorial trough. This suggests that air pollution during the NE monsoon should be studied more thoroughly. Further study of the role of synoptic wind flow on other air pollutants is crucial to expand the understanding of the atmospheric processes for better constrain on the local greenhouse gas and other air pollutant budgets.

A relatively new (in 2012) station at Bachok, Kelantan located 100 meters (m) from the east coast of Peninsular Malaysia has furthered inspired this study. This station, known as the Bachok Marine Research Station (BMRS), is in a tropical coastal environment and an ideal location to study the local, regional and long-range composition and transport of pollutants. This station is in a collaboration with the First Institute of Oceanography (FIO, China), the University of Cambridge and the University of East Anglia. It is equipped with several meteorological and air pollutants measuring equipment and has been accepted as a regional Global Atmospheric Watch (GAW) station by the World Meteorological Organization (WMO) in June 2016. A few studies involving this area has been conducted by Dominick et al. (2015) focusing on the particle mass and number concentration on the east coast of Peninsular Malaysia during the NE monsoon. Farren et al. (2019) also conducted studies on the chemical characterization of water-soluble ions in atmospheric particulate matter and clear difference in aerosol compositions originating from the continental East Asia regions and marine air masses found at BMRS. These studies also emphasized the need for more comprehensive studies on local and long-range effects consisting of a complete emission inventory as well as meteorological and gaseous parameters as input to the chemical transport models to gain a better understanding of the complex ambient air over BMRS.

Anthropogenic emissions of greenhouse gases are increasing annually and it contributed to widespread impacts on human and natural systems (IPCC, 2014). CH_4 and CO_2 are the two most important greenhouse gases that are continuously monitored and both exert a significant radiative forcing everywhere around the globe. Atmospheric aerosols are liquid or solid particles suspended in the air which have a direct and indirect radiative forcing in the atmosphere. Combinations of radiative forcing from greenhouse gases and atmospheric aerosols contribute to global warming and subsequently lead to climate variabilities (IPCC, 2001). Study on greenhouse gases and atmospheric aerosols

in every parts of the world is required to better quantify and prove their impacts in a global scale.

Main focus of the study is to determine the meteorological conditions over BMRS during the NE and SW monsoons and how it influences the variability and transport of CO_2, CH_4, PM_{10} and $PM_{2.5}$. The study investigates the meteorological conditions over BMRS using both in-situ and remote-sensing data. Two intensive case studies were conducted from 25 to 27 January 2016 (CS1) and from 3 to 5 June 2016 (CS2) focusing on the strong synoptic and land sea breeze events at BMRS. Through these case studies, more detailed meteorological conditions, variabilities and transport of CO_2, CH_4, PM_{10} and $PM_{2.5}$ at BMRS are examined.

1.2 Problem Statement

Malaysia is directly influenced by the two major Asian monsoons which are the NE and SW monsoons. The SW monsoon is attributed to stable and dry conditions which are usually prone to the transboundary air pollution episodes like haze This event released large amounts of terrestrially-stored carbon into the atmosphere (in the form of CO_2, CO and CH_4) e.g., haze episode in 2015 (Huijnen et al., 2016) and are detrimental to human health (Aditama, 2000; Afroz et al., 2003; Emmanuel, 2000; Sahani et al., 2014; World Health Organization, 2018). During the NE monsoon, transboundary transport of air pollution can also occur due to the synoptic scale of motions flowing from the Siberian-Mongolian High and East Asia e.g. Ashfold et al. (2017), Ashfold et al. (2015), Dominick et al. (2015) and Farren et al. (2019). The studies show ozone (Ashfold et al., 2017), perchloroethene (Ashfold et al., 2015), particulate matters (Dominick et al., 2015; Farren et al., 2019) and some chlorinated very short-lived substances (Cl-VSLS) are transported from the East Asian regions to the east coast of Peninsular Malaysia. There is a knowledge

gap on the effects of large circulation system i.e. synoptic events on other air pollutants like CO_2, CH_4 and particulate matters. Furthermore, the differences between different scales of meteorological conditions during the NE and SW monsoons on air pollutants at the east coast of Peninsular Malaysia have not yet been quantified satisfactorily. Besides that, the meteorological and air quality data at BMRS have not been fully explored to enhance its role as an ideal regional station under GAW. Hence, this study aims to fill the research gap on the variations and transport of CO_2, CH_4, PM_{10} and $PM_{2.5}$ as well as its relations to the meteorological conditions during the NE and SW monsoons.

1.3 Objectives of the Study

The objectives for this study are

1. To investigate the meteorological conditions at BMRS during the NE and SW monsoons;
2. To determine the potential sources of air pollutants at BMRS during different monsoon periods;
3. To examine the relations of CO_2, CH_4, PM_{10} and $PM_{2.5}$ with the meteorological conditions during the intensive case studies periods.

1.4 Research Questions and Challenges

Research questions that will be answered from this study are:

1. What are the significant meteorological features during the NE and SW monsoons at BMRS?
2. Which is the appropriate transport model that can be used to determine the origins of air masses during the NE and SW monsoons?

3. What are the major mechanisms for the transport and distribution of air pollutants to BMRS?
4. What are the relations and effects of meteorological conditions during the NE and SW monsoon periods to the variabilities of CH_4, CO_2, PM_{10} and $PM_{2.5}$?

The main challenge for this study is data quality. Observational data are carefully scrutinized to ensure their high quality by counter checking with the collaborated partners and comparing with those nearby stations belonging to the Department of Environment (DOE), Malaysia.

1.5 Research Importance

This research is crucial in supporting BMRS as a regional GAW station. More studies utilizing data from this station will facilitate contribution to a wider research community through data and knowledge sharing. This will also ensure continued refinement of good quality data at BMRS. In essence, studies on the transport of air pollutants during the NE monsoon will provide better understanding of the different meteorological conditions during this period as well as the precursor and distribution of air pollutants in the east coast of Peninsular Malaysia. In addition, comparison of studies during both the NE and SW monsoons will highlight accurately the differences of meteorological conditions during both periods and how these can affect the distribution of the air pollutants.

Technologies continue to evolve rapidly and more open access of high resolution meteorological and air quality data are and will be made available globally. The ability to utilize and interpret all these scientific data using the right tools and methods are undeniably very important and beneficial. Thus, this preliminary study serves as a fundamental step towards using big data and its analysis to understand the processes that influence air pollution in the region.

1.6 Thesis Structures

Chapter 1 gives the introduction, problem statement, objective and importance of the study. Chapter 2 provides the recent literature reviews on greenhouse gases and atmospheric aerosols, characteristics of the NE and SE monsoons, factors of air pollutant transport and possible transport models that can be used to examine the transport of air pollutants at BMRS. Data and methodologies used to examine the meteorological conditions and its effects on the variabilities and transport of air pollutants are elaborated in Chapter 3. Chapter 4 discusses the results. Finally, Chapter 5 summarizes and highlights the major findings of the research study with indication of possible future work.

CHAPTER 2: LITERATURE REVIEW

The study of air pollution is pervasively increasing and it has turned into a global issue from over the last 30 years. Variabilities of air pollution can be largely results due to different meteorological conditions from local to synoptic scales and the pathways of the air masses. Malaysia is exposed to two major monsoon periods namely the Northeast (NE) and the Southwest (SW) monsoon. The NE monsoon is usually characterized with strong winds and high rainfall rates (wet condition) while the SW monsoon is usually attributed to light winds and low rainfall rates (dry condition). Thus, it is important to understand how different meteorological conditions during these different monsoon periods can influence the distribution of air pollutants over Malaysia. There were many extensive studies conducted on the influence of meteorological parameters on air pollutants during the SW monsoon in Malaysia. However, there were less detailed studies on the distribution of pollutants during the NE monsoon especially during the strong synoptic influence – cold surge event. Section 2.1 describes the characteristics of greenhouse gases and atmospheric aerosols in terms of their sources, sinks and residence time. Section 2.2 details the characteristics of the NE and SW monsoon over Malaysia. Section 2.3 looks into the relations of meteorology with air pollution and Section 2.4 examines the transport model to determine the source regions of air pollutants.

2.1 Greenhouse gases and particulate matter (PM)

This section describes the characteristics of greenhouse gases and atmospheric aerosols in term of its sources, sinks and residence times. The troposphere is constituted of a mixture of gases as shown in APPENDIX A. The air is mostly comprised of nitrogen and oxygen with a percentage of 78.08% and 20.95% respectively. There is also argon and carbon dioxide which comprised of 0.93% and 0.03% respectively. Together, these

four gases constitute for 99.99% of the air volume. The remaining constituents of air are of prime importance in the atmospheric chemistry because of their reactivity. Tropospheric trace gases compositions have undergone changes with increasing quantity since 100 years ago (Wenig et al., 2003) due to anthropogenic influence.

Greenhouse gases and particulate matters which are currently measured at BMRS are the main focus for this study. Greenhouse gases like carbon dioxide (CO_2) and methane (CH_4) show high contribution to global warming and it subsequently lead to sea level rise, ocean acidification, and more extreme weather (Kellogg, 2019; Kweku et al., 2017; Letcher, 2019; Masson-Delmotte et al., 2018; Stocker et al., 2013). CO_2 is the most long-lived (50 to 200 years lifespan) greenhouse gases in the atmosphere (Kellogg, 2019; Ritchie & Roser, 2017; Stocker et al., 2013). In accordance to WMO report in October 2017, the globally averaged surface mole fraction of CO_2 is 403.3 ± 0.1 ppm and it has shown an increment of 3.3 ppm from 2015 to 2016 (World Meteorological Organization, 2017). Recent press release in November 2018 by WMO revealed another new record high for globally averaged concentration of CO_2 which is 405.5 ppm in 2017 (World Meteorological Organization, 2018). The ocean is the largest sink for CO_2, absorbing about 40 percent of CO_2 since the beginning of the industrial era (Kellogg, 2019; Khatiwala et al., 2013; Stocker et al., 2013; Zickfeld et al., 2017). CO_2 is naturally present in the atmosphere as part of the Earth's carbon cycle from the natural circulation of carbon between the atmosphere, oceans, soil, plants, and animals (Kellogg, 2019; Stocker et al., 2013; Wallace & Hobbs, 2006). However, the industrial revolution by human activities is altering the carbon cycle both by adding more CO_2 to the atmosphere and changing the natural sinks, like natural forests where CO_2 are mostly removed (Stocker et al., 2013). Among the main anthropogenic sources are through fossil fuel combustion for energy and transportation and land-use changes (Kellogg, 2019; Pearson et al., 2017; Stocker et al., 2013).. Recent concern for CO_2 emission in Southeast Asia is from palm oil production

(mainly produced in Indonesia and Malaysia). The growing production of palm oil threatens biodiversity (Fitzherbert et al., 2008; Pearson et al., 2017; Sheil et al., 2009; Wilcove & Koh, 2010). Tropical forests store large amounts of carbon both in primary forests and secondary forests (Feldpausch et al., 2005). When tropical forests are cleared to make way for oil palm plantations, carbon is released into the atmosphere like CO_2 which then enhances global warming(Achard et al., 2014; Baccini et al., 2012). Numerous global carbon-cycle modelling studies have been conducted which comprised tropical component however there were limitation on data in the global tropical regions (Defries et al., 2002; Houghton, 2005; Pearson et al., 2017; Schoot et al., 2011). Existence of BMRS as another observatory station in Malaysia will help reduce the uncertainties in regional estimates of CO_2 sources and sinks.

CH_4 is a potent greenhouse gas (Saunois et al., 2016; Stocker et al., 2013). It has efficient capability to trap radiation responsible for 20% of radiative forcing (Etminan et al., 2016; Yang et al., 2017) despite its shorter lifetime (9 years) as compared to CO_2 in the atmosphere. Global atmospheric methane has continued to in recent years (Reay et al., 2018). WMO reported that its concentration had undergone a slight increase of about 9 ppb (0.009 ppm) in 2015 to become 1853 ± 2 ppb (1.853 ± 0.002 ppm) in 2016 (World Meteorological Organization, 2017). In 2017, it reached a new high of 1859 ppb (1.859 ppm) (World Meteorological Organization, 2018). Anthropogenic CH_4 is produced from the production and transport of natural gas, coal, and oil; livestock, biomass burnings and landfills (Reay, 2007; Saunois et al., 2016; Stocker et al., 2013). About 40% of CH_4 is usually emitted into the atmosphere by natural sources (like wetlands and termites) while the rest of it is from anthropogenic sources. The primary natural sink of CH_4 is the atmosphere itself (in the troposphere) through oxidation process (react with the hydroxyl radical) to produce CO_2, H_2O, and O_3 (Holmes, 2018; Reay, 2007; Reay et al., 2018;

Saunois et al., 2016; Wallace & Hobbs, 2006). Besides that, CH_4 can also be removed through soil uptake where it is oxidized by bacteria.

Atmospheric aerosols have a profound impact on the climate, just like greenhouse gases, they are able to change the Earth's radiative or energy balance (Andreae & Crutzen, 1997; McNeill, 2017; Stocker et al., 2013). Atmospheric aerosols are the suspensions of small solid or liquid particles (excluding cloud particles) in the air (having negligible terminal fall speeds) (Stocker et al., 2013; Wallace & Hobbs, 2006). Particulate matters are categorized under atmospheric aerosols. Different ranges of particle sizes play different roles. For example, particles with diameter from 10^{-3} to less than 10^{2} μm play a role in the atmospheric chemistry including air pollution such as haze or fog episode (Andreae & Crutzen, 1997; Kolb & Worsnop, 2012; McNeill, 2017; World Health Organization, 2006). The residence time for the particles in the atmosphere depends on the particle sizes. The smaller the size of the particle, the longer its residence time in the atmosphere. Their lifetimes are approximately one to two weeks. They have more uneven distribution than greenhouse gases and is more concentrated near its source regions over continents and within the atmospheric boundary layer. The increase of uneven distribution of tropospheric aerosols causes high heterogeneous radiative forcing which can affect the regional as well as global climate (Chung, 2012; McNeill, 2017; Stocker et al., 2013). Particulate matters from around 0.05 to 10 micrometers (μm) in diameters are of greatest concern as the particles of this size range interact directly with the sunlight, and also make up the majority of the aerosol mass (Kolb & Worsnop, 2012; Remer et al., 2009; Stocker et al., 2013). There have been large numbers of particles injecting into the atmosphere directly and through the gas to particles (g-to-p) conversion. In general, 15% of the particles with the diameter sizes greater or equal to 5 μm is estimated to be produced from natural emissions while ~80% is from anthropogenic emissions (industrial processes, fuel combustion, and g-to-p conversion). The sources of anthropogenic

emissions are stationary and mobile sources. It can be emitted directly in the atmosphere or transformed into secondary organic particles originated from gaseous pollutants such as sulfur dioxide (SO_2) and nitrogen oxides (NO_x) (Krzyżanowski et al., 2005; McNeill, 2017; Stocker et al., 2013). Biomass burning is among one of the major source of particulate matters in Southeast Asia (Heil & Goldammer, 2001; Koe et al., 2001; Latif et al., 2018). It usually comprised of high amounts of organic pollutants and are able to move far from their sources due to their fine particle size and stability (Ramanathan & Feng, 2009). The two most frequently monitored particulate matters are PM_{10} (diameter is less than 10 μm; covered both coarse and fine particles) and $PM_{2.5}$ (diameter less than 2.5 μm; also known as fine particles). These PM are the most concern pollutant as it can affects the respiratory system especially $PM_{2.5}$. The fine particles also contribute to more dominant role in the formation of haze episodes (Betha et al., 2014; Heil & Goldammer, 2001; See et al., 2006). Dominick et al. (2015) emphasized that BMRS can be influenced by both primary and secondary natural and anthropogenic sources of fine particles. Primary natural sources mostly from sea spray and crustal material while secondary sources originated from oxidation of reduced precursor gases (Sulfur oxides, nitrogen oxides and organics) emitted from the sea. Meanwhile, the primary anthropogenic sources can be influenced by trace metals, agriculture, open burning and oily residues; secondary sources mostly are from fossil fuel combustion, motor vehicle exhaust, animal husbandry, fertilizer and sewage. Sea spray also was a significant source of coarse particles at coastal areas (Almeida et al., 2005; Stocker et al., 2013). The guideline or threshold values recommended by WHO for daily averaged of PM_{10} and $PM_{2.5}$ are $50 \mu g m^{-3}$ and $25 \mu g m^{-3}$ respectively. The $PM_{2.5}/PM_{10}$ ratio is useful in identifying the temporal and spatial sources of PM as different sizes of PM originate from different sources. Studies conducted by Chan and Yao (2008) and Zhou et al. (2019) in China, Munir (2017) in UK implemented this method and great heterogeneity exists at different regions. Particles,

unlike gases do not partition between air and water consistently and thermodynamically in a predictable way (Hemond & Fechner, 2014). Deposition of PM involves both dry and wet depositions (Wu et al., 2018). Dry deposition is associated with the deposition of particles or gases from the atmosphere through the direct delivery of mass to the surface (i.e. non-precipitation method) (Dolske & Gatz, 1985) while the latter is attributed to deposition under wet processes i.e. rain scavenging (Chate & Pranesha, 2004). Strong wind speed, high relative humidity and low temperature contributed to high dry deposition velocity (Hemond & Fechner, 2014).

Climate change is a global concern which requires greenhouse gases and aerosols inventory from different regions of the Earth for mitigation purposes (Houghton et al., 2001). Rising CH_4, CO_2, PM_{10} and $PM_{2.5}$ can contribute to the increase of total radiative forcing which can lead to dangerous temperature increase resulting in more extreme climate in the future (Caro, 2018; Stocker et al., 2013). Beside negative impact on public health (Afroz et al., 2003), PM_{10} and $PM_{2.5}$ can also indirectly affect the climate.

2.2 Northeast (NE) and Southwest (SW) monsoon in Malaysia

Monsoon are typically produced when there exists land-sea differential heating mainly caused when heat is released from the sun radiations (Lim & Samah, 2004). The temperature difference creates pressure differences which then allows the flows of air from within lands and seas. Besides that, seasonality is also affected by the Earth's deflection known as the Coriolis effect. When the Earth rotates and revolves around the Sun, different periods occur due to the different land masses of the northern and southern hemispheres. Northern hemisphere has larger land surface area than the southern hemisphere, thus it is warmer. This causes opposing seasons between the northern and southern hemispheres. Asian monsoon occurrence affects a spectacular part of the Earth's

climate system and could reach up to 60% of human inhabitants. The two types of Asian monsoons are the summer and winter monsoons. Their features are shown in Table 2.1. Summer monsoon originates from a high-pressure region near the Mascarene Island over the Indian Ocean which is known as the Mascarene High. Meanwhile, winter monsoon commences when there is a high-pressure region at Siberia which is in the north-eastern part of Eurasia near Lake Baikal and the high-pressure region is commonly known as the Siberian High. This causes a significant pressure difference between the high-pressure region (Siberian High) and the low region in the equatorial area, leading to the onset of the winter monsoon. Monsoon trough (low-pressure region) is usually observed over North India during the summer monsoon while during the winter monsoon, near-equatorial trough was observed over the equatorial region of Southeast Asia. Also, summer monsoon is usually associated with an existence of cross-equatorial low-level jet over East Africa while winter monsoon is usually associated with lower tropospheric surges or better known as cold surge. Summer monsoon is associated with rainfall over the northern India while rainfall during the winter monsoon usually affects mainly the Malaysia-Indonesia regions.

Table 2.1: Features of Asian monsoon – summer and winter monsoon.

Summer monsoon	Winter monsoon
Mascarene High over the Indian Ocean	Siberian High near Lake Baikal
Monsoon trough over North India	Monsoon trough near equatorial of Southeast Asia
Cross-equatorial low-level jet over East Africa	Lower tropospheric surges
Monsoon rainfall and cloud over northern India	Monsoon rainfall and cloud over Malaysia- Indonesia region

Source: (Lim & Samah, 2004)

In Malaysia, winter and summer monsoon periods are known as the NE and SW monsoons respectively (Lim & Samah, 2004). NE monsoon usually starts as Siberian-Mongolian High build-up and the northerly wind progresses rapidly southward affecting

the tropics in the vicinity of the South China Sea and it involves synoptic scale of motions (Chang et al., 2006; Chang et al., 1979; Wangwongchai et al., 2005; Yokoi & Matsumoto, 2008). There are also studies that suggesting it is variable depending on the Arctic Oscillation (Gong & Ho, 2003; Loo et al., 2015; Wu & Wang, 2002). The start of this monsoon can be detected with the presence of gusty winds and strong seas during the middle or end of November. One of the most intriguing aspects of NE monsoon is the development of cold surges. The cold outbreak (Chang et al., 2005) usually encompasses a large area from East Asia to the western Pacific and usually associate with heavy rainfall over the east coast of Peninsular Malaysia (Hai et al., 2017; Juneng et al., 2007; Shariff et al., 2015; Tangang et al., 2008). The cold surges can be characterized when there is a drastic drop in temperature, a strengthening of northerly winds and increase in surface pressure (Lim & Samah, 2004; Ooi et al., 2011; Shariff et al., 2015; Tangang et al., 2008). Cold surge index can also be used to determine the occurrences of cold surge (Chang et al., 2005; Ooi et al., 2011)

SW monsoon in Malaysia is not directly affected by any large-scale weather systems due to the absence of near-equatorial trough. Rather than the Mascarene High, this monsoon is more affected by the pressure differences from the Australia and the Western Pacific region. The monsoon trough lies far to the north mainly over the South China Sea and extends south-eastwards to the Philippines and Northwest Pacific (Chenoli et al., 2018; Lim & Samah, 2004). The generally dry condition during this period is also attributed by the passages of typhoon across the Philippines, activation of the Indian-Sumatra trough, and summer monsoon break. During the monsoon, land-sea breeze events are dominant. Land-sea breeze is a shallow circulation which is restricted to only 3 km of height. In Malaysia, this event is always associate with diurnal variability over a day (Lim & Samah, 2004). Interaction of this local meteorological events with several

other factors i.e. movement of strong westerly winds at lower troposphere allows the initiation of cloud development.

2.3 The meteorological influence on the air pollution

Meteorological conditions play a crucial role in the diffusion, deposition and transport of air pollutants. The mechanisms for the transport of air pollution and the review on the studies related to the meteorological conditions with air pollution in Malaysia are explained in this section.

2.3.1 The mechanisms for the transport of air pollution

The study on the relationships underlying big data such as air pollutants and meteorological data can provide important information in regards to the air pollution exposures. The mechanisms on the transport of air pollutants can be examined by analyzing several important factors. The three major factors of the air pollution distribution are winds, topography and atmospheric stability (Stull, 2016).

2.3.1.1 Wind

Wind generally describes the movement of air driven by forces. The strength of wind plays a major role in the distribution of air pollution. When pollutants spread into the air, the intensity of the wind determines how quickly the pollutants mix with the surrounding air and how fast they move away from their source. Typically, strong winds lower the concentration of pollutants by spreading them apart as they move downwind. Furthermore, stronger wind associated with more air turbulence which subsequently

produces swirling eddies that dilute the pollutants through mixing. Oppositely, light wind allows more accumulation of the air pollutants and they tend to become more concentrated.

Wind and associated meteorological conditions can act as a transport mechanism for transboundary air pollution. Sources and pathways of the wind can also influence how the wind impact the distribution of air pollutants. Akimoto (2003) emphasized that the effect of global air pollution on climate and the environment has become a new concern in atmospheric science particularly for air pollutants that have long atmospheric lifetimes (at least 1 week) such as ozone (O_3) and carbon monoxide (CO). In Southeast Asia, Pochanart et al. (2004) stressed that there is significant transport from East Asia through northerly winds flowing into the tropics which substantially impacts Hong Kong and Southeast Asia (in particular Thailand) during winter. Japan (Kaneyasu et al., 2000) and Taiwan (Lin et al., 2004) are affected too. The main mechanism for the transport is well explained in the studies too (Kaneyasu et al., 2000; Lin et al., 2004; Pochanart et al., 2001; Pochanart et al., 2004). The confluence of cold dry air from Siberia and warmer and moist air from the Pacific which subsequently lead to active frontal cyclones over coastal regions of East Asia which subsequently lead to the formation of cyclone that moves off the coast and tracks east or north-eastwards over the Western Pacific. These cyclones and the associated fronts provide the dominant export pathway for pollutant from East Asia. The low-level outflow in the air following the cold front is another important factor for this transport. This can cause pollutants from the heavily polluted regions of continental East Asia to accumulate and then be exported in the boundary layer and lower troposphere behind cold fronts. The dry, descending air stream behind the cold front may also draw high levels of stratospheric ozone down into the lower troposphere which may mix in with this polluted air. While this air is generally confined to the lower troposphere over the western Pacific, it may be entrained into the pre-frontal ascending flow in the

following cyclone thus lifting it to higher altitudes where it may be rapidly transported eastwards. Pochanart et al. (2004) and Ashfold et al. (2015) emphasized that there is a need to study air pollution transport in Southeast Asia as there are very few studies conducted in this region to explain better the intercontinental transport of air pollution and its impact in Southeast Asia. Another study by Ashfold et al. (2017) focused specifically on the effects of cold surge events on the air quality. Cold surge is the strong northerly winds initiated from the Siberian High. The significant finding is that the ozone recorded to higher levels during the cold surge events (2003 to 2012). Oram et al. (2017) also noted that the prevailing northeasterly winds from East Asia contributed to the high levels (than expected) of short-lived chlorine compounds (Cl-VSLS) at Bachok, Kelantan. Farren et al. (2019) study also indicated the strong anticyclone system (Siberian High) led to the arrival of strong northeasterly winds as well as the aged emissions from the highly polluted East Asian regions to areas along the east coast of Peninsular Malaysia. All of these studies show that strong winds from polluted regions are capable to transport air pollutants (with long atmospheric lifespan) to another regions. Therefore, the sources and pathways of the winds should be considered too.

2.4.1.2 Topography

Topography describes the shape of the landscape. It plays an important part in trapping pollutants. Valleys that are encased by mountain and hills are mostly prone to air pollution. At night, cold air tends to drain downhill where most of it settle into low-lying basins and valleys. Air pollution concentrations in mountain valleys also are the greatest during the colder months. In accordance to Dominick et al. (2015), BMRS is in a rural and coastal area where major activities are fishing and plantations. Being a coastal station, BMRS is exposed to land-sea interactions. This station can be influenced by a mixture of

local anthropogenic and biogenic emissions, clean air masses and aged emissions from regional sources during the Northeast monsoon (Farren et al., 2019).

2.4.1.3 Atmospheric stability

Atmospheric stability also affects air pollutions as it is related to the vertical movement of air. Stability is like the resistance of the atmosphere to the vertical motion. There are three types of atmospheric stability which are stable, neutral and unstable (Stull, 2006). Unstable atmosphere can be identified when the air temperature decreases in higher altitudes. This is when the warm air at the surface rises up and interacts with cooler air at the upper level leading to temperature decreases. However, stable atmosphere occurs when the air temperature decreases very slowly or increases as the altitude increases. This indicates that cooler air is at the lower level while warm air is at higher level of the atmosphere. An unstable atmosphere will enhance while stable atmosphere will suppress the vertical motion of air. Atmospheric stability also depends on the climatic circumstances. The unstable atmosphere can be clearly seen at noon (as sun produces solar radiations and heat the land surfaces) while the stable atmosphere is clearly seen at night and dawn. Unstable atmosphere is usually associated with turbulent flow where air pollution present tends to mix with the surrounding air thus decrease in its concentration. Meanwhile, stable atmosphere is usually attributed to laminar flow where the presence of air pollution tends to accumulate and increase in concentration.

The troposphere is generally constrained towards different types of vertical motion known as an atmospheric boundary layer (ABL) and free troposphere (FT). ABL is known as the bottom of the troposphere region which can be affected by the conditions of the Earth's surface. It is the key parameter in the description of the vertical processes of the lower troposphere including the distribution of air pollution. Stull (2006) has

highlighted the typical structure of the atmospheric boundary layer and evolutions over land in details during fair weather (Figure 2.1). During daytime, the ABL is comprised of unstable surface layer (SL), statically unstable mixed layer (ML), and strongly stable entrainment zone (EZ). Meanwhile, at night, the ABL usually comprised with the stable boundary layer (SBL) or known as a nocturnal boundary layer (NBL), statically neutral residual layer (RL), and statically stable capping inversion (CI). The RL can contain pollutants and moisture from the daylight's ML however it is less associated with turbulent flows.

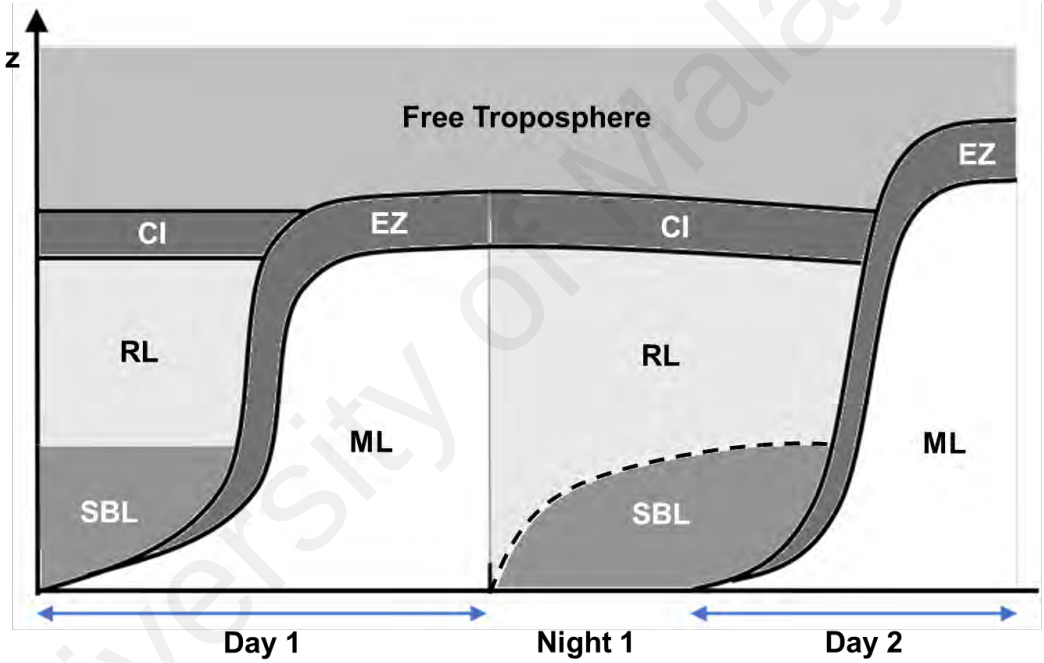

Figure 2.1: Components of ABL during summer over land (Stull, 2006) where SBL: Stable Boundary Layer, RL: Residual Layer, CI: Capping Inversion, ML: Mixed Layer and, EZ: Entrainment Zone. Color ranged from very unstable (white) to neutral (light grey) then to very stable (dark grey) atmospheric stability

Seibert et al. (2000) and Seidel et al. (2010) had reviewed several techniques to determine the structures of the ABL such as using the Parcel method, Richardson number and vertical profiles of specific parameters (potential temperature, specific humidity, relative humidity, and refractivity). Nair et al. (2011) highlighted that even though there

have been several methods suggested and techniques used, there is still no unique definition and single overall accepted method for the determination of ABL, especially at the coastal region. ABL at the coastal is usually more complicated as it is prone to be influenced by the synoptic or mesoscale meteorological conditions. Furthermore, it can also be affected to the thermal internal boundary layer height (TIBL) which usually reduced the ABL (Wei et al., 2018).

The relationship between atmospheric stability and the distribution of air pollutants is more complicated than explaining its relationships with the wind. Its variabilities are different during days and nights; cloudy and non-cloudy days and also under different scales of meteorological conditions. Therefore, typical atmospheric stability is considered for this study where unstable atmosphere is strong at noon while stable atmosphere is stronger at late night and pre-dawn. This subsequently implies that there is more presence of turbulent air at noon and laminar air at night.

2.4.2 Review on air pollution studies in Malaysia

There has been growing studies on air pollution episodes in Malaysia. The Malaysian government has adopted the Air Pollution Index (API) to monitor and improve air quality (Afroz et al., 2003; Mead et al., 2018).There were many studies on the seasonal and monthly variations of air pollutants during the NE and SW monsoon as shown in APPENDIX B. However, most of the extensive studies focused on the air pollution events, the contributing factors and impacts (Azam et al., 2018; Latif et al., 2018; Othman et al., 2014; Tajudin et al., 2019) are mainly focused during the SW monsoon (APPENDIX B) due to the transboundary pollution resulted from the biomass burning in Indonesia in addition to the dry and stable atmospheric condition (Afroz et al., 2003). During the SW monsoon, Malaysia experienced frequent haze episodes resulting mainly

from the forest fires in Sumatra and Kalimantan, Indonesia (Department Of Environment). Haze episode during the SW monsoon 2015 was the worst one where 34 areas in the country recorded unhealthy air quality status. Besides transboundary pollution transported from the Indonesia region, the atmospheric condition was influenced by the extended drought period associated with a strong El-Nino (Huijnen et al., 2016). The study also estimated the carbon emissions from the 2015 forest fires which were the largest seen in the maritime Southeast Asian as compared to that in 1997. Furthermore, records from 49 monitoring stations in Malaysia showed that almost 40% of the Malaysian population was on average exposed to PM_{10} concentrations higher than 100 μgm^{-3} during the episode (Mead et al., 2018).

The study on air pollution associated during the NE monsoon is less as it is prone to the wet conditions and the air pollutants are able to be washed out. However, NE monsoon which is usually attributed to synoptic flows and presence of transient disturbances known as cold surges can also allow transboundary pollution to be transported at Malaysia. The tropics are well known to be associated with deep convection in which air can be lifted quickly into the primary gateway of the stratosphere through the Tropical Tropopause Layer (TTL). Southeast Asia and the Western Pacific are a particularly important source region of air that enters the TTL. A lot of studies revealed transport of air pollutants from East Asia to another parts of Asia and Southeast Asia (Akimoto, 2003; Ashfold et al., 2017; Oram et al., 2017; Pochanart et al., 2004). Ashfold et al. (2015) emphasized that during the Northern Hemisphere winter, pollution originating from polluted East Asia land mass contributed to high (double the typical background level) levels of perchloroethene (C_2Cl_4) at Borneo. Ashfold et al. (2017) also showed there is an exceedance in the concentration of O_3 (according to the World Health Organization's air quality) at Kota Bharu during cold surge events. In addition, Oram et al. (2017) also revealed high levels of chlorinated very short-lived substances (VSLSs) are present in the

surface and upper tropospheric air in East and Southeast Asia. Farren et al. (2019) emphasized that emissions from East Asian regions during this monsoon period contributed to differences in aerosol compositions at BMRS where more elevated sulphate (SO_4^{2-}) concentration and increase chlorine Cl^- depletion were observed from the continental air masses that originated from the industrialized regions of East Asia compared to marine air masses. More studies on Southeast Asia are needed to quantify the relations of meteorological conditions with air pollutants during NE monsoon (Ashfold et al., 2015; Pochanart et al., 2001).

2.5 Transport models

Transport of pollution from continental source regions can take place in the boundary layer (BL) and free troposphere (FT) region. Meanwhile, the characteristics of atmosphere at certain locations are also very dependent on its local and regional pollutions. To determine the potential sources contributing to air pollution at certain sites, data analysis and modelling are necessary. Air pollution modelling is a numerical tool used to describe the relationship between emissions, meteorology, atmospheric concentration, and deposition (Daly & Zannetti, 2007). Transport model is required to determine the sources, compositions, sinks, and transport of the air pollutants in various parts of the world (Lal, 2007; Lin et al., 2014; Palmer, 2008; Qian et al., 2010; Strode & Zhu, 2010). The usage of air pollution modelling could give a more complete deterministic description of the air quality problem such as analysis of factors and causes (emission sources, meteorological processes, and physical and chemical changes) and some guidance on the implementation of mitigation measures. Generally, the transport phenomena are characterized by the mean velocity of the fluid while the study of diffusion

and mixing are characterized by its type of atmospheric flows such as laminar or turbulent motions.

The transport model is required to prove whether there is a transport of pollutants from other regions to BMRS or not. Thus, the focus of the literature for this section is on the transport model for trace gases and aerosols as shown in APPENDIX C. There are different types of transport models for air pollutants depending on the purpose of usage or study. For example, the Gaussian Plume model is used to determine the maximum ground-level impact of the plumes and its maximum impact from the source. Meanwhile, Lagrangian modelling is run in which an air parcel is followed along a trajectory and it is assumed to conserve its identity through the same path. However, Eulerian modelling is run in which an area studied is divided into grid cells both in vertical and horizontal directions. In other words, the Lagrangian model is often used over a large distance and longer time periods while the Eulerian model is used over urban areas and restricted to an episodic phenomenon.

APPENDIX C shows that most of the study related to the transport of trace gases and aerosols using Chemistry version of Weather Research and Forecasting (WRF-Chem) and Hybrid Single Particle Lagrangian Integrated Trajectory (HYSPLIT) models. HYSPLIT model is a complete system in computing simple air parcel trajectories as well as its complex transport, dispersion, chemical transformation and deposition simulations (NOAA; Stein et al., 2015) while WRF-Chem is a weather research and forecasting model integrated with chemistry to represent the emission, mixing, transport and chemical transformation of pollutants simultaneously with meteorology (Grell et al., 2005; NCAR). In general, the WRF model is a state-of-the-art atmospheric modelling system for meteorological research and numerical weather prediction. It was an excellent choice for a broad range of applications across scales from tens of meters to thousands of kilometers

including meteorological studies, real-time numerical weather prediction, idealized simulations, data assimilation, earth system model coupling and etc. (Michalakes et al., 2001). It is related to data assimilation system and software architecture supporting parallel computation with system extensibility. It allows researchers to produce simulations based on actual atmospheric conditions (from observations or reanalysis data) or in idealized conditions. Meanwhile, WRF-Chem is an extended version of WRF and it includes the atmospheric chemistry and aerosols part. It can simulate the trace gases and particles in an interactive way thus allowing for feedbacks between the meteorology and radiative active gases and particles. Since this model involves meteorology and chemical processes, it thus requires more details and the process is more complex. It uses advanced research WRF (ARW) as its dynamic core (transport) which is the mass coordinate version of the model. The atmospheric chemistry mechanism used are the Regional Acid Deposition Model version 2 (RADM2); it has been widely used to predict concentrations of oxidants and other air pollutants by using quasi-steady-state approximation method and the time integrations are solved by Backward Euler approximation. (Grell et al., 2005). Mead et al. (2018) used WRF-Chem to study the impact of the 2015 wildfires on air quality in Malaysia by examining the concentration of carbon monoxide (CO) and PM_{10}. The study also emphasized the need for incorporation of detailed ground-based observational data to accurately simulate variation and transport of air pollutants.

HYSPLIT has been evolved for more than 30 years from the single trajectories based on radiosonde data to multiple interacting pollutants transported, dispersed and deposited from local to global scales. It is widely used to study the potential sources of atmospheric pollutants because the model simulates airflow patterns from the receptor site which is a major mechanism for pollutant transport. The fundamental of this model's calculation is based on a hybrid between the Lagrangian approach (use a moving frame of reference for the advection calculations as the trajectories of the air parcels move from their initial

location) and the Eulerian methodology (use fixed three-dimensional grid as a frame of reference). One of the most common model applications is a back trajectory analysis to determine the origin of air masses and provide relationships on source-receptor (Ding et al., 2013; Fleming et al., 2012; Han et al., 2005). Other application includes tracking and forecasting the release of radioactive material, wildfire smoke, wind-blown dust, volcanic ash and etc. (Stein et al., 2015). Preparation on the meteorological input data and analysis of the simulation outputs are needed to run the HYSPLIT model. Pre-processing for this model involves preparing the meteorological model data source (either small, large, mesoscale or global scales) into an HYSPLIT-compatible format. There are meteorological data that are already formatted for HYSPLIT and are publicly available from NOAA's Air Resources Laboratory (ARL) such as Global Data Assimilation System (GDAS), National Centre for Atmospheric Research (NCAR) reanalysis data and etc. Postprocessors are needed to analyze multiple trajectory outputs and concentration ensembles. The multiple forward and backward trajectory analysis to forecast air mass movement and to track the air mass history respectively allows for the depiction of airflow patterns over different spatial and temporal ranges and able to account for the uncertainty in the associated wind patterns. Grouping trajectories that share some commonalities in space and time are also available to simplify the analysis and interpretation thus reducing the uncertainty in the determination of the atmospheric transport pathways. The multiple trajectories that are near to each other can also be merged into a group known as cluster trajectory. This method had been used by in the study of Baker (2010) about pollutant concentrations within Birmingham, Markou and Kassomenos (2010) on back trajectories reached Greater Athens, Karaca and Camci (2010) and Borge et al. (2007) on the long range transport on particulate matter (PM).

WRF simulations needed to be carried out on high-performance computing (HPC) clusters as they require an effective compute resource to handle the complex and parallel

simulations. At this instant, the configuration of the WRF model is still incomplete so it is not feasible to use it to examine the transport of the air pollutants for this study. Thus, HYSPLIT model is used to examine the possible transports of air pollutants at BMRS.

2.5.1 Concentration Weighted Trajectory (CWT)

In order to examine the source regions of the air masses in more detailed, there is a need to couple the trajectory analysis with the air pollutants at BMRS. This method is also known as the conditional probability function (CPF). It has been successfully utilized to analyze the point source impacts of many studies and it was a simpler method compared to non-parametric regression method (Kim & Hopke, 2004). It estimates the probability of a given source contribution from a given source wind direction that exceeds a predetermined threshold criterion. The two frequently used source techniques to identify the source regions coupled with the back trajectories known as the Potential Source Contribution Function (PSCF) and secondly is based on Concentration Weighted Trajectory (CWT). PSCF calculates the probability of a source that is located at latitude i and longitude j (Byčenkienė et al., 2014). Its basis is if a source is located at (i, j), an air parcel that passed through that location can collect material at the source and transport it along the trajectory. This method solves by following (Equation 2.1) where m_{ij} is the number of trajectories that arrived at a receptor site with pollutant concentrations higher than a specified criterion. Common criteria for m_{ij} is controlled by a percentile value of 90 percentiles. n_{ij} is the number of trajectories the trajectories passed through the cell (i, j).

$$\boldsymbol{PSCF} = \frac{\boldsymbol{m_{ij}}}{\boldsymbol{n_{ij}}} \qquad \text{(Equation 2.1)}$$

CWT method used the same grid domain however for each grid cell, the mean concentration species was calculated. In this method, every concentration is used as a weighting factor for the residence time of all trajectories in each grid cell and divided by the cumulative residence time for all trajectories. Increased in the dwelling time of air mass over emission source areas can facilitate the embodiment of air pollutants thus is strongly related with the species concentrations at the receptor site (Dimitriou et al., 2015). For each grid cell, the mean concentration of the pollutant is calculated using Equation 2.2 where *i* and *j* are the indices of the grid, *k* is the index of trajectory, *N* is the total number of trajectories in the analysis, C_k is the concentration of pollutant measured corresponding to the arrival of trajectory *k*, and τ_{ijk} is the residence time of trajectory *k* in grid cell *(i, j)*. A high value of $\bar{C}_{ij}$ defines that air parcels passing over the cell (*i, j*) would (on average) cause high concentration at the receptor site.

$$\left(\overline{\boldsymbol{C}}_{\boldsymbol{ij}}\right) = \frac{\sum_{k=1}^{N} \boldsymbol{C}_{\boldsymbol{k}} \boldsymbol{\tau}_{\boldsymbol{ijk}}}{\sum_{k=1}^{N} \boldsymbol{\tau}_{\boldsymbol{ijk}}} \qquad \text{(Equation 2.2)}$$

CWT was chosen for this study because it provides more accurate source regions based on the concentration of a pollutant at the receptor site. Carslaw and Ropkins (2012) also emphasized the main limitations in using the PSCF method is that the grid cells can show the same source regions when the concentration of the pollutant is slightly higher or much higher than the criterion. The implementation of CWT formula has been adopted by several recent studies. It indicated that PM containing lead (Pb) and vanadium (V) at Fukue Island, Japan were emitted from industrial combustion in China and ships in the Pacific respectively (Hidemori et al., 2014). Using this method, Byčenkienė et al. (2014) have revealed that aerosol sources influencing Vilnius (Lithuania) are seasonally dependent and can be highly influenced by the heavily industrialized areas in Poland, Germany and Czech Republic. This method also determines the source regions of $PM_{2.5}$

that affects Athens (Dimitriou et al., 2015) and for mercury at the urban coastal site in Nova Scotia, Canada (Cheng et al., 2013).

Overall, understanding the variabilities of CO2, CH4, PM10, and PM2.5 in relations with different meteorological conditions in different monsoon periods at BMRS will further increase the understanding of the transport of air pollutants from East Asia to the deep tropic during the NE monsoon. Studies described the NE monsoon are prone to the influence of strong northeasterly winds while the SW monsoon is more influenced by light southwesterly winds. Among the major factors described in Section 2.3, the main mechanism that will be focused on this study are on the strength, sources and pathways of the winds. Studies also show that WRF-Chem and HYSPLIT model is among the most commonly used to examine the transport of air pollutants. HYSPLIT model is chosen due to its easier application and feasibility to determine the origins of air masses at BMRS. Studies show that CWT are capable to incorporate the back-trajectory analysis with the concentration at the receptor site. Hence, this study will implement the HYSPLIT-CWT method to examine the transport of CO_2, CH_4, PM_{10} and $PM_{2.5}$ at BMRS.

CHAPTER 3: DATA AND METHODOLOGY

This chapter provides a description of the data and methods employed for this study. Data used are observational and remote-sensing data. R Software, GrADS, and HYSPLIT model were mainly used for data analysis and visualization.

3.1 Observational Data

The observational data are based at the BMRS located at 102.4259 °E and 6.0086 °N, i.e. in the eastern coast of Peninsular Malaysia and is located 100 m from the water edge of the South China Sea. There were two categories of observational data used for this study.

3.1.1 Atmospheric Laboratory (Tower) Data

The data was obtained from the instruments mounted on a tower with a height approximately 30 m above the ground level (Figure 3.1) namely Los Gatos Research (LGR's) greenhouse gases analyser, EDM 180 Ambient dust monitor (GRIMM AEROSOL) (Spielvogel et al., 2009), and LSI LASTEM Automated Weather Station (AWS). The data processing from GRIMM was well described by (Dominick et al., 2015). It is equipped with a global positioning system (GPS), the aerosol monitoring system also consisted of an aerosol spectrometer which is attached directly to the Nafion inlet drying tube where the air enters (GRIMM, 2018; Grimm & Eatough, 2009). The aerosol spectrometer uses the state-of-the-art optical particle counter enabling in-situ measurements of the particle distribution with a diameter size ranging from 0.27 μm and 34 μm. Using a volume-controlled pump at a rate of 1.2 L min^{-1}, the ambient air is pumped into the measuring cell and passes through the GRIMM spectrometer cell which was

designed as a single particle detection and counting system. All the aerosol particles that move through the measurement chamber are classified by their distribution channels of 31 sizes. The particle mass measurement is obtained by applying the theoretical mass equation and the principle of measurement is based on the light-scattering technology for single particle counts (Grimm & Eatough, 2009). The particle diameter data are first converted to particle volume by using the mean particle diameter between the thresholds of 31 different channels. Then the volume data are converted to a particle mass distribution by using a corresponding density factor. Finally, these were added to the total mass of each channel of particulate matter. This technique complies with some international guidelines for ambient air monitoring such as EN12341, EN14907, and US-EPA Designated Reference and Equivalent Method and GOST-R (Dominick et al., 2015).

Figure 3.1 BMRS's atmospheric laboratory

The dry mole fractions of CO_2, CH_4 and water vapor (H_2O) were determined by using Off-Axis Integrated Cavity Output Spectroscopy at a frequency of 1Hz for LGR's

greenhouse gases analyser. The analyser calibration was carried out every 45 hours using three secondary gas standards prepared in the Cylinder Filling Facility (CFF) and calibrated against NOAA primary gas standards (Scales) in the Carbon Related Atmospheric Measurement Laboratory (CRAM), both of which are based at the University of East Anglia (UEA) in the UK. A secondary working standard consisting of non-calibrated compressed air was measured every 7 hours to assess and account for drift in the analyzer response between calibrations. The performance of the analyser was evaluated using a target gas cylinder measured every 10 hours. This target gas cylinder was calibrated against NOAA primary gas standards in the CRAM lab and was introduced to the analyzer as an air sample and treated as an air sample during data processing. The ambient air was added to the analyser without being dried during the study period. Therefore, we used the measurements of the H_2O analyzers to convert the wet air mole fractions to dry air mole fractions. Due to inaccuracies in CO_2 and CH_4 dry air mole fractions reported using the analyzers built-in water correction, the relationship between the wet air mole fractions of CO_2 and CH_4 reported by the analyser and the corresponding dry air mole fractions was independently determined. This test was conducted at the Facility for Airborne Atmospheric Measurements (FAAM) in the UK using the experimental setup used by O'Shea et al. (2013). AWS data were observed together with meteorological data measured in GRIMM AEROSOL to ensure the accuracy of the data. LGR's greenhouse gases analyser measured carbon dioxide (CO_2) and methane (CH_4) data in each 1-second while GRIMM AEROSOL and AWS produced data in each 1-minute. Two years of data (November 2014 to September 2016) were collected from the atmospheric laboratory for this study.

3.1.2 Radiosonde Data

The second observational data is the upper-air data measured by Vaisala radiosonde RS92-SGP (Nash et al., 2005). Vaisala radiosonde is widely used type of sonde in the global radiosonde network for the measurement of the upper- air meteorological parameters (Dirksen et al., 2014). This radiosonde scored 4.96 in a performance score of all climate variables and it qualified for Global Climate Observing System (GCOS) Upper Air Network (GUAN) use (Nash et al., 2011). It is the only radiosonde that incorporated working protection against evaporative cooling and it protects the input data from exhibiting biases upon emerging from clouds. This allows it to provides excellent quality radiosonde data for wide range of applications such as climatology, numerical weather prediction models and synoptic meteorology (Nash et al., 2011). As shown in Figure 3.2, it was equipped with a temperature sensor, humidity sensor, pressure sensor, Global Positioning Sensor (GPS) antenna and allows wind measurement by GPS receiver. The filled-balloon are attached to it to raise it up into higher altitudes. The upper-air data are recorded in 2-second interval and able to measure up until 20 km above the ground level.

Figure 3.2: Vaisala's radiosonde RS92-SGP used to measure the upper air data during case studies period

Radiosonde attached to a balloon filled with helium gas (Figure 3.3) was launched specifically during case study periods to measure the upper-air meteorological data over BMRS and to compare it with the reanalysis data. Case study 1 (CS1) was conducted from 25 to 27 January 2016 and 17 radiosondes were launched during this period starting at 1100 LT (local time). Meanwhile, the second case study (CS2) was conducted from 3 to 5 June 2016 and 18 radiosondes were launched also starting at 1100 LT. Measurements are collected for every 3-hour intervals.

Figure 3.3: Radiosonde attached to balloon and released to the atmosphere during case study period

3.2 ERA5 Reanalysis Data

ERA5 is the fifth generation of climate reanalysis dataset from the European Centre for Medium Range Weather Forecasting (ECMWF). It has higher spatial (31km vs. 79 km) and temporal resolution (hourly vs. three hourly) than ERA-Interim (4th generation

of reanalysis dataset from ECMWF) (Hersbach, 2018; Hoffmann et al., 2019; Urraca et al., 2018). To study the seasonal patterns of NE and SW monsoon from 2014 to 2016, three hours interval of 925 hPa zonal (u) wind, meridional (v) wind, mean sea level pressure (MSLP), and geopotential height (gph) at 500 hPa were collected. For this study, data on the 925 hPa pressure level was utilized because it is likely a representative of boundary layer conditions (Ashfold et al., 2017) and provides the most prominent meteorological characteristic of the study region (Kavitha et al., 2018). MSLP and gph at 500 hPa data used to determine the pressure differences at the surface and at the mid troposphere respectively. The results subsequently will be able to determine on the presence of the synoptic winds. For case studies analysis, one-hour interval data as mentioned above were used; 10 m u and v winds were also downloaded to specifically examine the surface winds of the study regions.

3.3 Global Data Assimilation System (GDAS) Data

GDAS data is the numerical weather prediction (NWP) data from the National Oceanic and Atmospheric Administration (NOAA) Air Resources Laboratory. It was used by the National Centre for Environmental Prediction (NCEP), Global Forecast System (GFS) model to place observations data (such as 3-D, model space, surface observations, balloon data, wind profiler data, aircraft reports, buoy observations, radar observations, and satellite observations) into gridded model space to start, initialize or weather forecasts (Stein et al., 2015). The output for GDAS is World Meteorological Organization (WMO) Gridded Binary (GRIB) and there are two types of GDAS data available which are 1° by 1° (GDAS1) and 0.5° by 0.5° (GDAS0P5) horizontal resolutions; it corresponds to 100 km × 100 km and 50 km × 50 km respectively. Both of the data assimilated from the same observations but they differed in several aspects such as horizontal resolutions and

vertical velocity fields. The major difference between GDAS1 and GDAS0P5 is on the vertical velocity; GDAS0P5 does not include the vertical velocity and it has to be calculated by the vertical integration of the horizontal velocity divergence while the vertical motion of the trajectory generated from GDAS1 can be calculated directly from its model output vertical wind velocity. HYSPLIT backward trajectories differed with different input meteorological data. Areas with complicated topography is encouraged to use GDAS1 (Su et al., 2015) so this data was used for this study to observe the backward trajectories at BMRS. The data is in 3-hourly archive data and it was run four times a day (00, 06, 12, 18 UTC). In addition, the data are in 360 by 181 latitude-longitude with the lower-left corner (1,1) is (0W, 90S) and the upper-right corner (360, 181) is (1W, 90N) (NOAA). The data downloaded for this study is also ranged from 2014 to 2016.

3.4 Hotspots Data

Active fires or hotspots data are collected from the National Aeronautics and Space Administration (NASA's) Earth Science Data and Information System (ESDIS)- Fire Information for Resource Management System (FIRMS). These data are only collected during case studies period. This near-real time fire data is extracted from the Moderate Resolution Imaging Spectrometer (MODIS) (Giglio et al., 2016) and the Visible Infrared Imaging Radiometer Suite (VIIRS) (Schroeder et al., 2014). MODIS and VIRRS is attached to Aqua and Terra and Suomi-National Polar-orbiting Partnership (NPP) satellite respectively. The spatial resolutions for the fire detection are 1 km and 375 m respectively. MODIS data (Collection 6) utilized is the latest and the best active fires or hotspots product through remote sensing available with improved detection of small fires. These data were also used by Dominick et al. (2015), Khan et al. (2016) and Price et al. (2012) to investigate the impact of biomass burnings within different study areas in Asia

and Australia. A new approach on fire radiative power (FRP) has been retrieved for the fire detection of these data (Giglio et al., 2016) and the method has been shown able to better estimates remote biomass burning (Wooster et al., 2005). However, Ichoku et al. (2012) stressed the characterization of biomass burning by observing the active fire location from satellite is only qualitative and it is not adequate to quantify the biomass burning quantitatively. Despite the argument, the data are still able to identify the geographic positions of the active fire (Ichoku et al., 2012), which is helpful in providing the general estimates on the possible biomass burning activities within the case studies period.

3.5 Rainfall Data

The rain rate data is derived from Tropical Rainfall Measuring Mission (TRMM) satellite. It was a research satellite designed with the main purpose is to improve the distribution and variability of the precipitation in the tropics which is an important part of water cycle in the current climate system. The data collected is in 3-hour temporal resolution and 0.25° × 0.25° latitude-longitude resolution (Huffman et al., 2010; Huffman et al., 2007). The output of the rain rate is in TRMM Algorithm 3B-42 which involves the merging of high quality/infrared (IR) precipitation and root mean-square (RMS) precipitation-error estimates. It provides high quality estimation thus the rainfall characteristics in BMRS during case studies can be examined and specified closely. Varikoden et al. (2010) shows strong positive correlation ($r = 0.96$) achieved between this TRMM rain rate data with rainfall data in Kota Bharu measured by Malaysian Meteorology Department (MMD). A lot of studies concerning the characteristics of rainfall in Peninsular Malaysia has been using this data too (Juneng et al., 2007; Semire et al., 2012; Tangang et al., 2008; Varikoden et al., 2011; Varikoden et al., 2010). The

intensity of the rainfall are determined in accordance to Varikoden et al. (2010) which are classified into low, medium and high class intensities. The low-class intensity is when the rain is less than $4\,mm/hr$, medium class when it is ranged between $4\,mm/hr$ and $8\,mm/hr$ and high intensity when it is more than $10\,mm/hr$. These data are also collected during case studies periods.

3.6 Statistical Analysis

The basic statistical data such as mean, median, maximum, minimum, and standard deviation for all the observational data are analyzed using R Software. Pearson correlation is calculated to determine the relation or association between meteorological variables and air pollutants. The most frequently used correlation is known as the Pearson Product-Moment Correlation Coefficient, r (Crawford, 2006; Wilks, 2011) using (Equation 3.3) where $\bar{x}$ and $\bar{y}$ represent the mean of the respective variable.

$$r_{xy} = \frac{\sum(x-\bar{x})(y-\bar{y})}{\sqrt{\sum(x-\bar{x})^2 \sum(y-\bar{y})^2}} \qquad \text{(Equation 3.3)}$$

The Pearson correlation bounded by −1 and 1; that is $-1 \leq r_{xy} \geq 1$. If $r_{xy} = -1$ then there is a perfect negative linear association between x and y. Oppositely, if $r_{xy} = 1$, then there is a perfect positive linear association. This correlation had been widely used to examine the relationship of meteorological parameters (except wind direction) with the air pollutants (Vardoulakis & Kassomenos, 2008; Xu et al., 2006). . It was interpreted into three categories namely weak (0.0 to 0.3), moderate (0.3 to 0.7) and strong (0.7 to 1.0) (Ratner, 2009). This correlation cannot be used to examine the relationship of wind direction with the air pollutants as the 2-dimensional direction is a circular variable. Thus, the wind rose is also generated to examine the relationships of winds with the distribution of air pollution using R with Openair packages (Carslaw & Ropkins, 2012).

Hypothesis testing is a method often used to decide whether the results contain enough information (data) to cast any doubts, inferences and conclusions. There are two types of hypothesis testing namely parametric (has normal distributions) and non-parametric (free distributions) tests. The probability level or p-value is the most frequent parametric test used to determine the level of significance on the relations between air pollutants and meteorological parameters in Malaysia (Ashfold et al., 2015; Dominick et al., 2015; Mohd Talib Latif et al., 2014). R (Langfelder & Horvath, 2012) was also used to determine the p-value where if it the values is < 0.05 and < 0.01, then the correlation between x and y is considered significant and strongly significant respectively.

Nonparametric hypothesis testing for correlation coefficient was also implemented since the case studies data are only short-term and there are particularly some gaps on the CS2 data. Non parametric tests are generally designed for real data, skew, lumpy, outliers and gaps scattered (Wilks, 2011). Bootstrapping method have been chosen as the non-parametric test for this study considering the short-termed periods of CS1 and CS2. Through this method, a finite sample is treated as similarly as possible to the unknown distribution leads to resampling with replacement. This means that some of the original data will be drawn into a given bootstrap sample for multiple times and some will not be drawn at all. This resampling process is repeated using a large number, $n = 10000$. Then the 95% bootstrap bias-corrected and accelerated (BCa) confidence interval (CI) was calculated using R to investigate the significance level of the correlation coefficient. BCa CI is a second-order accurate interval which considers both the estimate of the original data and adjust the skewness in the bootstrap distribution (Mudelsee, 2003).

3.7 Grid Analysis and Display System (GrADS)

The GrADS is an interactive desktop tool that is commonly used to easy access, manipulation and visualization of earth science data (Berman et al., 2001). It was able to handle both gridded data and stationary data and supports many data file formats namely binary, gridded binary (GRIB), Network Common Data Form (NetCDF), Hierarchical Data Format (HDF) and Binary Universal Form for the representation of meteorological data (BUFR). This system uses a 5-dimensional data environment which is consisted of the four conventional dimensions (longitude, latitude, vertical level and time) with an optional 5th dimension for grids that is generally implemented but designed to be used for ensembles. FORTRAN-like expressions are used in command line to execute the operation interactively. GrADS was used for both gridded (ERA5) and station data (radiosonde) for this study.

An area covering tropical Southeast (SE) Asia between 85 °E to 145 °E and 5 °S to 235 °N are the main concern for this study. ERA5 data from 2014 to 2016 were averaged from November to March for the NE monsoon and from May to August for the SW monsoon (following the criteria of monsoon period provided by the Meteorological Department of Malaysia) to investigate the variation of winds and the effect of synoptic motions during the two monsoon periods.

3.7.1 Cold Surge

One of the interesting aspects of NE monsoon is the development of the cold surge (Chang et al., 2006). The cold surge is typically referred as cold air outbreaks from the Siberian-Mongolian High (SMH). It is usually attributed with the strengthening of the northeasterly winds, a drastic drop in temperature and increase in surface pressure (Lim & Samah, 2004). Its criteria over the Equatorial South China Sea and over the eastern

coast of Peninsular has been well studied (Chang et al., 2005; Ooi et al., 2011; Samah et al., 2016; Shariff et al., 2015). It can occur once to twice a month and can last from a few days to a week or more. In order to understand the synoptic influence on BMRS, the cold surge index was calculated. A cold surge index defined by Chang et al. (2005) was also calculated in GrADS using the daily averaged of v wind at 925 hPa between 110.0 °E and 117.5 °E along 15.0 °N to evaluate the cold surge index. Cold surge occurs when the cold surge index is < -8 ms^{-1}, while a strong cold surge is said to occur when it is < -12 ms^{-1}(Chang et al., 2005; Hai et al., 2017).

3.8 Determination of sea breeze

Borne et al. (1998) established a method of selecting days of sea breeze under synoptic conditions in an archipelago. Furberg et al. (2002) also have followed this approach focusing on a sea breeze event at a region with strong effects from coastlines. Through this method, a sea breeze event was determined by identifying a distinct change in surface wind direction within 24-hour period. It consists of six filters but the only the last two filters were implemented and adjusted in this study due to data limitation (for example sea surface temperature and geostrophic wind at 700 hPa). The criteria utilize to separate sea breeze from synoptic motions are:

1) Changes in hourly wind direction from 8 a.m. (sunrise + 1) to 2 p.m. (sunset ° 5) must be larger than 30°, and
2) The east coastline of BMRS are aligned from 337.5° to 135°, thus the winds originated from 337.5° to 135° are considered as onshore winds. Thus, the sharp changes of hourly averaged wind direction (ppeak) must be outside of the offshore

wind direction and the hourly averaged of wind directions for consecutive 5 hours following ppeak must be within the onshore wind direction.

3.9 Polar Plot

Polar plot is one of the functions in Openair package of R. It plots a bivariate polar plot of concentrations and it included some additional enhancements than Polar frequency (Carslaw, 2012). Bivariate polar plots provide a graphical method that shows the joint wind speed and wind direction dependence of air pollutant concentrations. It has been proved to be useful for quickly representing a graphical impression of potential sources influences at a monitoring site (Carslaw & Beevers, 2013; Westmoreland et al., 2007). The additional enhancements involve the plots are shown as a continuous surface and surfaces are calculated through modelling using smoothing techniques. The CPF probability was used rather than mean values to show the wind directions that dominate a (specified) high concentration of a pollutant; showing the probability of such concentrations occurring by wind direction. The CPF is defined as CPF = $m_{\theta,j}/n_{\theta,j}$ where $m_{\theta,j}$ is the number of samples in the wind sector θ and wind speed interval j with values within the specified intervals of percentiles or ranges, and $n_{\theta,j}$ is the total number of samples in the same interval of wind direction and wind speed (Grange et al., 2016; Uria-Tellaetxe & Carslaw, 2014). The wind direction data are generally rounded to each 10 degrees and surface measurements of wind speed within 0 to 30 ms^{-1}(Carslaw & Beevers, 2013). Using several intervals of percentiles allowed more sources to be identified and characterised (Uria-Tellaetxe & Carslaw, 2014).

3.10 HYSPLIT coupled with CWT Analysis

HYSPLIT window version was used in this study through Graphical User Interface (GUI) in which its methodology is well described in its tutorial and user-guide (Draxler & Hess, 1998; Stein et al., 2015). This model is particularly used for trajectory purpose and its operation involves three basic steps namely setup run, model run and display. The setup run is used to enter information such as the starting time, location, and height for the tracer release. Besides that, the trajectory duration (or total run time) and meteorological data were also included. Then, when the 'model run' is invoked, the trajectory was generated based on the advection of a particle or puff equation that is computed from the average of the three-dimensional velocity vectors at the initial position P(t) and the first-guess position P`(t+Δt) as shown on Equation 3.4 and Equation 3.5 respectively.

$$\boldsymbol{P`(t+\Delta t) = P(t) + V\,(P,t)\,\Delta t} \quad \text{(Equation 3.4)}$$

And the final position is:

$$\boldsymbol{P(t+\Delta t) = P(t) + 0.5\left[V(P,t) + V\left(P`, t+\Delta t\right)\right]\Delta t} \quad \text{(Equation 3.5)}$$

Trajectory during monsoon period is constituted of hundreds of trajectories. Thus, it tends to obscure the dominated individual trajectories. Hence, trajectories that are near to each other were merged by its mean trajectory known as a cluster (Stein et al., 2015) using a Ward's method. This is where the differences within a cluster are minimized while differences between clusters are maximized. In other words, trajectories in the same group (trajectory mean) will have a minimum difference with each other. The clustering allows a large number of trajectory outputs to be converted to a smaller number which subsequently ease the explanation. To execute the cluster, HYSPLIT computes the spatial variance (SV), cluster spatial variance (CSV) and total spatial variance (TSV). Through

many iterations over each trajectory, the final increase in TSV is described as the merging of disparate clusters which are no longer similar. Thus, the optimum number of clusters is when the objective percentage change criterion is > 30% and the number of clusters is between 2 and 10 (2 < cluster < 10). This method is adopted from (Draxler et al., 2009) and also been applied by Byčenkienė et al. (2014), Cheng et al. (2013), Dimitriou et al. (2015) and (Hidemori et al., 2014) to examine the atmospheric pollutant sources.

Coupling air pollutants data with the calculated trajectory leads to refined information on local or regional sources (Petit et al., 2017). Tools that can be used to compute this analysis were TrajStat (Wang et al., 2009) and Openair (Carslaw & Ropkins, 2012). TrajStat is an independent program that is based on the Geographical Information System (GIS). Openair is one of R package which its main purpose is to analyze air pollution data (Carslaw & Ropkins, 2012). There has been a lot of development in this package, especially in trajectory analysis function. The latter tool is chosen to generate the CWT due to its easier application with a programming background. Thus, the Openair package (Carslaw & Ropkins, 2012) in R (using Equation 2.2) was utilized to implement the CWT method where the source area of the air pollutants (CO_2, CH_4, PM_{10} and $PM_{2.5}$) are determined. The mean (CWT) concentrations for each grid cells were calculated based on the concentration at the receptor site. Then, the active fire/hotspots data are added as an additional layer on top of the map to examine the relationships of biomass burning to the air pollutants concentration.

CHAPTER 4: RESULTS AND DISCUSSION

This chapter presents the results and discussions of the study. Section 4.1 deals with the variations of meteorological parameters and air pollutants during the NE and SW monsoons at BMRS using data ranging from November 2014 to September 2016. Meteorological conditions, trends and transport of air pollutants associated with these two monsoon periods are also explained. Section 4.2 examines the variations of meteorological parameters and air pollutants extensively during the case studies. Two case studies were specifically conducted from 25 to 27 January 2016 (Case study 1: CS1) and from 3 to 5 June 2016 (Case study 2: CS2) which are in the respective NE and SW monsoon periods. The significant differences on the meteorological conditions during these two periods and their effects on the variability and transport of air pollutants are emphasized.

4.1 Variabilities of meteorological parameters and air pollutants at BMRS during the NE and SW monsoon periods

Seasonal and diurnal cycles are the fundamental modes in the variability of the global climate system as it is associated with large and well-defined variations in the solar forcing (Krishna Moorthy et al., 2003; Patra et al., 2009). Thus, the seasonal as well as diurnal variations and the relationship between meteorological parameters with air pollutants during the NE and SW monsoon over BMRS and its surrounding areas from 2014 to 2016 are elaborated in this section. In addition, the possible transport of air pollutants during both monsoon periods based on the HYSPLIT cluster back-trajectories, Polar plot and CWT analysis are included in this section.

4.1.1 Meteorological conditions associated over BMRS during the NE and SW monsoon periods

The weather conditions in Malaysia are well described by Lim and Samah (2004). In general, Malaysia is influenced by the NE, SW and two inter-monsoon seasons. The Peninsular of Malaysia (Figure 4.1) particularly features some of the complex terrain in the maritime continent, being signified by mountain ranges (Titiwangsa) with peaks above 2000 m and separated by narrow valleys (Joseph et al., 2008). This region experiences a year-round warm and humid climate. The relative humidity is 80% and the temperatures range from 21°C to 32°C throughout the year (Peng et al., 2006). The NE monsoon is typically categorized as the wet season while the SW monsoon is generally the dry season on the east coast of Peninsular Malaysia (Chenoli et al., 2018; Lim & Samah, 2004).

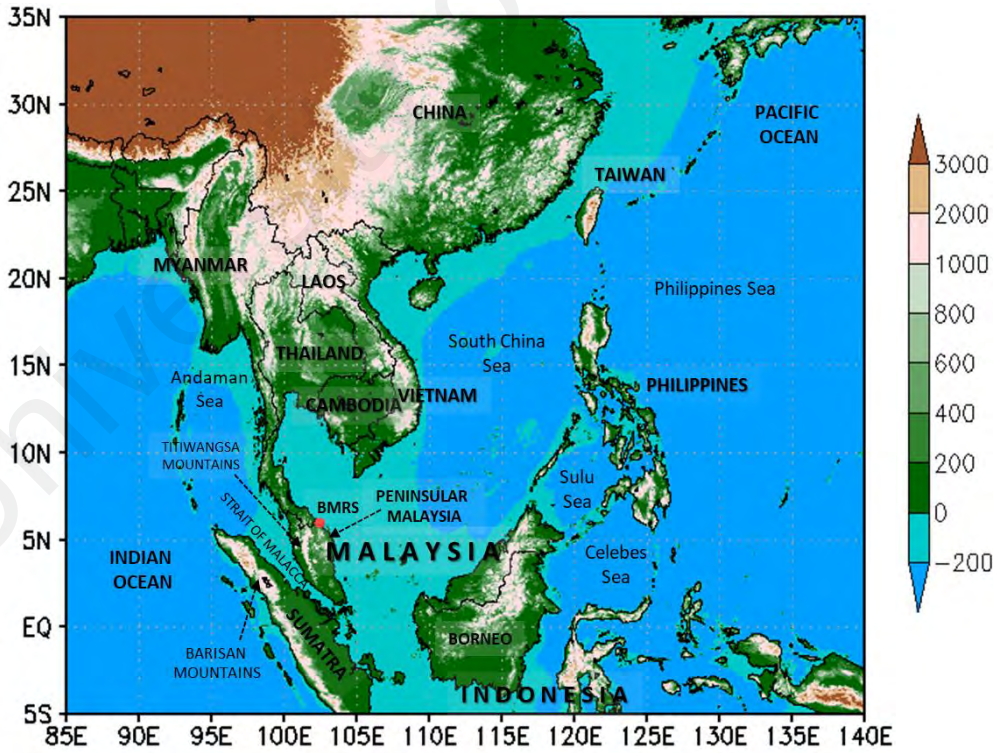

Figure 4.1: Map of BMRS and its surrounding areas. The background of the map represents the variation of elevation (m). The red dot (●) is the location of BMRS

BMRS is situated at the northeastern coast of Peninsular Malaysia (Figure 4.1), a rural area with fishing and agriculture as major economic activities (Dominick et al., 2015). During the NE monsoon, areas along the east coast of Peninsular Malaysia are particularly susceptible to prolonged strong winds and heavy rainfalls leading to severe flooding (Hai et al., 2017; Juneng et al., 2007). These severe weather events are usually associated with cold air outbreaks from the Siberian-Mongolian High (SMH) which then spread toward the equator in the form of strong northeasterly winds known as cold surges (Lim & Samah, 2004). Figure 4.2 (a) and (c) show the average 925 hPa zonal (u) and meridional (v) wind components respectively during the NE monsoon. BMRS and the east coast of Peninsular Malaysia were clearly influenced by the strong (wind speed > 10 ms^{-1}) north-easterly winds. Figure 4.2 (e) shows the characteristics of mean sea level pressure (MSLP) and the 500 hPa geopotential height during the NE monsoon. There are significant pressure gradients shown between 30°N (East of Siberian High) and 5°N (Asiatic land), thus BMRS is clearly influenced by this synoptic aspect during the NE monsoon. Other studies (Chang et al., 1979; Wangwongchai et al., 2005; Yokoi & Matsumoto, 2008) also have demonstrated the existence of synoptic scale motions during the NE monsoon. Cold surges occurred when there is a decrease in the surface temperature at the east and south of the SMH (Chang et al., 2006; Chang et al., 1979) or when the cold surge index reaches −8 ms^{-1} and lower. Its characteristics over the equatorial SCS and over the eastern coast of Peninsular Malaysia were studied well (Ooi et al., 2011; Samah et al., 2016; Shariff et al., 2015; Tangang et al., 2008). Cold surge event can occur once or twice a month and its effects can last from a few days to a week or longer (Chang et al., 2005; Lim & Samah, 2004). This phenomenon can also affect the rate of rainfall on the eastern and southern coasts of Malaysia (Hai et al., 2017; Juneng et al., 2007; Shariff et al., 2015; Tangang et al., 2008) and the air quality over Southeast Asia (Ashfold et al., 2017; Farren et al., 2019; Oram et al., 2017; Pochanart et al., 2004). Figure 4.3 shows the cold surge indices derived

during the NE monsoon. During the NE 2014/2015 (Figure 4.3 (a)), twelve cold surge events were detected (five of them were strong cold surges (cold surge index < -12 ms^{-1} (Hai et al., 2017)). The strongest cold surge occurred in December and became weaker in February. In the meantime, eleven cold surge events were observed (three were strong cold surges) during the NE 2015/2016 as shown in Figure 4.3 (b). Differences on the occurrences of cold surge events during both periods are attributed to the development and evolution of the Siberian High (Loo et al., 2015; Park et al., 2011). There are several studies that indicated frequency of cold surges is dependant on the Arctic Oscillation (Gong et al., 2001; Loo et al., 2015; Wu & Wang, 2002).

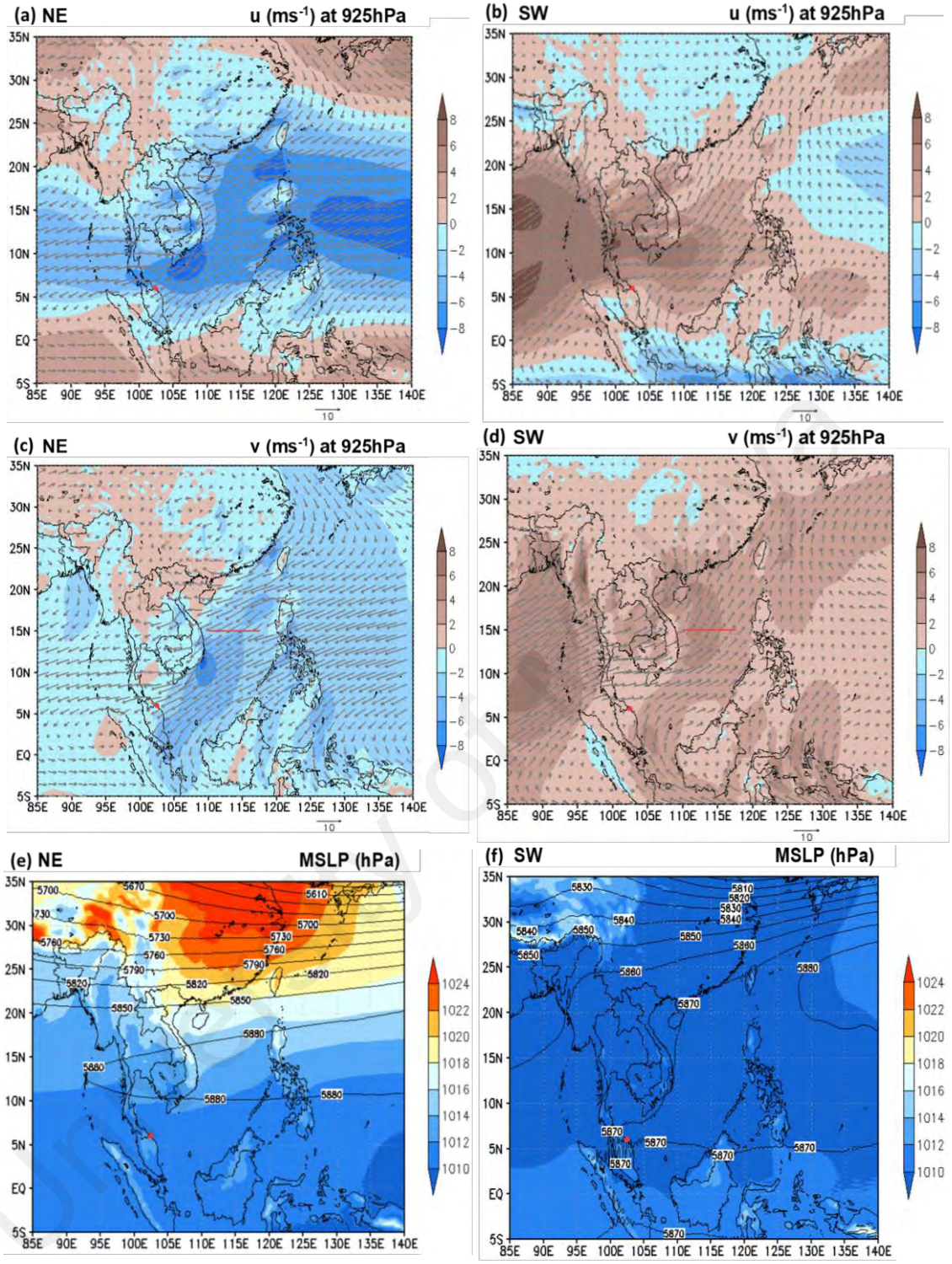

Figure 4.2: Average 925 hPa winds, mean sea level pressure (MSLP) and geopotential heights (gph) at 500 hPa (contour lines) during NE and SW monsoon. First column (a, c and e) shows for NE monsoon while second column (b, d and f) is for SW monsoon. The red dot (●) is the location of BMRS. Grey wind vectors are superimposed on (a) to (d) and each wind vector represents 10 ms^{-1} of wind speed. Red lines in variation of v winds (c and d) indicated is the position over which cold surge index is calculated. The labelled black contours in variations of MSLP (e and f) show the gph at 500 hPa

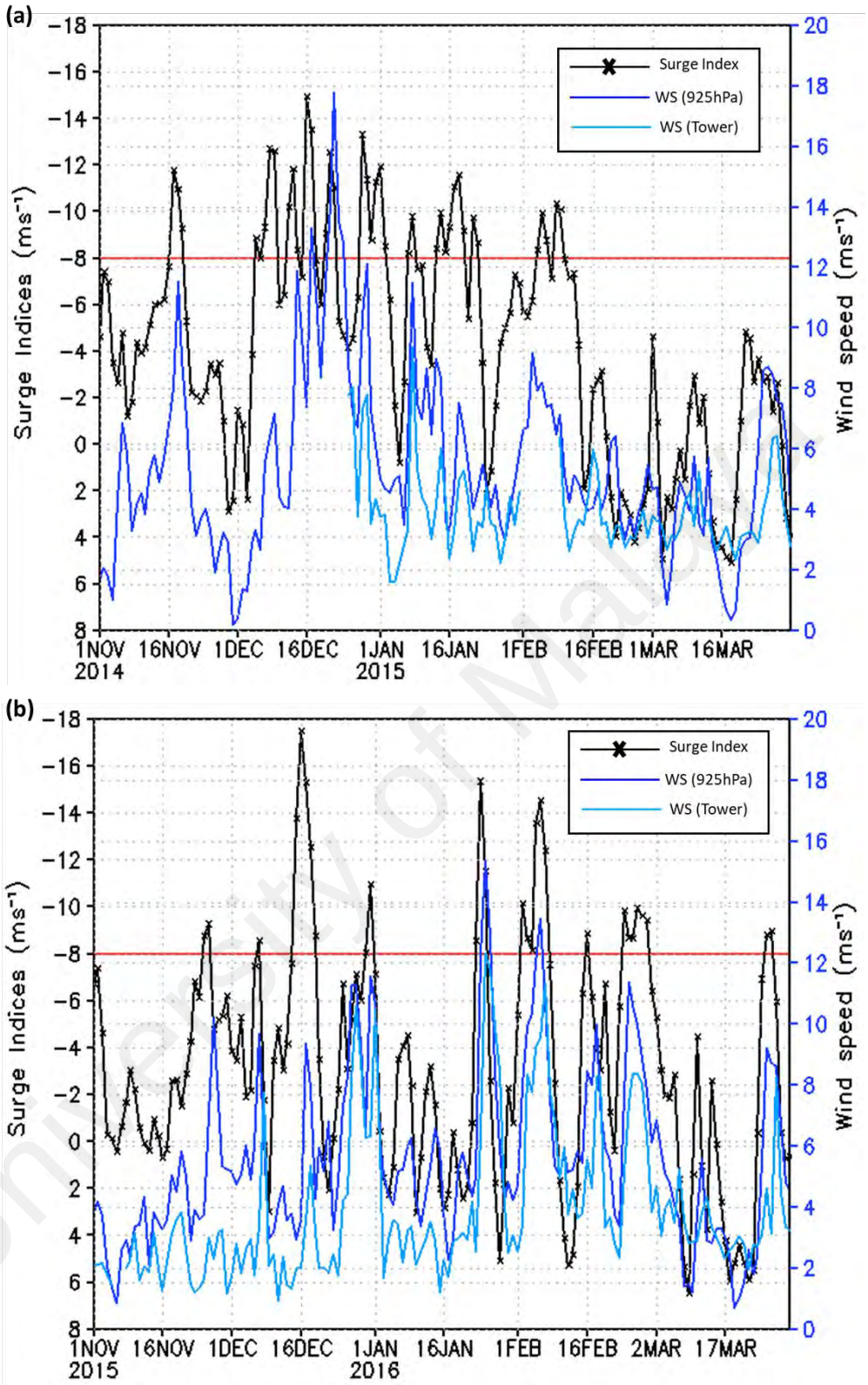

Figure 4.3: Time series of cold surge index and wind speed during (a) NE 2014/2015 and (b) NE 2015/2016. Red lines indicate the baseline where cold surge occurred (cold surge indices < −8 ms^{-1}). Light blue colored time series shows the daily averaged wind speed calculated based on the AWS data at BMRS tower meanwhile the dark blue colored time series shows the 925 hPa wind speed at BMRS

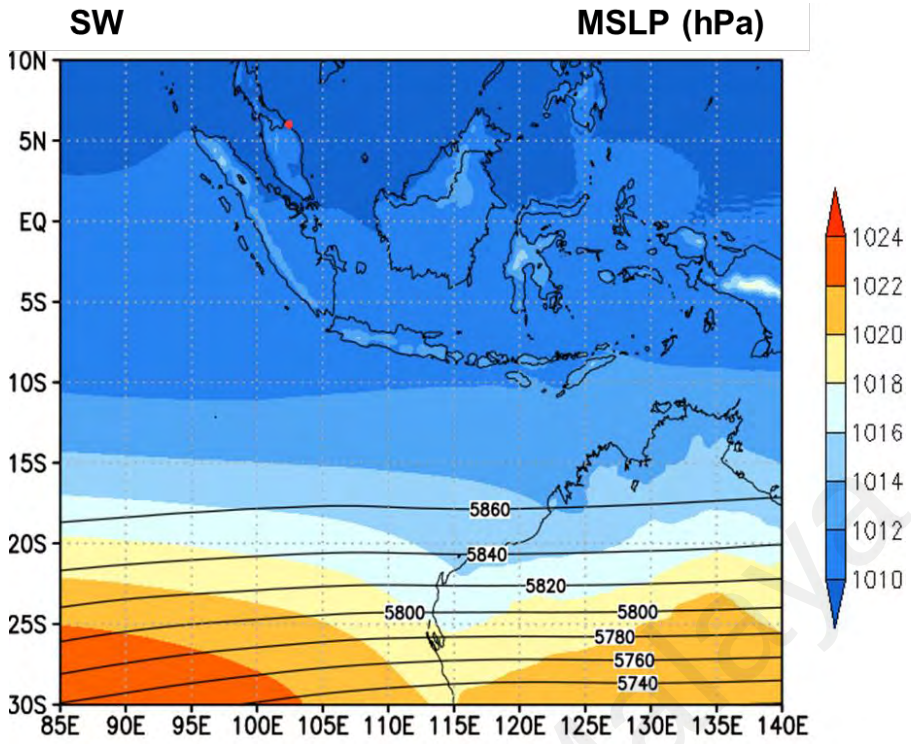

Figure 4.4: Average MSLP and 500hPa gph (contour lines) from 10°N to 30°S (latitude) and 85°E to 140°E (longitude) during the SW monsoons. The red dot (●) is the location of BMRS

During the SW monsoon, Malaysia is not directly influenced by any large scale weather system due to the monsoon trough which lies far north mainly over the South China Sea (SCS) and extending southwestward to the Philippines and Western Pacific (Chenoli et al., 2018; Lim & Samah, 2004). It is usually characterized with high outgoing long-wave radiation (OLR), less cloud, low precipitation and dry epoch (Chenoli et al., 2018). This contributes to a dry condition during this monsoon period. Figure 4.2 (b) and (d) clearly show the presence of light (wind speed < 5 ms^{-1}) south-westerly winds heading towards BMRS and it flowing continuously to the SCS during the SW monsoon. Figure 4.2 (f) shows no strong pressure gradient between 35°N and 5°N. However there exists slight pressure gradient existed between 5°N with 30°S (Figure 4.4). Therefore, BMRS can also be affected by weak synoptic flows during the SW monsoon.

4.1.2 Statistical summary of BMRS Tower data during the NE and SW monsoons

The summary for each respective monsoon period is calculated and shown in Table 4.1 and Table 4.2. The data are not 100 percent available for both of the monsoon periods due to some technical issues, maintenance periods and data quality. Greenhouse gases (CO_2 and CH_4) are only available from November 2015 to September 2016. Thus, the available percentages during both monsoon periods shown are below 50%. The basic statistical terms used are minimum, median, mean, maximum, 1st quartile, 3rd quartile and standard deviation. Clear statistical differences are shown during both of these monsoon periods especially the temperature, wind speed and the air pollutants. During the NE monsoon, normal mean temperature is 26.6°C (Range of temperature (daily average) at Kota Bharu is from 23°C to 32°C) with maximum temperature of 30.5°C. The average wind speed recorded is 4.0 ms^{-1} and the maximum is 14.29 ms^{-1}. During the SW monsoon, higher temperature is recorded as compared to the NE monsoon with mean temperature of 27.2°C and maximum temperature of 33.7°C. Meanwhile, the mean wind speed recorded during the SW monsoon is lower than NE monsoon with average of 2.13 ms^{-1} and maximum of 11.27 ms^{-1}. All air pollutants (CO_2, PM_{10} and $PM_{2.5}$) except CH_4 show higher mean, maximum and standard deviation values during the SW monsoon (Table 4.1 and Table 4.2).

Table 4.1: Descriptive analysis of 1-hour average meteorological and air pollutants data during NE monsoon at BMRS

	T (°C)	P (hPa)	WS (ms^{-1})	CH_4 (ppm)	CO_2 (ppm)	PM_{10} (μgm^{-3})	$PM_{2.5}$ (μgm^{-3})
Available data	70%	82%	82%	46%	46%	81%	81%
Min	19.6	1004	0.1	1.836	399.0	0.0	0.0
Q1	25.4	1008	1.5	1.877	405.1	10.13	8.20
Median	26.8	1010	3.3	1.912	408.3	15.76	13.06
Mean	26.6	1010	4.0	2.050	417.8	19.73	16.65
Q3	28.1	1011	6.0	2.067	419.0	24.47	19.85
Max	30.5	1016	14.9	4.176	531.7	223.76	212.96
SD	1.88	2.03	2.85	0.311	22.23	16.43	15.20

Note: Min: Minimum; Q1: Quartile 1; Q3: Quartile 3; Max: Maximum; SD: Standard Deviation

Table 4.2: Descriptive analysis of 1-hour average meteorological and air pollutants data during SW monsoon at BMRS

	T (°C)	P (hPa)	WS (ms^{-1})	CH_4 (ppm)	CO_2 (ppm)	PM_{10} (μgm^{-3})	$PM_{2.5}$ (μgm^{-3})
Available data	82%	66%	82%	37%	37%	31%	31%
Min	21.3	1000	0.0	1.789	396.7	0.477	0.467
Q1	24.8	1005	1.19	1.863	409.2	9.391	8.982
Median	27.7	1007	1.70	1.919	417.4	18.855	18.282
Mean	27.2	1006	2.13	2.021	430.7	40.593	39.416
Q3	29.5	1008	2.66	2.110	445.7	43.364	42.036
Max	33.7	1013	11.27	3.871	567.7	454.83	428.90
SD	2.60	1.84	1.40	0.236	29.36	56.66	55.10

Note: Min: Minimum; Q1: Quartile 1; Q3: Quartile 3; Max: Maximum; SD: Standard Deviation

4.1.3 Time series of meteorological parameters and air pollutants at BMRS during the NE and SW monsoons

This section describes all the time series from seasonal to diurnal variations of meteorological parameters and air pollutants during the NE and SW monsoons. Its general variations and relations in both monsoon periods are first explained. BMRS can

be influenced by both local and synoptic influence. Days influenced with local and synoptic meteorological conditions are separated between one another and the variations of meteorological parameters and air pollutants under the influence of synoptic flow (only) are explained in the next subsection. The last subsection described its diurnal variations associated with local and synoptic influence in both monsoon periods.

4.1.3.1 General variations of meteorological parameters and air pollutants

The hourly variations of all parameters in each of the NE and SW monsoon periods from November 2014 to September 2016 are shown in Figure 4.5 to Figure 4.14. From general perspective, wind fluctuated within 50° to 200° (black line in Figure 4.5 (a) and (c)) during the NE monsoon. Wind rose (Figure 4.7 (a)) shows more than 50% of northeasterly winds dominated BMRS and 10% of it were strong winds. It then followed by 12% winds flowing from each east and southwest directions. This monsoon period was also attributed to great fluctuations of wind speed from light to strong winds (Figure 4.6 (a) and (c)) and consistent fluctuations of temperature (Figure 4.8 (a) and (c)) within its mean (26.6 °C). Station pressure also shows great fluctuation in its variation during the NE monsoon which ranged from 1005 to 1013 hPa (Figure 4.9 (a) and (c)). On the other hand, overall variations of CO_2 during the NE monsoon (Figure 4.10 (a)) fluctuated between 410 to 440 ppm. CH_4 fluctuated between 1.8 to 2.5 ppm during this period as shown in Figure 4.10 (c). There are statistically significant strong and moderate negative correlations shown between CO_2 with temperature and wind speed respectively as shown in Table 4.3. CO_2 also shows strong positive correlations with CH_4 and both PM (PM_{10} and $PM_{2.5}$). CH_4 shows similar relationship with temperature, wind speed and PM as CO_2 (Table 4.3). These indicate that the variations of CO_2 and CH_4 is in inverse relation with temperature and wind speed while it is in direct (or positive) relation with CO_2 and PM

during the NE monsoon. These further imply that CO_2 and CH_4 decrease under the influence of higher temperature and stronger winds where these conditions are usually associated with more formation of turbulences and stronger mixing processes in the atmosphere. The positive relations resulted between all the pollutants imply it is originated from the same sources. These are explained with more details in Section 4.2.5 using transport model. PM_{10} showed low level of concentrations during this monsoon period (Figure 4.11 (a) and (c)) with daily average values mostly below 100 μgm^{-3}. These variations are in statistically significant moderate positive correlation ($r = 0.39$) with PM_{10} measured at Kota Bharu station operated under DOE (Figure 4.12). Kota Bharu is a more urbanized area with higher volume of traffic (Dominick et al., 2015) compared to BMRS. Therefore, there were more exposures of PM at Kota Bharu and hence contributed to the less strong positive correlations. At BMRS, only 3 days were associated with values exceeded WHO's guideline value (50 μgm^{-3} for 24-hour). Overall variations of $PM_{2.5}$ were also attributed with daily average below 100 μgm^{-3} as shown in Figure 4.13 (a) and (c). However, $PM_{2.5}$ showed more days (35 days in total) exceeded WHO's guideline value which is 25 μgm^{-3} for 24-hour. The clearest and prolonged exceedance occurred in March 2016. The fine particles at BMRS can be affected by the primary and secondary sources from both the natural and anthropogenic emissions (Dominick et al., 2015). Primary – natural sources are primarily due to the sea spray and crustal materials, while the secondary sources are caused by the oxidation of reduced precursor gases such as oxidation of reduced precursor gases namely sulfur oxides (SO_x) and nitrogen oxides (NO_x) from the oceans and wetlands. Meanwhile, primary – anthropogenic sources can be originated from the trace metals, oily residues, agriculture and open burning whereas the secondary sources are caused by the fossil fuel combustion, motor vehicle exhaust, animal husbandry, sewage and fertilizer. Thus, the days associated with an exceedance of the guideline level of $PM_{2.5}$ can be caused by all these sources. Other possible reasons for

these exceedances are further explained in subsequent sections where its diurnal variations and sources were considered. There were statistically significant moderate and weak negative correlations attained between PM (PM_{10} and $PM_{2.5}$) with temperature and wind speed respectively as shown in Table 4.3. These imply that the concentrations of PM_{10} and $PM_{2.5}$ also decrease under the influence of higher temperature and stronger winds in this period. Ratio $PM_{2.5}/PM_{10}$ (RPM) is very beneficial in providing information on its formation process and particle origin (Xu et al., 2017). Higher RPM means more influence from anthropogenic sources and lower RPM indicates more influence of coarse particles where it is originated mostly from the natural sources (Sugimoto et al., 2016). A ratio of 0.5 is typical of developing country urban areas and is at the range of 0.5 to 0.8 in developed country urban areas (WHO, 2005). However, a different value for this ratio can be employed to better reflects the local conditions if the relevant data were available. Overall daily variations of RPM during this monsoon period show fluctuations between 0.5 to 1.0 (Figure 4.14 (a) and (c)). There were very high ratios in March 2016 which suggest great presence of fine particles.

During the SW monsoon, BMRS experienced daily fluctuation in wind direction ranging from 100° to 260° (black line in Figure 4.5 (b) and (d)). Wind rose shows even percentages (26%) of northeast and southwest winds dominated BMRS during this monsoon period (Figure 4.7 (b)). It is followed by 12% of southerly and 10% of westerly winds. Wind speed variations (Figure 4.6 (b) and (d)) during this period fluctuated consistently within its average around 2.1 ms^{-1} (Table 4.2) and the highest wind mainly flowed from the northeast direction (onshore) (Figure 4.7 (b)). Temperature fluctuated between 24°C to 30°C (Figure 4.8 (b) and (d)) while pressure fluctuated between 1004 to 1010 hPa (Figure 4.9 (b) and (d)) during this monsoon period. On the other hand, CO_2 fluctuated between 410 to 450 ppm while CH_4, between 1.9 to 2.2 ppm during this period as shown in Figure 4.10 (b) and (d) respectively. There were statistically significant

moderate negative correlations between these pollutants with wind speed and temperature as shown in Table 4.4. These imply that CO_2 and CH_4 decrease under the influence of higher temperature and stronger winds during this monsoon period. These pollutants also show strong positive correlations with PM (PM_{10} and $PM_{2.5}$) which demonstrate pollutants are originated from the same source regions. Further details on the sources of these pollutants are explained in Section 4.2.5 using transport model. PM_{10} (Figure 4.11 (b) and (d)) and $PM_{2.5}$ (Figure 4.13 (b) and (d)) showed great fluctuation in its concentrations during this monsoon period. PM_{10} recorded 24 times exceedance of WHO's guideline value while $PM_{2.5}$ demonstrate triple times of exceedance of the WHO's guideline value (71 times). Overall daily variations of RPM during the SW monsoon ranged from 0.9 to 1.0. This describes higher presence of fine particles over BMRS during the SW monsoon as compared to the NE monsoon. The dry condition and low wind speed during the SW monsoon caused more accumulation of pollutants.

Table 4.5 shows brief descriptions of the variations of meteorological parameters and air pollutants during the NE and SW monsoons. BMRS shows lower temperatures and higher wind speed during the NE monsoon in comparison to the SW monsoon. Furthermore, lower average CO_2, PM_{10} and $PM_{2.5}$ were shown in the NE monsoon. Only CH_4 shown a higher average in the NE monsoon. The variations of the air pollutants are greatly influenced by the variability of temperature and wind speed in both the NE and SW monsoon i.e. significant negative correlations shown between all air pollutants with the temperature and wind speed.

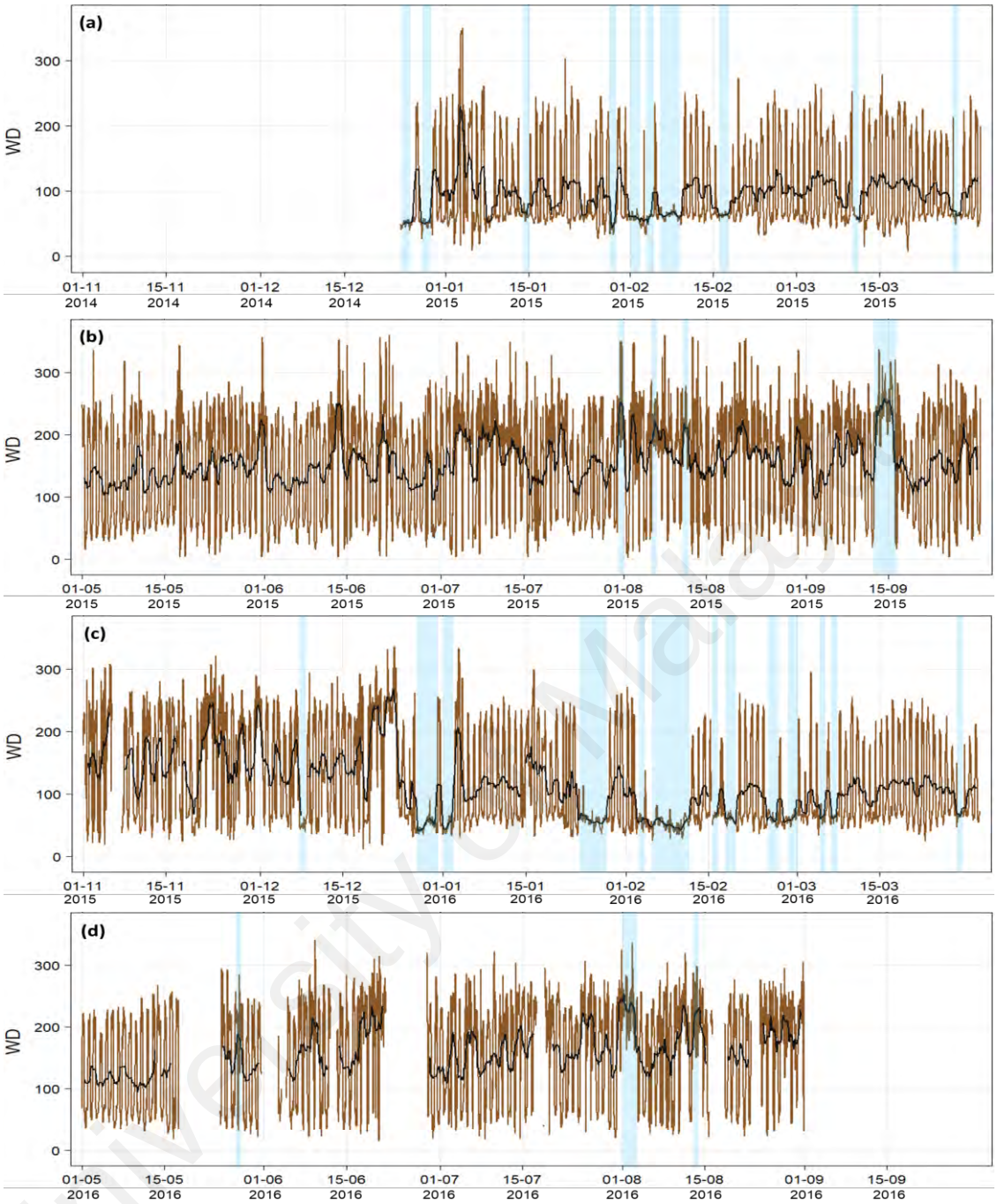

Figure 4.5: Hourly time series (in local time) of wind direction, WD (°) during (a) NE 2014/2015, (b) SW 2015, (c) NE 2015/2016 and (d) SW 2016. The blue shaded regions represent the days with suppressed land-sea breeze. The black line represents the daily variation resulted using moving average filter

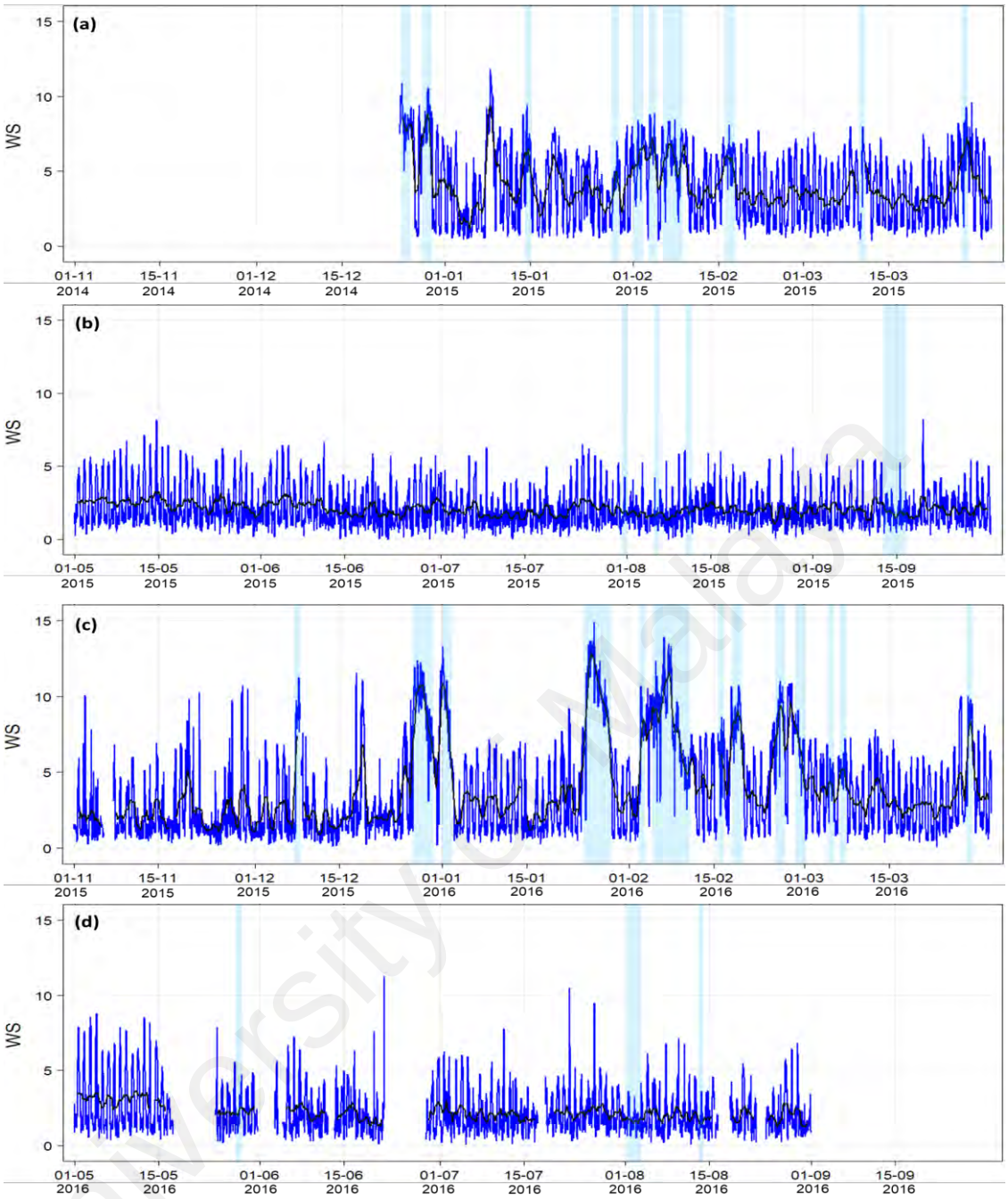

Figure 4.6: Hourly time series (in local time) of wind speed, WS (ms^{-1}) during (a) NE 2014/2015, (b) SW 2015, (c) NE 2015/2016 and (d) SW 2016. The blue shaded regions represent the days with suppressed land-sea breeze. The black line represents the daily variation

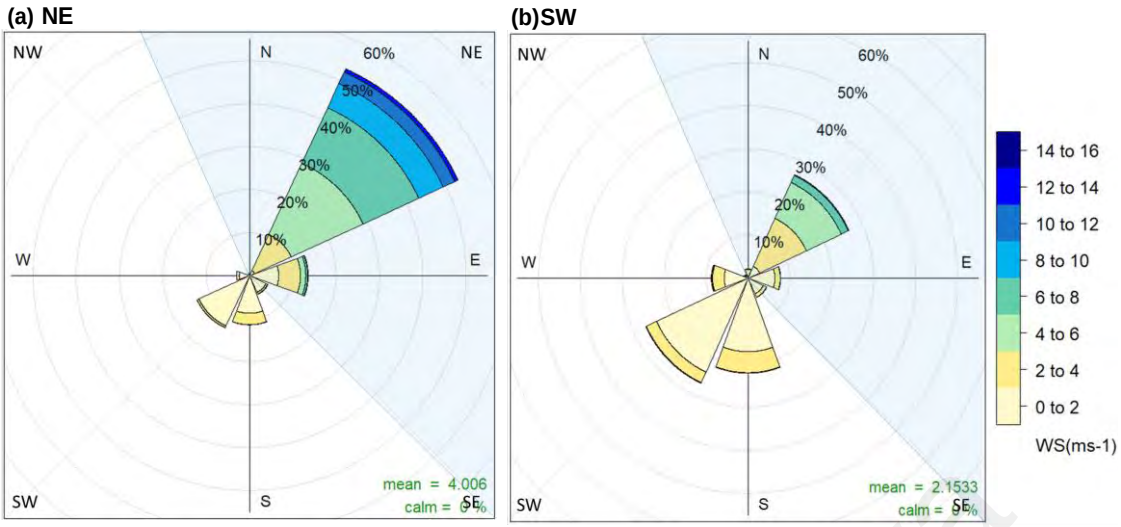

Figure 4.7: Wind roses from hourly averaged of wind data during the (a) NE and (b) SW monsoon periods from 2014 to 2016 at BMRS. The wind rose use 8 cardinal directions namely north (N), south (S), east (E) and west (W), NE, NW, SE, and SW. The light blue shaded sectors represent the wind directions from 337.5° to 135°

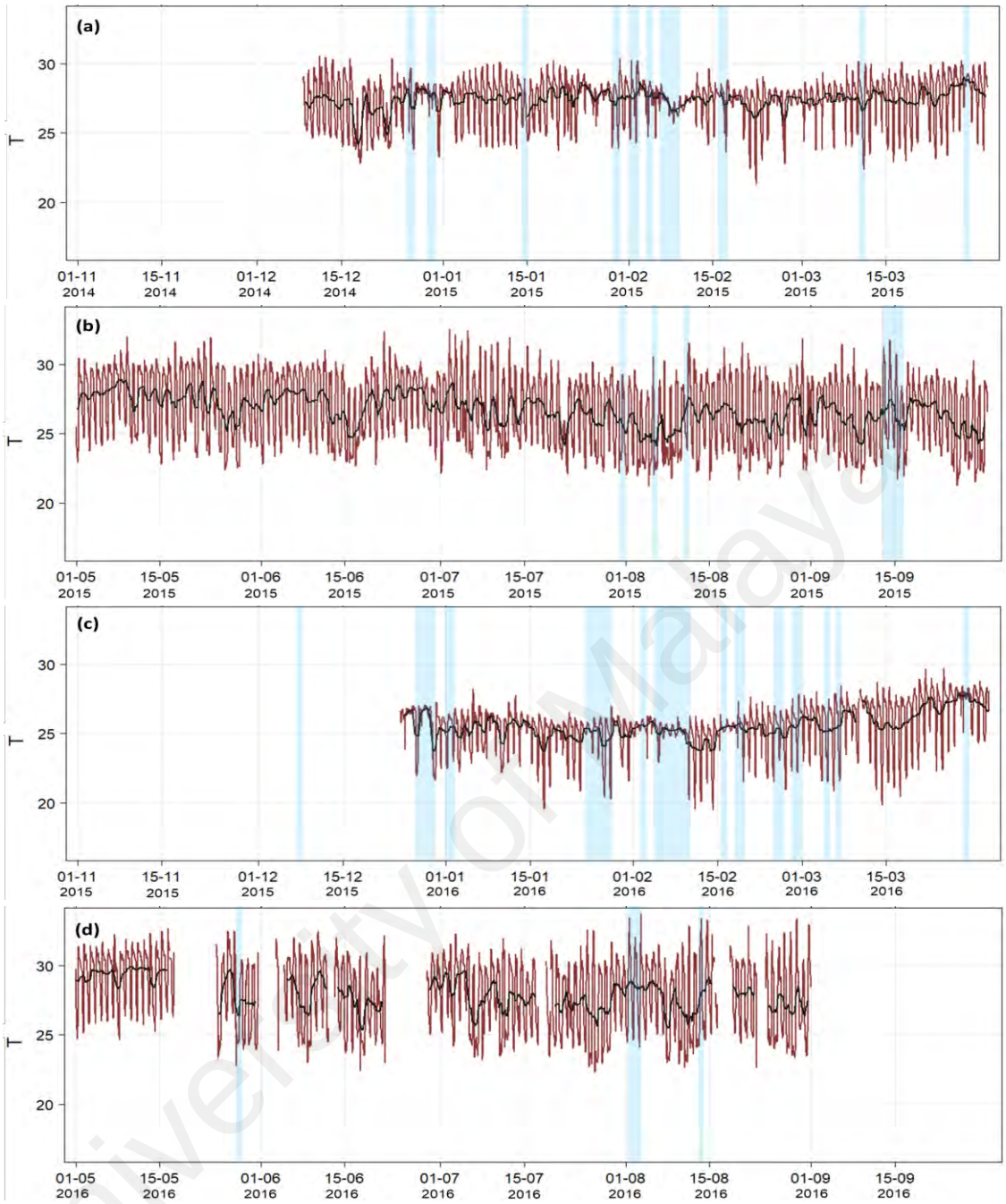

Figure 4.8: Hourly time series (in local time) of air temperature, T (°C) during (a) NE 2014/2015, (b) SW 2015, (c) NE 2015/2016 and (d) SW 2016. The blue shaded regions represent the days with suppressed land-sea breeze. The black line represents the daily variation

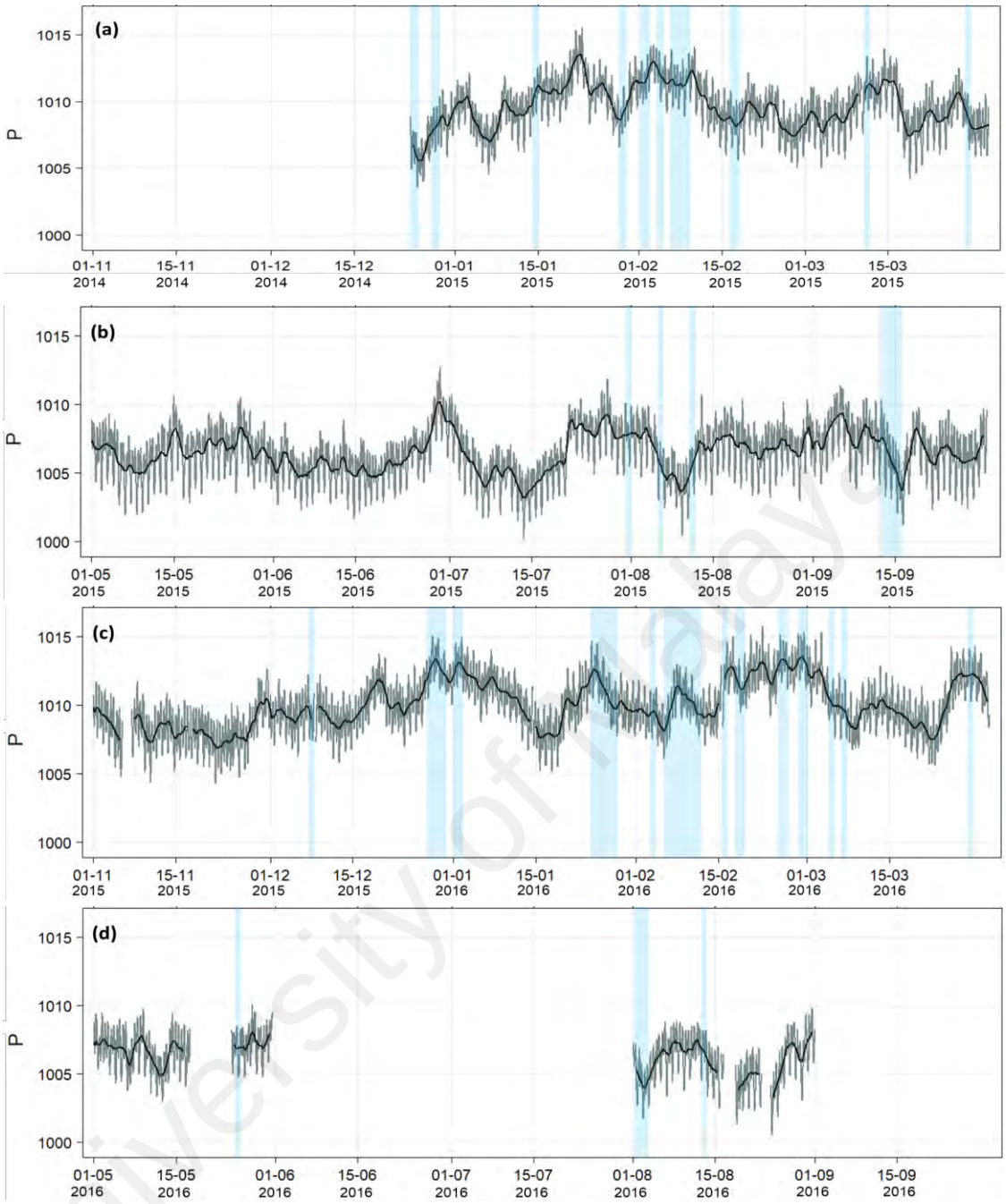

Figure 4.9: Hourly time series (in local time) of air pressure, P (hPa) during (a) NE 2014/2015, (b) SW 2015, (c) NE 2015/2016 and (d) SW 2016. The blue shaded regions represent the days with suppressed land-sea breeze. The black line represents the daily variation

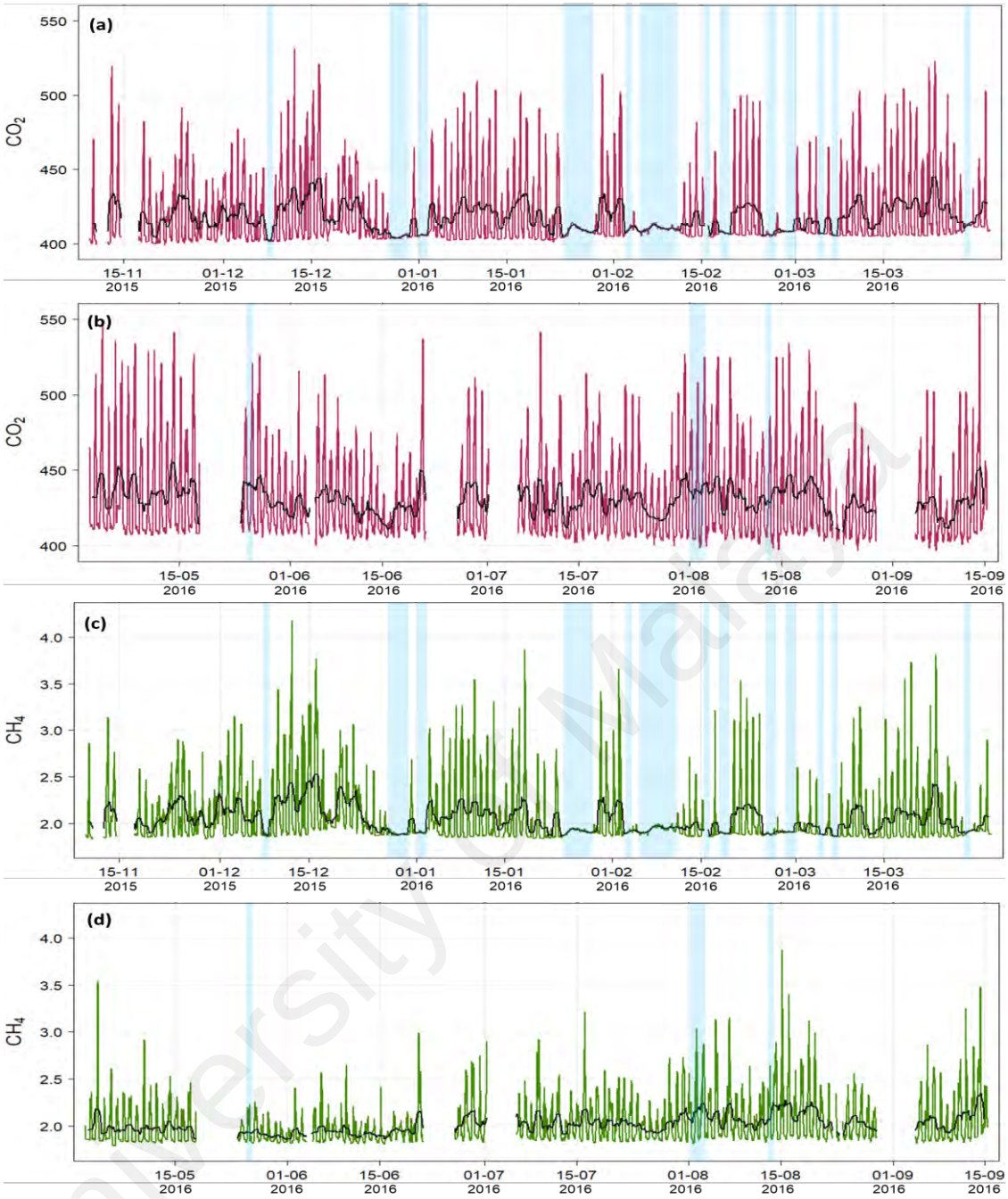

Figure 4.10: Hourly time series (in local time) of CO_2 (ppm) and CH_4 (ppm) during NE 2015/2016 ((a) and (c) respectively) and SW 2016 ((b) and (d) respectively). The blue shaded regions represent the days with suppressed land-sea breeze. The black line represents the daily variation

Figure 4.11: Hourly time series (in local time) of PM10 (µgm-3) during (a) NE 2014/2015, (b) SW 2015, (c) NE 2015/2016 and (d) SW 2016. The blue shaded regions represent the days with suppressed land-sea breeze. The dashed lines represent the WHO's guideline value for PM_{10} (for 24-hour average) = 50 µgm-3. The black line represents the daily variation

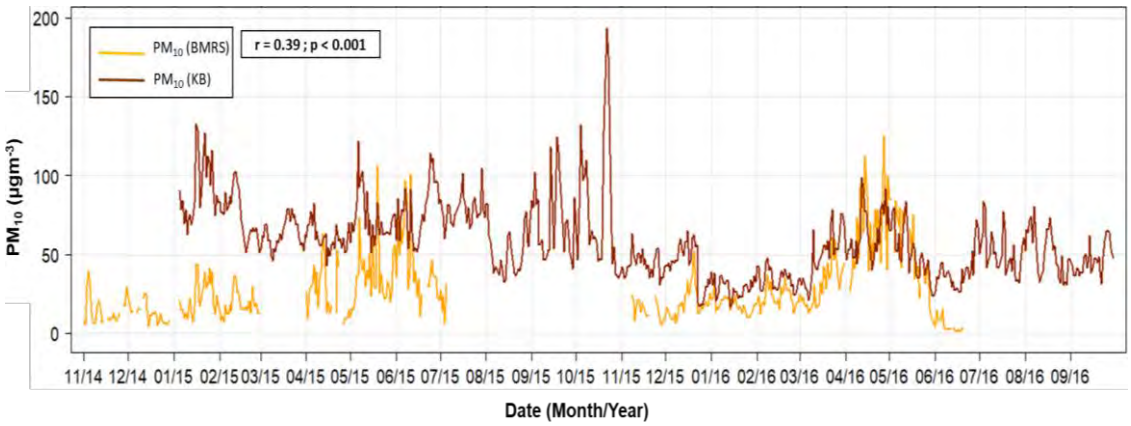

Figure 4.12: Hourly time series of PM10 at BMRS and Kota Bharu (KB) from November 2014 to September 2016

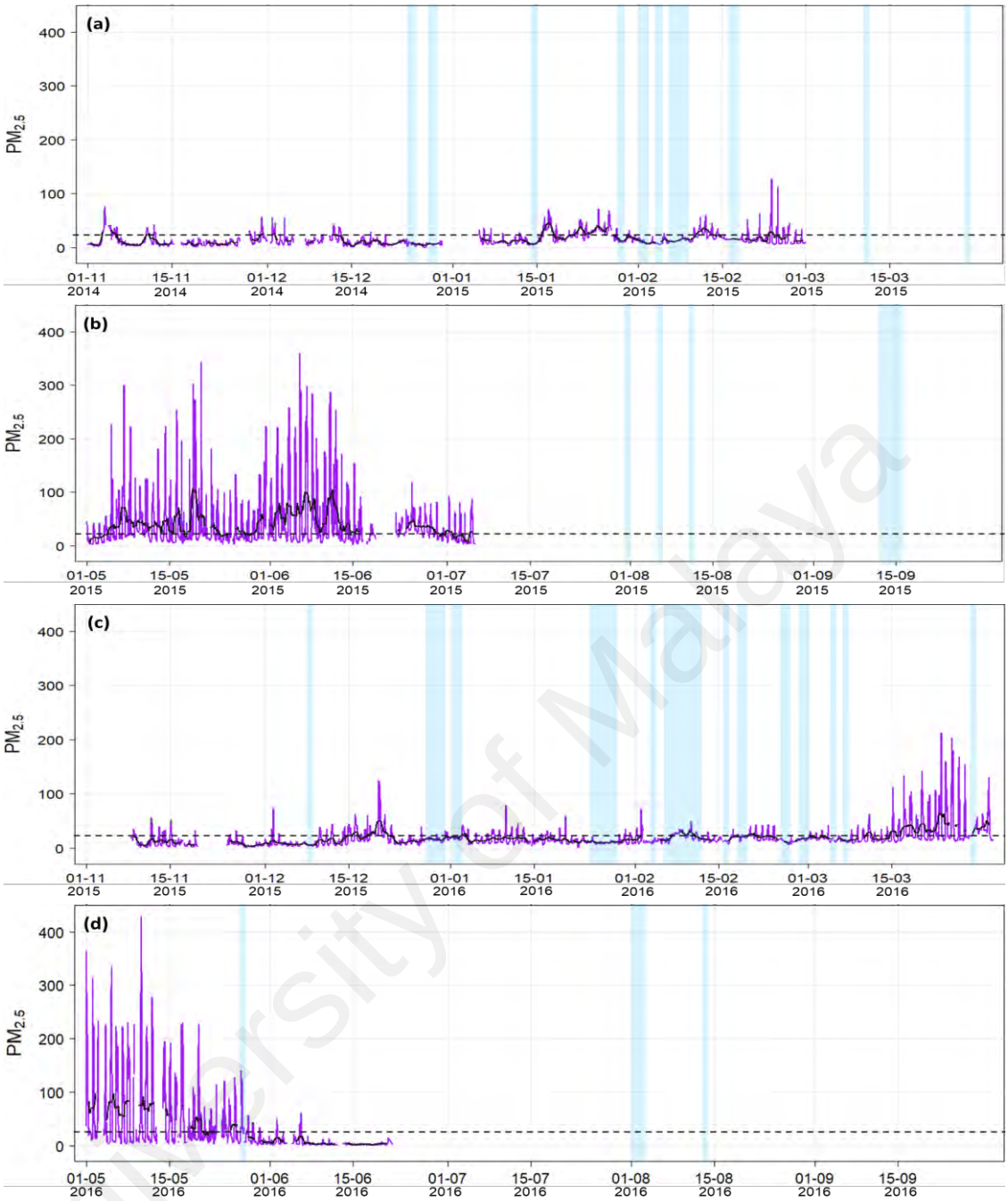

Figure 4.13: Hourly time series (in local time) of $PM_{2.5}$ (μgm^{-3}) during (a) NE 2014/2015, (b) SW 2015, (c) NE 2015/2016 and (d) SW 2016. The blue shaded regions represent the days with suppressed land-sea breeze. The dashed lines represent the WHO's guideline value for $PM_{2.5}$ (for 24-hour average) = 25 μgm^{-3}. The black line represents the daily variation

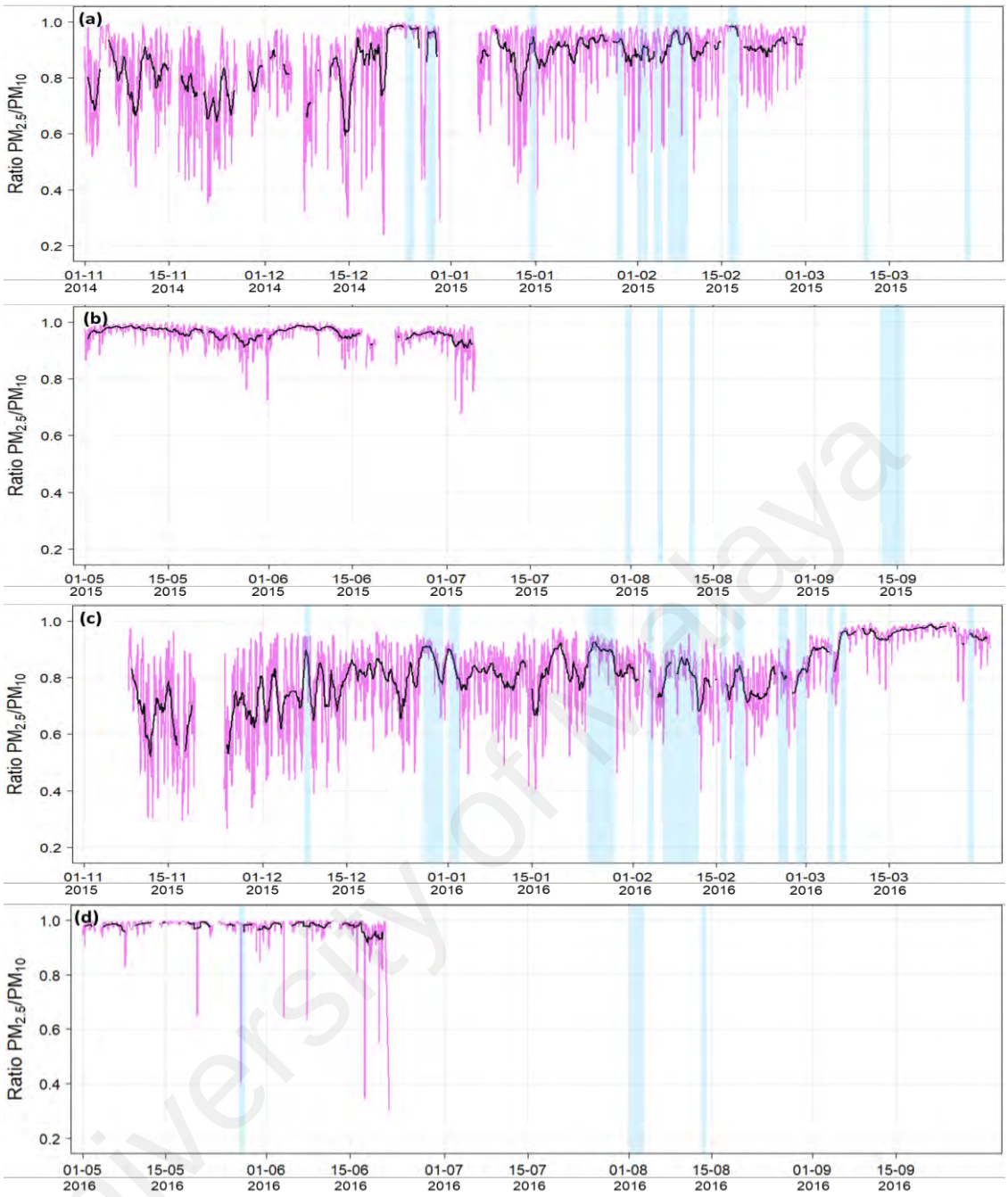

Figure 4.14: Hourly time series (in local time) of RPM during (a) NE 2014/2015, (b) SW 2015, (c) NE 2015/2016 and (d) SW 2016. The blue shaded regions represent the days with suppressed land-sea breeze. The black line represents the daily variation

Table 4.3: Correlation coefficient (r) between all variables during the NE monsoon at BMRS. Values in bold are statistically highly significant correlation (p <0.001). The values ranged from –1 (perfect negative correlation: dark red) to 0 (no correlation: white) to +1 (perfect positive correlation: dark blue)

	T	WS	P	PM_{10}	$PM_{2.5}$	CO_2	CH_4
T	1.00						
WS	**0.33**	1.00					
P	**0.06**	**0.08**	1.00				
PM_{10}	**-0.32**	**-0.29**	**0.15**	1.00			
$PM_{2.5}$	**-0.33**	**-0.23**	**0.13**	**0.98**	1.00		
CO2	**-0.78**	**-0.44**	**-0.14**	**0.60**	**0.60**	1.00	
CH4	**-0.72**	**-0.40**	**-0.11**	**0.50**	**0.50**	**0.95**	1.00

Table 4.4: Correlation coefficient (r) between all variables during the SW monsoon at BMRS. The descriptions for the values and colors are same as Table 4.3

	T	WS	P	PM_{10}	$PM_{2.5}$	CO_2	CH_4
T	1.00						
WS	**0.41**	1.00					
P	**-0.30**	**-0.31**	1.00				
PM_{10}	**-0.31**	**-0.30**	**0.08**	1.00			
$PM_{2.5}$	**-0.31**	**-0.29**	**0.08**	**1.00**	1.00		
CO2	**-0.59**	**-0.40**	0.07	**0.73**	**0.73**	1.00	
CH4	**-0.53**	**-0.38**	-0.06	**0.82**	**0.82**	**0.85**	1.00

Table 4.5: Summary on the general variations of meteorological parameters and air pollutants during the NE and SW monsoon

1. In comparison to SW monsoon, NE monsoon shows:
   - Lower temperatures and higher magnitude of wind
   - Lower CO_2, PM_{10} and $PM_{2.5}$
   - Higher CH_4
2. In both monsoon periods:
   - Strong winds and high temperature increased the level of air pollutants

4.1.3.2 Variations of meteorological parameters and air pollutants under synoptic influence

The east coastline of Peninsular Malaysia near the BMRS is aligned from 337.5° to 135.0° (blue shaded regions in Figure 4.7), indicating that the winds blowing from these wind directions are onshore winds (blue shaded sectors), while the remaining winds from other directions are associated with offshore winds. Using a method elaborated in Section 3.8 where the daily surface wind directions are evaluated individually (Borne et al., 1998); the days with typical land sea breeze are separated from the days without land sea breeze (or days with suppressed land sea breeze). BMRS was found to experience 20 and 29 days with suppressed land sea breeze during the NE 2014/2015 and NE 2015/2016 respectively (blue shaded regions in the time series). This period was associated with dominant wind direction ranging from 45° (northeasterly) to 90° (easterly) (Figure 4.5 (a) and (c)); indicating a great influence of onshore winds. The wind speed during this period varied from moderate to strong winds (shaded areas in Figure 4.6 (a) and (c)). Only five cold surge events during the NE 2014/2015 and six cold surge events during the NE 2015/2016 led to the strong winds at BMRS (blue colored lines in Figure 4.3 (a) and (b) respectively). The effects of the cold surge on the strength of wind at BMRS are closely linked to the location of the near-equatorial trough (Chen et al., 2013; Lim & Samah, 2004). If the trough is situated farther north of the Peninsular Malaysia, then the areas along the east coast of Malaysia are not affected by strong winds and heavy rainfall. However, if it is situated towards the south, then strong winds and rainfall are experienced at the northern fringe of the trough (east coast of Malaysia). The days with suppressed land sea breeze at BMRS during the NE monsoon can also be attributed by other synoptic influence beside cold surge event namely easterly surge (Wang, 2006) or other synoptic weather systems (Chang et al., 2005; Lim & Samah, 2004; Tangang et al., 2008). Other synoptic events like monsoon disturbance, tropical storm and tailed effect of tropical storms (Tan et al.,

2013) could hinder the differential heating between the land and sea, hence causing dominant onshore winds at BMRS. This period is associated with a decrease of temperature and it is most visible during two or more days of prolonged onshore winds (shaded areas in Figure 4.8 (a) and (c)). On the other hand, air pollutants resulted within its lowest level during this period. CO_2 (shaded area in Figure 4.10 (a)) and CH_4 (shaded area in Figure 4.10 (c)) resulted to around 410 ppm and 1.85 ppm respectively while PM (shaded areas of (a) and (c) in Figure 4.11 (PM_{10}) and Figure 4.13 ($PM_{2.5}$)) resulted to concentration below 30 μgm^{-3}. This period is also attributed with inconsistent levels of RPM (Figure 4.13 (a) and (c)) however most of the days show a decreasing pattern of RPM.

BMRS experienced ten days with suppressed land sea breeze during the SW monsoon in which 6 days occurred in the SW 2015 and the remaining days are shown in the SW 2016. This period was dominated by consistent offshore winds (135.0° < wind direction < 337.5°) as shown in shaded region of Figure 4.5 (b) and (d). This is possible due to the influence of southwesterly synoptic flow during this period. The dominant flows from southwesterly direction may hinder the onshore winds to flow over BMRS causing the resultant winds to be in the direction of offshore wind and hence suppressing the typical land-sea breeze event. No significant differences shown in the variation of wind speed (Figure 4.6 (b) and (d)), temperature (Figure 4.8 (b) and (d)), and air pollutants (Figure 4.10 to Figure 4.13 - (b) and (d)) during this period in comparison to days with land sea breeze.

4.1.3.3 Diurnal variations of meteorological parameters and air pollutants under synoptic and local meteorological conditions

All of the meteorological parameters and air pollutants during days with and without land sea breeze (under local and synoptic influence respectively) in both of monsoon periods were presented in the form of boxplots. A boxplot is a standardized method of displaying the distribution of data based on its statistical summary. The boxplots (Figure 4.15 to Figure 4.23) show the level of minimum, first quartile (Q1) median, third quartile (Q3), top outliers, bottom outliers and the ranges of the data. The mean value was also shown in the diurnal boxplot as red dot.

Days with suppressed land sea breeze during the NE monsoon exhibited no diurnal cycle signals as proven by the variation of wind direction (Figure 4.15 (a)), wind speed (Figure 4.16 (a)) and temperature (Figure 4.17 (a)). There were consistent wind direction (around 60° - northeasterly), moderate wind speed of 8 ms^{-1} and temperature varied around the mean value of 27°C. Diurnal variation of pressure has little influence on other meteorological parameters and is usually shown as a semi diurnal variation (Haurwitz, 1965). This is justified by Figure 4.18 (a) where the minimum are shown at 05:00 LT and 17:00 LT and intermediate maximum levels are at 11:00 LT and 23:00 LT. Pressure variation is more influenced by the latitude and the solar tide in the atmosphere (Dai & Wang, 1999; Haurwitz, 1965). This period is also associated with low levels of CH_4 (about 1.8 ppm), CO_2 (around 410 ppm), PM_{10} (within 20 μgm^{-3}) and $PM_{2.5}$ (about 20 μgm^{-3}) as shown in Figure 4.19 (a), Figure 4.20 (a), Figure 4.21 (a) and Figure 4.22 (a) respectively. Interestingly, there was high RPM shown during this period within 0.90 (Figure 4.23 (a)), proving dominant presence of fine particles.

Meanwhile, days with land sea breeze during the NE monsoon were associated with clear diurnal cycle as shown in each (b) of Figure 4.15 to Figure 4.23. Land sea breeze

are strongly influenced by the differential heating between the land and sea; thus, the variation of temperature is fundamental precursor for any changes of variations during this period. The minimum mean of temperature (around 24°C) is shown 1 hour after sunrise which is at 08:00 LT. Temperature then increases until it reaches the maximum at 12:00 LT to 17:00 LT (around 28°C). The temperature subsequently decreases over night to dawn and reaching its minimum level. The diurnal cycle of wind direction is used to investigate the onset of land and see breeze. Mean wind direction at 08:00 LT is 200° (south-southwesterly (SSW)) and from 14:00 LT to 18:00 LT are shown around 70° (east-northeasterly (ENE) (Figure 4.15 (b)). As explained in the previous sub-section, the winds from the 337.5° to 135.0° of wind direction were attributed to onshore winds and associated as a sea breeze, while the remaining winds were attributed to offshore winds (land breeze). There was time lag with respect to the onset of the sea breeze where it did not occur immediately with the sunrise or at the time of minimum temperature (08:00 LT). The increase of temperature from 08:00 LT to 11:00 LT demonstrates a transformation period of land breeze to sea breeze. Thermal contrast is needed between the land and sea to reach certain threshold conditions for the formation of sea breeze thus resulted to this lag in the formation of sea breeze event. Furthermore, the time lag also varies depending on the atmospheric conditions, soil moisture and location (Kavitha et al., 2018). Figure 4.15 (b) also indicates the sea breeze lasted for 14 hours starting at 11:00 LT and ending at 01:00 LT (in midnight) while land breeze lasted for 8 hours (from 02:00 LT to 10:00 LT). Beside differential heating between the land and sea, the prolonged sea breeze is influenced by the great pressure gradient formed between the 30°N and 5°N implying presence of synoptic forcing. However, this synoptic condition is in its moderate to weak form. Thus, this period was attributed to interaction between the local and weak synoptic meteorological conditions. The minimum levels of wind speed (around 2 ms^{-1}) are shown from 07:00 LT to 09:00 LT while maximum level shown

at 19:00 LT (around 6 ms^{-1}) (Figure 4.16 (b)). The diurnal variation of pressure (Figure 4.18 (b)) shows similar pattern as the days with suppressed land sea breeze, demonstrating its little influence on other meteorological factors. The diurnal variations of air pollutants demonstrate influences by both the temperature and wind. CH_4 and CO_2 show maximum level (mean) at 07:00 LT (around 2.5 ppm and 460 ppm respectively) and minimum level from 12:00 to 18:00 LT (around 1.9 ppm and 420 ppm respectively). Meanwhile, PM_{10} and $PM_{2.5}$ show maximum level (mean) at 08:00 LT (around 40 μgm^{-3}) and minimum level from 12:00 to 19:00 LT (around 30 μgm^{-3}). There is slight difference experienced by CH_4 and CO_2 due to lack in data availability (No data available during the NE 2014/2015). The air pollutants started to decrease when temperature started to increase from its minimum level at 08:00 LT. Then, the presence of sea breeze which started at 11:00 LT with a rapid increase in wind speed directly contributed to the depletion of air pollutants until 19:00 LT. Subsequent decrease of wind speed contributed to rapid increase of air pollutants until sea breeze ended at 01:00 LT (on the next day). Air pollutants continuously increased during land breeze where there was rapid decrease of wind speed and temperature. Increase in temperature and wind speed demonstrates formation of unstable atmosphere with presence of more turbulence flows. This condition allows more distribution of pollutants and thus decreases the level of air pollutants efficiently. RPM (Figure 4.23 (b)) shows interesting relations with wind speed and temperature. The minimum mean level of RPM shown at 10:00 LT (RPM ~ 0.75) while the maximum level reached at 18:00 to 21:00 LT (RPM ~ 0.90). Rapid increase of temperature from its minimum level decreases the RPM. However, RPM increases to its maximum level when sea breeze started to prevail (with an increase in wind speed). It continuously decreases (with a rapid decrease of wind speed) until sea breeze ends at 01:00 LT. Land breeze contributes to consistent level of RPM ~ 0.85 from 02:00 LT to

08:00 LT. This demonstrates that a rapid increase of wind speed during the sea breeze event contributes to more transport of fine particles.

Days with suppressed land sea breeze during the SW monsoon exhibited a dominant offshore wind (mean level between 200° to 250°) with light wind speed (Figure 4.15 (c) and Figure 4.16 (c)) respectively. However, there was a weak diurnal cycle shown by the diurnal variation of temperature (Figure 4.17 (c)) where the maximum level was shown at 15:00 LT and minimum level at 00:00 LT. CH_4 (Figure 4.19 (c)) and CO_2 (Figure 4.20 (c)) also show a slight diurnal effect where it gradually decrease as temperature increase. PM_{10} (Figure 4.21 (c)) and $PM_{2.5}$ (Figure 4.22 (c)) showed inconsistent variations due to the lack of data during this period.

Meanwhile, days with land sea breeze during the SW monsoon were associated with clearer diurnal cycle as shown in each (d) of Figure 4.15 to Figure 4.23. Figure 4.17 (d) shows minimum mean temperature at 07:00 LT (about 26°C) and maximum level at 13:00 LT (around 30°C). Temperature decreased slightly over the day (until 18:00 LT) and rapidly over night to dawn until its maximum level was reached. The consistent wind direction from the SSW (around 200°) from 00:00 LT to 09:00 LT gradually changed to ENE (within 50°) from 12:00 LT to 19:00 LT (Figure 4.15 (d)). The figure also indicates the sea breeze prevailed at 12:00 LT until 19:00 LT (7 hours) while land breeze started at 20:00 LT and ended at 11:00 LT. Based on Figure 4.16 (d), sea breeze was associated with an increase in wind speed from 11:00 LT until it reached its maximum level at 16:00 LT (4 ms^{-1}), then wind speed decreased continuously until end of sea breeze. The wind speed continuously decreased during the land breeze until minimum level at 00:00 LT to 10:00 LT (around 2 ms^{-1}). Pressure showed similar patterns during days with and without land sea breeze in the SW monsoon as shown in Figure 4.18 (c) and (d) respectively. The air pollutants registered maximum level (mean(at 07:00 LT (CH_4 ~2.3 ppm; CO_2 ~ 480

ppm; PM_{10} ~ 90 μgm^{-3} and $PM_{2.5}$ ~ 90 μgm^{-3}), then it decreased rapidly to the minimum level at 12:00 LT to 19:00 LT (CH_4 ~ 1.8 ppm; CO_2 ~ 415 ppm; PM_{10} ~ 30 μgm^{-3} and $PM_{2.5}$ ~ 30 μgm^{-3}). The air pollutants increased rapidly afterwards until maximum level was reached. The diurnal variations of the air pollutants clearly influenced by the temperature and wind. The levels of pollutants started to decrease when temperature increased (since the atmosphere became more unstable which increased the turbulence and mixing process) and when sea breeze prevailed, the air pollutants decreased from 12:00 LT to 19:00 LT. Land breeze which is associated with rapid decrease in temperature and consistent light winds rapidly increased the level of air pollutants to its maximum level. RPM showed minimum mean level at 08:00 LT to 11:00 LT with value ~ 0.95 and this was associated with an increase in temperature. The rest of the hours was shown within its maximum level within RPM ~ 0.97. This demonstrates very strong dominance of fine particles during days with land sea breeze in the SW monsoon.

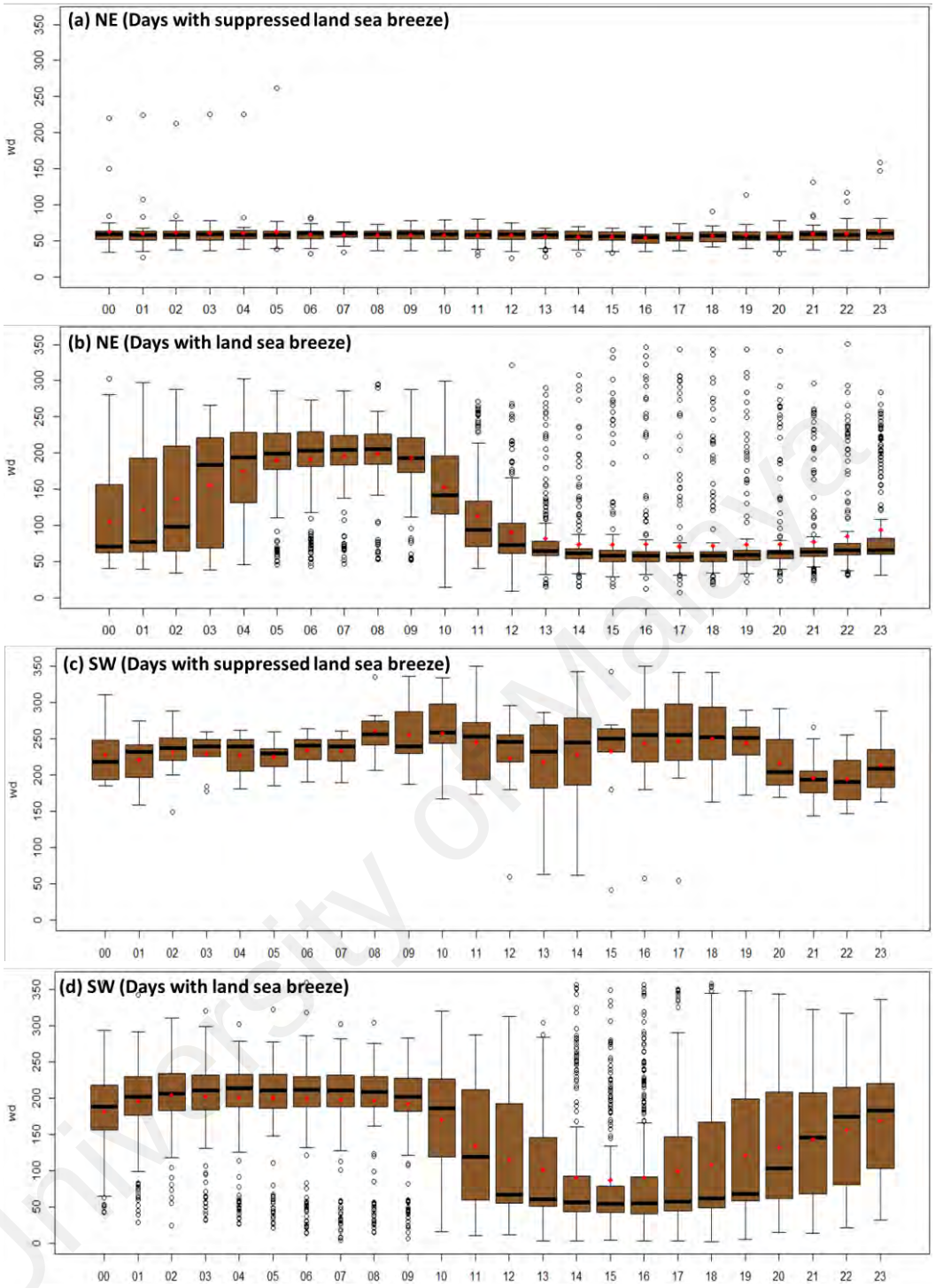

Figure 4.15: Boxplot of diurnal variations of WD (°) based on local time (LT) for days with and without land sea breeze in NE and SW monsoon periods. The red dots (•) represent the mean values and (○) represent the outliers

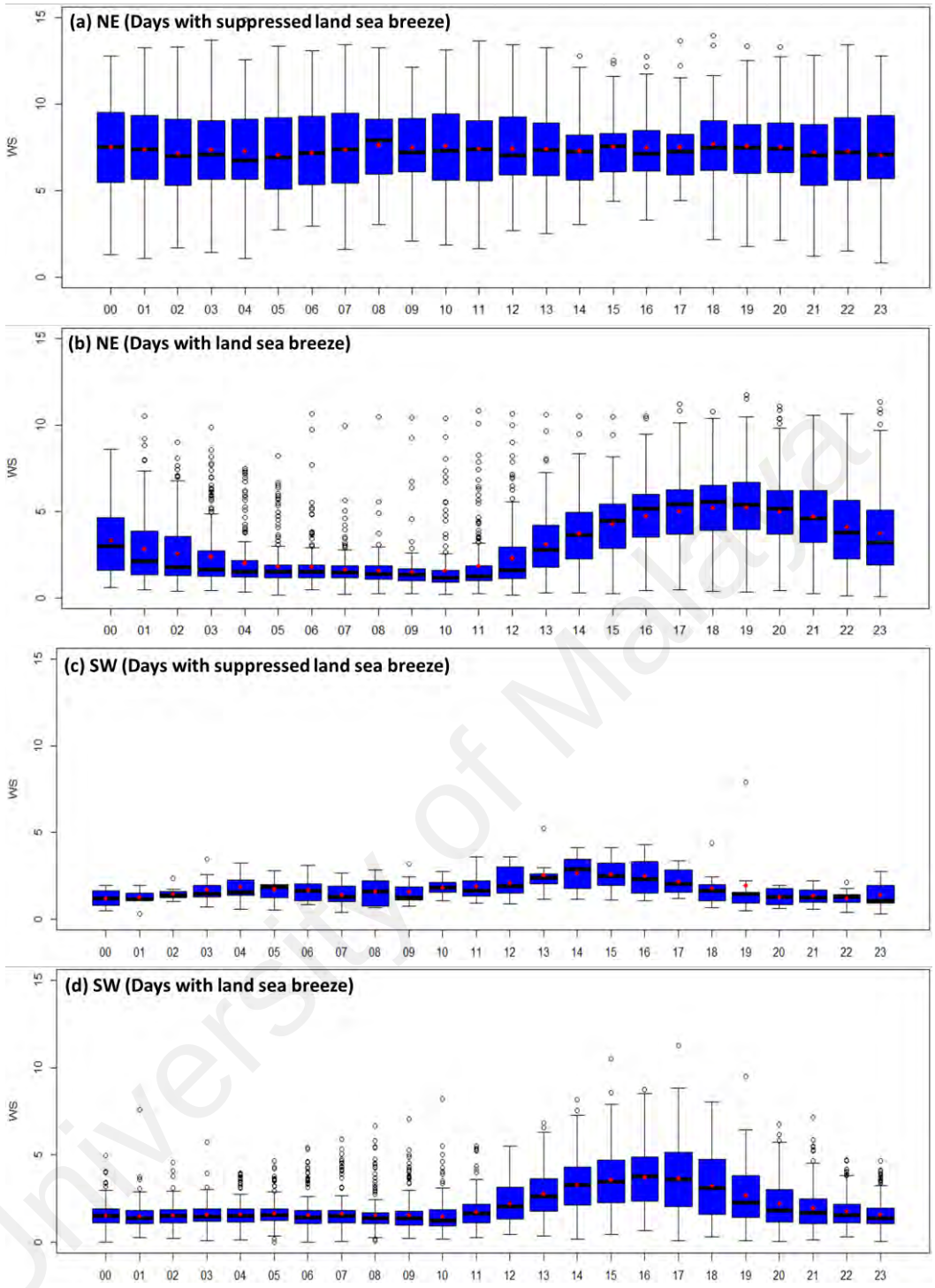

Figure 4.16: Boxplot of diurnal variations of WS (ms-1) based on local time(LT) for days with and without land sea breeze in NE and SW monsoon periods. The red dots (•) represent the mean values and (○) represent the outliers

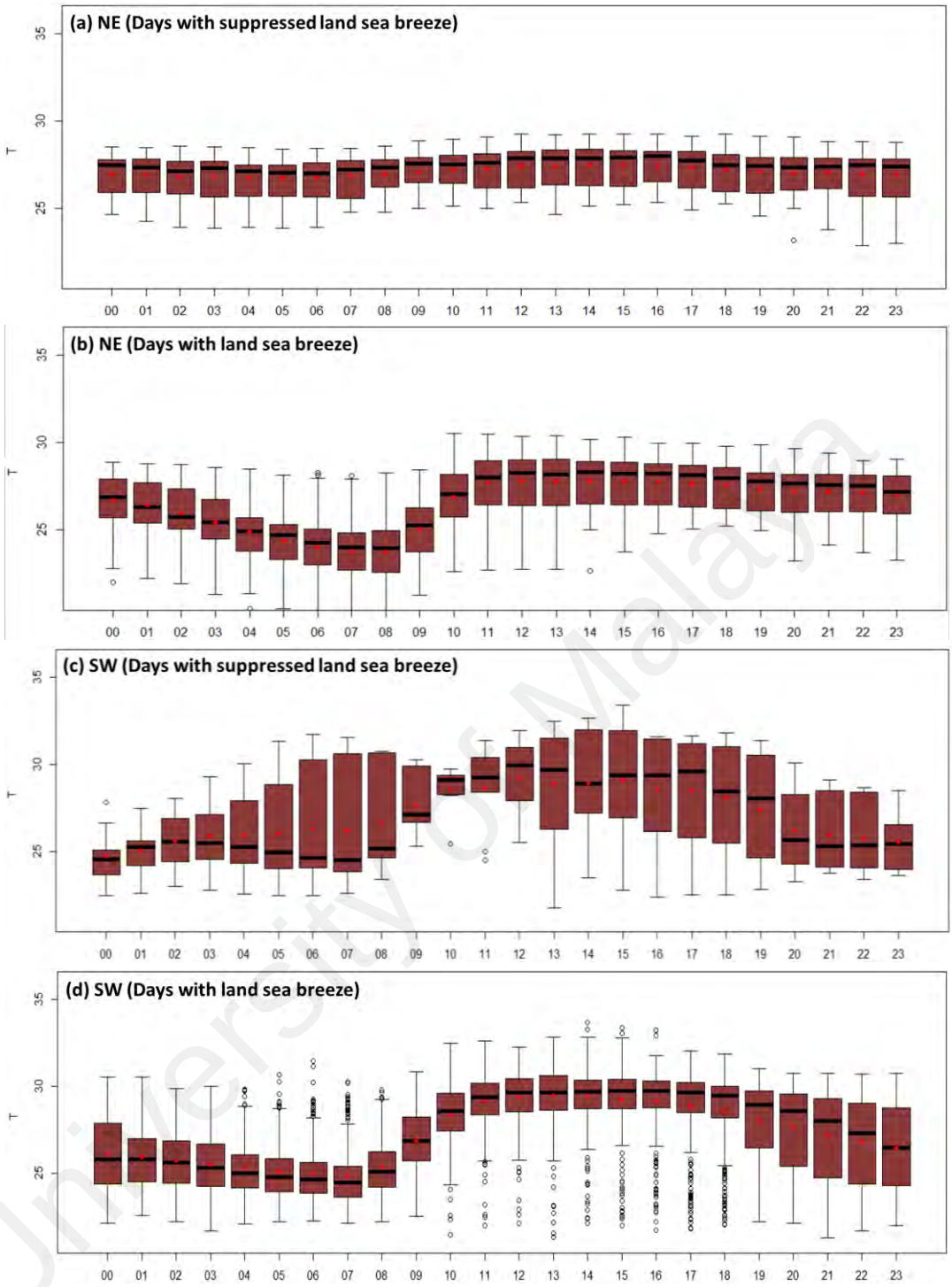

Figure 4.17: Boxplot of diurnal variations of T (°C) based on local time (LT) for days with and without land sea breeze in NE and SW monsoon periods. The red dots (•) represent the mean values and (○) represent the outliers. The hours shown is based on local time (LT)

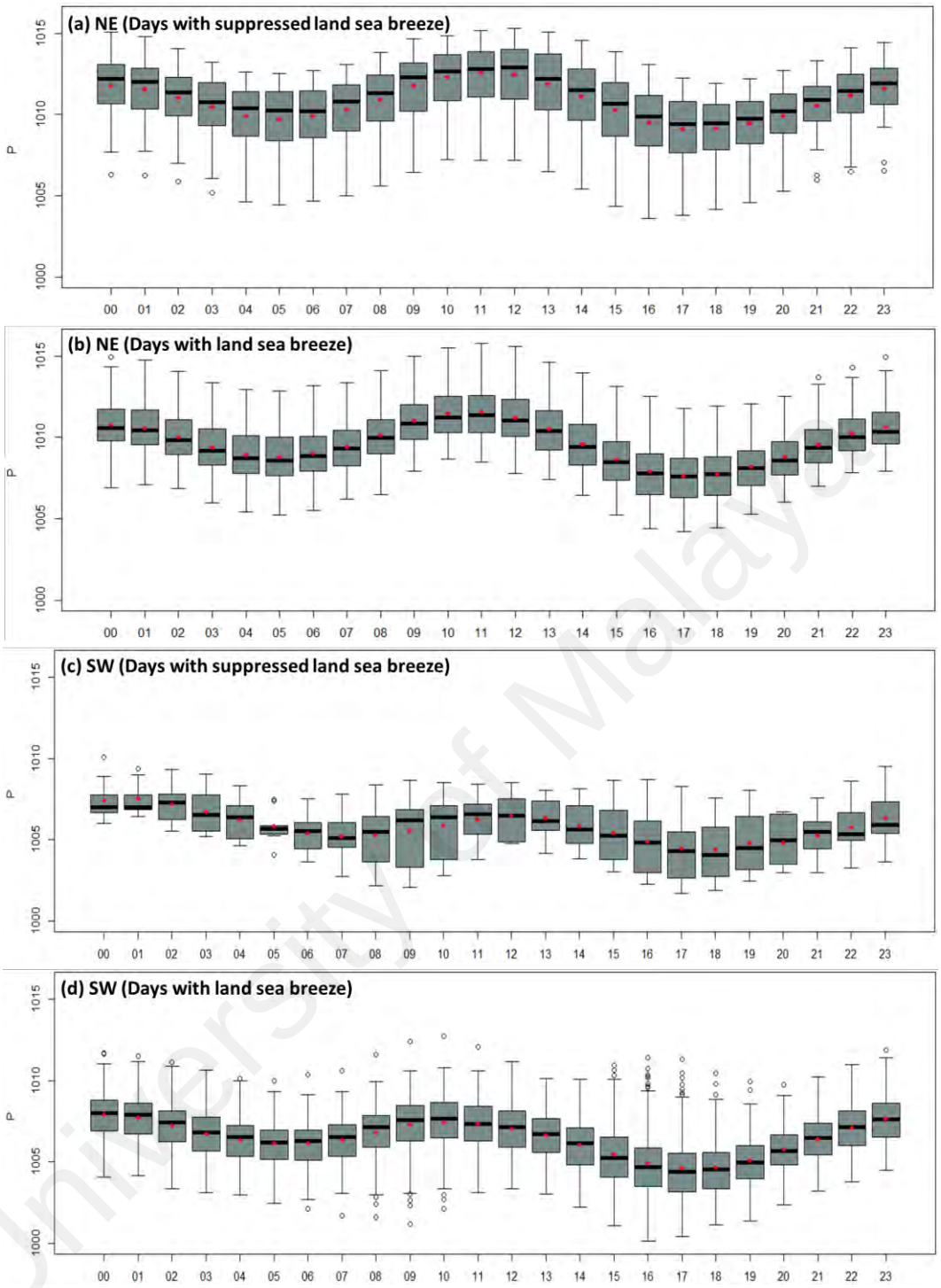

Figure 4.18: Boxplot of diurnal variations of P (hPa) based on local time (LT) for days with and without land sea breeze in NE and SW monsoon periods. The red dots (•) represent the mean values and (○) represent the outliers

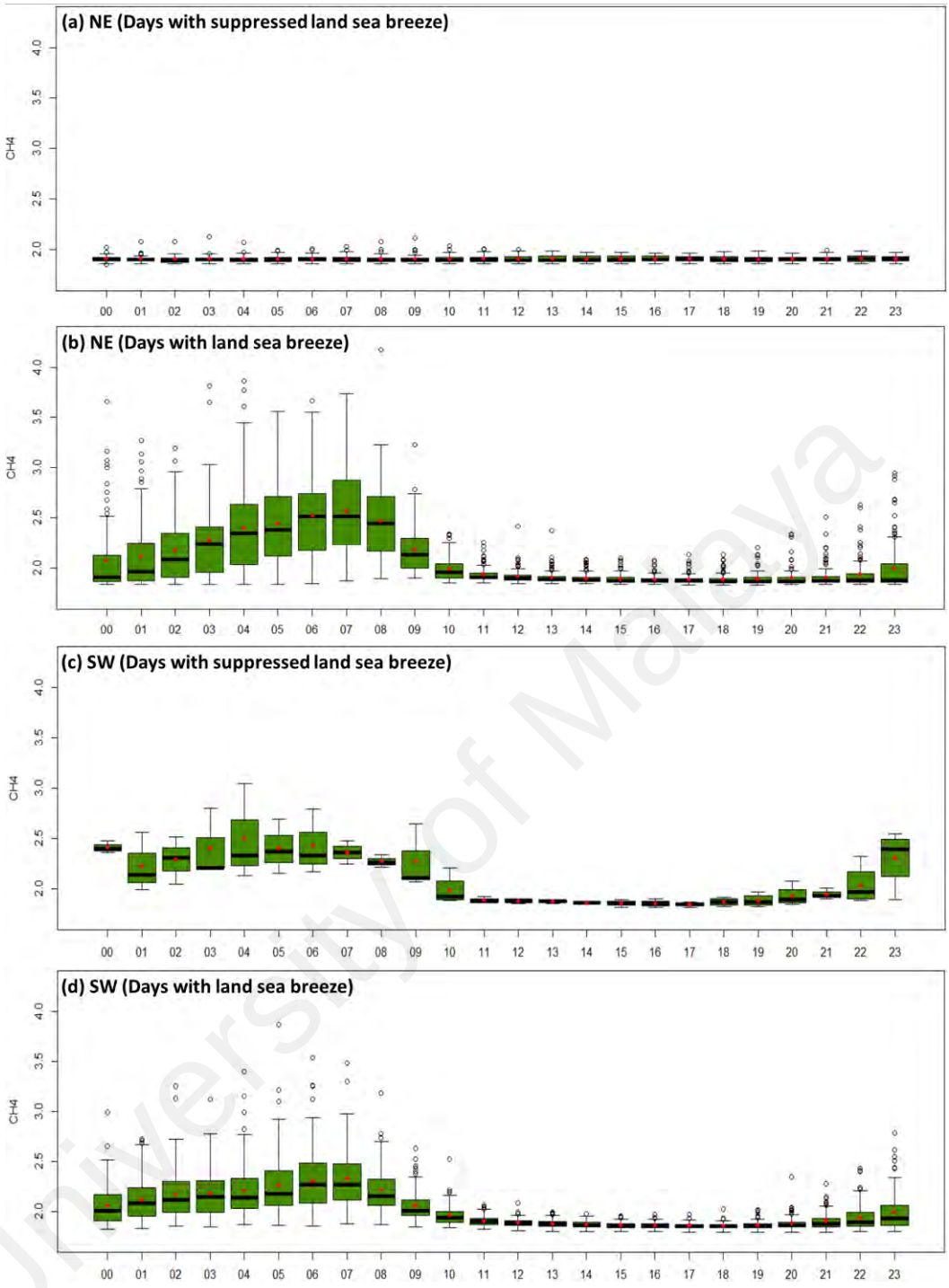

Figure 4.19: Boxplot of diurnal variations of CH4 (ppm) based on local time(LT) for days with and without land sea breeze in NE and SW monsoon periods. The red dots (•) represent the mean values and (○) represent the outliers

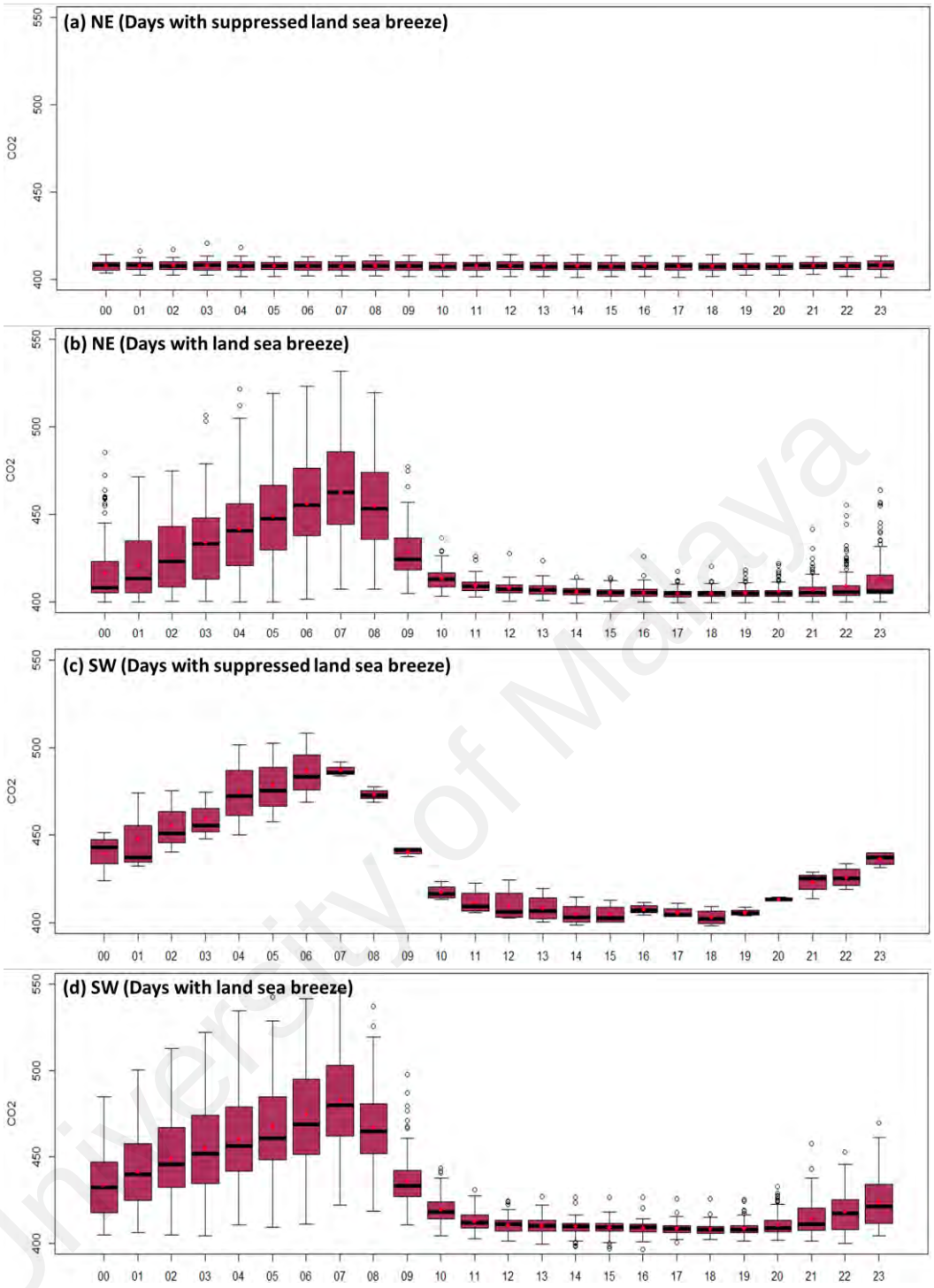

Figure 4.20: Boxplot of diurnal variations of CO2 (ppm) based on local time (LT) for days with and without land sea breeze in NE and SW monsoon periods. The red dots (•) represent the mean values and (○) represent the outliers

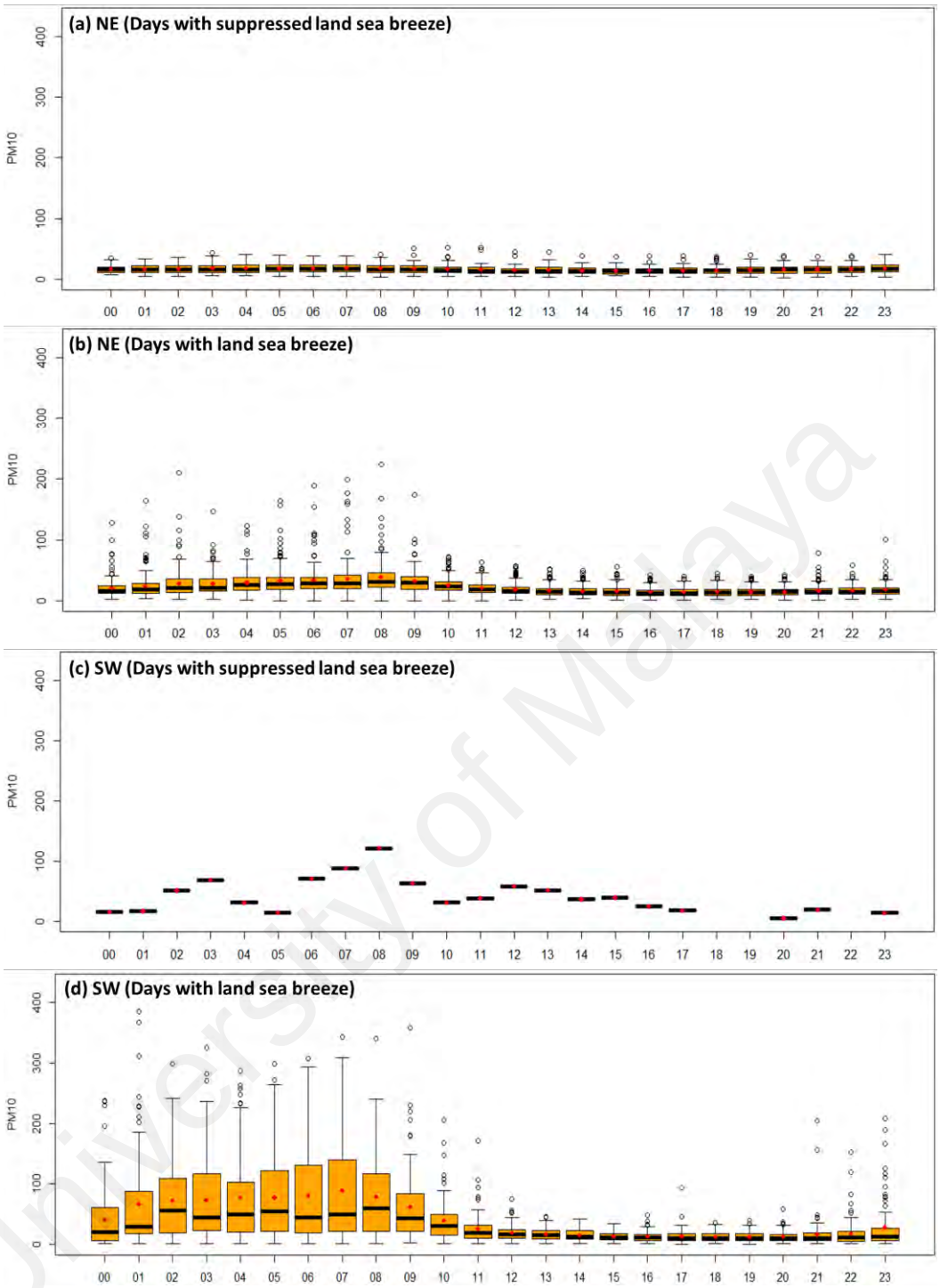

Figure 4.21: Boxplot of diurnal variations of PM10 (µgm-3) based on local time(LT) for days with and without land sea breeze in NE and SW monsoon periods. The red dots (•) represent the mean values and (○) represent the outliers

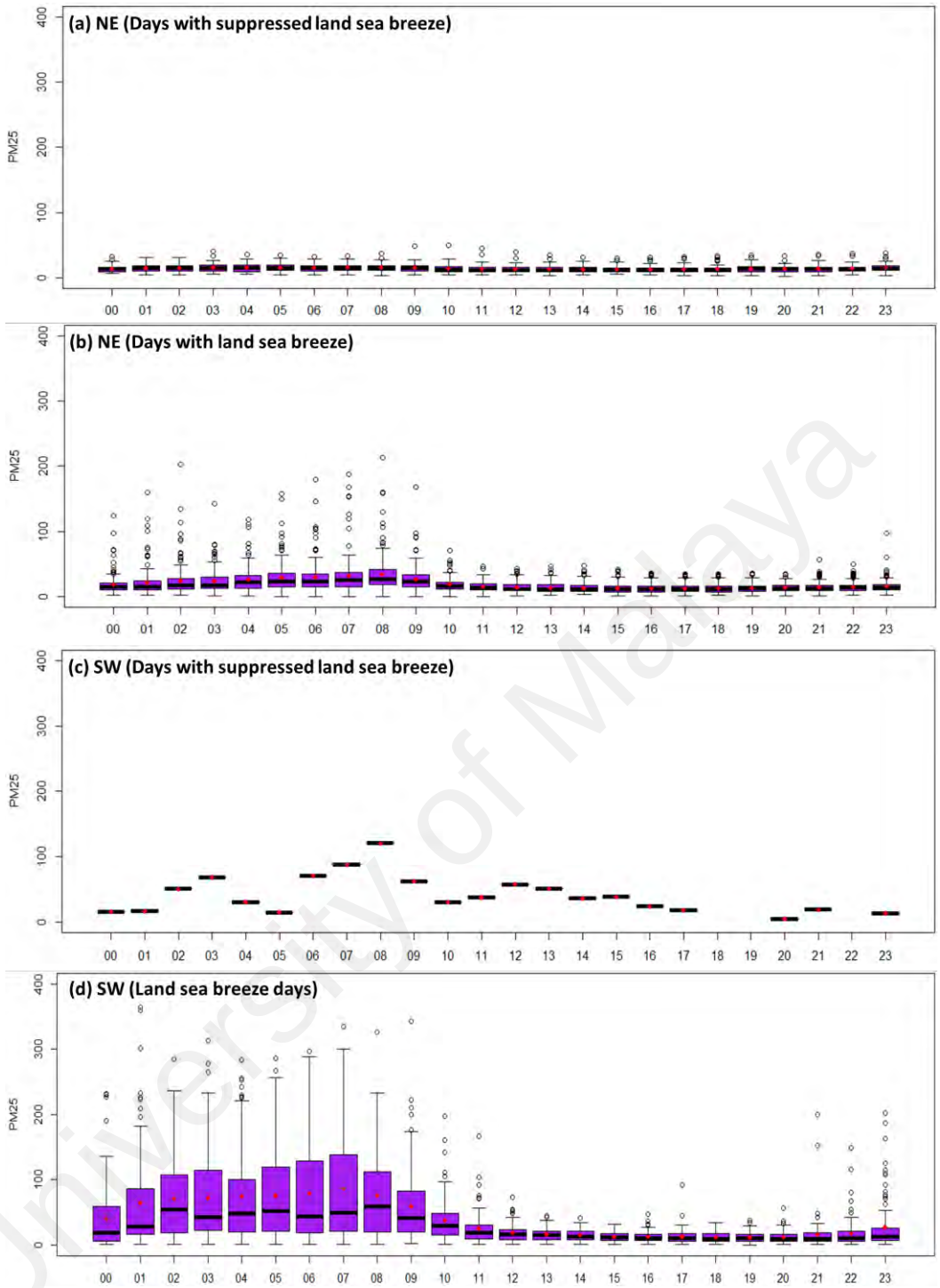

Figure 4.22: Boxplot of diurnal variations of $PM_{2.5}$ (μgm^{-3}) based on local time(LT) for days with and without land sea breeze in NE and SW monsoon periods. The red dots (•) represent the mean values and (○) represent the outliers

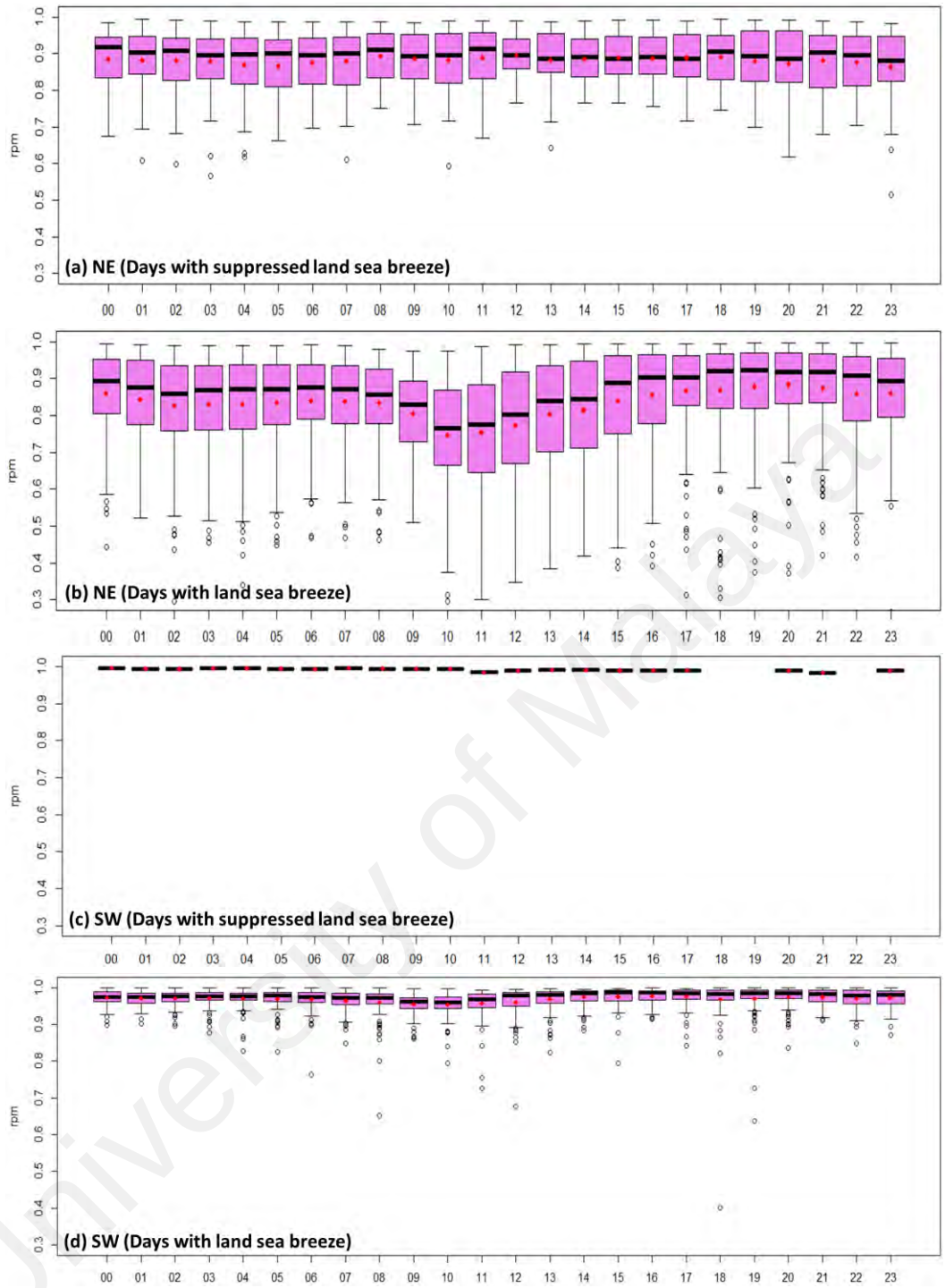

Figure 4.23: Boxplot of diurnal variations of RPM based on local time (LT) for days with and without land sea breeze in NE and SW monsoon periods. The red dots (•) represent the mean values and (○) represent the outliers

Table 4.6: Summary on the variations of meteorological parameters and air pollutants during days with and without suppressed land sea breeze in the NE and SW monsoon

Meteorological conditions and variations of air pollutants during days with suppressed land sea breeze	
NE monsoon	**SW monsoon**
1. Total 49 days 2. This period is caused by a cold surge event associated with a strong event and other events like tropical storms, monsoon disturbances etc. 3. Dominant influence of onshore wind 4. No significant diurnal effect is shown on the meteorological parameters and air pollutants 5. Low level air pollutants 6. Presence of more fine particles compared to coarse particles (RPM ~ 0.90)	1. Total 10 days 2. This period is caused by an influence of southwesterly synoptic flows (weak) 3. Dominant influence of offshore wind 4. Weak diurnal cycle shown on air pollutants 5. No significant change on level of air pollutants (as compared with days with land sea breeze) 6. No significant change of RPM
Meteorological condition and variations of air pollutants during days with land sea breeze	
NE monsoon	**SW monsoon**
1. Land-sea breeze occurred every day. • Sea breeze occurred for 14 hours; land breeze occurred for 7 hours 2. A clear diurnal cycle is shown on the variations of meteorological parameters and air pollutants 3. Variations of air pollutants affected by temperature and wind • Strong wind and high temperature reduced level of air pollutants • Presence of more fine particles during sea breeze event	1. Land-sea breeze occurred every day • Sea breeze occurred for 7 hours; land breeze occurred for 17 hours 2. A clear diurnal cycle is shown on the variations of meteorological parameters and air pollutants 3. Variations of air pollutants affected by temperature and wind

Table 4.6 shows summary on the variations of meteorological parameters and air pollutants at BMRS under the influence of local and synoptic meteorological conditions in the NE and SW monsoons. Days with suppressed land sea breeze in the NE monsoon (49 days) was attributed to strong synoptic effect where there were consistent presence of northeasterly wind (onshore), moderate to strong wind and no diurnal effect shown on the variations of meteorological parameters and air pollutants. This period also was

associated with low level of all air pollutants and high RPM. Only ten days in SW monsoon are attributed as days with suppressed land sea breeze. This period was dominated with light offshore wind and weak diurnal effect on the variations of temperature and air pollutants. Days with land sea breeze in both NE and SW monsoon are associated with strong local meteorological condition where it occurred every day and clear diurnal cycle shown on the variations of meteorological parameters and all air pollutants. The main differences are on the period of sea breeze and land breeze events. In the NE monsoon, sea breeze event occurred from 11:00 LT to 01:00 LT (14 hours) while it occurred from 12:00 LT to 19:00 LT (7 hours) in the SW monsoon. This is due the consistent pressure gradient formed between the 30°N and 5°N and implied a presence of moderate to low synoptic forcing over BMRS. Sea breeze with the presence of higher temperature and wind speed reduced the level of all air pollutants in both monsoon periods. However, higher wind speed during this event in the NE monsoon shows an increase of RPM. This demonstrated more fine particles brought over BMRS from the sea during the NE monsoon.

4.1.4 Transport of air pollutants at BMRS during the NE and SW monsoon

The transport of air pollutants is associated to the movement of air masses and HYSPLIT model is very well-known model that can be utilized to examine the origin of the air masses. HYSPLIT cluster back trajectories were firstly produced to show the dominant origins of air masses during the NE and SW monsoon. Then, using CPFP plots, the associated bivariate plots of air pollutants in association with wind speed and wind direction over BMRS are shown. Afterward, using HYSPLIT-CWT analysis, possible sources of air pollutants during days with suppressed land sea breeze and days with land sea breeze in both monsoon periods were explained. The HYSPLIT-CWT analysis for all

the air pollutants were analyzed using 120-hour residence time considering the lifespan of all the air pollutants. It was calculated based on each individual trajectory (based on 6-hours interval) and concentration of air pollutants at BMRS.

BMRS is strongly affected by the transboundary transport of air masses during the NE monsoon. Figure 4.24 (a) indicates that BMRS has already been exposed to long-range transport of air masses flowing from the SCS within 1 24-hour span. This in advance led to the increase in the hours where sea breeze prevailed at this station (during days with land sea breeze in the NE monsoon) as shown in the diurnal variations in the previous sub-section. The 120-hour cluster back trajectory (Figure 4.24 (b)) revealed transboundary air masses primarily flowing from the SCS (25%), areas between the SCS and East China Sea (ESC) (46%) and the continental region of China (29%).

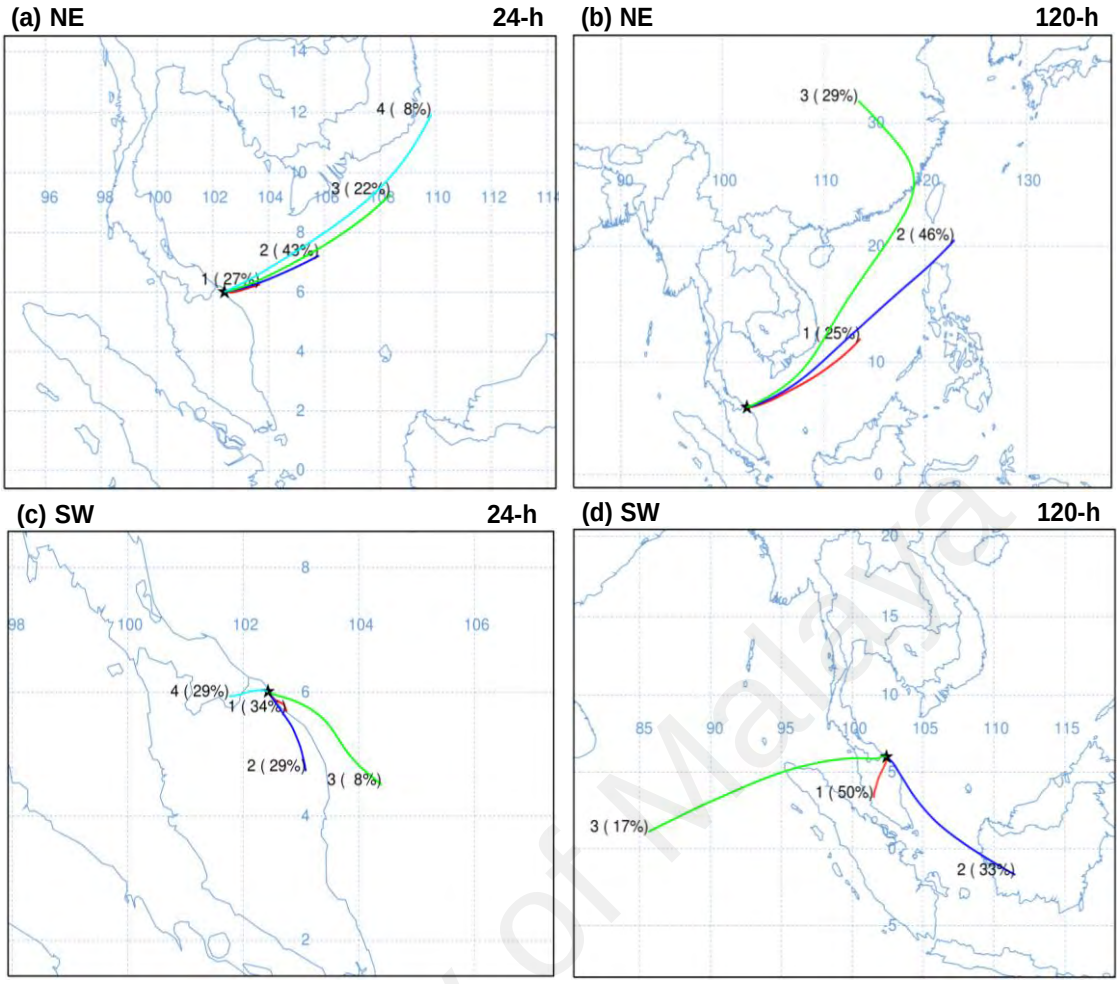

Figure 4.24: HYSPLIT cluster back-trajectories during different monsoon periods and trajectory times from 2014 to 2016 using GDAS1 data. Source ★ is at 6.0086 °N and 102.4259 °E (BMRS location). Colored lines represent the mean trajectory of each cluster. The values at the end each line represent the percentages of individual backward air trajectories included in each cluster

Conditional Probability Function Polar (CPFP) plots for all air pollutants during the days with suppressed land sea breeze in the NE monsoon are shown in Figure 4.25 to Figure 4.27. Figure 4.25 (a) to (d) show onshore wind (shaded areas in figure) contributed to most of CH_4, ranging between the minimum to 95th percentile. The onshore wind was associated with various wind speed from light to strong winds. Meanwhile, Figure 4.25 (e) shows that the CH_4 greater than the 95th percentile contributed by both onshore and offshore winds. Figure 4.26 shows the CPFP plot for CO_2 during this period. Onshore wind strongly contributed to all ranges of CO_2 from the minimum to maximum levels.

Figure 4.26 (e) shows that the CO_2 greater than the 95th percentile originated by both the strong onshore (northeasterly) and light offshore (south-southeasterly) winds. Figure 4.27 shows onshore wind strongly contributed to the high RPM (above 0.90). Offshore wind only contributed to within the minimum to 50th percentile of RPM (Figure 4.27 (a) and (b)) ranging from 0.51 to 0.90. This indicates coarse particles are contributed more from the land areas while fine particles are originated from the sea. The individual trajectories associated with suppressed land sea breeze days during the NE monsoon are shown in Figure 4.31 (a) and (b). BMRS was influenced with direct, dominant and greater synoptic flows of air where there were higher flows from the regions near Siberia and Mongolia. HYSPLIT-CWT analysis indicates that the principal (high) sources of CH_4 and CO_2 (as shown in Figure 4.32 (a) and (c) respectively) at BMRS were originated from the SCS, ECS and the continental regions of China. Figure 4.32 (e) shows principal (high) sources RPM were also originated from these regions and it suggests strong presence of fine particles.

CPFP plots for all air pollutants during the days with land sea breeze in the NE monsoon are shown in Figure 4.28 to Figure 4.30. Figure 4.28 (a) shows strong dominance of onshore wind for the minimum to 25th percentile of CH_4. Then, CH_4 within the 25th to 75th percentiles were contributed by both the onshore and offshore winds (Figure 4.28 (b) and (c)). The remaining CH_4 ranging from the 75th percentile to maximum were highly associated with light southwest wind as shown in Figure 4.28 (d) and (e). In comparison to CPFP plot for CH_4, CO_2 (Figure 4.29) also shows similar wind directions and wind speed contributed to the respective interval of percentiles. Figure 4.30 shows the CPFP plot for RPM. The minimum to 95th percentile of RPM contributed by combination of onshore and offshore winds (Figure 4.30 (a) to (d)) and various wind speed. RPM greater than the 95th was strongly dominated by the moderate onshore wind (east-northeasterly). This indicates very high fine particles are contributed from the SCS

area. Individual trajectories during this period indicated various sources of air from different directions and weaker influence of synoptic flows (Figure 4.31 (c) and (d)) (as compared to days with suppressed land sea breeze). HYSPLIT-CWT analysis shows stronger principal influences of CH_4, CO_2 and RPM (as shown in Figure 4.32 (b), (d) and (f) respectively) were originated from the SCS and ECS.

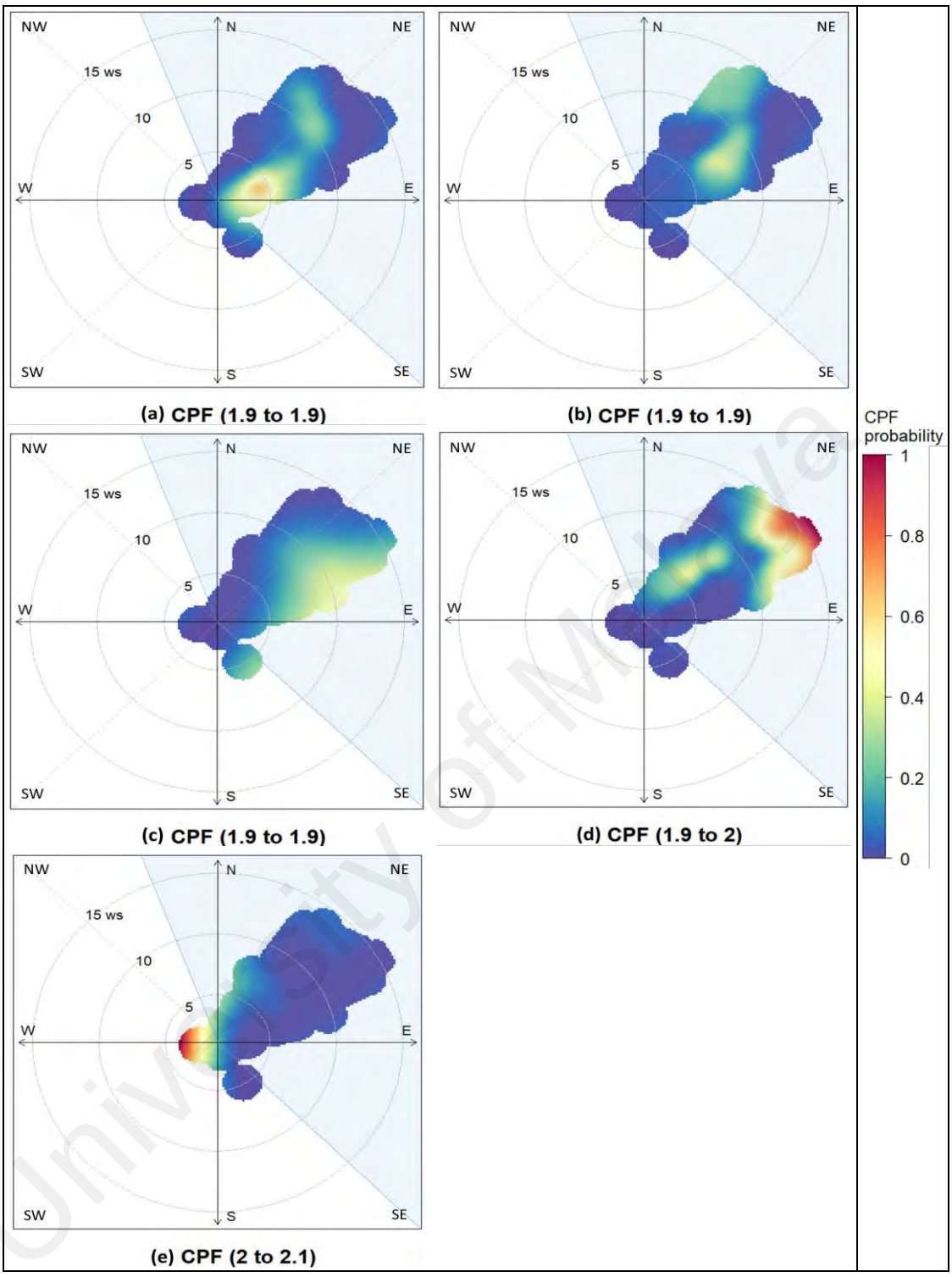

Figure 4.25: Polar plot of hourly CH_4 (ppm) at BMRS based on the CPF function for a range of percentile intervals from (a) Minimum to Q1 (b) Q1 to Q2 (c) Q2 to Q3 (d) Q3 to 95th percentile and (e) 95th percentile to maximum during days with suppressed land sea breeze in the NE monsoon. The color scale shows the CPF probability and the radial scale shows the wind speed. The light blue shaded sectors represent the onshore wind (Same indications used for the all the preceded CPFP plots)

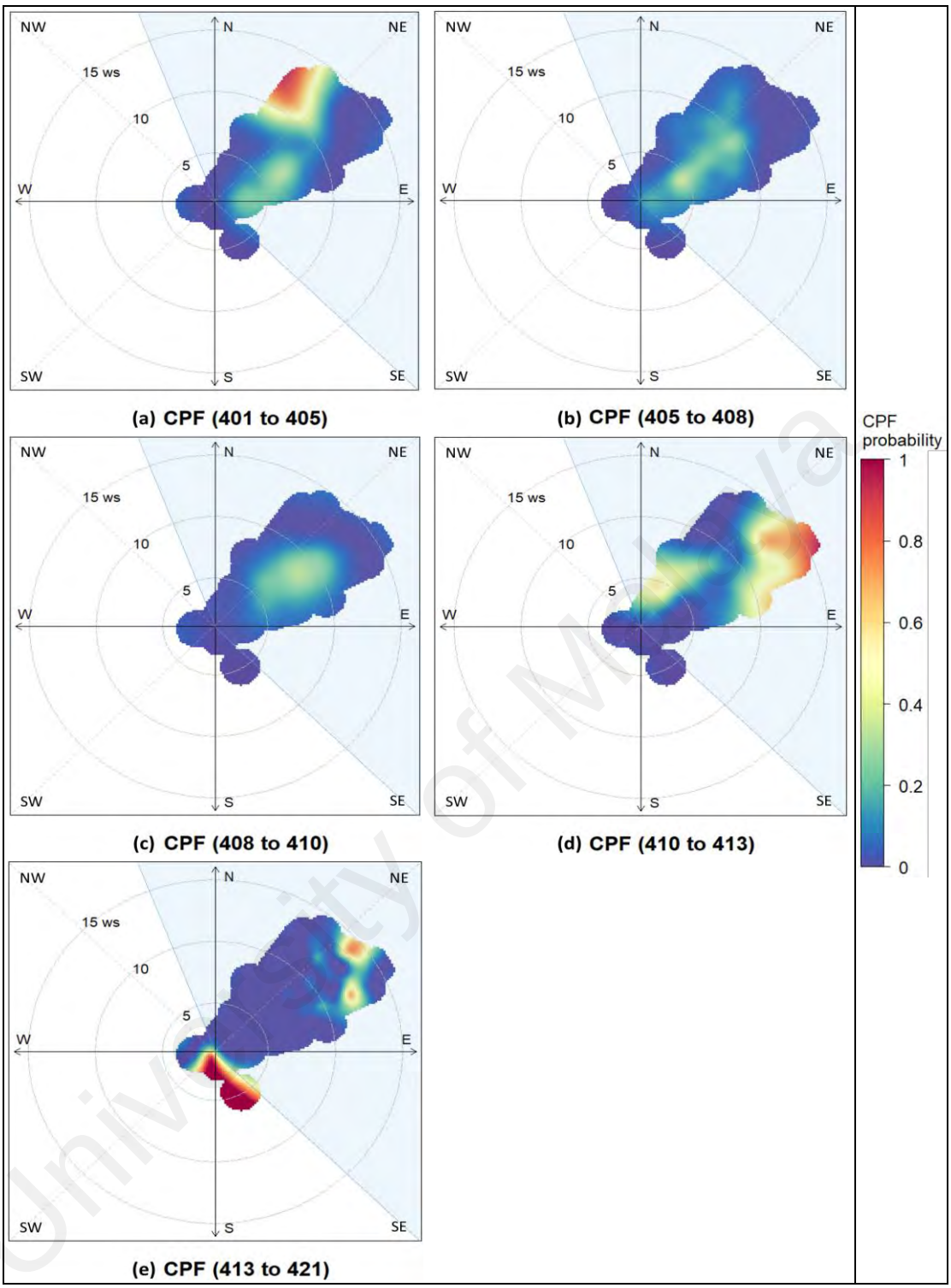

Figure 4.26: Polar plot of hourly CO_2 (ppm) at BMRS based on the CPF function for a range of percentile intervals from (a) Minimum to Q1 (b) Q1 to Q2 (c) Q2 to Q3 (d) Q3 to 95th percentile and (e) 95th percentile to maximum during days with suppressed land sea breeze in the NE monsoon

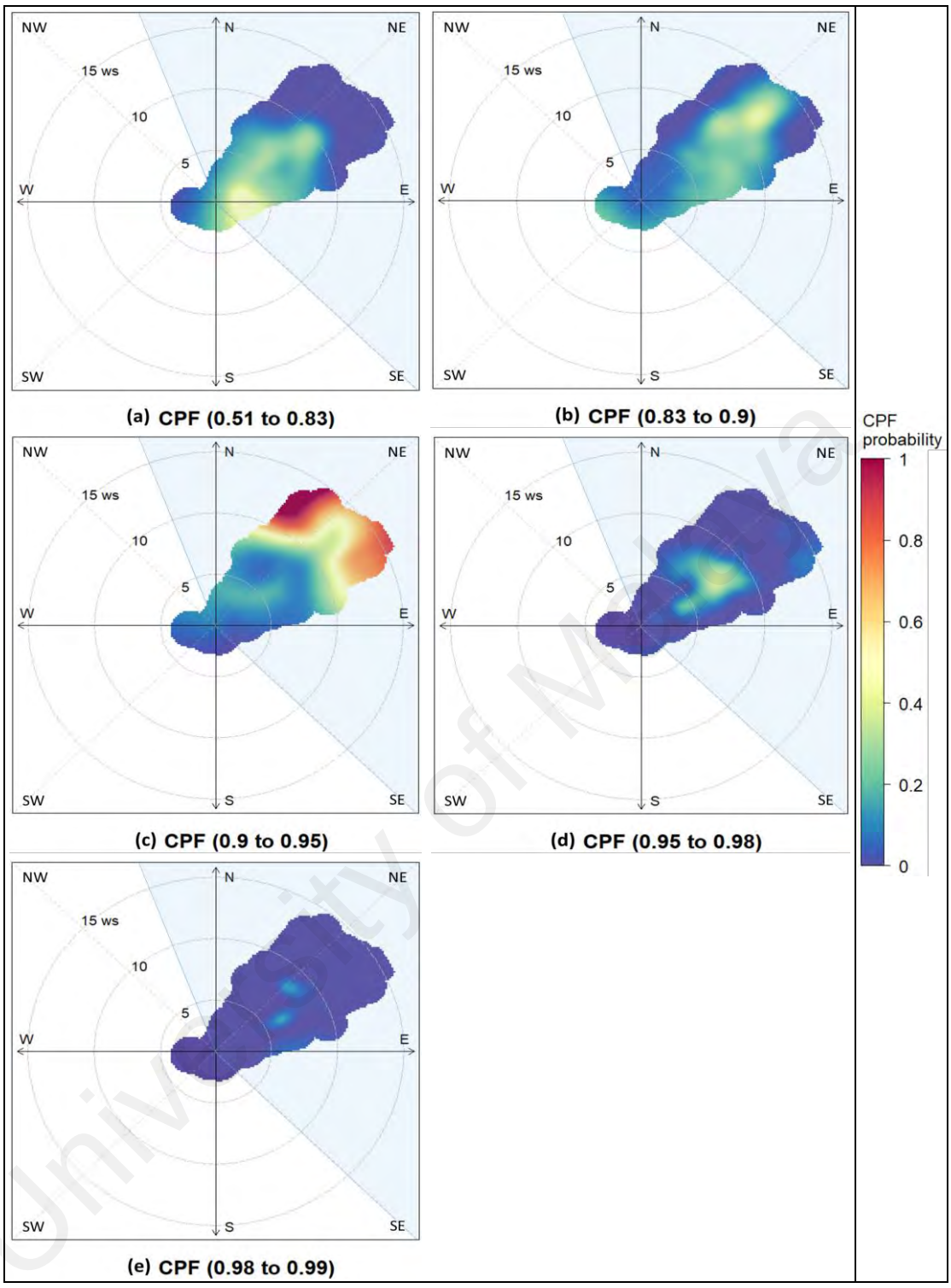

Figure 4.27: Polar plot of hourly RPM at BMRS based on the CPF function for a range of percentile intervals from (a) Minimum to Q1 (b) Q1 to Q2 (c) Q2 to Q3 (d) Q3 to 95th percentile and (e) 95th percentile to maximum during days with suppressed land sea breeze in the NE monsoon

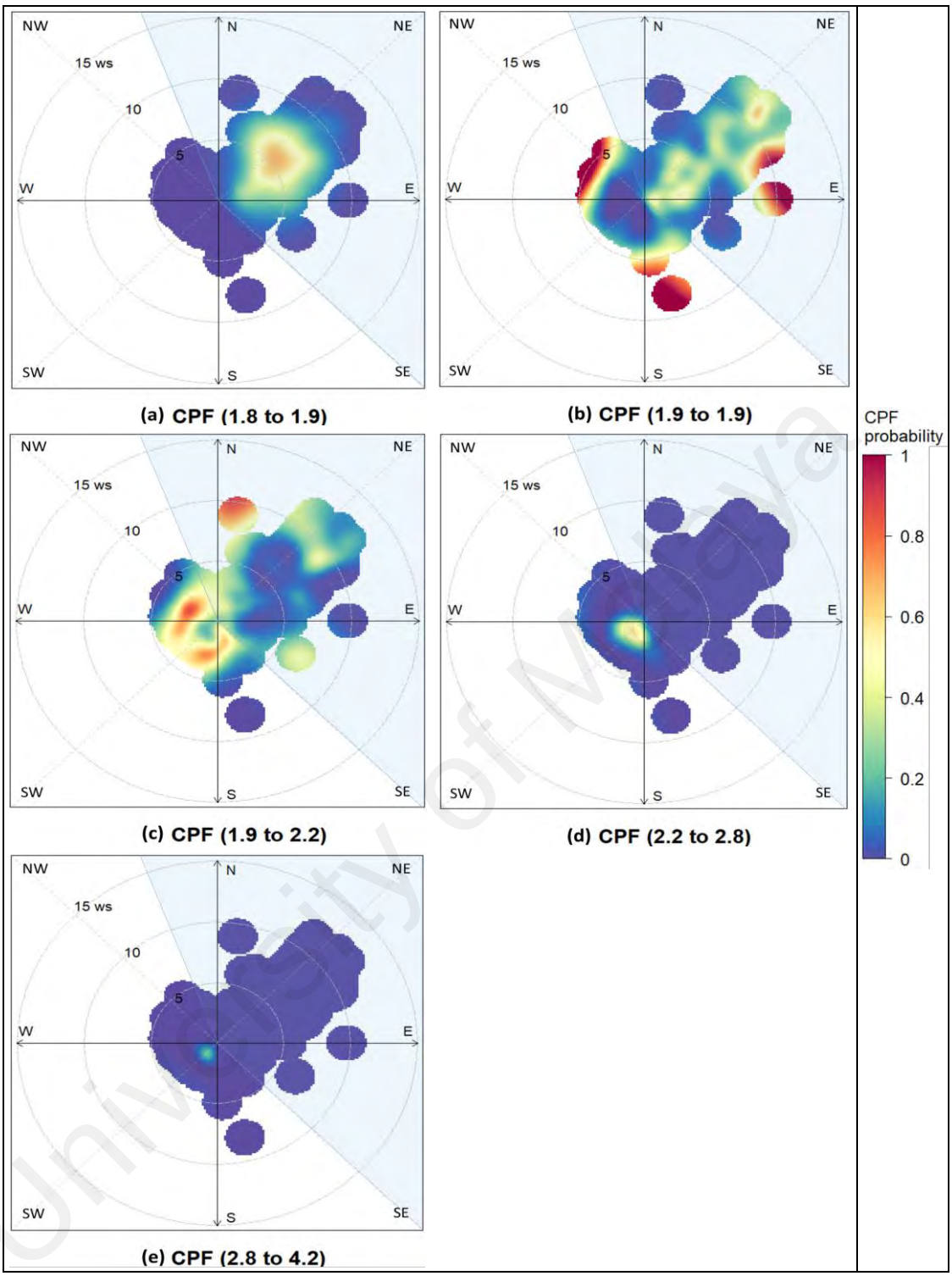

Figure 4.28: Polar plot of hourly CH_4 (ppm) at BMRS based on the CPF function for a range of percentile intervals from (a) Minimum to Q1 (b) Q1 to Q2 (c) Q2 to Q3 (d) Q3 to 95th percentile and (e) 95th percentile to maximum during days with land sea breeze in the NE monsoon

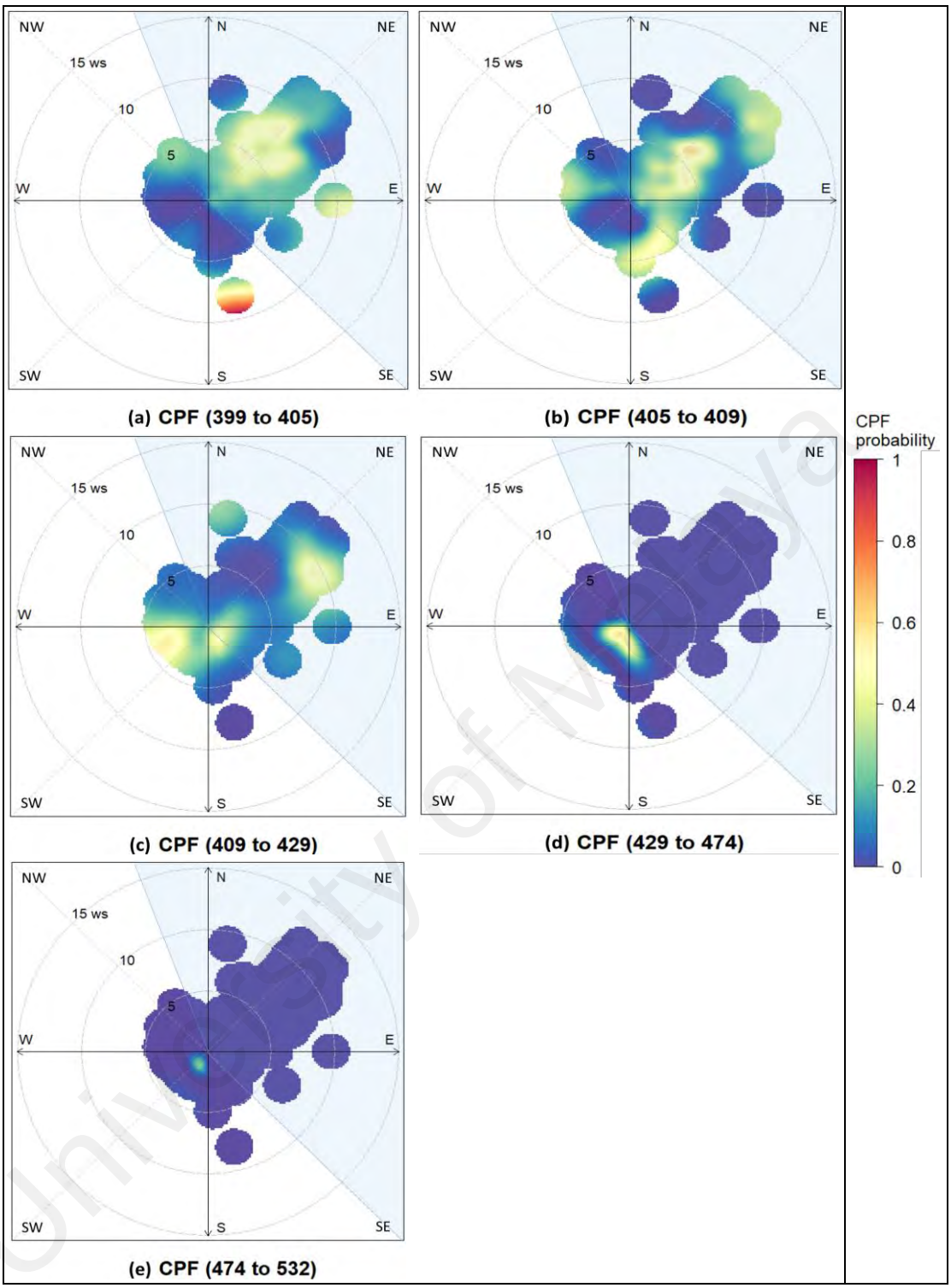

Figure 4.29: Polar plot of hourly CO_2 (ppm) at BMRS based on the CPF function for a range of percentile intervals from (a) Minimum to Q1 (b) Q1 to Q2 (c) Q2 to Q3 (d) Q3 to 95th percentile and (e) 95th percentile to maximum during days with land sea breeze in the NE monsoon

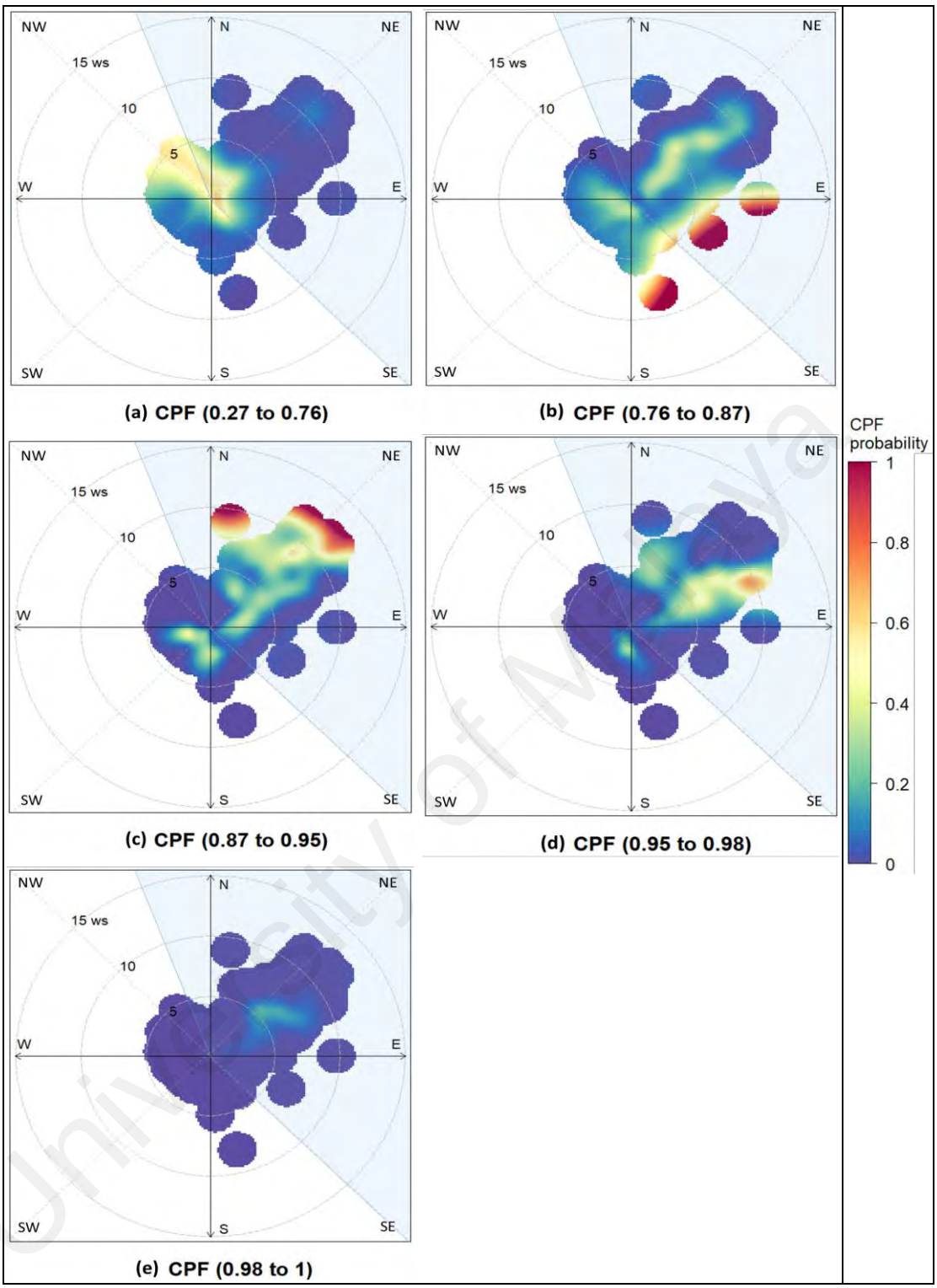

Figure 4.30: Polar plot of hourly RPM at BMRS based on the CPF function for a range of percentile intervals from (a) Minimum to Q1 (b) Q1 to Q2 (c) Q2 to Q3 (d) Q3 to 95th percentile and (e) 95th percentile to maximum during days with land sea breeze in the NE monsoon

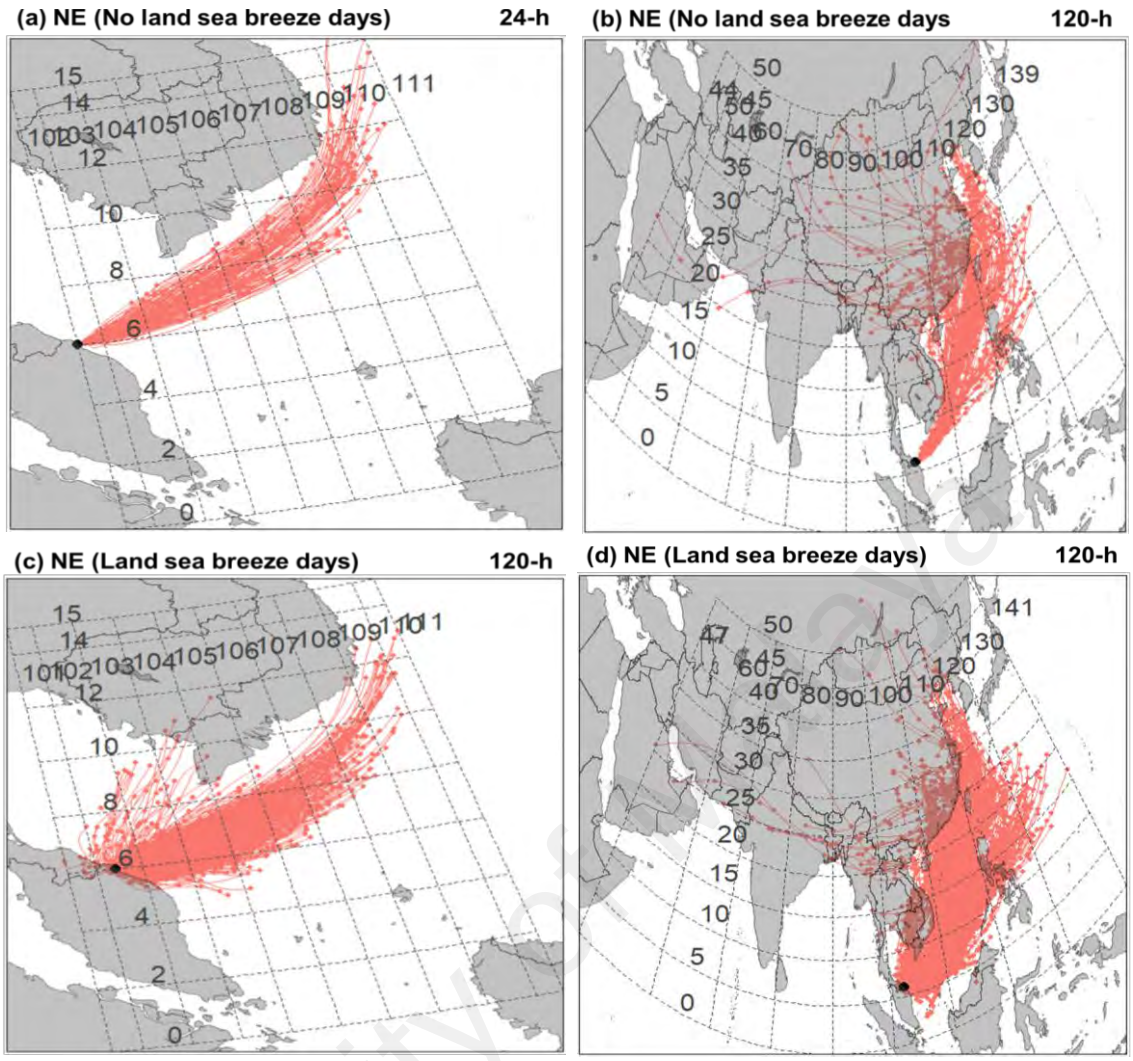

Figure 4.31: Individual back-trajectories during days with land sea breeze ((b) and (d)) and days with suppressed land sea breeze ((a) and (c)) in the NE monsoon. Source ● is at 6.0086 N and 102.4259 E (BMRS location)

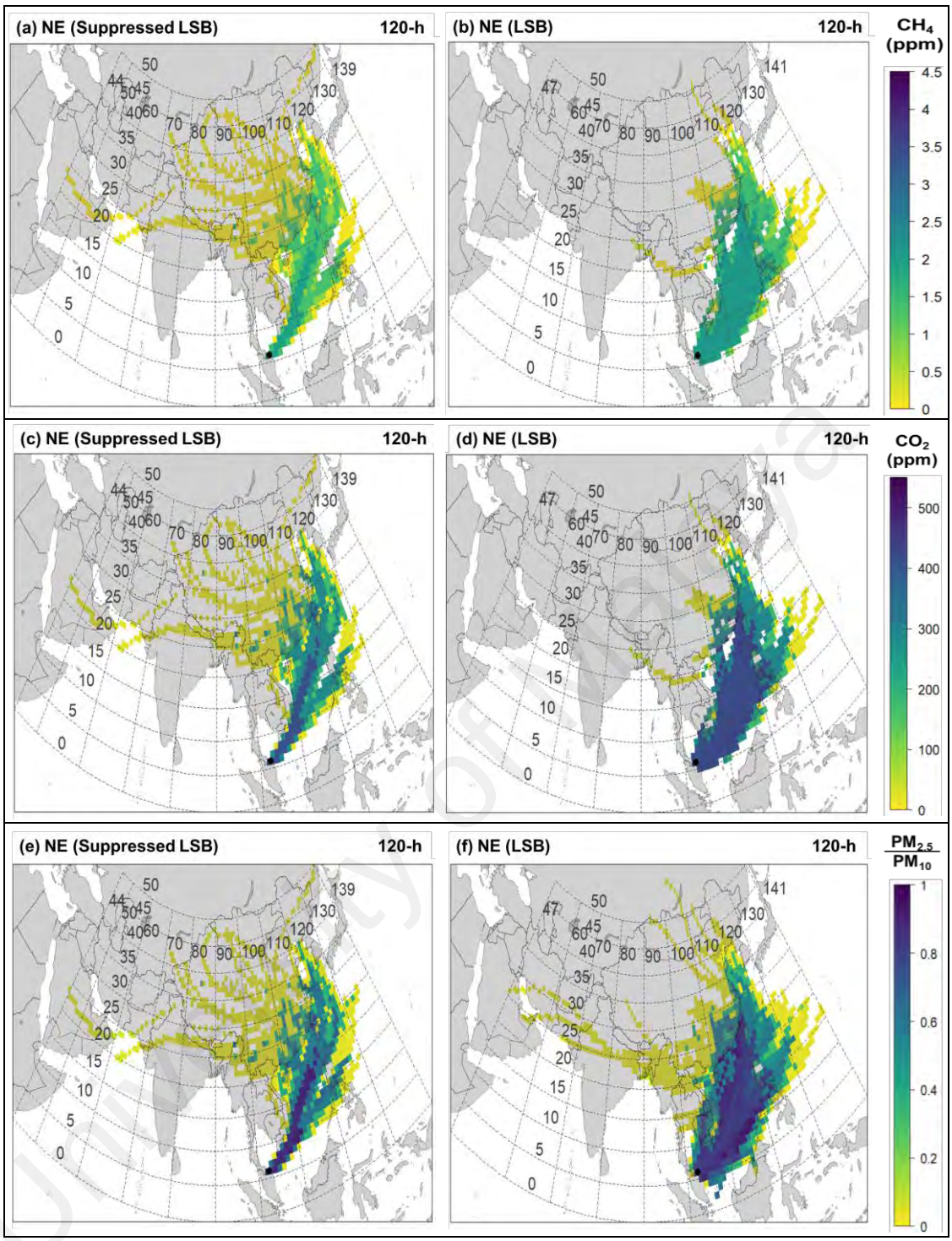

Figure 4.32: CWT for CH4 (a and b), CO2 (c and d) and RPM (e and f) during days with land sea breeze (2nd column) and days with suppressed land sea breeze (1st column) in NE monsoon. Source ● is at 6.0086 N and 102.4259 E (BMRS location). Range of colors for the CWT described from non-source areas (yellow) to strongest source areas (dark blue) of pollutants at BMRS

BMRS was associated with strong influence of local and regional sources during the SW monsoon. Figure 4.24 (b) shows that the air originates from both the land (blue lines – 58%) and sea (green and red lines – 42%) regions within 24-hour trajectories time. This also shows the formation of land sea breeze at BMRS. The 120-hour cluster trajectory (Figure 4.24 (d)) also shows that the air can be affected by the regional sources which contributed to 50% percentages from the overall trajectories. BMRS can also be influenced by the long-range transport of air which originated from the Indian Ocean (17%) and Kalimantan, Indonesia (33%).

CPFP plots for all CH_4 and CO_2 during the days with suppressed land sea breeze in the SW monsoon are shown in Figure 4.33 and Figure 4.34 respectively. The CPFP plot for RPM is not able to be generated owing to the lack of data in respective wind direction – wind speed sectors. CPFP plot for CH_4 and CO_2 also show less definite source areas due to the lack of data. However, the 75th to 95th percentiles of CH_4 and CO_2 were associated with light offshore wind (Figure 4.33 and Figure 4.34 respectively). The individual trajectories associated without land sea breeze days during the SW monsoon are shown in Figure 4.38 (a) and (b). BMRS was influenced by higher flows of air from the land area which originated from the west and southwest directions (Figure 4.38 (a)). There is transboundary transport of air masses based on the 120-hour trajectories as shown in Figure 4.38 (b). HYSPLIT-CWT analysis indicates that the principal (high) sources of the CH_4 (Figure 4.39 (a)) and CO_2 (Figure 4.39 (c)) during this period was mainly originated from the northern region of Peninsular Malaysia and area near the border of Malaysia-Thailand.

On the other hand, CPFP plots for air pollutants during the days with land sea breeze in the SW monsoon are shown in Figure 4.35 to Figure 4.37. Figure 4.35 (a) and (b) show that CH_4 within the minimum to 50^{th} percentile was associated with both onshore and

offshore winds. Meanwhile, CH_4 ranging from the 50th percentile to its maximum were highly originated from the southwest direction (offshore wind) as shown in Figure 4.35 (c) to (e). CO_2 (Figure 4.36) also shows similar wind directions and wind speed contributed to the respective interval of percentiles as CH_4. Figure 4.37 shows the CPFP plot for RPM. This plot shows light offshore wind highly contributed to the minimum to 25th percentile of RPM and this range (RPM within 0.40 to 0.96) indicates a presence of both fine and coarse particles. Then, RPM within 25th to 75th percentiles were originated from both land (offshore wind) and sea (onshore wind) areas (Figure 4.37 (b) and (c)). The remaining RPM ranging from its 75th percentile to maximum shown high influence of moderate onshore wind (northeasterly). Individual backward trajectories during this period reveals that BMRS was strongly influenced by the local and mesoscale flows of air from the Peninsular Malaysia region within 24-hour trajectories time (Figure 4.38 (c)). This period was also attributed to more transboundary transport of air masses from the areas over the SCS, Indian Ocean, Java Sea (Figure 4.38 (d)). HYSPLIT-CWT analysis shows the principal sources of CH_4 (Figure 4.39 (b)) and CO_2 (Figure 4.39 (d)) were originated from the central regions of Peninsular Malaysia, the SCS, Indian Ocean and Java Sea. These source regions were also associated with strong presence of fine particles based on the HYSPLIT-CWT analysis for RPM as shown in Figure 4.39 (e).

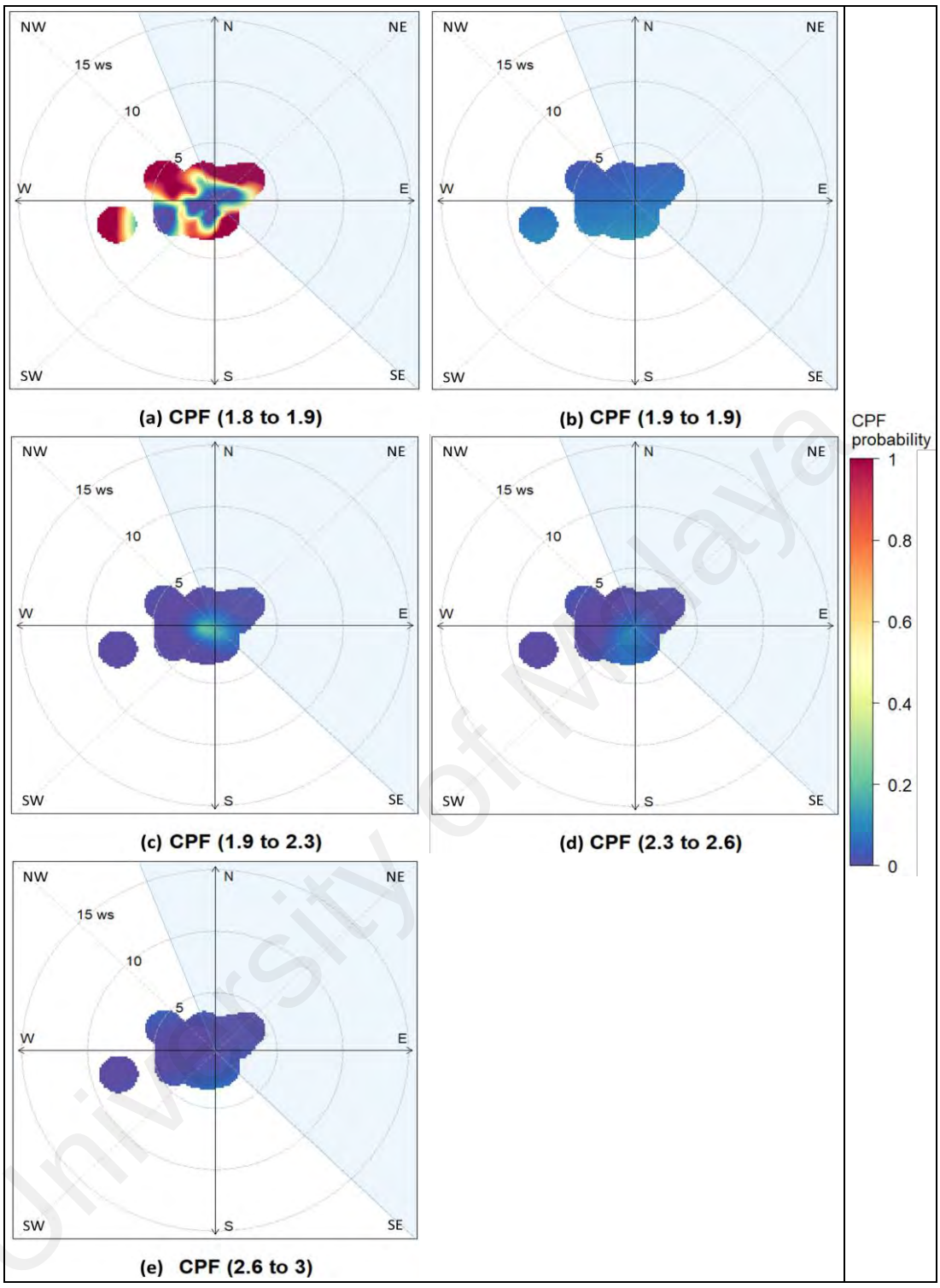

Figure 4.33: Polar plot of hourly CH_4 (ppm) at BMRS based on the CPF function for a range of percentile intervals from (a) Minimum to Q1 (b) Q1 to Q2 (c) Q2 to Q3 (d) Q3 to 95th percentile and (e) 95th percentile to maximum during days with suppressed land sea breeze in the SW monsoon

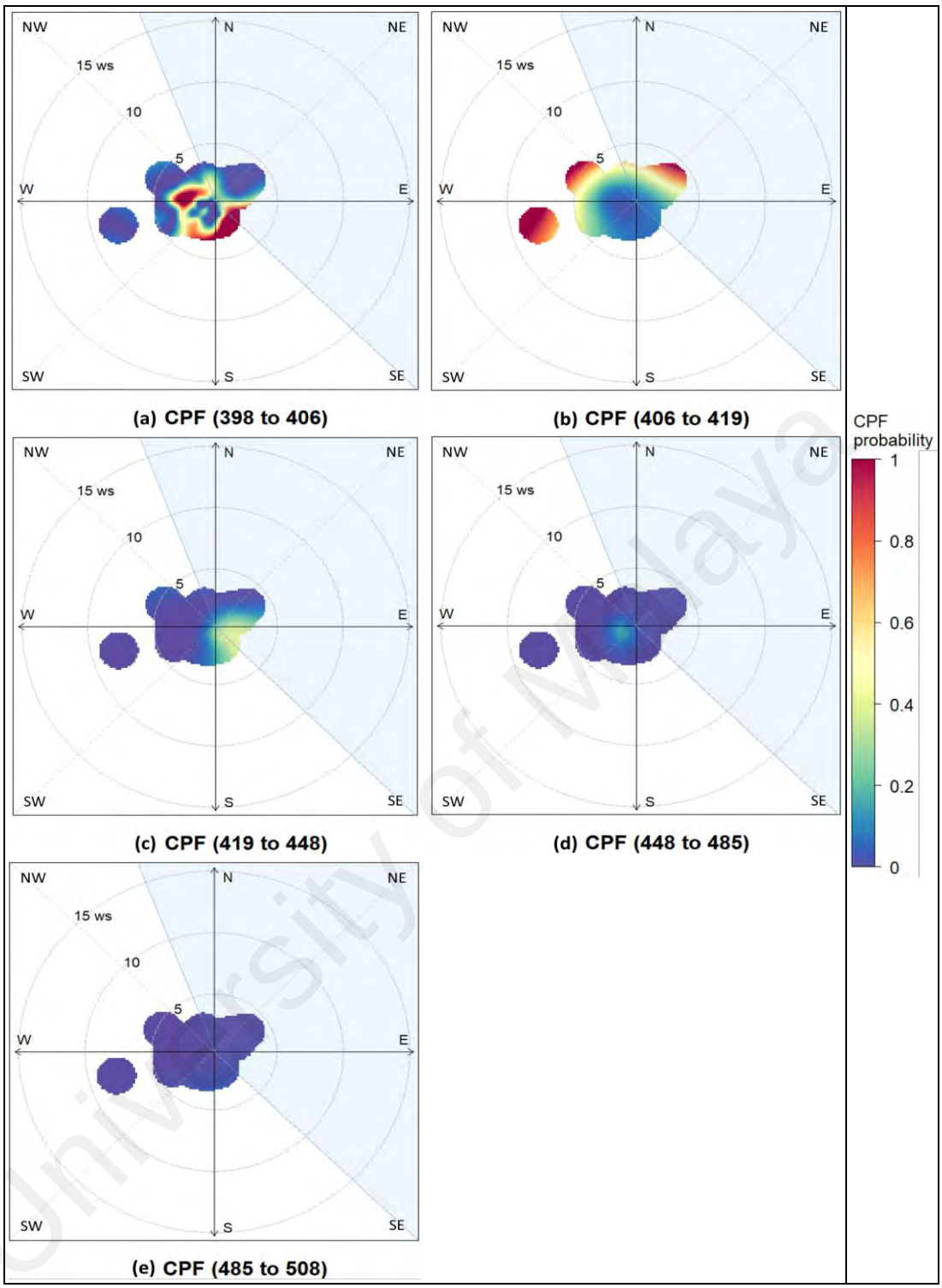

Figure 4.34: Polar plot of hourly CO_2 (ppm) at BMRS based on the CPF function for a range of percentile intervals from (a) Minimum to Q1 (b) Q1 to Q2 (c) Q2 to Q3 (d) Q3 to 95th percentile and (e) 95th percentile to maximum during days with suppressed land sea breeze in the SW monsoon

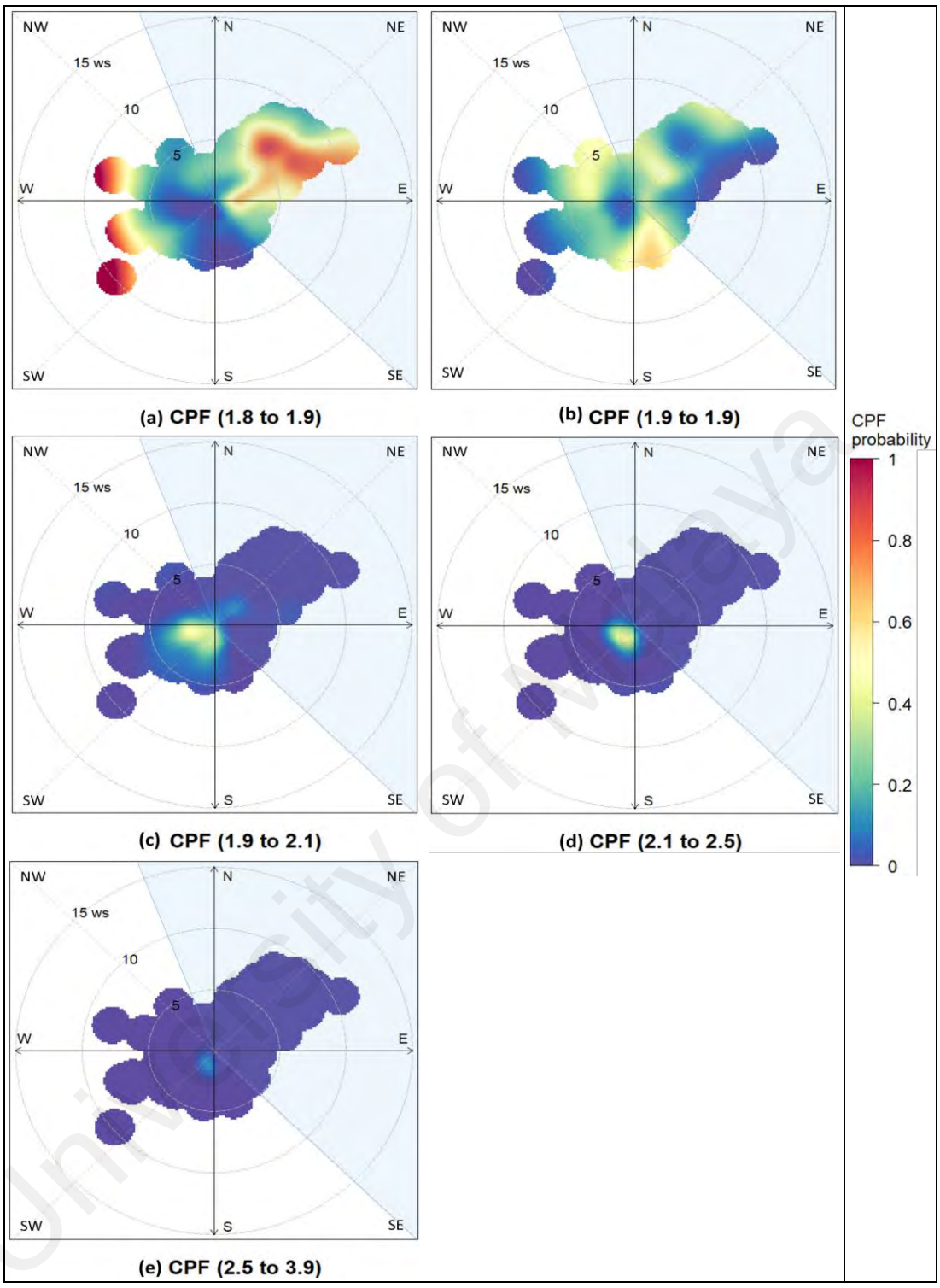

Figure 4.35: Polar plot of hourly CH_4 (ppm) at BMRS based on the CPF function for a range of percentile intervals from (a) Minimum to Q1 (b) Q1 to Q2 (c) Q2 to Q3 (d) Q3 to 95th percentile and (e) 95th percentile to maximum during days with land sea breeze in the SW monsoon

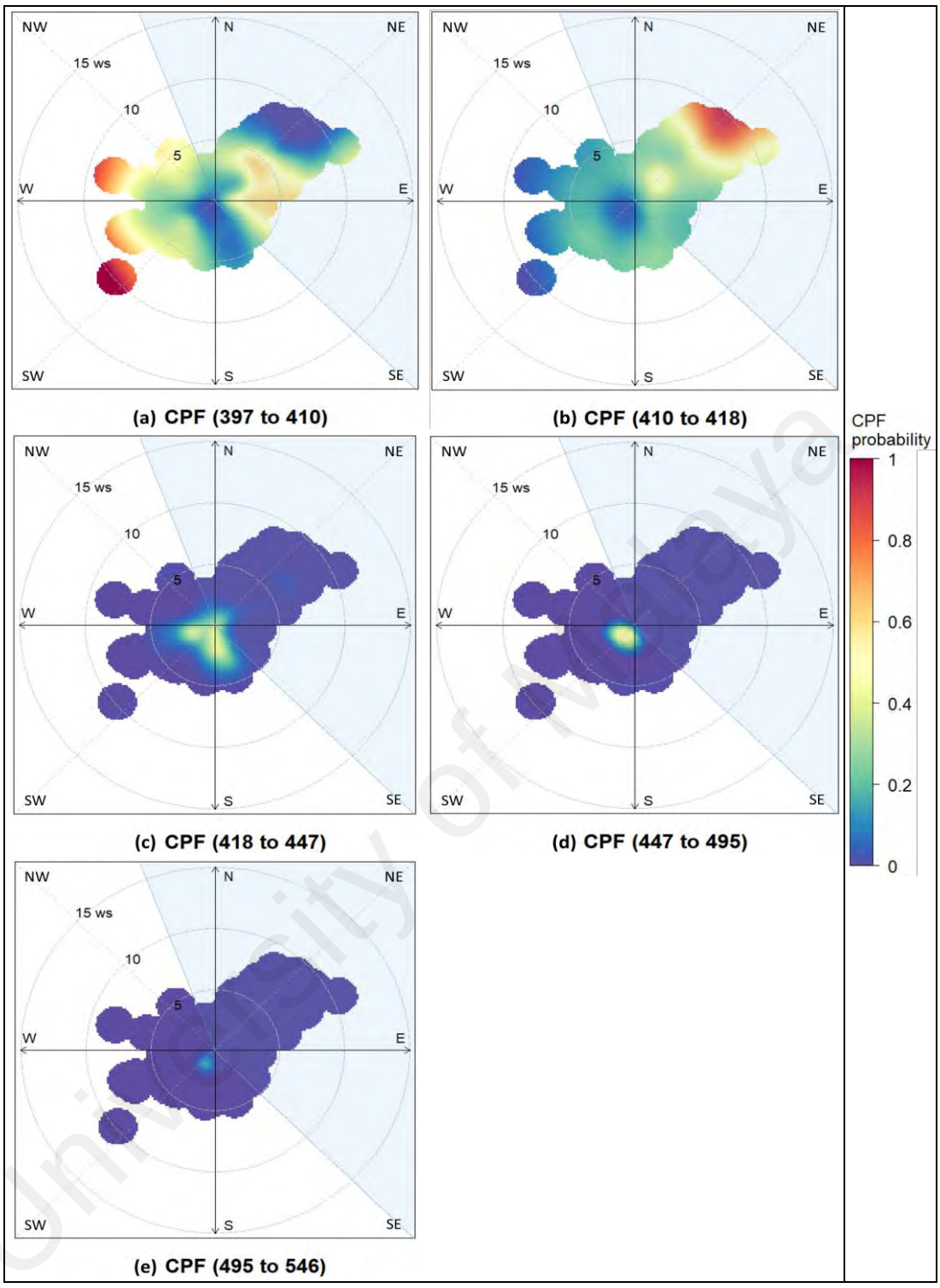

Figure 4.36: Polar plot of hourly CO_2 (ppm) at BMRS based on the CPF function for a range of percentile intervals from (a) Minimum to Q1 (b) Q1 to Q2 (c) Q2 to Q3 (d) Q3 to 95th percentile and (e) 95th percentile to maximum during days with land sea breeze in the SW monsoon

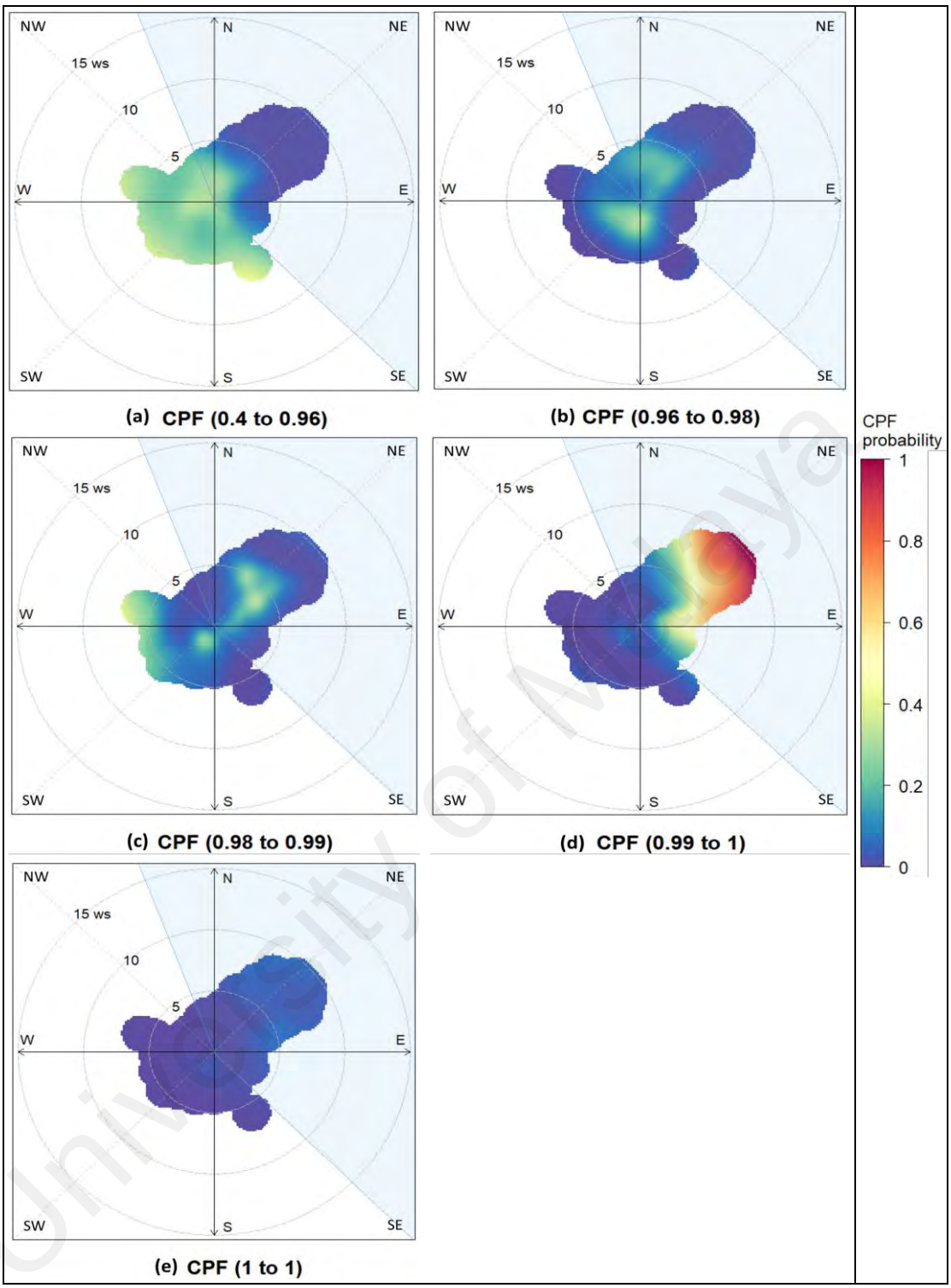

Figure 4.37: Polar plot of hourly RPM at BMRS based on the CPF function for a range of percentile intervals from (a) Minimum to Q1 (b) Q1 to Q2 (c) Q2 to Q3 (d) Q3 to 95th percentile and (e) 95th percentile to maximum during days with land sea breeze in the SW monsoon

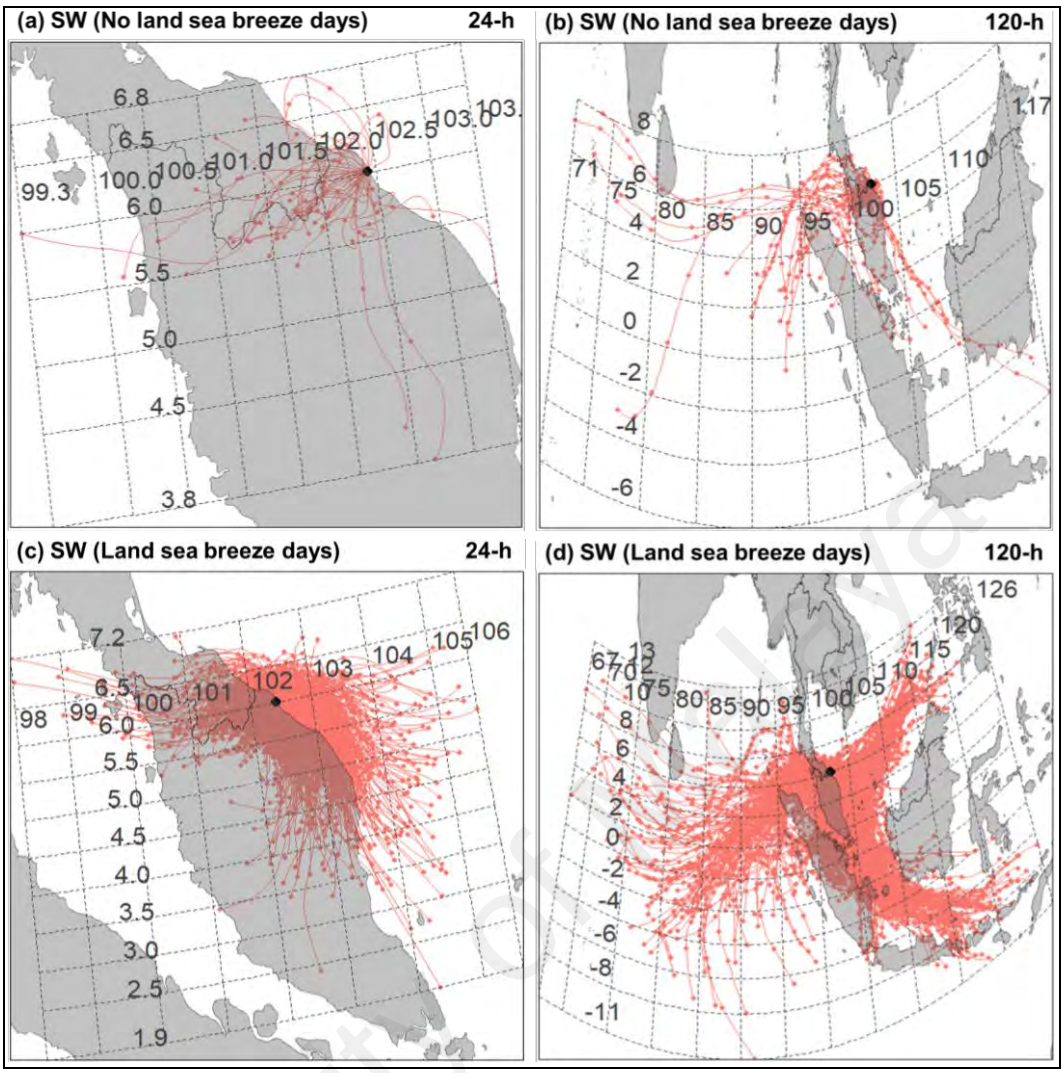

Figure 4.38: Individual back-trajectories days with land sea breeze ((b) and (d)) and days with suppressed land sea breeze ((a) and (c)) in SW monsoon. Source ● is at 6.0086 N and 102.4259 E (BMRS location)

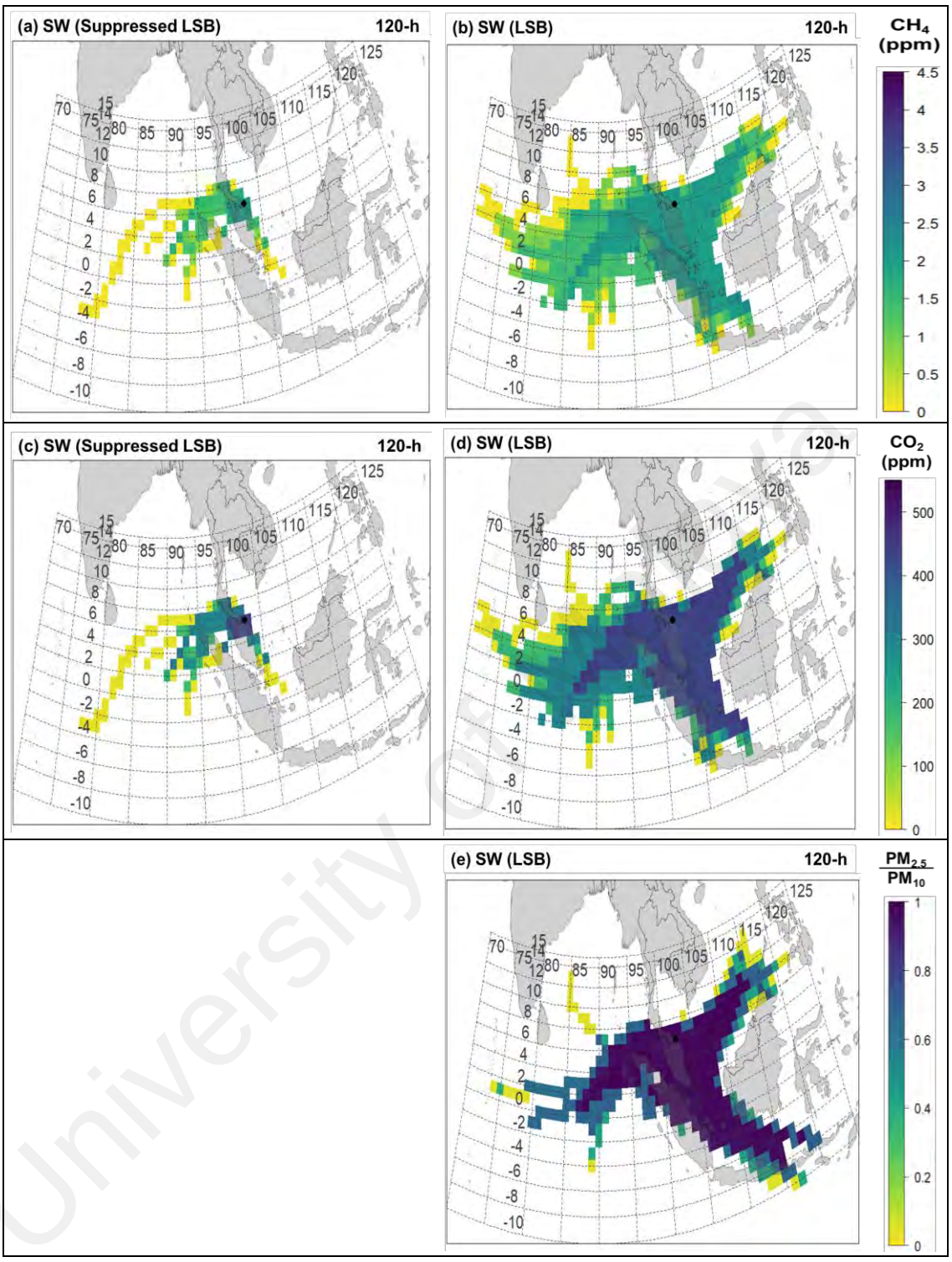

Figure 4.39: CWT for CH4 (a and b), CO2 (c and d) and RPM (e) during days with suppressed land sea breeze (1st column) and days with land sea breeze (2nd column) in SW monsoon. Source ● is at 6.0086 N and 102.4259 E (BMRS location). Range of colors for the CWT described from non-source areas (yellow) to strongest source areas (dark blue) of pollutants at BMRS

The CPFP plot is a useful tool for source identification and characterisation of air pollutants at BMRS while HYSPLIT-CWT analysis is beneficial to determine potential regional or transboundary sources of the air pollutants based on its respective lifetimes and wider flows of air masses. Table 4.7 shows the summary on the transport of air pollutants at BMRS under the dominant influence of local and synoptic meteorological conditions in the NE and SW monsoons. BMRS is influenced by low levels of air pollutants during days with suppressed land sea breeze in the NE monsoon. HYSPLIT-CWT show that BMRS is highly influenced by long-range transport of CO_2 and CH_4 from the East Asia, ECS and SCS. However, high CO_2 and CH_4 during this period are both associated with both onshore and offshore wind using the CPFP plots. This indicate a combination of local and transboundary sources of air pollutants. Hence, case studies are conducted to specifically examine the transboundary sources of air pollutants during the NE monsoon. Meanwhile, days with suppressed land sea breeze in SW monsoon shows no significant difference in regard to its transport of air pollutants as compared to days with land sea breeze. Both periods are attributed by local and regional transport of air pollutants around BMRS.

Table 4.7: Summary on the transport of air pollutants at BMRS during days with and without suppressed land sea breeze in the NE and SW monsoon

Transport of air pollutants during days with suppressed land sea breeze	
NE monsoon	**SW monsoon**
1. CPFP plots show high CO_2 and CH_4 (above its 95th percentile values) are influenced by both onshore and offshore winds – an indication of both local and long-range transport of pollutants respectively; while high RPM (above its 95th percentile) are influenced by onshore wind. 2. HYSPLIT-CWT analysis shows the principal (high) sources of CO_2, CH_4 and RPM (within 120 hours) are the SCS, ECS and continental regions of China.	1. CPFP plots show high CO_2 and CH are influenced by offshore wind 2. HYSPLIT-CWT analysis shows the principal (high) sources of CO_2 and CH_4 are the northern region of Peninsular Malaysia and area over the border of Malaysia-Thailand.
Transport of air pollutants during days with land sea breeze	
NE monsoon	**SW monsoon**
1. CPFP plots show high CO_2 and CH_4 are influenced by offshore wind – an indication of local sources of pollutants; while high RPM are influenced by onshore wind. 2. HYSPLIT-CWT analysis shows the principal (high) sources of CO_2, CH_4 and RPM are the SCS and ECS	1. CPFP plots show high CO_2 and CH are influenced by offshore wind; while high RPM are influenced by offshore and onshore wind 2. HYSPLIT-CWT analysis shows the principal (high) sources of CO_2, CH_4 and RPM are the areas along the east coast of Peninsular Malaysia, the Indian Ocean, SCS and the Java Sea.

4.2 Variabilities of meteorological parameters and air pollutants at BMRS during case studies

The results shown below are based on the case study undertaken three days each during the NE and SW monsoon periods in 2016. CS1 was conducted from 25 to 27 January 2016 while CS2 was conducted from 3 to 5 June 2016. These two case studies were conducted thoroughly to examine the effects of the strong synoptic and local meteorological conditions on the atmospheric concentration of CH_4, CO_2, PM_{10} and

$PM_{2.5}$. Hourly ERA5 reanalysis winds data at 10 m and radiosonde data were added to examine these case studies in depth. It should be noted that there is a period of missing data during CS2 due to technical issues. However, the important features of local meteorological condition and its impact are able to be captured and described. For both case studies, the bootstrapping approach was also implemented for both case studies to prove the significance of the correlation achieved between the pollutants and the meteorological parameters at BMRS.

Table 4.8 and Table 4.9 show the statistical summary of 1-minute averaged data during CS1 and CS2 respectively. The basic statistical terms used are: minimum, median, mean, maximum, 1st quartile, 3rd quartile and standard deviation. Average results indicated lower temperature and higher wind speed were present during CS1 compared to CS2. During CS2, standard deviations suggested that the data was distributed over a broader range of values compared to CS1.

Table 4.8: Descriptive analysis of the 1-minute averaged of CH_4, CO_2, PM_{10}, $PM_{2.5}$, T, WS and WD at BMRS (tower data) during CS1

	CH_4 (ppm)	CO_2 (ppm)	PM_{10} (μgm^{-3})	$PM_{2.5}$ (μgm^{-3})	T (°C)	WS (ms^{-1})	WD (°)
Available data (%)	80.6	80.6	100.0	100.0	99.9	99.9	99.9
Min	1.899	407.50	3.50	3.20	24.26	5.30	26.80
Q1	1.918	409.00	8.50	7.90	27.59	10.20	49.80
Median	1.934	410.50	10.00	9.20	27.85	11.40	55.90
Mean	1.933	410.60	10.35	9.37	27.79	11.48	55.10
Q3	1.947	412.40	11.80	10.60	28.16	12.70	60.70
Max	1.999	415.10	30.30	21.60	28.73	18.50	83.90
SD	0.017	1.92	2.83	2.19	0.57	1.83	7.74

Note: Min: Minimum; Q1: Quartile 1; Q3: Quartile 3; Max: Maximum; SD: Standard Deviation

Table 4.9: Descriptive analysis of the 1-minute average of CH_4, CO_2, PM_{10}, $PM_{2.5}$, T, WS and WD at BMRS (tower data) during CS2

	CH_4 (ppm)	CO_2 (ppm)	PM_{10} (μgm^{-3})	$PM_{2.5}$ (μgm^{-3})	T (°C)	WS (ms^{-1})	WD (°)
Available data (%)	54.6	54.6	71.5	71.5	56.4	56.4	56.4
Min	1.822	398.70	0.60	0.60	25.75	0.30	2.90
Q1	1.841	407.00	3.00	2.90	29.44	1.00	57.50
Median	1.852	412.50	4.40	4.30	29.91	1.80	69.80
Mean	1.901	424.00	7.08	6.99	29.52	2.68	110.30
Q3	1.928	426.30	9.80	9.70	30.50	4.50	172.70
Max	2.440	513.00	39.70	39.50	33.23	10.70	354.70
SD	0.105	26.98	5.98	5.96	1.54	2.06	69.99

Note: Min: Minimum; Q1: Quartile 1; Q3: Quartile 3; Max: Maximum; SD: Standard Deviation

4.2.1 Meteorological conditions and its effect on air pollutants during CS1

For CS1, seventeen radiosondes were specifically launched in every three hours from 11:00 LT on 25 January 2016 to 11:00 LT on 27 January 2016. The meteorological conditions, its characteristics, effects on the variations and transport of air pollutants during CS1 are examined in this section.

4.2.1.1 Characteristics of strong synoptic condition during CS1

NE monsoon in Southeast Asia are frequently influenced by the synoptic scale flows (Chang et al., 1979; Chang et al., 2005; Lim & Samah, 2004). Synoptic flows are able to affect air pollution at a regional and across the basin (Beaver & Palazoglu, 2009). Cold surge is considered as an event that is affected by the strong synoptic condition between the SMH and Southeast Asia regions. Figure 4.40 shows that there is strong pressure gradient between 5°N and 30°N, indicating mechanism on the synoptic influence at BMRS during this period. The shaded grey rectangle in Figure 4.41 indicates the indices of the cold surge during CS1. It demonstrates an onset of cold surge started to commence

two days before the CS1 (23 January 2016). It strengthened on 24 January then weakened to mild cold surge (cold surge index = −10 ms^{-1}) on 25 January and stopped on the following two days of CS1. Despite no cold surge detected on the second and third day of CS1, the northeasterly winds were still strong and persisted consistently over BMRS throughout the whole period of CS1 as shown by ERA5's wind speed at 10 m (Figure 4.42 (a)), radiosonde's data (Figure 4.43), and tower's data (blue lines of Figure 4.41 and Figure 4.49 (d)) with mean values of ~11 ms^{-1} (Table 4.8). Figure 4.42 (a) also shows strong onshore (northeasterly) winds flowing from the northern SCS to the coastal areas of Vietnam and then flowed towards BMRS. Meanwhile, Figure 4.42 (b) shows the strong winds that penetrated inland for about 60 km from BMRS and other areas along the east coast of Peninsular Malaysia were also affected. The figure also shows the evolution of frictional convergence. As the strong winds hit coast, the mechanical forcing formed due to the discontinuity in the surface roughness, thus induce lifting and cloud formations (Roeloffzen et al., 1986) along the east coast or at the northeastern part of Peninsular Malaysia. This condition was also associated with the presence of strong easterly winds at BMRS which prevailed from the surface up to 2500 m (Figure 4.43 and Figure 4.46 (a)) with high relative humidity (> 80%) (Figure 4.45). Strong northeasterly winds were clearly shown within 1000 m height as shown by the averages u and v component of winds in Figure 4.46 (a) and (b) respectively. The 1-minute time series of wind (Figure 4.49 (b), (c) and (d)) from BMRS tower also shows strong northeasterly wind dominated the wind flow during the whole period of CS1. This characteristic is accompanied with weakened vertical thermal gradient as shown by the temperature evolutions over BMRS (Figure 4.44) where clear thermal gradient only shown within 600 m. Subsequently, this condition led to the suppression of the local meteorological condition – land sea breeze at BMRS. The 1-minute time series of temperature (Figure 4.49 (a)) from AWS at BMRS tower shows similar surface variations as radiosonde data where significant drop of

temperature clearly shown from 02:00 to 05:00 LT, 26 January 2016. Daily averaged of TRMM data (Figure 4.48) shows slight rain (following Department of Environment of Malaysia rainfall rate index) occurred over SCS along the northeast coast of Peninsular Malaysia on the second and third day of CS1. Formation of clouds were also clearer during days with the presence of rain as shown in Figure 4.47.

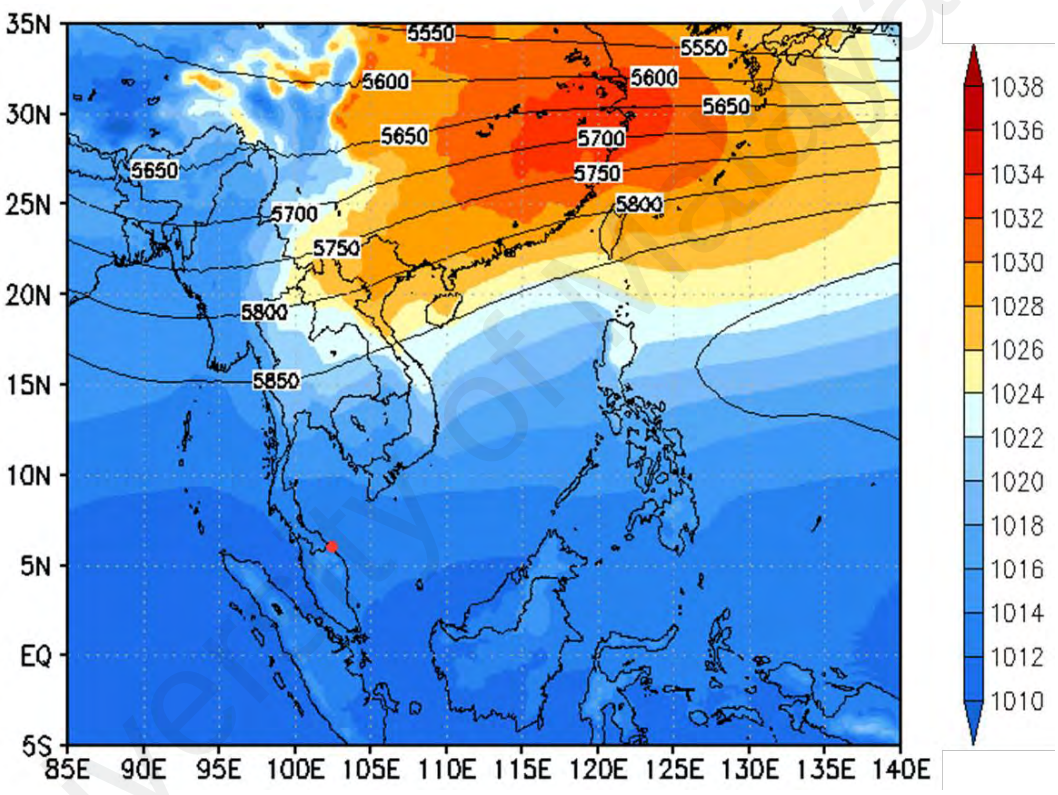

Figure 4.40: Average MSLP (hPa) (shaded regions) with geopotential height at 500 hPa (contour lines) during CS1. The red dot (●) is the location of BMRS

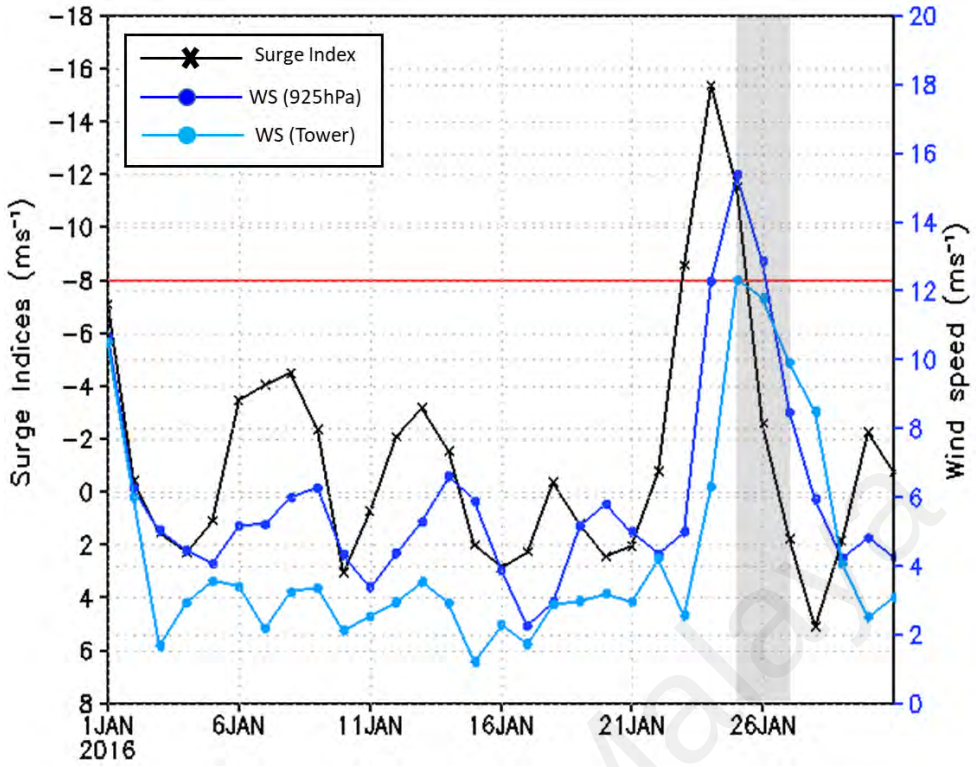

Figure 4.41: Cold surge indices calculated for January 2016. Red lines indicate the baseline where cold surge occurred (cold surge indices < −8 ms-1). Light blue colored time series shows the daily averaged wind speed calculated based on the AWS data at BMRS tower meanwhile the dark blue colored time series shows the 925 hPa wind speed at BMRS. The grey shaded area represents the cold surge indices during CS1

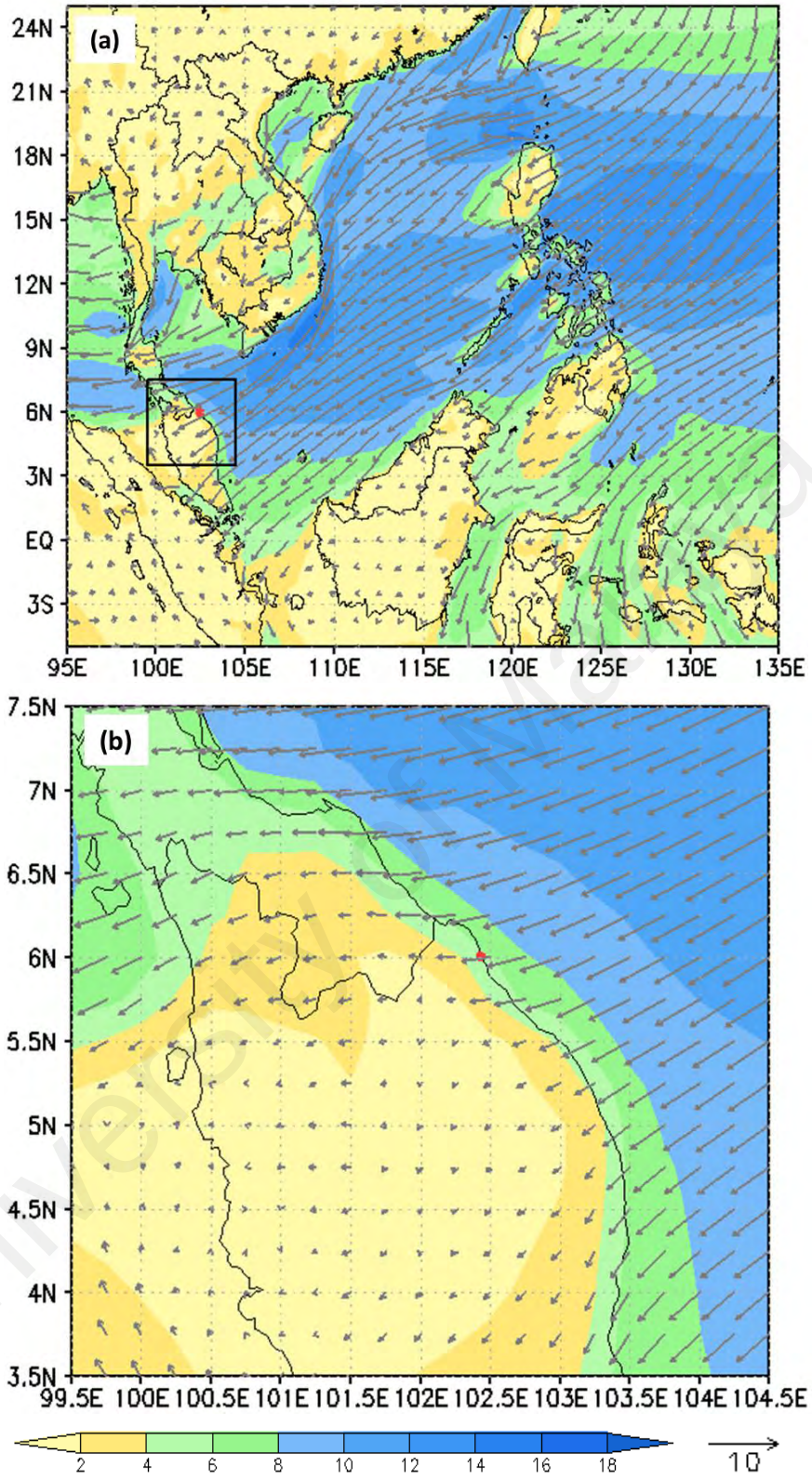

Figure 4.42: Average ERA5's wind speed and wind vectors at 10 m during CS1 where (a) Regions covered from 5°S to 24°N and 95°E to 135°E and (b) Regions covered from 3.5 °N to 7.5 °N and 99.5°E to 105°E zoomed from (a) (Small black box). Each wind vector represents 10 ms-1 wind speed. The red dot (●) is the location of BMRS

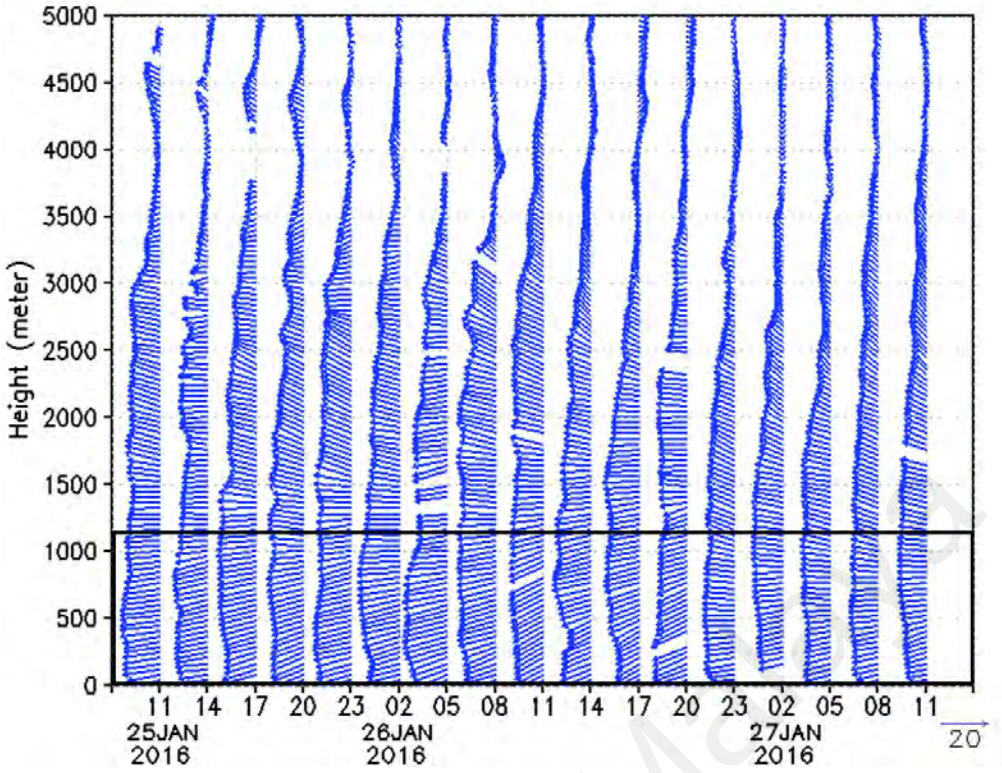

Figure 4.43: Time-height evolutions of wind vectors during CS1 from 1100 LT on 25 January 2016 to 1100 LT on 27 January 2016 within 5000 m height. Small black box in represents height at 1200 m. Each wind vector represents in the unit of ms-1

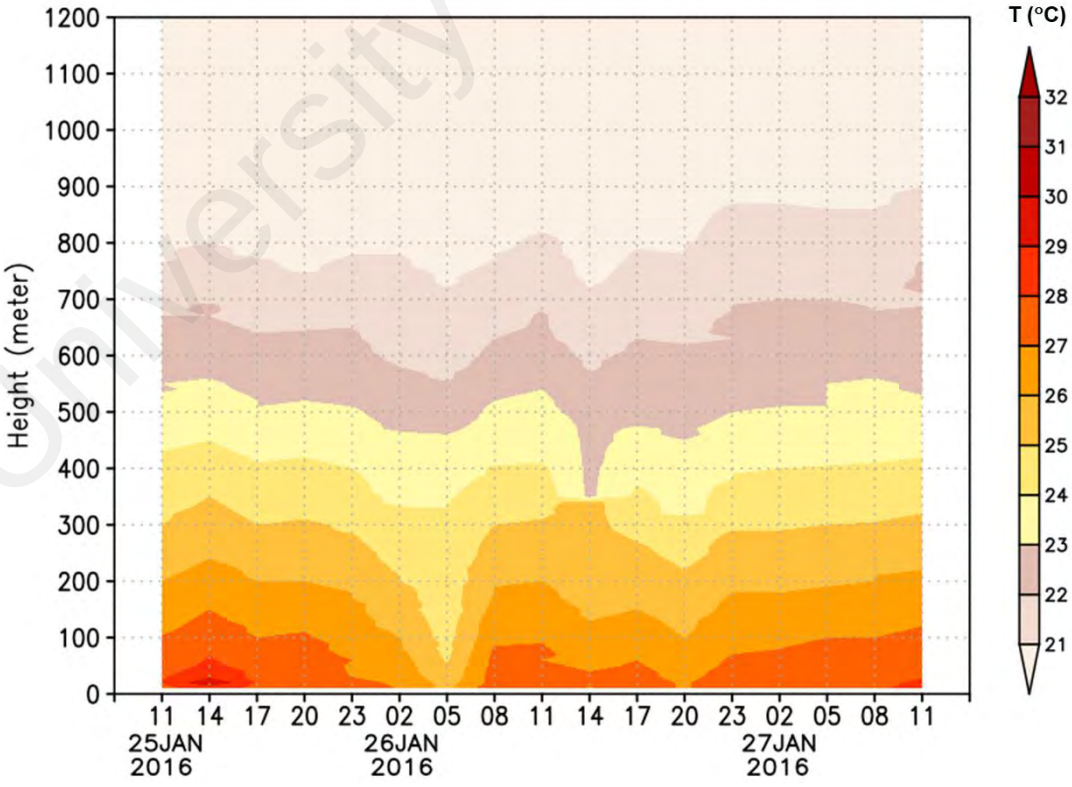

Figure 4.44: Time-height evolutions of air temperature (T) during CS1 within 1200 m height (within the black box of Figure 4.40)

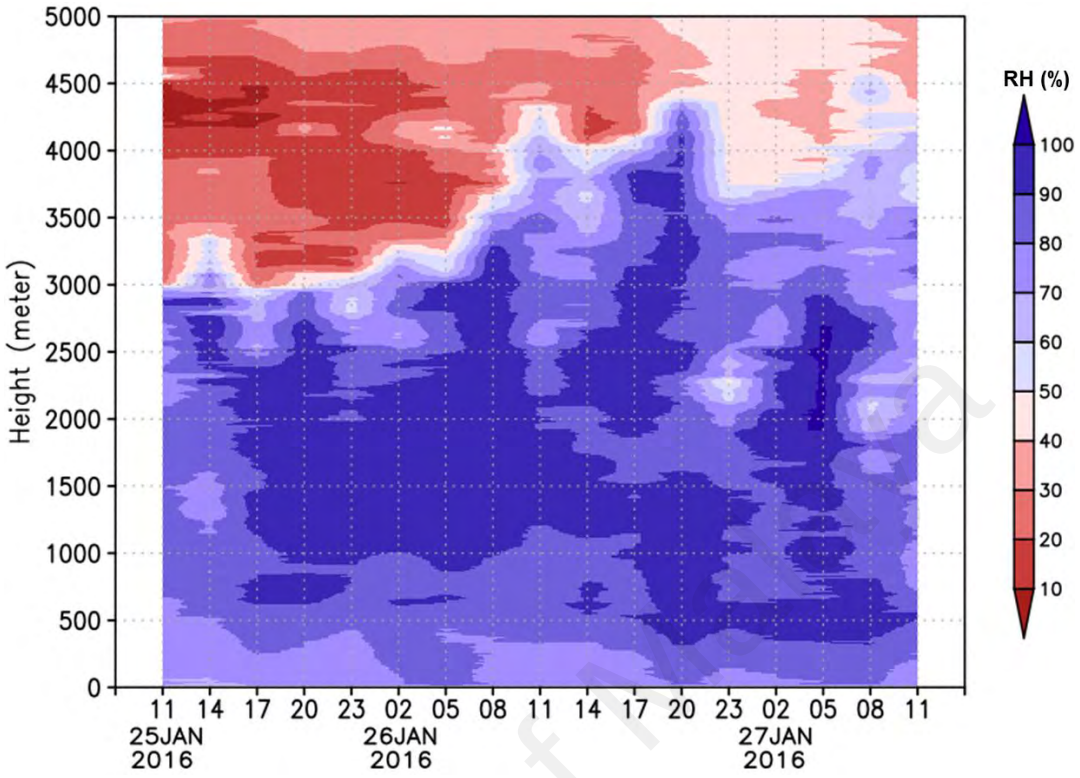

Figure 4.45: Time-height evolutions of relative humidity (RH) during CS1 within 5000 m height

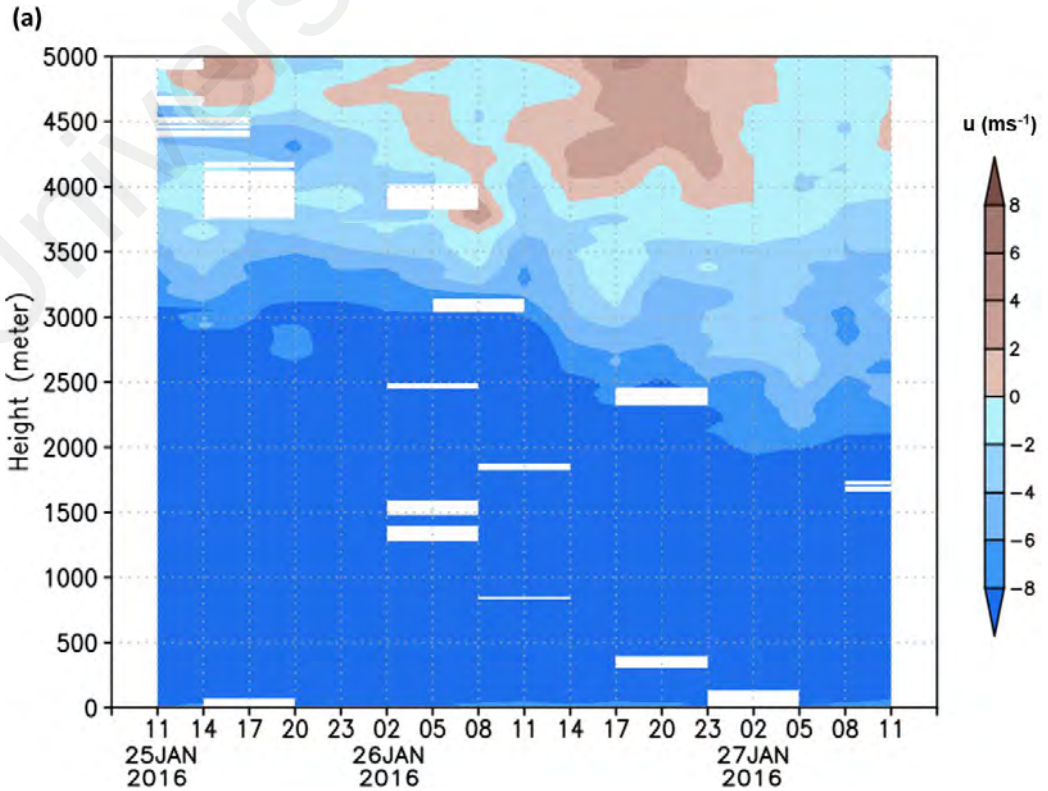

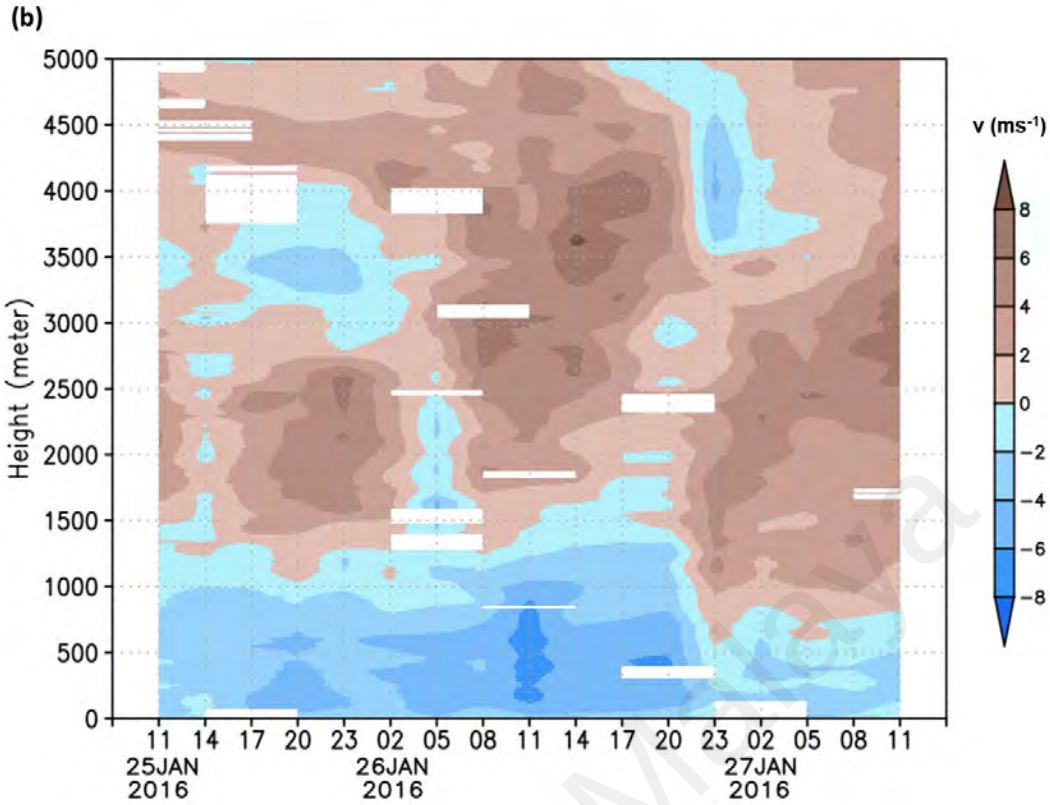

Figure 4.46: Time-height evolutions of (a) zonal winds (u) and (b) meridional winds (v) during CS1 within 5000 m height

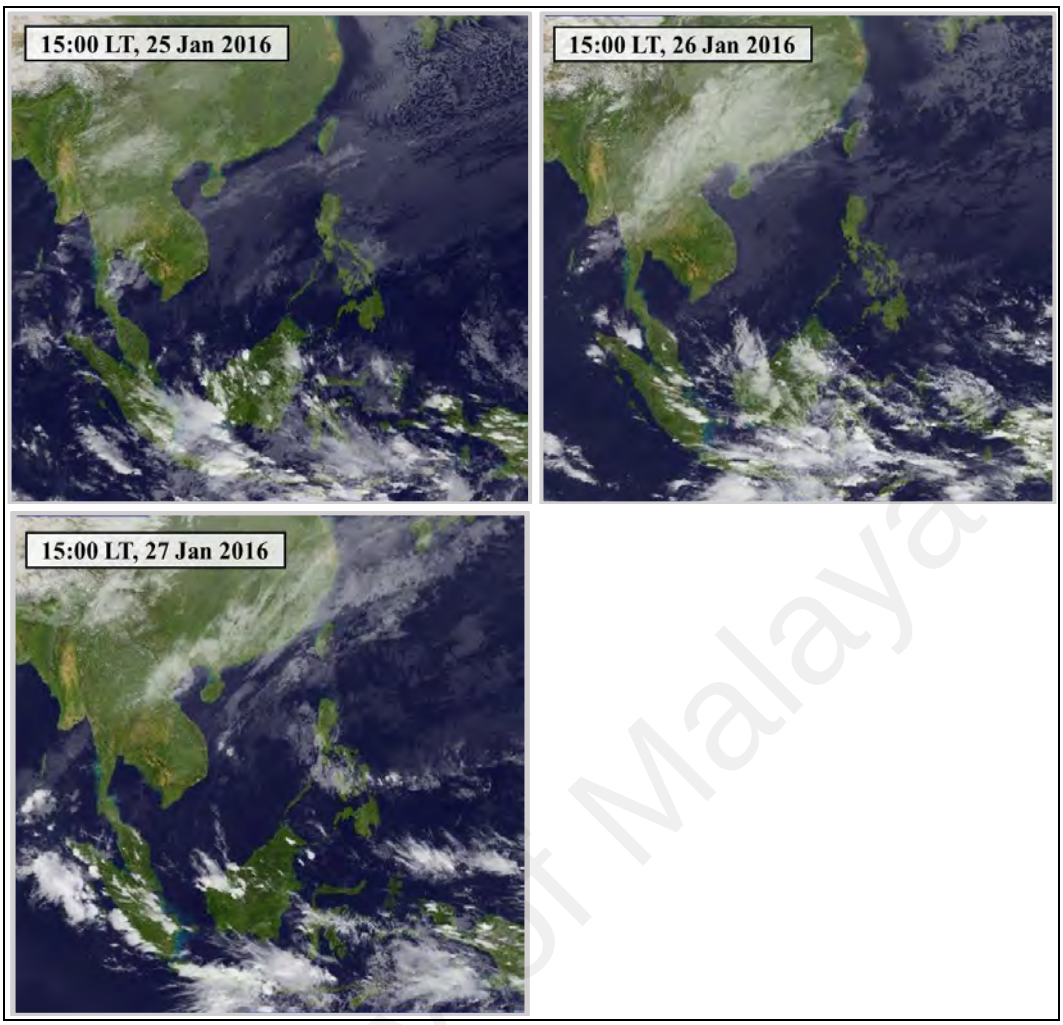

Figure 4.47: Himawari-9 satellite images at 15:00 LT for each day in CS1

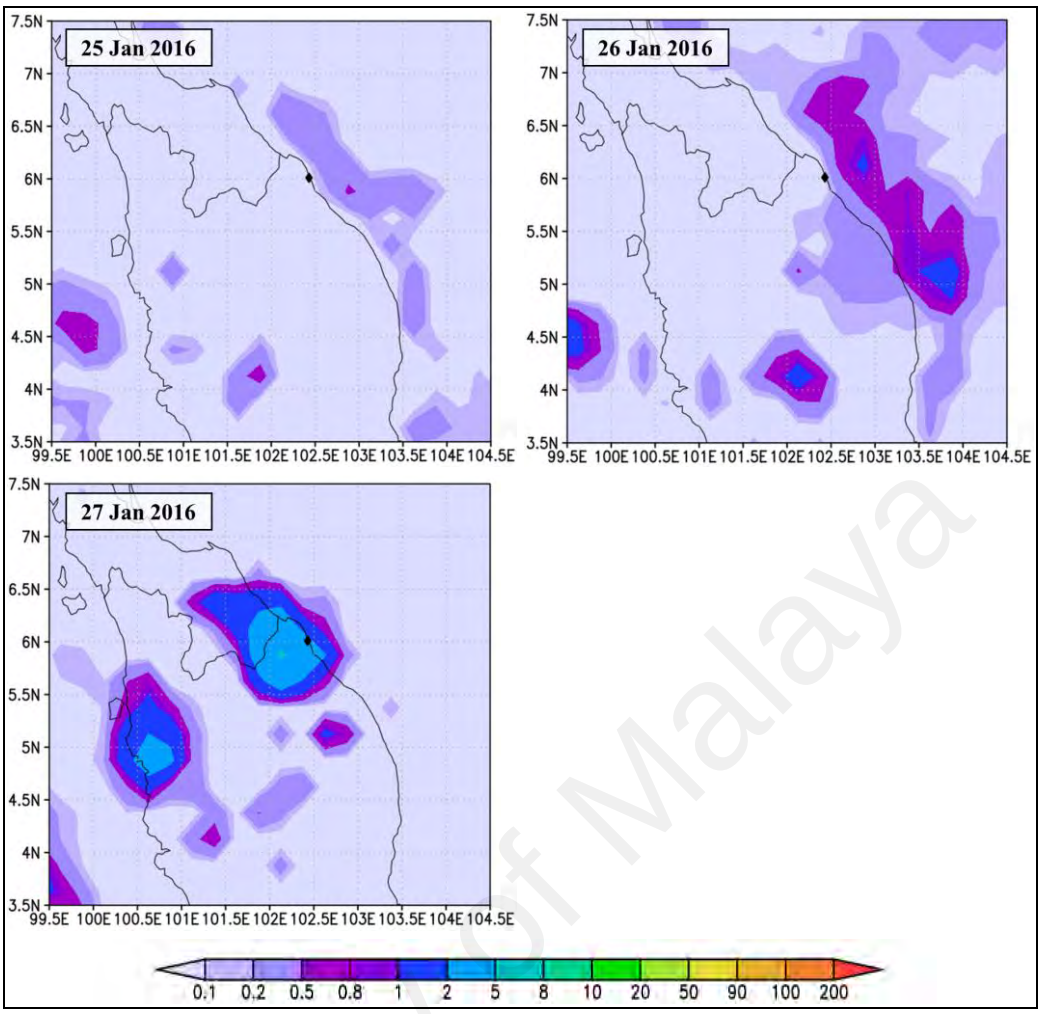

Figure 4.48: Daily averaged of TRMM rain rate (mm/hr) at BMRS during CS1. The black (♦) is the location of BMRS

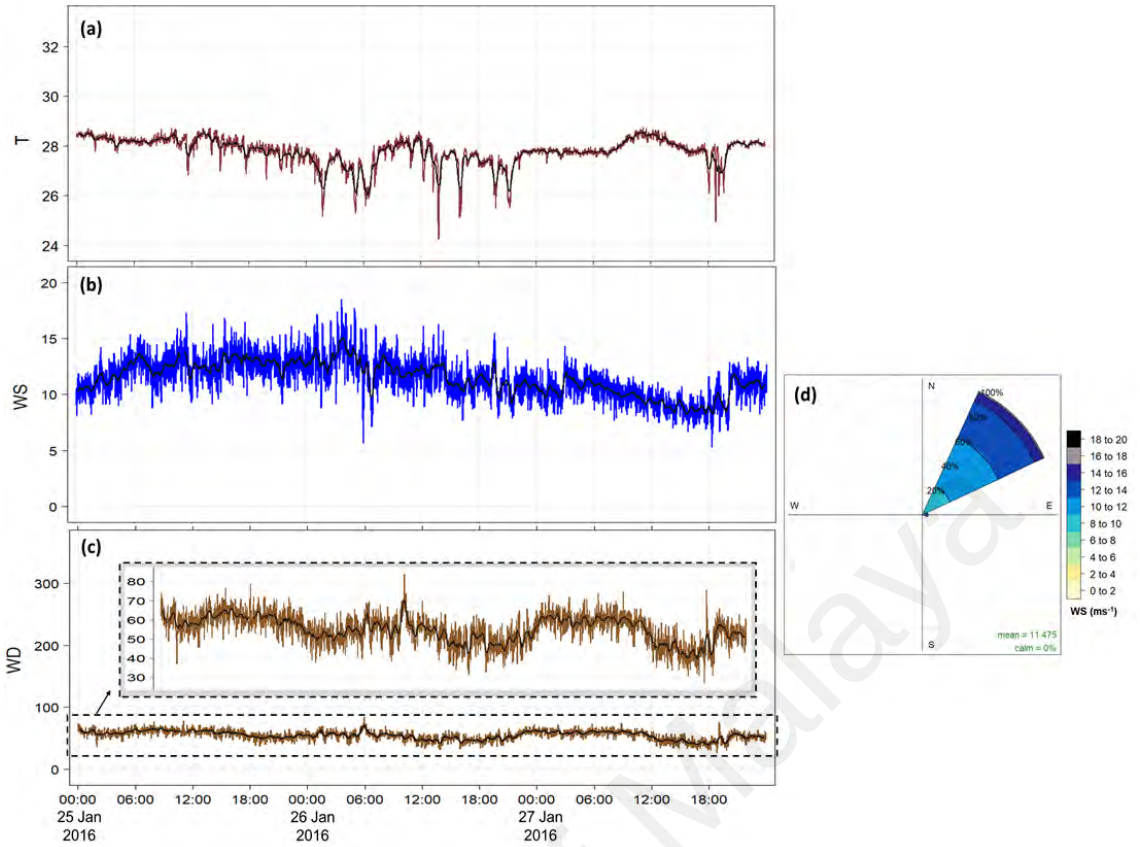

Figure 4.49: 1-minute time series of (a) T (° C) (b) WS (ms^{-1}) (c) WD (°) and (d) Wind rose at BMRS during CS1 (Local time). The black line in each time series represents the variation resulted using moving average filter (at each 30 data points)

4.2.1.2 Effects of strong synoptic condition on air pollutants during CS1

Overall, air pollutants during CS1 resulted within its low levels. However, there was an interesting relation between the air pollutants and the meteorological condition during this period. Figure 4.50 (b) shows variation of CO_2 decreased following the decrease of cold surge indices (shaded areas in Figure 4.41). In general, CH_4 also decreased as shown in Figure 4.50 (a). There are statistically significant moderate positive associations between wind speed with CO_2 (r = 0.55) and CH_4 (r = 0.31) respectively as shown in Table 4.10. CH_4 can also be removed through the chemical reaction in the troposphere through oxidation process where it reacts with hydroxyl radicals to produce CO_2, H_2O and O_3 (Holmes, 2018). This explains the weaker positive relations with wind speed as compared to CO_2. The positive correlations attained between CO_2 and CH_4 with wind

speed are contrary to the typical relationship between wind and air pollutants where strong winds usually minimised the quantity of air pollutants (negative correlation). In addition to that, there were statistically significant weak positive correlations between temperature with CH_4 (r = 0.10) and CO_2 (r = 0.15) (Table 4.10). These unusual relations suggest the strong northeasterly winds in weakened vertical gradient of temperature favored the transport of CO_2 and CH_4 at BMRS. Meanwhile, PM_{10} and $PM_{2.5}$ fluctuated ±2.0 within its mean: 10.4 μgm^{-3} and 9.4 μgm^{-3} respectively (Figure 4.50 (c) and (d)). Correlations for PM_{10} and $PM_{2.5}$ with wind speed were −0.40 (moderate) and −0.37 (weak) indicating that strong winds decrease the concentrations of PM (Table 4.10). In the meantime, both PM_{10} and $PM_{2.5}$ indicate non-significant correlations with temperature. High dry deposition velocity of PM is accomplished with strong wind speed, high relative humidity and low temperature (Hemond & Fechner, 2014) whereas high wet deposition occurs when there are high rate of rainfalls. During this case study, the PM were associated to both type of depositions where there were strong northeasterly winds, high relative humidity, moderate temperature and slight rain during the second and third day were present. Thus, this explains the low PM concentration. Variation of RPM shows that it ranged between 0.7 to 1.0 (Figure 4.50 (e)) and this implies the presence of both coarse and fine particles.

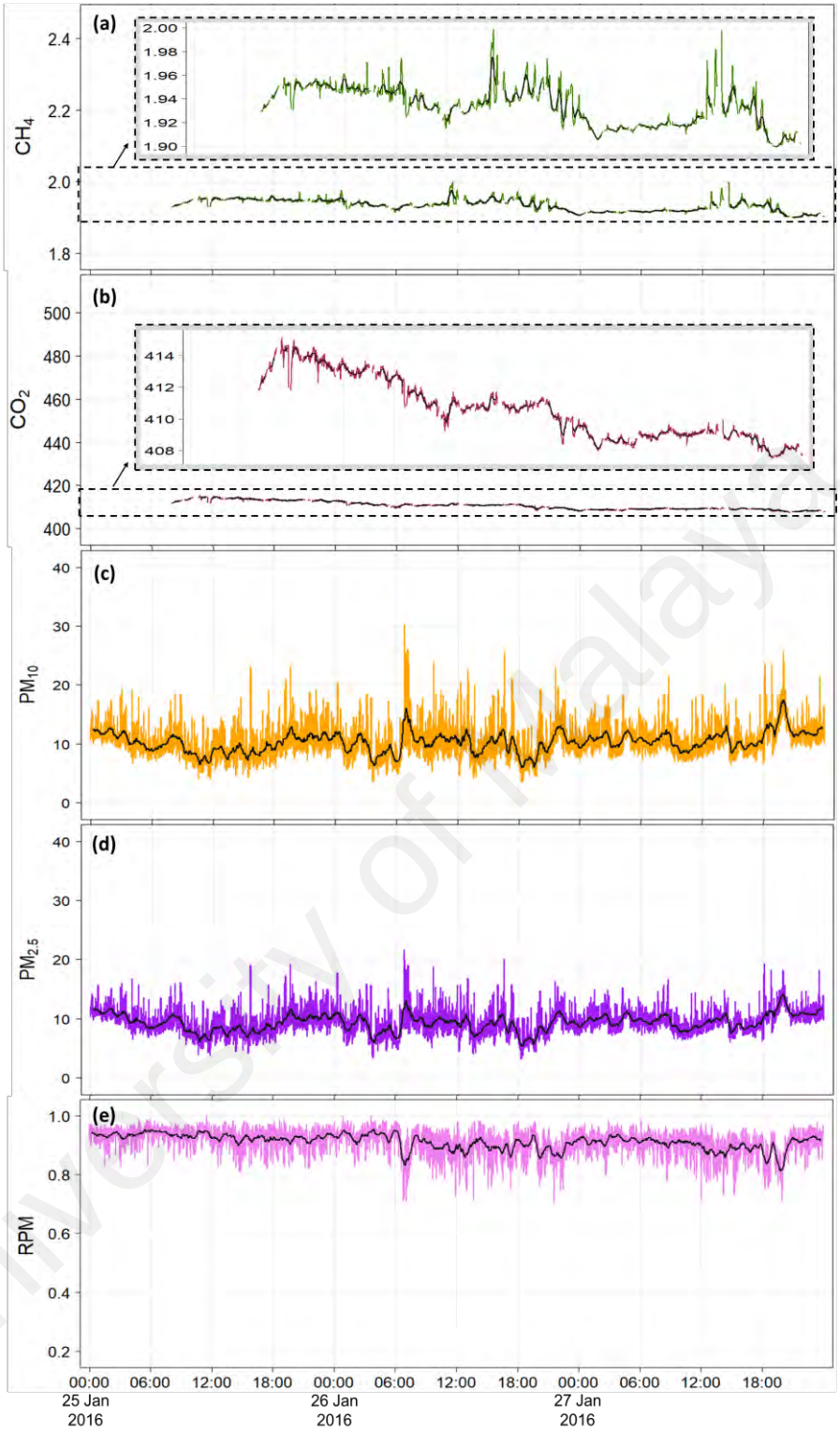

Figure 4.50: 1-minute time series of (a) CH4 (ppm) (b) CO2 (ppm) (c) PM10 (µgm-3) (d) PM2.5 (µgm-3) and (e) RPM, RPM during CS1 (Local time). The black line in each time series represents the variation resulted using moving average filter (at each 30 data points)

Table 4.10: Pearson Correlation (r) between air pollutants with wind speed (WS) and temperature (T) during CS1. 95% CI shown is the 95% bootstrapping BCa CI. The shaded boxes (grey-colored) represents non-significant correlation coefficient.

	CH_4	CO_2	PM_{10}	$PM_{2.5}$
WS	r = 0.31; 95% CI = [0.29, 0.34]; p-value < 0.001	r = 0.55; 95% CI = [0.53, 0.57]; p-value < 0.001	r = −0.42; 95% CI = [−0.43, −0.38]; p-value < 0.001	r = −0.39; 95% CI = [−0.40, −0.34]; p-value < 0.001
T	r = 0.10; 95% CI = [0.07,0.13]; p-value < 0.001	r = 0.15; 95% CI = [0.12, 0.18]; p-value < 0.001	r = −0.01; 95% CI = [−0.07, 0.00]; p-value > 0.05	r = 0.01; 95% CI = [−0.07,0.00]; p-value > 0.05

Table 4.11: Pearson Correlation (r) among all air pollutants during CS1. 95% CI shown is the 95% bootstrapping BCa CI.

	CH_4	PM_{10}	$PM_{2.5}$
CO_2	r = 0.79; 95% CI = [0.77, 0.80]; p-value < 0.001	r = −0.17; 95% CI = [−0.20, −0.13]; p-value < 0.001	r = −0.16; 95% CI = [−0.19, −0.13]; p-value < 0.001
CH_4		r = −0.13; 95% CI = [−0.16, −0.10]; p-value < 0.001	r = −0.16; 95% CI = [−0.19, −0.13]; p-value < 0.001
PM_{10}			r = 0.99; 95% CI = [0.98, 0.99]; p-value < 0.001

The CPFP plots for all air pollutants during the CS1 are shown in Figure 4.51 to Figure 4.53. All air pollutants were highly associated with onshore wind. CH_4 being within 25th to 50th percentiles were associated with strong wind from 70° (east-northeasterly) while the next interval of percentile associated with light to strong winds from the 315° (northwesterly) and 30° (north-northeasterly) of wind direction respectively. Highest

mixing ratio CH_4 during this period was associated with strong 45° (northeasterly) wind. Meanwhile, highest and largest association of CPF probability of CO_2 was shown ranging from 50th to 75th percentiles (Figure 4.52 (c)). This is also associated with strong wind speed from 30° to 50° of wind direction (northeasterly). The highest mixing ratio of CO_2 was mainly originated within the 60° of wind direction (east-northeasterly). Figure 4.53 (a) demonstrates a presence of both the fine and coarse particles based on the RPM being within 0.71 to 0.89. Meanwhile, the highest RPM was associated with strong wind from within 60° of wind direction (Figure 4.53 (e)). All the results suggest the high levels of air pollutants associated with strong onshore winds.

The HYSPLIT-CWT result indicates BMRS was influenced by the long-range transport of air pollutants. Back trajectories during this period indicate air travel from continental regions of East Asia and through the SCS before arriving at BMRS. The figure also shows that the main (high) sources of the pollutants are the continental region of China and coastal area of Vietnam. show air travelling from continental regions of East Asia and across the SCS before arriving at BMRS. The figure also shows that the principal (high) sources of the pollutants are the continental region of China and coastal area of Vietnam. A research study conducted by Oram et al. (2017) using Numerical Atmospheric-dispersion Modelling (NAME) as transport model during January and February 2014 also shows that the same source regions dominated the high concentrations of short-lived anthropogenic chlorocarbons observed at BMRS. Figure 4.54 (c) shows finer particles within BMRS and Vietnam are more attributed at the SCS. The location of active fire/hotspots were also superimposed in Figure 4.54. During this period, there were high number of hotspot locations throughout the continental China and Indo-China (especially Vietnam, Thailand and Cambodia) regions. East Asia (including China) is one of the main regions for air pollution especially in terms of acid deposition, regional haze and increase of trace gases due to its high population and rapid economic development

(Nguyen et al., 2019; Wu et al., 2017). Shanghai, Beijing and the Pearl River Delta region – including Shenzhen, Guangzhou, Hong Kong and their immediate vicinities are well known as economically diverse regions in China (Chan & Yao, 2008). On the other hand, Indo-China is highly influenced by biomass burning from forest fires (Chuang et al., 2013). Khan, Latif, Amil, et al. (2015) study shows that the concentration of PM in Indo-China are correlated with the intermingling of both coarse and fine particles where over the southern Vietnam (Mekong Delta), it is attributed to high biomass burning particularly from crop residues (Le et al., 2014). Additional emissions could have been gathered over parts of Vietnam as the winds subsided (Figure 4.42) hence accumulated the pollutants in its coastal area before it reached BMRS. The relations of air pollutants between one another are shown in Table 4.11. There are statistically significant very weak negative associations between the greenhouse gases (CO_2 and CH_4) and PM (PM_{10} and $PM_{2.5}$). This may be linked to atmospheric lifetimes of these air pollutants. CO_2 and CH_4 can remain in atmosphere for years (over 5 years) (Trogler, 1995). However, PM can only live for weeks in the atmosphere (WHO, 2005). During this case study, given the regional transport of air pollutants, the PM may also undergo multiple and rapid intermingling processes within different sizes of particles and interactions between the atmosphere and sea (Hemond & Fechner, 2014) thus contributing further to the low correlations with other types of air pollutants (especially CO_2 and CH_4).

Table 4.12 shows a description of the meteorological conditions, relationships and transport of air pollutants during the CS1. Overall, CS1 shows that strong synoptic meteorological condition allows the transboundary transport of CO_2 and CH_4 over central of China and Vietnam at BMRS.

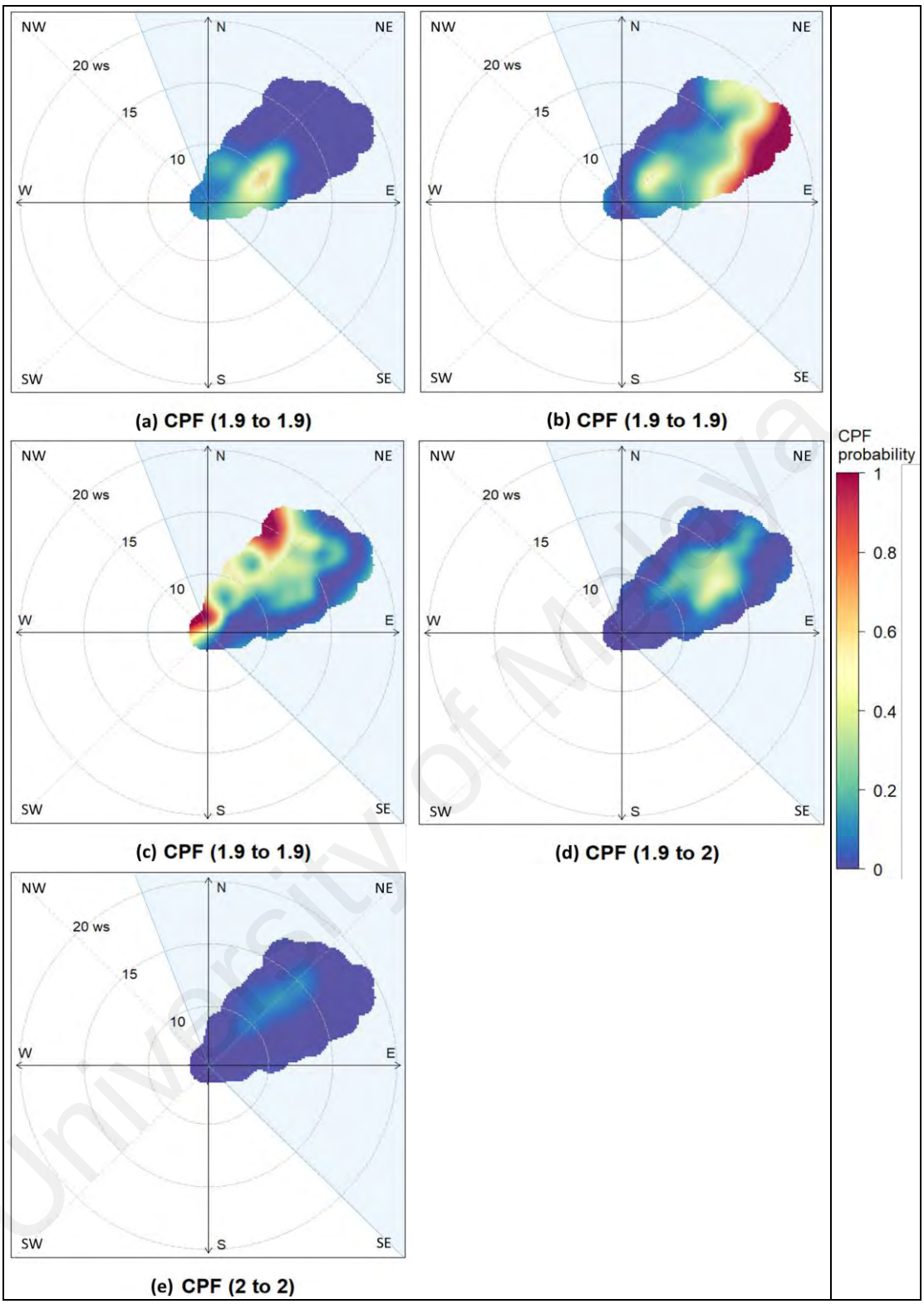

Figure 4.51: Polar plot of hourly CH_4 (ppm) at BMRS based on the CPF function for a range of percentile intervals from (a) Minimum to Q1 (b) Q1 to Q2 (c) Q2 to Q3 (d) Q3 to 95th percentile and (e) 95th percentile to maximum during CS1. The color scale shows the CPF probability and the radial scale shows the wind speed. The light blue shaded sectors represent the onshore wind. (Same indications used for the all the preceded CPFP plots)

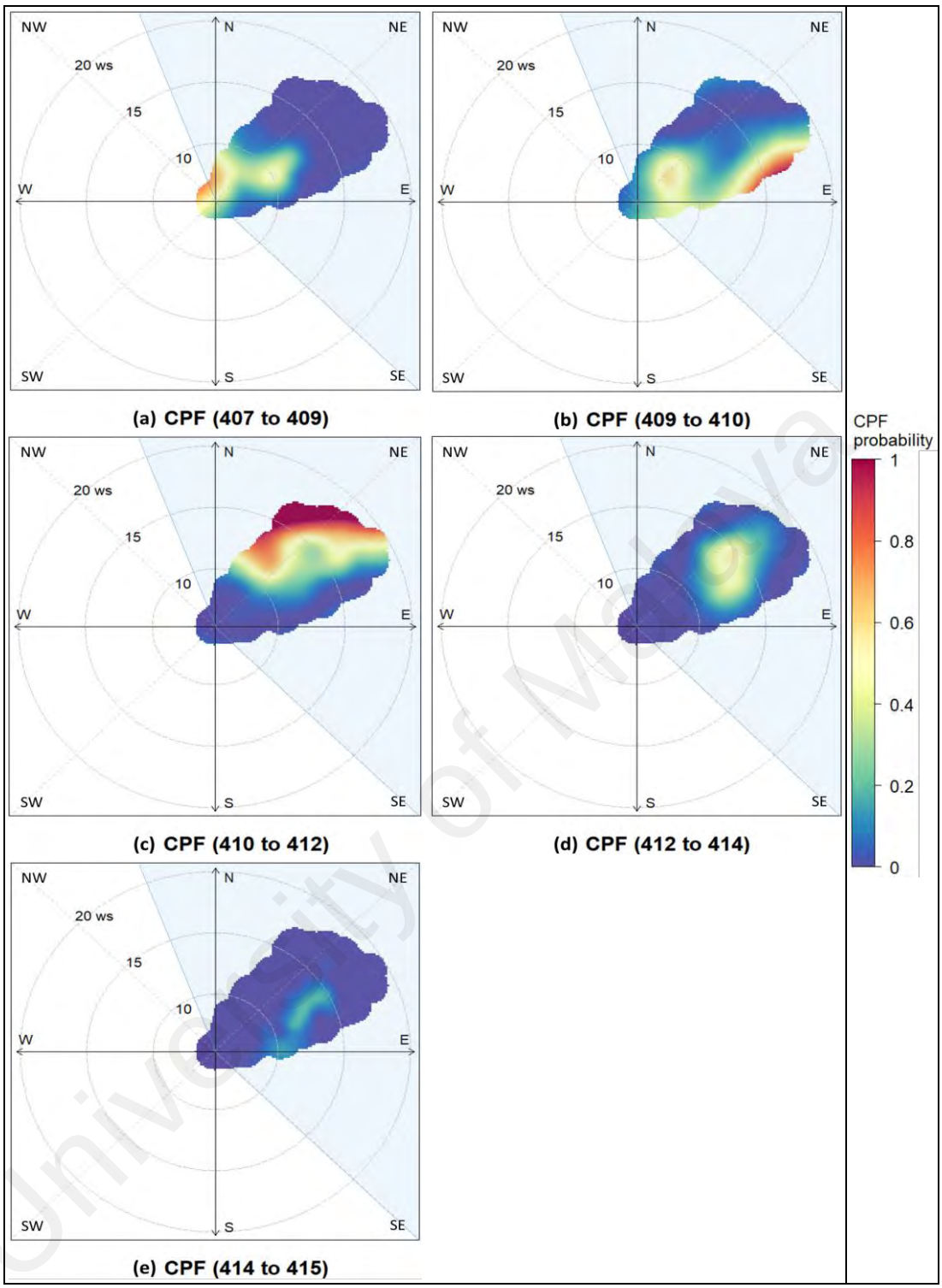

Figure 4.52: Polar plot of hourly CO_2 (ppm) at BMRS based on the CPF function for a range of percentile intervals from (a) Minimum to Q1 (b) Q1 to Q2 (c) Q2 to Q3 (d) Q3 to 95th percentile and (e) 95th percentile to maximum during CS1

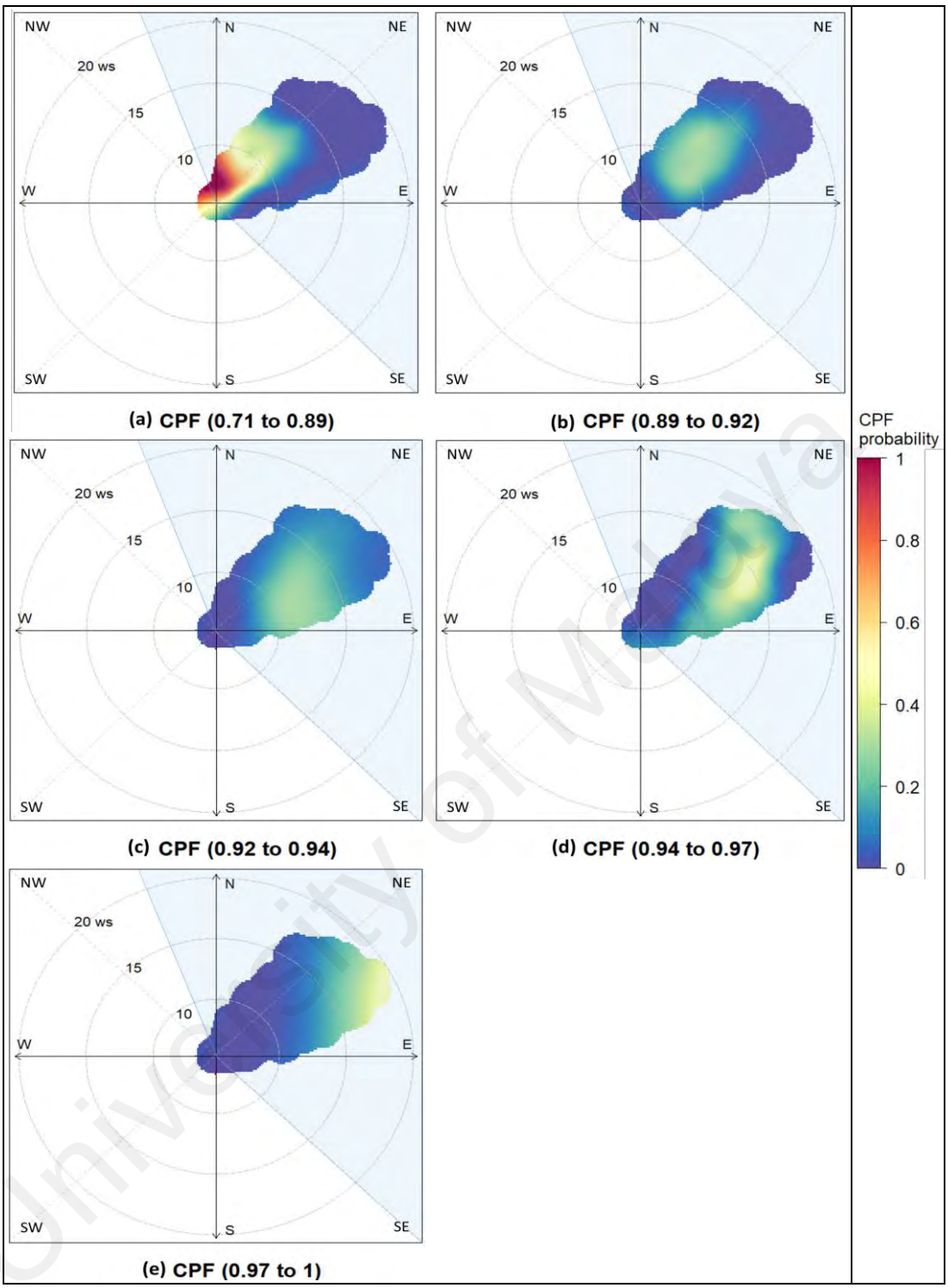

Figure 4.53: Polar plot of hourly RPM at BMRS based on the CPF function for a range of percentile intervals from (a) Minimum to Q1 (b) Q1 to Q2 (c) Q2 to Q3 (d) Q3 to 95th percentile and (e) 95th percentile to maximum during CS1

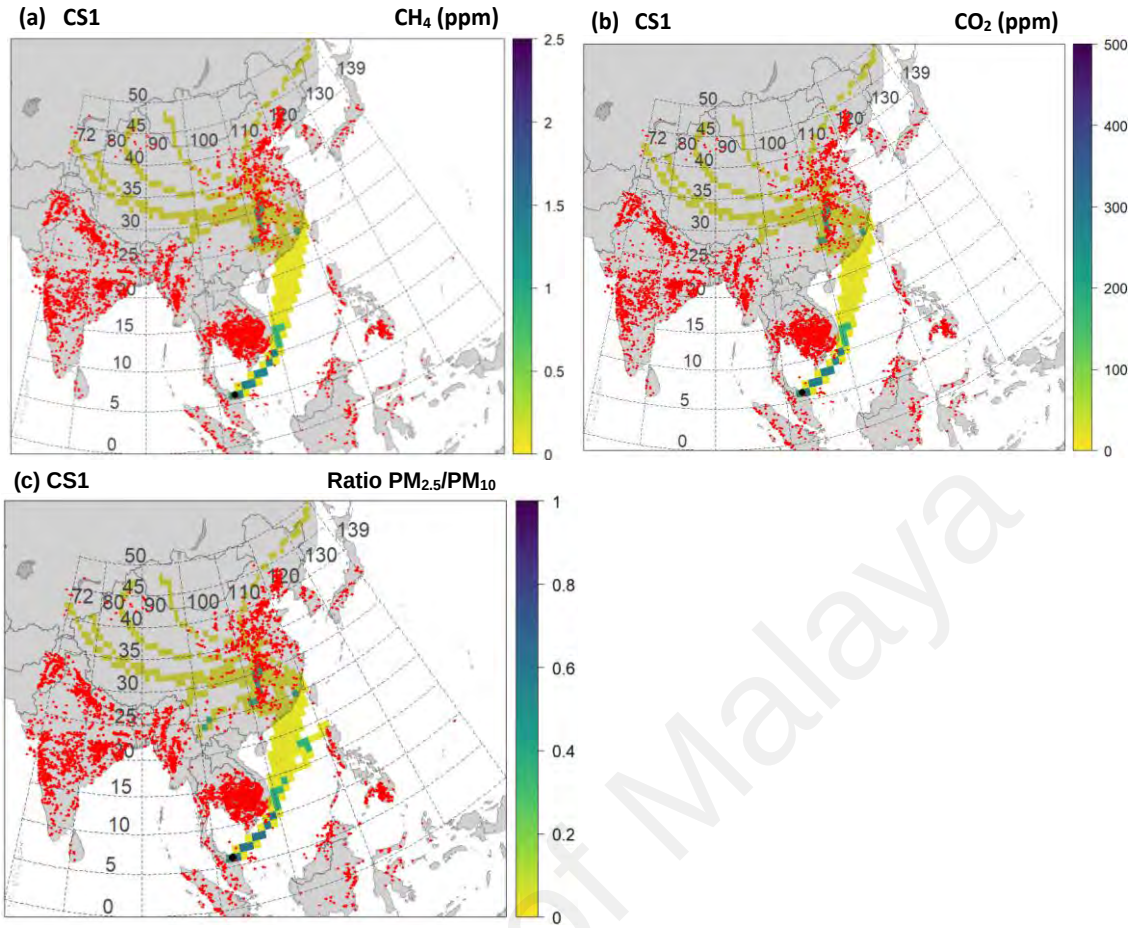

Figure 4.54: CWT coupled with hotspot data for CS1. Total trajectory run time is 120 hours. Source ● is at 6.0086 N and 102.4259 E (BMRS location). Points ◆ show the hotspot locations. Range of colors for the CWT described from non-source areas (yellow) to strongest source areas (dark blue) of pollutants at BMRS

Table 4.12: Summary on the meteorological conditions, relations and transport of air pollutants during CS1

Meteorological conditions and its characteristics
1. Strong synoptic meteorological condition – cold surge event 2. BMRS was influenced by strong northeasterly during the whole period of CS1 3. The strong easterly wind penetrated for about 60 km inland along the east coast of Peninsular Malaysia and prevailed from surface up to 2500 m height with high relative humidity 4. Clear vertical thermal gradient shown within 600 m – an indication of suppression of local meteorological condition (land sea breeze)
Relations and transport of air pollutants
1. Low level of air pollutants 2. CO_2 and CH_4 show significant positive correlations with wind speed 3. CPFP plots and HYSPLIT-CWT analysis superimposed with hotspots data show the principal (high) CO_2, CH_4 and RPM are associated with onshore wind and originated from the continental region of China and areas along the coastal of Vietnam (transboundary sources).

4.2.2 Meteorological conditions and its effect on air pollutants during CS2

In this case study, 18 radiosondes were launched from 11:00 LT on 03 June 2016 to 14:00 LT on 05 June 2016 for each three hours. The meteorological condition, its characteristics and its impact on the levels and transport of air pollutants during CS2 are discussed in this section.

4.2.2.1 Characteristics of local meteorological condition during CS2

CS2 indicates the characteristic of an atmosphere without the effect of synoptic flow. There is slight pressure difference between 5°N and 30°S during this period as shown in Figure 4.55 thus indicating poor influence of synoptic flow at BMRS. The location of BMRS which is only 100 m from the sea (SCS) is highly associated with the land sea breeze owing to the presence of strong differential heating. These events often require

diurnal fluctuations over a day (Lim & Samah, 2004) where convection peaks around mid-afternoon (Joseph et al., 2008). When the synoptic-scale motions are weak, sea breezes are able to completely develop and can lead in the development of convergent zones on land and divergent zones at sea (Bouchlaghem et al., 2008). During this period, light winds (Figure 4.57) were present at BMRS with mean values = 2.68 ms^{-1} (Table 4.9). Hourly evolutions of wind speed from 10 m (ERA5) and 30 m observational data at BMRS indicate land sea breeze occurred every day. Figure 4.56 (a) and (c) indicate the wind variations during the onset of sea breeze and land breeze associated with onshore (337.5° to 135°) and offshore winds respectively.

The sea breeze started on 1) 14:00 LT to 20:00 LT on 3 June 2016, 2) 09:00 LT on 4 June 2016 to 00:00 LT on 5 June 2016 and 3) 14:00 LT on 5 June 2016 to 01:00 LT on the following day. There was time lag regarding the start of the sea breeze where it didn't occur immediately with the sunrise particularly on 03 and 05 June 2016 (Figure 4.57). Thermal contrast is required between the land and sea to exceed some threshold level for this event to occur. The time lag also varies depending on the conditions of the atmosphere, soil moisture and location (Kavitha et al., 2018). In Peninsular Malaysia, the lag on the occurrence of sea breeze event is not unusual especially for a location located near the coastal areas. The sea breeze eventually started in late afternoon (at 16:00 LT) over the west coast of Peninsular Malaysia (Joseph et al., 2008). During this case study, the deepest inland penetration of the sea breeze events was seen in the late afternoon (Figure 4.56 (b)) where the easterly winds advanced inland within 30 to 90 km towards the Titiwangsa Range. The figure also indicates sea breeze events penetrating inland from the west coast of Peninsular Malaysia. Joseph et al. (2008) stresses that due to high orography, the collision between the sea breeze from the east and west coast at the northern part of Peninsular Malaysia is impossible. However, when there is an interaction of lee waves and the sea breeze front, the deep convective clouds can be developed. Figure

4.60 shows there were clouds formed at the intersection of those westerly and easterly winds (Figure 4.56 (b)). Therefore, this indicates that convective zones are formed as a result of the sea breeze events. Radiosondes data shows the sea breeze events at BMRS extends to a maximum height of 1000 m uniformly at 20:00 LT during 03 June and 04 June 2016 (Figure 4.57). Increasing in temperatures (Figure 4.58 (a)) and strengthening of easterly zonal winds (Figure 4.59 (a)) contributed to these vertical rises. The land breeze starts when offshore winds flowed consistently toward the sea (SCS) as shown in Figure 4.56 (c). In particular, BMRS experiences land breeze events in the northeastern part of Peninsular Malaysia where the offshore wind flows either southwesterly towards the SCS or blends with the southeasterly wind from areas along the eastern coast of Peninsular Malaysia. The winds then drifted more southeastward along the coast or southwestward of the SCS as shown in Figure 4.56 (c) and (d). Radiosonde data shows land breeze events during CS2 were associated with westerly and southwesterly winds (Figure 4.57 and Figure 4.59). CS2 were also associated with inconsistent variations of relative humidity during land and sea breeze event Figure 4.58 (b) which may be caused by complex interaction between land-sea temperature, meridional winds and zonal winds in SW monsoon. Daily averaged of TRMM rain rate (Figure 4.61) shows no rain over BMRS during this case study. 1-minute time series of BMRS tower shows similar values in its temperature (Figure 4.62 (a)) and wind (Figure 4.62 (c), (d) and (e)) as recorded by radiosonde (at surface level). It also implies a formation of clearer diurnal cycle on 05 June 2016 where sea breeze events were associated with higher temperature (around 30°C), higher wind speed (moderate level) and lower wind direction (around 90° - easterly wind).

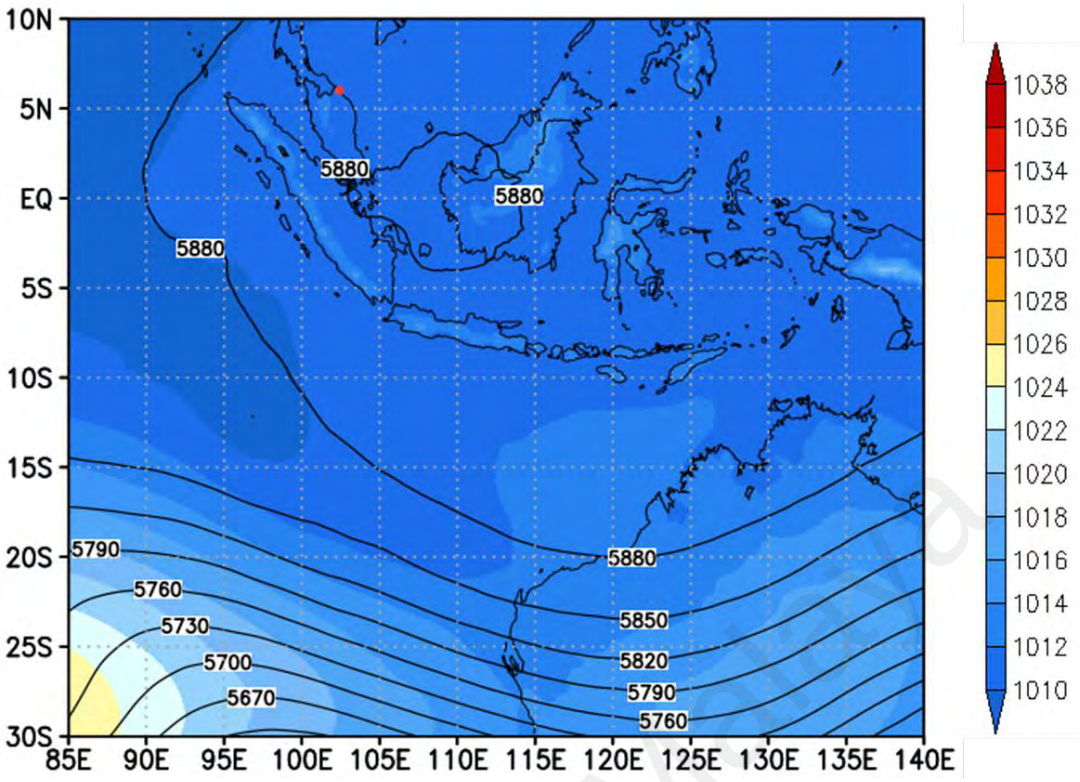

Figure 4.55: Average MSLP (hPa) with geopotential height (gph) at 500 hPa (contour lines) during CS2. The red dot (●) is the location of BMRS

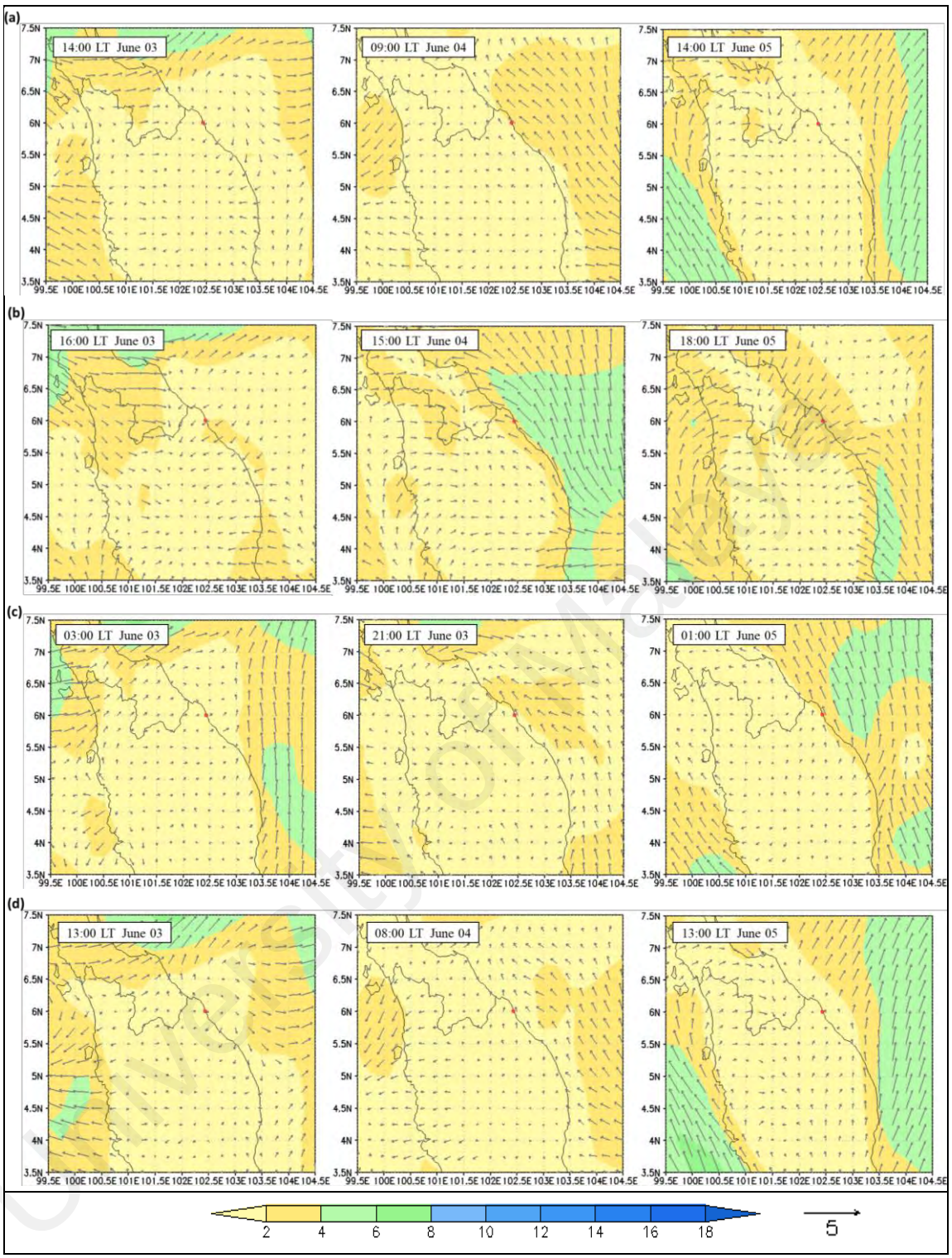

Figure 4.56: Variations of wind speed (hourly averaged) during CS2. Regions covered same as Figure 10 (b) for specific events namely (a) Onset of sea breeze (b) Deepest sea breeze inland penetration (c) Onset of land breeze and (d) Offset of land breeze. The red dot (●) is the location of BMRS

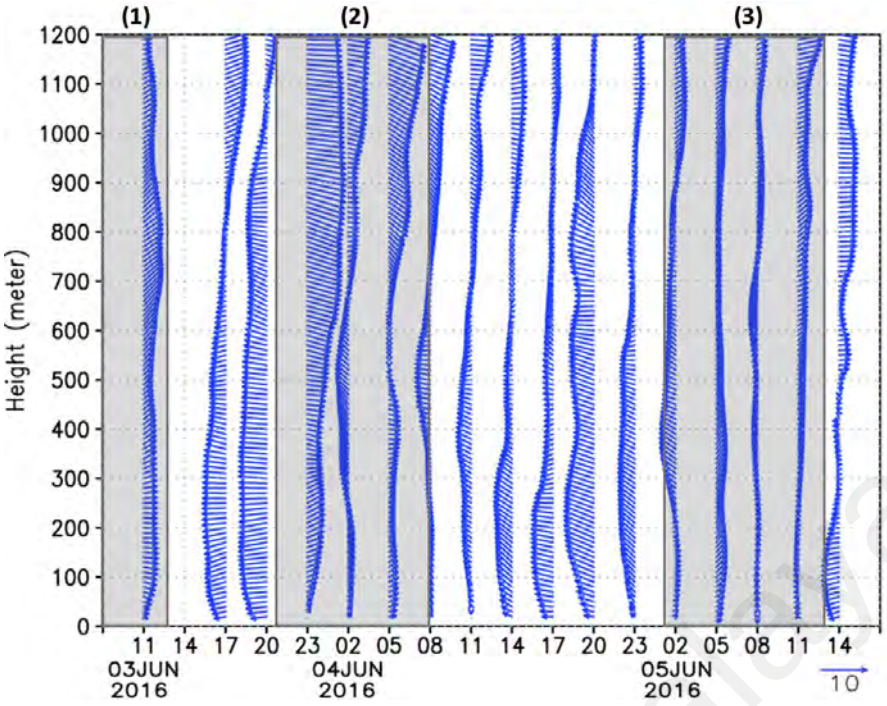

Figure 4.57: Time-height evolutions of wind vectors during CS2 from 1100 LT on 3 June 2016 to 1400 LT on 5 June 2016 within 1200 m height. Each wind vector represents in the unit of ms^{-1}. The grey shaded rectangles represent land breeze events where (1) 03:00 to 13:00, 03 June 2016 (2) 21:00, 03 June to 08:00, 04 June 2016 and (3) 01:00 to 13:00, 05 June 2016

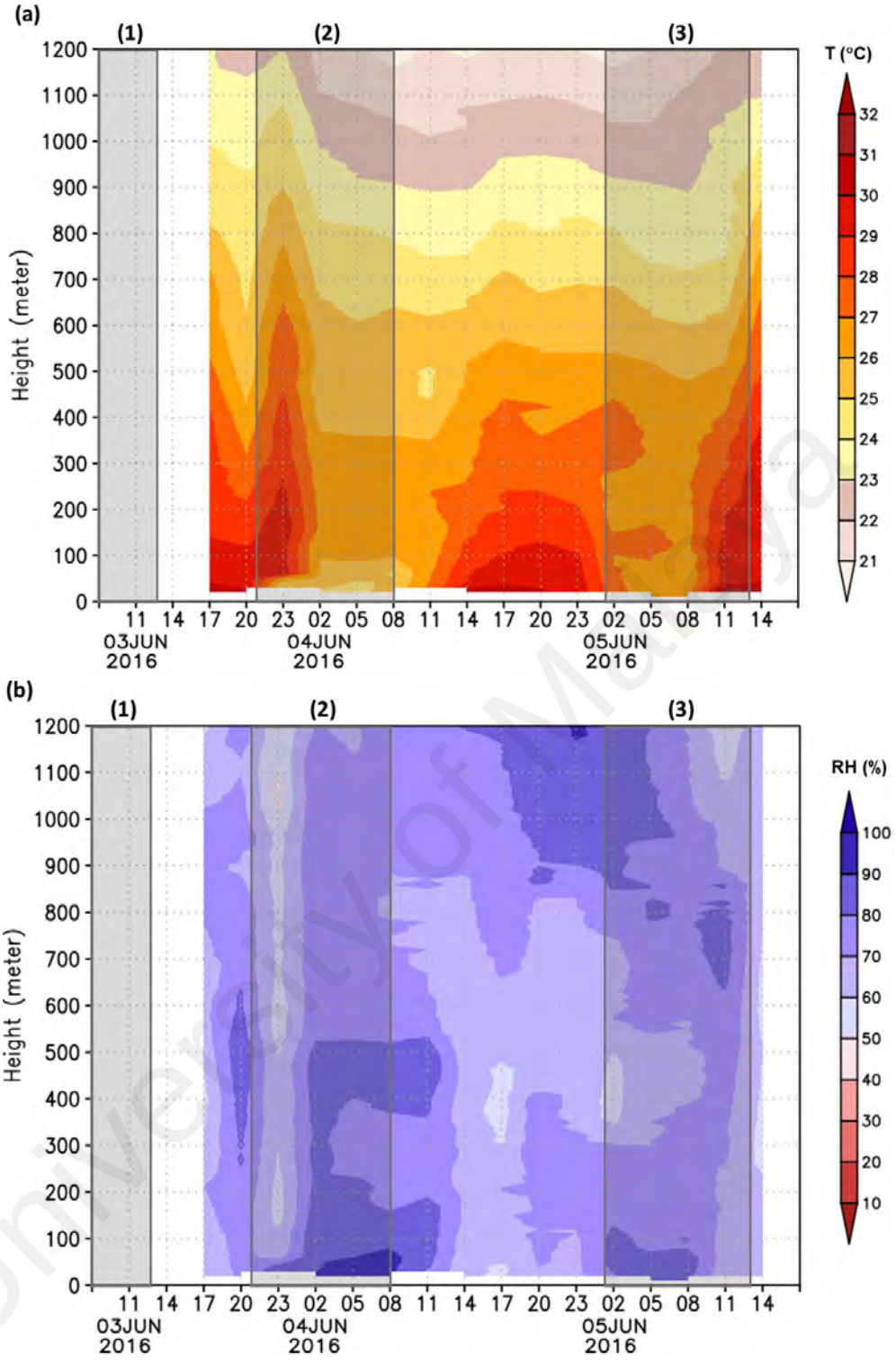

Figure 4.58: Time-height evolutions of (a) Air temperature (T) and (b) Relative humidity (RH) within 1200 m height during CS2. The grey shaded rectangles represent land breeze events

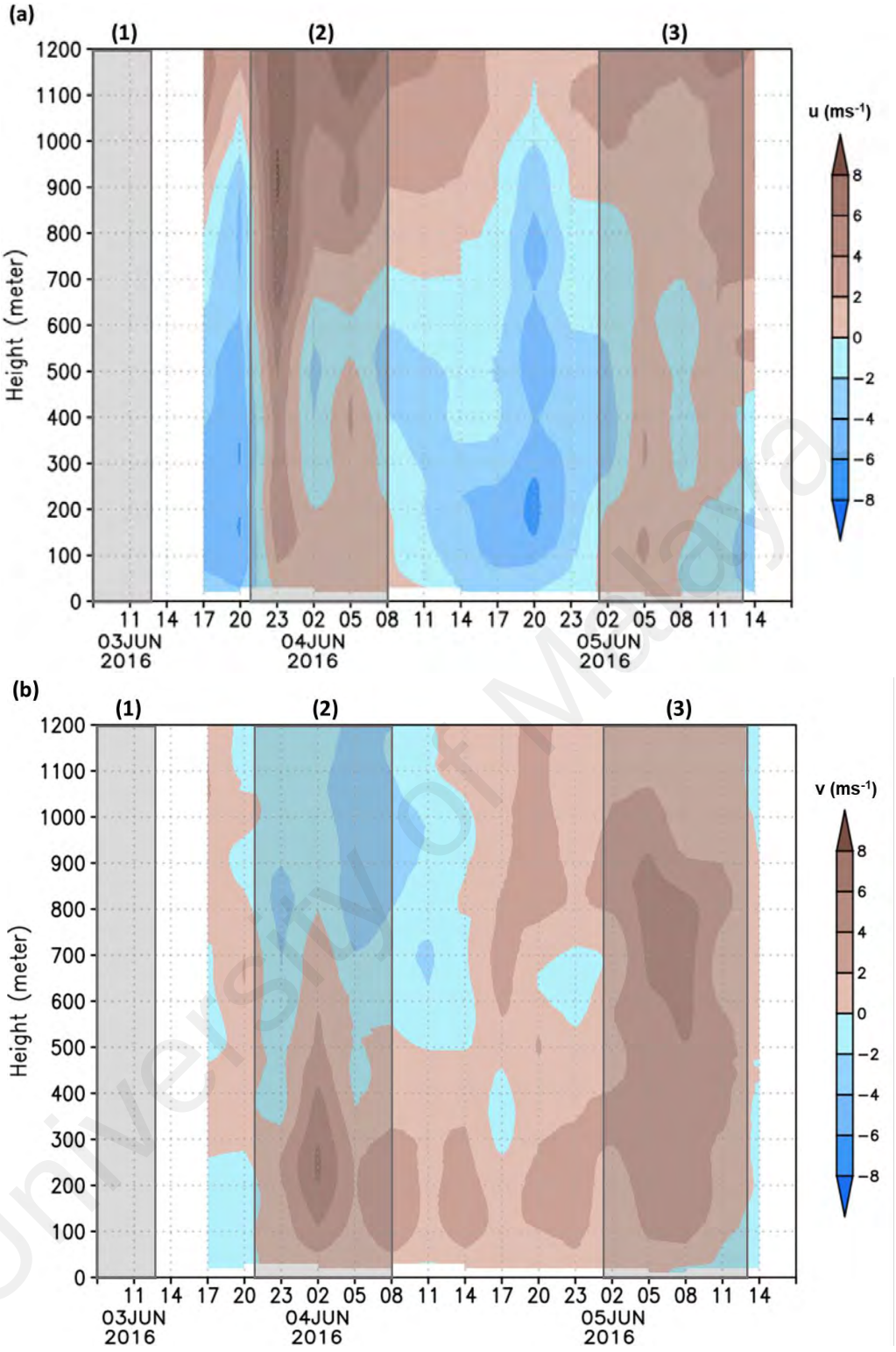

Figure 4.59: Time-height evolutions of (a) Zonal winds (u) and (b) Meridional winds (v) within 1200 m height during CS2. The grey shaded rectangles represent land breeze events

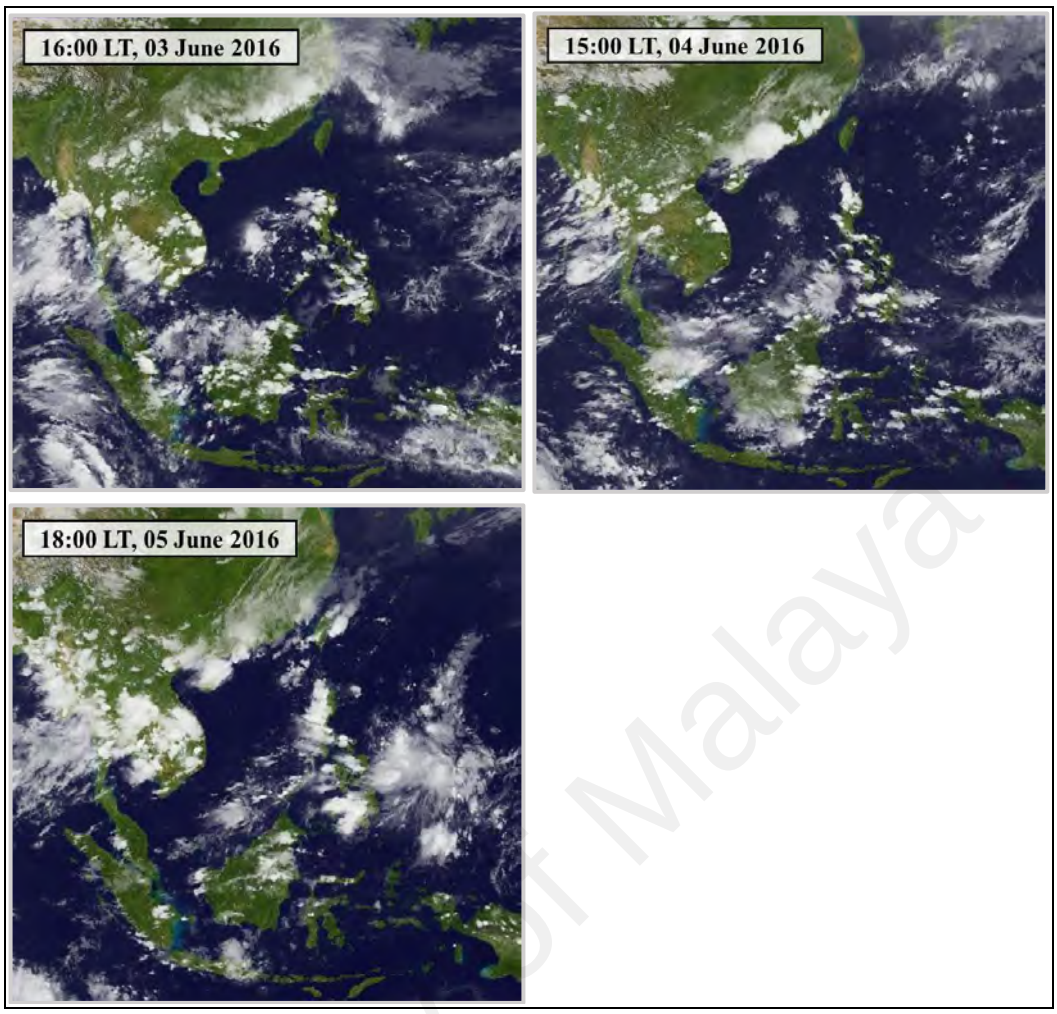

Figure 4.60: Himawari-9 satellite images during deepest inland penetration of sea breeze of CS2

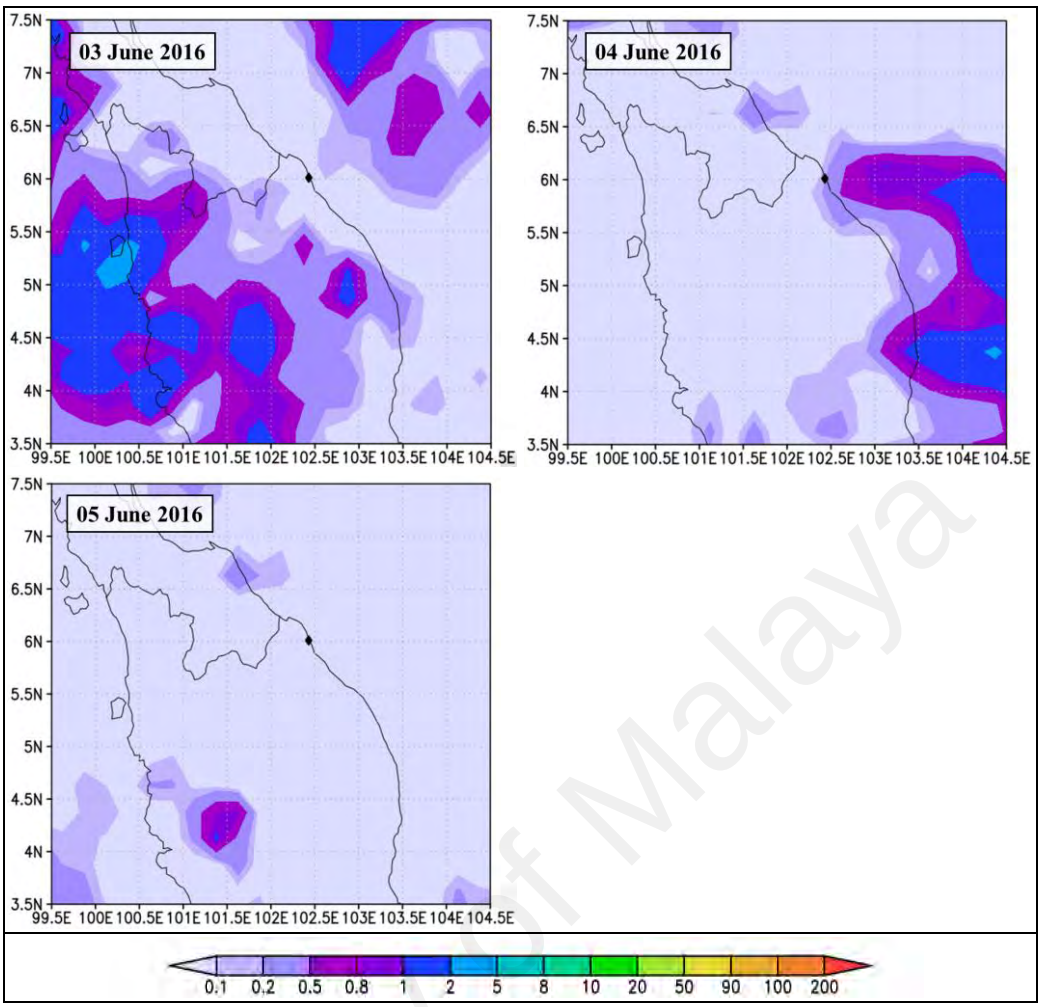

Figure 4.61: Daily averaged of TRMM rain rate (mm/hr) at BMRS during CS2. The black (♦) is the location of BMRS

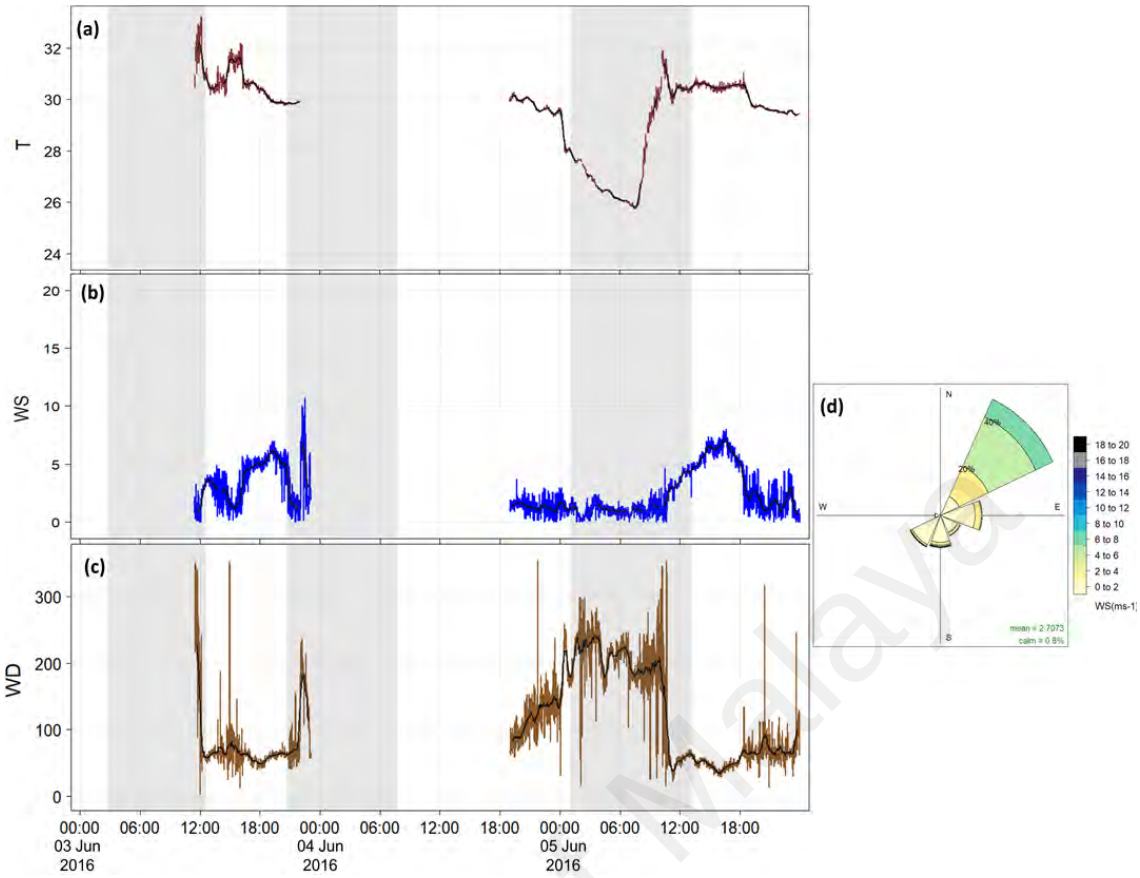

Figure 4.62: 1-minute time series of (a) T (°C) (b) WS (ms-1) (c) WD (°) and (d) Wind rose at BMRS during CS2 (Local time). The black line in each time series represents the variation resulted using moving average filter (at each 30 data points). The grey shaded rectangles represent land breeze events

4.2.2.2 Effects of local meteorological condition on air pollutants during CS2

Numerous experimental and computational simulations have shown the impacts of breeze circulation on the evolution of air pollutants (Bouchlaghem et al., 2008). Photochemical transformations (Dominick et al., 2015) coupled with the dynamic circulations such as breezes play an important role in the production, transport, and redistribution of reactive chemical species in the low levels of the atmosphere (Kavitha et al., 2018). Figure 4.63 shows the time series of all air pollutants during CS2. There were statistically significant moderate negative associations between the wind speed and all of the air pollutants as shown in Table 4.13. It is also shown that there were moderate and strong negative correlations between the PM (PM_{10} and $PM_{2.5}$) and greenhouse gases

(CO_2 and CH_4) respectively. These suggests that the wind and temperature variations during this case study played a major role in the variation of air pollutants. Strong winds and high temperature have led to a more unstable atmosphere, causing more turbulence, increase mixing processes and provide wider distribution of air pollutants in the atmosphere hence decreased its levels.

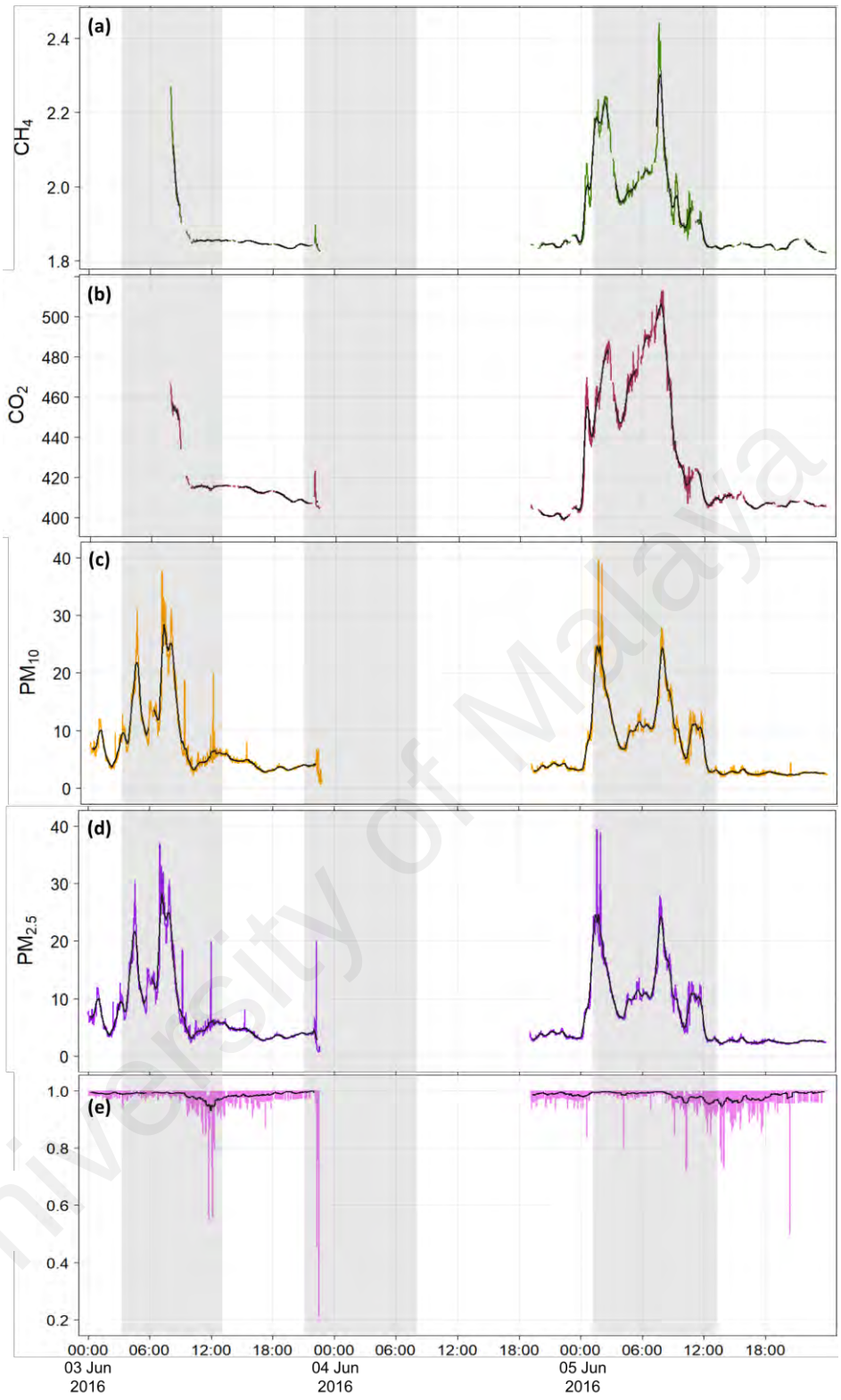

Figure 4.63: 1-minute time series of (a) CH_4 (ppm (b) CO_2 (ppm) (c) PM_{10} (μgm^{-3}) (d) $PM_{2.5}$ (μgm^{-3}) and (e) RPM, RPM at BMRS during CS2 (Local time). The black line in each time series represents the variation resulted using moving average filter (at each 30 data points). The grey shaded rectangles represent land breeze events

Table 4.13: Pearson Correlation (r) between air pollutants with wind speed (WS) and temperature (T) during CS2. 95% CI shown is the 95% bootstrapping BCa CI

	CH_4	CO_2	PM_{10}	$PM_{2.5}$
WS	r = −0.42; 95% CI = [−0.44, −0.40]; p-value < 0.001	r = −0.40; 95% CI = [−0.42, −0.38]; p-value < 0.001	r = −0.41; 95% CI = [−0.44, −0.40]; p-value < 0.001	r = −0.41; 95% CI = [−0.44, −0.40]; p-value < 0.001
T	r = −0.70; 95% CI = [−0.73, −0.67]; p-value < 0.001	r = −0.77; 95% CI = [−0.80, −0.73]; p-value < 0.001	r = −0.57; 95% CI = [−0.60, −0.53]; p-value < 0.001	r = −0.58; 95% CI = [−0.60, −0.53]; p-value < 0.001

Table 4.14: Pearson Correlation (r) between air pollutants during CS2. 95% CI shown is the 95% bootstrapping BCa CI

	CH_4	PM_{10}	$PM_{2.5}$
CO_2	r = 0.91; 95% CI = [0.90, 0.91]; p-value < 0.001	r = 0.82; 95% CI = [0.80, 0.84]; p-value < 0.001	r = 0.82; 95% CI = [0.80, 0.84]; p-value < 0.001
CH_4		r = 0.93; 95% CI = [0.91, 0.93]; p-value < 0.001	r = 0.93; 95% CI = [0.91, 0.93]; p-value < 0.001
PM_{10}			r = 0.99; 95% CI = [0.991, 0.998]; p-value < 0.001

The CPFP plots for all air pollutants during the CS2 are shown in Figure 4.64 to Figure 4.66. CH_4 and CO_2 within its respective minimum to 75th percentile contributed by combination of onshore and offshore winds (Figure 4.64 and Figure 4.65 respectively). Meanwhile, the remaining CH_4 and CO_2 ranging from the 75th percentile to its respective maximum strongly associated with offshore wind. CPFP plot of RPM during CS2 demonstrates high dominance of fine particles based on high presence of RPM from 0.97 to 1.0.

Overall back trajectories at BMRS during CS2 indicates strong local circulation. Strong positive associations (statistically significant) are observed between all of the air pollutants as shown in Table 4.14. This means that all the air pollutants are closely related and derive from the same regions of source. Sea breezes produce stable and low greenhouse gases mixing ratios (CO_2 and CH_4) and PM concentrations (PM_{10} and $PM_{2.5}$). Time series of RPM as shown in Figure 4.63 (e) during this event show lower ratio compared to in land breeze event; indicating more presence of coarse particles or due to more distribution process in the atmosphere. There were presence of more mild winds (between 5 to 10 ms^{-1}) (Figure 4.62 (b)) and vertical thermal gradient Figure 4.58 (a) during this event too. This favored more turbulence flow formation and thus led to low levels of pollutants. Figure 4.67 shows the CWT during this event; the principal (high) sources of the CO_2 and CH_4 are at Malaysia-Thailand border and areas along the east coast of Peninsular Malaysia. CWT for RPM (Figure 4.67 (c)) also suggests fine particles are more dominant (ratio ~ 1.0) within Malaysia-Thailand border and Terengganu area. On the other hand, land breezes lead to higher levels and more fluctuations on CO_2, CH_4, PM_{10} and $PM_{2.5}$ as shown in Figure 4.68 (grey shaded areas of (a) to (d)). Presence of light offshore winds lead to higher accumulation of air pollutants, thus increasing its levels. Shaded areas in Figure 4.68 (e) also demonstrates more dominance of fine particles based on high ratio of $PM_{2.5}/PM_{10}$. Figure 4.68 shows the CWT for the land breeze event. The principal sources are mostly originated from continental local areas (within Kelantan and Terengganu). The east coast of Peninsular Malaysia is characterized by agriculture (Dominick et al., 2015) and mid-sized cities. Hence, agricultural burning, forest fire activities, and industrial sources may have contributed to principal (high) sources of pollutants at BMRS during this period. The areas which contributed to principal (high) sources of pollutants during this event matched well with the principal sources during sea

breeze event. This further strengthens the evidence that local meteorological condition (land-sea breeze) at BMRS is associated greatly with local sources of air pollutants.

Table 4.15 shows the summary on the meteorological conditions, relations and transport of air pollutants during CS2. Overall, CS2 shows that local meteorological condition – land sea breeze event allows strong diurnal effect on the variations of CO_2, CH_4, PM_{10} and $PM_{2.5}$ at BMRS. These pollutants are mainly associated with local and regional sources of emissions surrounding BMRS.

Table 4.15: Summary on the meteorological condition, relations and transport of air pollutants during CS2

Meteorological conditions and its characteristics
1. Local meteorological condition – land-sea breeze 2. Variations of meteorological parameters at BMRS were influenced by a clear diurnal effect on each day of CS2. 3. The sea breeze events (easterly wind) can penetrate within 30 to 90 km inland in the late afternoon and can prevail for about 1000 m height. 4. Clear vertical thermal gradient is shown within 1000 m.
Relations and transport of air pollutants
1. Sea breeze and land breeze associated with low level and high level of air pollutants respectively 2. CO_2 and CH_4 show significant negative correlations with wind speed and temperature 3. CPFP plots and HYSPLIT-CWT superimposed with hotspots data show the principal (high) CO_2, CH_4 are influenced by offshore wind originated from areas along the east coast of Peninsular Malaysia (local and regional sources)

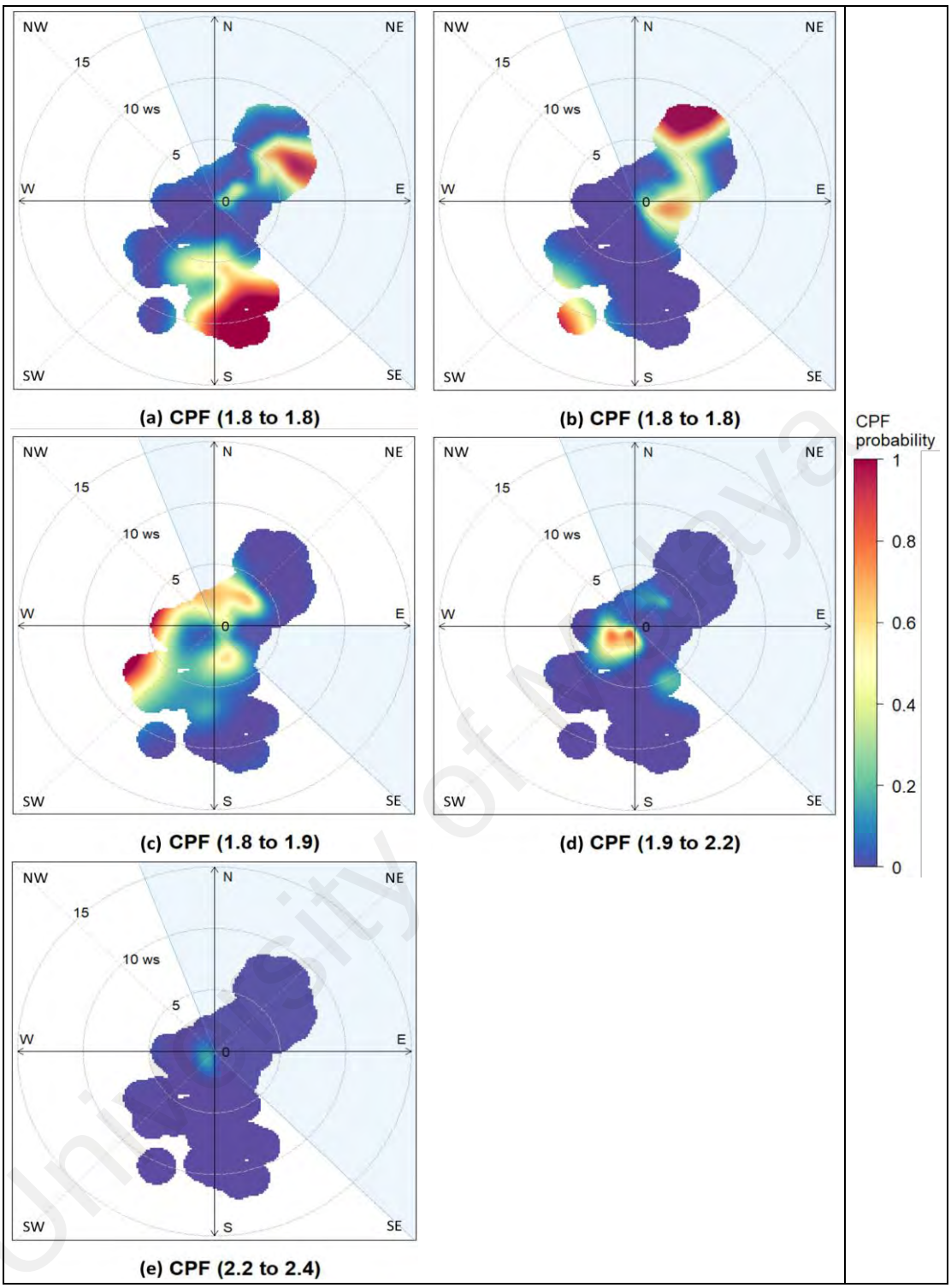

Figure 4.64: Polar plot of hourly CH_4 (ppm) at BMRS based on the CPF function for a range of percentile intervals from (a) Minimum to Q1 (b) Q1 to Q2 (c) Q2 to Q3 (d) Q3 to 95th percentile and (e) 95th percentile to maximum during CS2

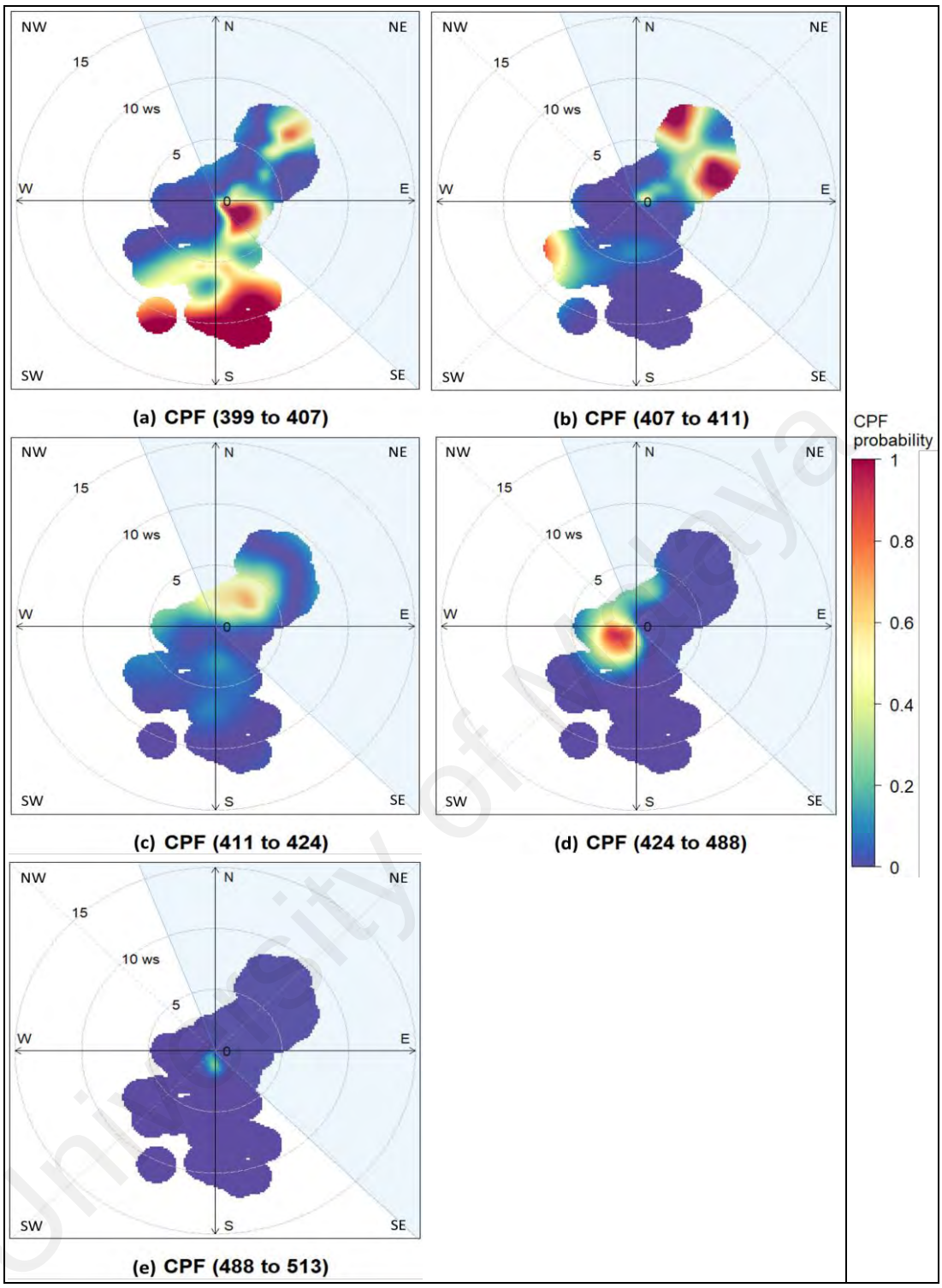

Figure 4.65: Polar plot of hourly CO_2 (ppm) at BMRS based on the CPF function for a range of percentile intervals from (a) Minimum to Q1 (b) Q1 to Q2 (c) Q2 to Q3 (d) Q3 to 95th percentile and (e) 95th percentile to maximum during CS2

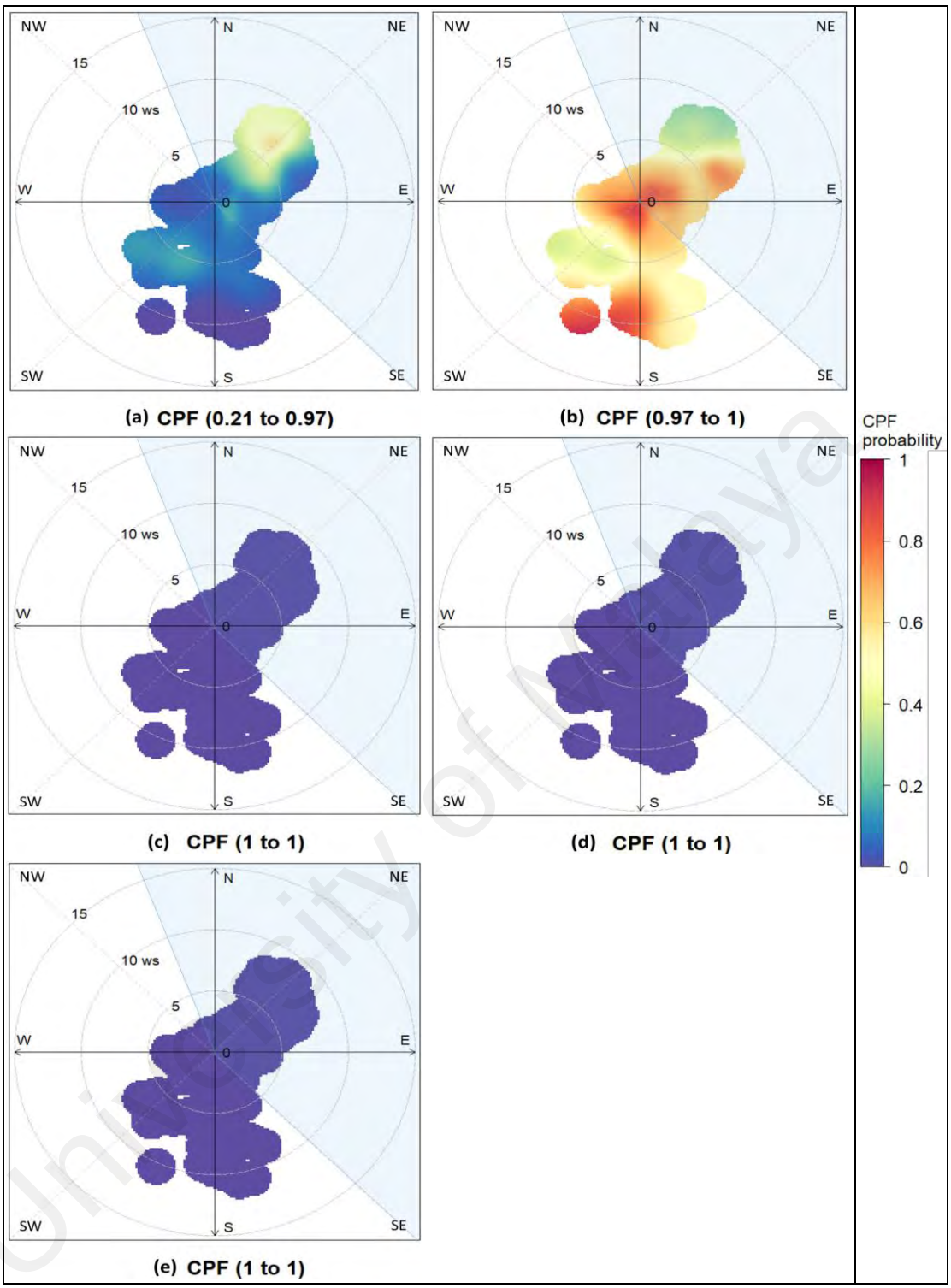

Figure 4.66: Polar plot of hourly RPM at BMRS based on the CPF function for a range of percentile intervals from (a) Minimum to Q1 (b) Q1 to Q2 (c) Q2 to Q3 (d) Q3 to 95th percentile and (e) 95th percentile to maximum during CS2

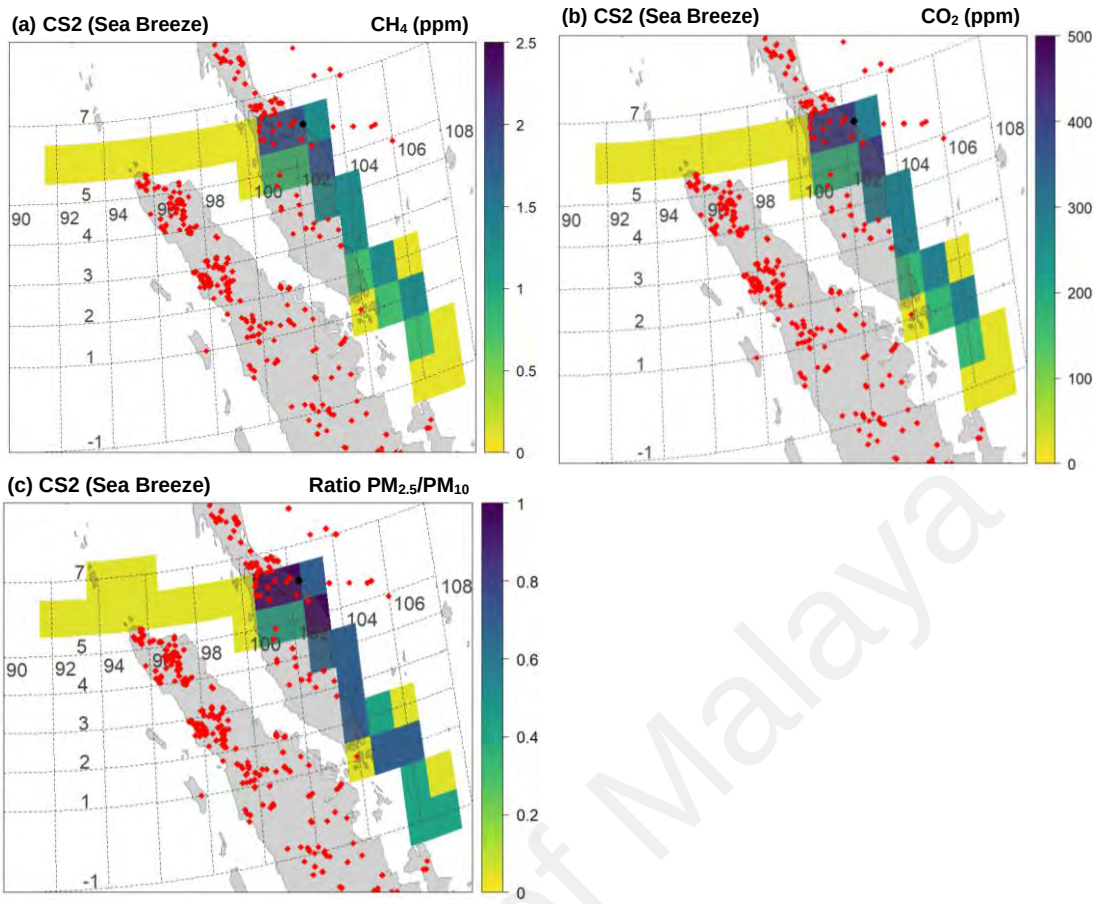

Figure 4.67: CWT during the sea breeze events coupled with hotspot data for (a) CH_4 (b) CO_2 and (c) RPM in CS2. The total trajectory time is 120-hour. Source ● is at 6.0086 °N and 102.4259 °E (BMRS location) . Points ◆ show the hotspot locations. Range of colors for the CWT described from non-source areas (yellow) to strongest source areas (dark blue) of pollutants at BMRS

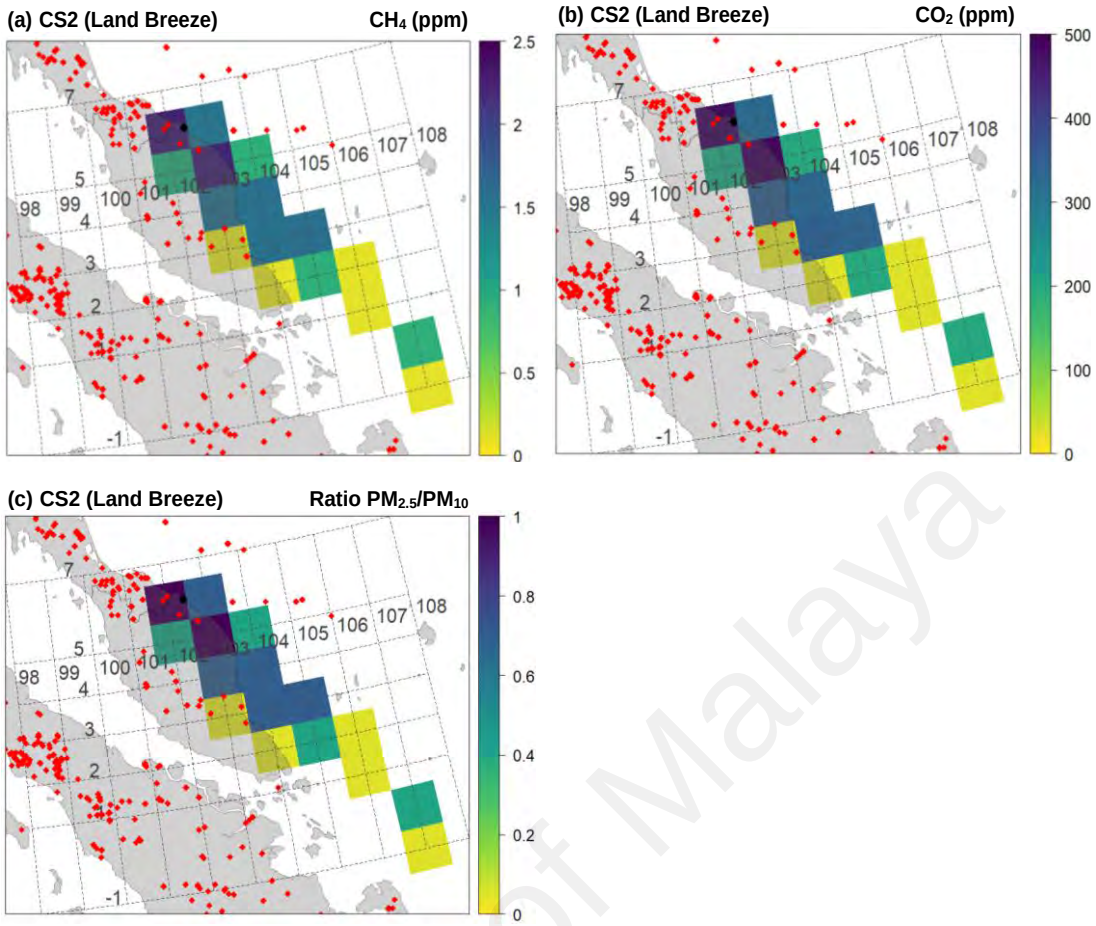

Figure 4.68: CWT during the land breeze events coupled with hotspot data for (a) CH_4 (b) CO_2 and (c) RPM in CS2. The total trajectory time is 120-hour. Source ● is at 6.0086 °N and 102.4259 °E (BMRS location) . Points ◆ show the hotspot locations. Range of colors for the CWT described from non-source areas (yellow) to strongest source areas (dark blue) of pollutants at BMRS

Atmospheric conditions played a key role in the distribution of air pollutants (Ahrens, 2011; Stull, 2016; Zhou et al., 2018). Using data from November 2014 to September 2016, this chapter shows that BMRS is influenced by the different meteorological conditions during the NE and SW monsoon differently. BMRS experienced both synoptic and local (land-sea breeze) meteorological conditions but only the local condition (land sea breeze) is dominant during the SW monsoon. More days with suppressed land sea breeze occurred during the NE monsoon in comparison to the SW monsoon. During the NE monsoon, this period was due to the strong synoptic event (cold surge) and other events like tropical storm, disturbance and tailed effect of the tropical storms. At BMRS, this period was attributed to dominant and strong onshore winds, no diurnal effect, low

levels of air pollutants (CO_2, CH_4, PM_{10} and $PM_{2.5}$). In addition, CWT analysis shows the principal sources of these pollutants were originated from the continental regions of China, SCS and ECS. The days with suppressed land sea breeze during the SW monsoon were also caused by the influence of synoptic flows which contributed to dominant and light offshore winds. Despite no clear changes of offshore and onshore winds shown, the temperature and the air pollutants during this period still experienced diurnal effect (weak). CWT analysis during this period show principal sources of air pollutants mostly dominated from the northern part of Peninsular Malaysia and area over the Malaysia-Thailand border. On the other hand, days with land sea breeze during both monsoon periods were associated with daily occurrence of land sea breeze and strong diurnal effect. During the NE monsoon, sea breeze event prevailed for longer period of times (14 hours) than land breeze event. Meanwhile, the sea breeze event only prevailed for 7 hours compared to land breeze event (17 hours) during the SW monsoon. The distribution of air pollutants during this period in both monsoon periods were strongly influenced by the variation of temperature and wind. Results from intensive case studies shows that CS1 was influenced by strong synoptic meteorological condition – cold surge event. This is attributed by dominance of strong easterly winds up to an altitude of 2500 m, weakened vertical thermal gradient and low levels of air pollutants at BMRS. However, this period was associated with regional source of pollutants from the continental region of China and coastal areas of Vietnam. Meanwhile, CS2 was influenced by local meteorological condition - land sea breeze, strong diurnal effect and closely linked to the local source of pollutants from areas along east coast of the Peninsular Malaysia.

CHAPTER 5: SUMMARY AND CONCLUSION

This chapter describes the summary and conclusions of this study. In addition, future works that can supplement this study is also presented.

5.1 Overall summary

This study assesses the meteorological conditions and the transport of CO_2, CH_4, PM_{10} and $PM_{2.5}$ over Bachok Marine Research Station (BMRS) (6.0086 °N and 102.4259 °E) during the NE and SW monsoon period using the observational data (BMRS) and remote sensing data from November 2014 to September 2016. The transport of the air pollutants at BMRS was examined using the CPFP plots, HYSPLIT model and CWT analysis.

In general, a statistical summary of observational data at BMRS during the NE and SW monsoon were attributed to different mean values of the meteorological parameters and air pollutants. The NE monsoon is associated with stronger wind speed and lower temperature. compared to the SW monsoon. CO_2, PM_{10} and $PM_{2.5}$ recorded to lower mean values in the former monsoon period while CH_4 recorded to the higher mean value.

BMRS experienced different meteorological conditions and characteristics in its transport of air pollutants during the NE and SW monsoon. During the NE monsoon, BMRS was influenced by the synoptic as well as local (land sea breeze) meteorological conditions. The significant pressure gradient between 30°N and 5°N during this monsoon period was the mechanism for the frequent influence of northeasterly synoptic flows at BMRS. 20% of the days in this monsoon period were attributed to suppressed land sea breeze over BMRS. This is influenced by the strong synoptic event like cold surge (20% of the days related to this event). Other synoptic events such as easterly surge, tropical storm, tropical disturbance and tailed effects of the tropical storm can also be the

precursor for this condition. At BMRS, this period was associated with dominant onshore winds (easterly and northeasterly winds), moderate to strong wind speed, very weak diurnal effect, low levels of air pollutants (CO_2, CH_4, PM_{10} and $PM_{2.5}$) and RPM within 0.9 (demonstrates the strong presence of fine particles). CPFP plots of show high CO_2 and CH_4 (above 95th percentile) are influenced by both offshore and onshore winds which indicated an interaction of both local and long-range transport of air pollutants respectively. Meanwhile, high RPM (above 95th percentile) is only associated with onshore wind. HYSPLIT-CWT analysis shows the long-range transport are associated with air pollutants emerged from the continental region of China, SCS and ECS.

Days with land sea breeze (local meteorological condition) during the NE monsoon were associated with clear diurnal effect in the variations of all meteorological parameters (except pressure) and air pollutants. The diurnal variation shows minimum mean temperature is at 08:00 LT (24°C) and maximum at 12:00 LT to 17:00 LT (within 28°C). Sea breeze event started at 11:00 LT and ended at 01:00 LT (14 hours) and followed by land breeze event which prevailed in the next 8 hours. The prolonged sea breeze during this monsoon period is influenced by moderate synoptic forcing. The diurnal cycle of air pollutants at BMRS is influenced by both the variations of temperature and wind. Initially, the rapid increase in temperature caused the decrease of air pollutants. Subsequent formation of sea breeze coupled with the increase of wind speed rapidly decreases the air pollutants within its lowest values. Then, the second phase of sea breeze with a gradual decrease in wind speed increases the level of the air pollutants. This is followed by land breeze event which continuously increases the air pollutants (under consistent light wind and decreases of temperature) to its maximum values. RPM also decreases with an increase in temperature however the first phase of sea breeze (with an increase in wind speed) increases RPM rapidly to its maximum value. The second phase of sea breeze (with a decrease in wind speed and temperature) and land breeze (consistent light wind

and decrease in temperature) decreases the RPM until its minimum value was reached. This demonstrates strong transport of fine particles during the high intensity of wind in the sea breeze event. CPFP plots show high CO_2 and CH_4 are influenced by offshore wind. However, high RPM are associated with onshore wind. HYSPLIT-CWT analysis shows the long-range transport of CO_2, CH_4 and RPM are mainly originated from the SCS and ECS.

During the SW monsoon, land sea breeze was strongly dominant where it occurred in 95% of the days. The remaining of the days were dominated by the southwesterly synoptic influence owing to the slight pressure differences existed between 5°N with 30°S. At BMRS, this period was associated with dominant and light offshore winds. Despite no land sea breeze, the hourly variations of temperature and the air pollutants during this period still show a diurnal effect (weak). CPFP plots show high CO_2 and CH_4 are associated with offshore wind. HYSPLIT-CWT analysis shows the principal sources air pollutants during this period are the northern region of Peninsular Malaysia and area over the border of Malaysia-Thailand.

Days with land sea breeze during the SW monsoon were also associated with clear diurnal effect in all of the meteorological parameters (except pressure) and air pollutants. The minimum temperature is shown at 07:00 LT (26°C) and maximum at 13:00 LT (30°C). The sea breeze event started in the afternoon at 12:00 LT and ended after sunrise at 19:00 LT (7 hours) while land breeze event prevailed for 17 hours. The diurnal cycle of air pollutants in this monsoon period also was influenced by both the temperature and wind. Sea breeze event during this period rapidly reduced the level of air pollutants where high temperature and strong wind decreased the level of air pollutants. The air pollutants increased rapidly in the land breeze event where it is associated with constant light wind and decreasing temperature. RPM shows very weak rate of changes (2% to 3%) from day

to night where clear changes only shown in early morning (from 07:00 LT to 10:00 LT). The remaining hours were dominated by a higher and consistent value (RPM ~ 0.97). This demonstrates very strong presence of fine particles. CPFP plots show high CO_2 and CH_4 are influenced by offshore wind while high RPM are associated to both onshore and offshore winds. HYSPLIT-CWT analysis generated during this period shown the principal sources of CO_2, CH_4 and RPM are the central regions of Peninsular Malaysia, the SCS, Indian Ocean and Java Sea.

Two case studies were conducted to examine the transport of air pollutants during specific meteorological conditions in the NE and SW monsoon extensively. The first case study (CS1) was conducted from 25 to 27 January 2016 while the second case study (CS2) was from 3 to 5 June 2016. Hourly ERA5 reanalysis wind data at 10 m, TRMM rain rate data, radiosonde data and hotspots data (from MODIS and VIRRS) were added to examine these case studies in depth. Results from case studies demonstrated the local and strong synoptic meteorological conditions from surface to lower troposphere in the SW and NE monsoon respectively. Hence, its relations and effects to the transport of air pollutants are allowed to be described in details.

CS1 was influenced by the strong synoptic meteorological condition - cold surge event. BMRS was associated with strong easterly winds up to an altitude of 2500 m, reduced vertical thermal gradient (clear vertical gradient seen only within 600 m), slight rain, and low levels of air pollutants during the whole period of CS1. Even though low levels of air pollutants resulted at BMRS, there were significant positive correlations shown between CO_2 and CH_4 with wind speed. This showed that the strong northeasterly wind favored the transport of CO_2 and CH_4 in moderate temperature conditions. CPFP plots and HYSPLIT-CWT analysis also justified the long-range transport of these air pollutants. The main (high) sources of the air pollutants at BMRS were the continental

region of China and areas along the coasts of Vietnam. These sources were possibly attributed to the industrial emissions and biomass burnings.

CS2 shows a characteristic of local meteorological condition – land sea breeze at BMRS. This condition was attributed with strong diurnal effect and significant negative correlations were shown between air pollutants with temperature and wind speed. The sea breeze event began at 1) 14:00 LT to 2000 LT on 3 June 2016; 2) 09:00 LT on 4 June 2016 to 00:00 LT on 5 June and 3) 14:00 LT on 5 June to 01:00 on the next day. The sea breeze extended up to a maximum of 1000 m uniformly at 20:00 LT and able to penetrate up to 30 to 90 km deep inland. This event was also associated with consistent and low level of air pollutants. The land breeze starts when offshore winds flowed consistently towards the SCS. This occurrence has contributed to higher and greater increases in air pollutant levels. CPFP plots and HYSPLIT-CWT analysis for both events demonstrate main (high) sources of the air pollutants were mainly originated from local and regional sources surrounding BMRS.

Overall, BMRS provides a valuable opportunity to research the impact of regional and local atmospheric conditions on air pollutants variability and thus allow better understanding and providing a key guide for formulating successful pollution abatement strategies in Malaysia and its neighbouring regions.

5.2 Major Conclusions

1. During the NE monsoon, BMRS is affected by the synoptic and local (land sea breeze) meteorological conditions while it is dominated by land sea breeze during the SW monsoon.

2. Days with suppressed land sea breeze at BMRS indicate an influence of synoptic flows during both the NE and SW monsoons. However, NE monsoon shows more and greater influence of synoptic flows like cold surge event and other events like tropical storm and monsoon disturbance. In BMRS, this period is dominated by onshore wind, no diurnal effect, moderate to strong wind speed, low level of air pollutants and high RPM (~ 0.90). The principal sources of air pollutants were highly originated from the continental region of China, SCS and ECS.
3. Days with land sea breeze at BMRS demonstrate strong diurnal effect and daily occurrences of land sea breeze during both the NE and SW monsoons. Sea breeze event during the NE monsoon is longer (14 hours) compared to the SW monsoon (7 hours) due to influences of synoptic forcing. Variations of air pollutants during this event is strongly influenced by the variations of temperature and wind. During the NE monsoon, principal (high) sources of pollutants were from the SCS and ECS, while the central region of Peninsular Malaysia, ECS, Indian Ocean and Java Sea were the principal sources of air pollutants during the SW monsoon.
4. CS1 has demonstrated characteristics of strong synoptic meteorological condition in the NE monsoon. BMRS was associated with strong easterly winds up to an altitude of 2500 m, weakened vertical thermal gradient and low levels of air pollutants. The main (high) sources of air pollutants at BMRS are the continental region of China and coastal areas of Vietnam.
5. CS2 indicated a characteristic of local meteorological condition in the SW monsoon. BMRS was associated with daily occurrences of land sea breeze and all the meteorological parameters and air pollutants strongly affected by the diurnal effect. The main sources of the air pollutants are the Malaysia-Thailand border and areas along the east coast of Peninsular Malaysia.

6. Overall, BMRS is continuously under- observed region and it provides a valuable opportunity to research the impact of regional and local atmospheric conditions to the variabilities of air pollutants in Malaysia and its neighborhood regions.

5.3 Suggestions for future work

The present study has shown that there is transport of regional sources of air pollutants from the continental regions of China and Vietnam under the influence of synoptic conditions during the NE monsoon. Investigating the variabilities of CO_2 and CH_4 over a longer period of time would be extremely beneficial. Another advance studies on the transport and biogeochemical interactions of these pollutants over the SCS would be beneficial in the study of climate change. Studies on many other chemical pollutants contained in the atmosphere during this monsoon period are also crucial for better understanding on the impact of regional air masses.

Oram et al. (2017) stressed that very short-lived anthropogenic chlorinated substances (Cl-VSLSs) can be transported routinely to Western Pacific tropical regions and further uplifted into the tropical upper troposphere. During CS1, heavy easterly winds and low temperatures prevailed at and above 600 m of altitude. This implies that more stagnant atmosphere and various amounts of air pollutants might be present there. Therefore, more air quality studies at higher altitudes are needed for further understanding on the effects of synoptic events on air pollution distribution.

REFERENCES

Achard, F., Beuchle, R., Mayaux, P., Stibig, H. J., Bodart, C., Brink, A., . . . Eva, H. D. (2014). Determination of tropical deforestation rates and related carbon losses from 1990 to 2010. *Global Change Biology, 20*(8), 2540-2554.

Aditama, T. Y. (2000). Impact of haze from forest fire to respiratory health: Indonesian experience. *Respirology, 5*(2), 169-174.

Afroz, R., Hassan, M. N., & Ibrahim, N. A. (2003). Review of air pollution and health impacts in Malaysia. *Environmental Research, 92*(2), 71-77. doi:http://dx.doi.org/10.1016/S0013-9351(02)00059-2

Ahrens, C. D. (2011). *Essentials of Meteorology: An Invitation to the Atmosphere*: Cengage Learning.

Akimoto, H. (2003). Global air quality and pollution. *Science, 302*(5651), 1716-1719.

Almeida, S. M., Pio, C. A., Freitas, M. C., Reis, M. A., & Trancoso, M. A. (2005). Source apportionment of fine and coarse particulate matter in a sub-urban area at the Western European Coast. *Atmospheric Environment, 39*(17), 3127-3138.

Andreae, M. O., & Crutzen, P. J. (1997). Atmospheric aerosols: Biogeochemical sources and role in atmospheric chemistry. *Science, 276*(5315), 1052-1058.

Ashfold, M., Latif, M., Samah, A., Mead, M. I., & Harris, N. R. (2017). Influence of Northeast Monsoon cold surges on air quality in Southeast Asia. *Atmospheric Environment, 166*, 498-509.

Ashfold, M. J., Pyle, J. A., Robinson, A. D., Meneguz, E., Nadzir, M. S. M., Phang, S. M., . . . Harris, N. R. P. (2015). Rapid transport of East Asian pollution to the deep tropics. *Atmospheric Chemistry and Physic, 15*, 3565-3573.

Azam, M., Alam, M. M., & Hafeez, M. H. (2018). Effect of tourism on environmental pollution: Further evidence from Malaysia, Singapore and Thailand. *Journal of Cleaner Production, 190*, 330-338.

Azmi, S. Z., Latif, M. T., Ismail, A. S., Juneng, L., & Jemain, A. A. (2010). Trend and status of air quality at three different monitoring stations in the Klang Valley, Malaysia. *Air Quality, Atmosphere & Health, 3*(1), 53-64.

Baccini, A., Goetz, S. J., Walker, W. S., Laporte, N. T., Sun, M., Sulla-Menashe, D., . . . Houghton, R. A. (2012). Estimated carbon dioxide emissions from tropical deforestation improved by carbon-density maps. *Nature Climate Change, 2*(3), 182-185. doi:10.1038/nclimate1354

Baker, J. (2010). A cluster analysis of long range air transport pathways and associated pollutant concentrations within the UK. *Atmospheric Environment, 44*(4), 563-571.

Beaver, S., & Palazoglu, A. (2009). Influence of synoptic and mesoscale meteorology on ozone pollution potential for San Joaquin Valley of California. *Atmospheric Environment, 43*(10), 1779-1788.

Berman, F., Chien, A., Cooper, K., Dongarra, J., Foster, I., Gannon, D., . . . Mellor-Crumme, J. (2001). The GrADS project: Software support for high-level grid application development. *The International Journal of High Performance Computing Applications, 15*(4), 327-344.

Betha, R., Behera, S. N., & Balasubramanian, R. (2014). 2013 Southeast Asian smoke haze: fractionation of particulate-bound elements and associated health risk. *Environmental Science & Technology, 48*(8), 4327-4335.

Borge, R., Lumbreras, J., Vardoulakis, S., Kassomenos, P., & Rodríguez, E. (2007). Analysis of long-range transport influences on urban PM 10 using two-stage atmospheric trajectory clusters. *Atmospheric Environment, 41*(21), 4434-4450.

Borne, K., Chen, D., & Nunez, M. (1998). A method for finding sea breeze days under stable synoptic conditions and its application to the Swedish west coast. *International Journal of Climatology: A Journal of the Royal Meteorological Society, 18*(8), 901-914.

Bouchlaghem, K., Nsom, B., Lattrache, N., & Haj, H. (2008). *Characterization of sea breezes and their effects on Air Pollution in the Tunisian Mediterranean region.* Paper presented at the WSEAS International Conference. Proceedings. Mathematics and Computers in Science and Engineering.

Byčenkienė, S., Plauškaitė, K., Dudoitis, V., & Ulevicius, V. (2014). Urban background levels of particle number concentration and sources in Vilnius, Lithuania. *Atmospheric Research, 143*, 279-292.

Caro, D. (2018). Greenhouse gas and livestock emissions and climate change *Encyclopedia: Reference Module in Food Science*.

Carslaw, D. (2012). The openair manual–open-source tools for analysing air pollution data. *Manual for version, 1*.

Carslaw, D. C., & Beevers, S. D. (2013). Characterising and understanding emission sources using bivariate polar plots and k-means clustering. *Environmental Modelling & Software, 40*, 325-329.

Carslaw, D. C., & Ropkins, K. (2012). Openair—an R package for air quality data analysis. *Environmental Modelling & Software, 27*, 52-61.

Chan, C. K., & Yao, X. (2008). Air pollution in mega cities in China. *Atmospheric Environment, 42*(1), 1-42. doi:http://dx.doi.org/10.1016/j.atmosenv.2007.09.003

Chang, C.-P., Wang, Z., & Hendon, H. (2006). The Asian winter monsoon *The Asian Monsoon* (pp. 89-127): Springer.

Chang, C., Erickson, J., & Lau, K. (1979). Northeasterly cold surges and near-equatorial disturbances over the winter MONEX area during December 1974. Part I: Synoptic aspects. *Monthly Weather Review, 107*(7), 812-829.

Chang, C., Harr, P. A., & Chen, H.-J. (2005). Synoptic disturbances over the equatorial South China Sea and western Maritime Continent during boreal winter. *Monthly Weather Review, 133*(3), 489-503.

Chate, D., & Pranesha, T. (2004). Field studies of scavenging of aerosols by rain events. *Journal of Aerosol Science, 35*(6), 695-706.

Chen, T.-C., Tsay, J.-D., Yen, M.-C., & Matsumoto, J. (2013). The winter rainfall of Malaysia. *Journal of Climate, 26*(3), 936-958.

Cheng, I., Zhang, L., Blanchard, P., Dalziel, J., & Tordon, R. (2013). Concentration-weighted trajectory approach to identifying potential sources of speciated atmospheric mercury at an urban coastal site in Nova Scotia, Canada. *Atmospheric Chemistry and Physics, 13*(12), 6031-6048.

Chenoli, S. N., Jayakrishnan, P., Samah, A. A., Hai, O. S., Mazuki, M. Y. A., & Lim, C. H. (2018). Southwest monsoon onset dates over Malaysia and associated climatological characteristics. *Journal of Atmospheric and Solar-Terrestrial Physics, 179*, 81-93.

Chuang, M.-T., Chou, C. C.-K., Sopajaree, K., Lin, N.-H., Wang, J.-L., Sheu, G.-R., . . . Lee, C.-T. (2013). Characterization of aerosol chemical properties from near-source biomass burning in the northern Indochina during 7-SEAS/Dongsha experiment. *Atmospheric Environment, 78*, 72-81.

Chung, C. E. (2012). Aerosol direct radiative forcing: a review *Atmospheric Aerosols-Regional Characteristics-Chemistry and Physics*: IntechOpen.

Crawford, S. L. (2006). Correlation and regression. *Circulation, 114*(19), 2083-2088.

D'Amato, G., Cecchi, L., D'Amato, M., & Annesi-Maesano, I. (2014). Climate change and respiratory diseases: Eur Respiratory Soc.

Dai, A., & Wang, J. (1999). Diurnal and semidiurnal tides in global surface pressure fields. *Journal of the atmospheric sciences, 56*(22), 3874-3891.

Daly, A., & Zannetti, P. (2007). Air pollution modeling–An overview. *Ambient air pollution*.

De Sario, M., Katsouyanni, K., & Michelozzi, P. (2013). Climate change, extreme weather events, air pollution and respiratory health in Europe. *European Respiratory Journal, 42*(3), 826-843.

Defries, R., Houghton, R., Hansen, M., Field, C., Skole, D., & Townshend, J. (2002). Carbon emissions from tropical deforestation and regrowth based on satellite observations for the 1980s and 1990s. *Proceedings of the National Academy of Sciences of the United States of America, 99*, 14256-14261. doi:10.1073/pnas.182560099

Department Of Environment. Official Portal of Department of Environment (DOE). Retrieved from https://www.doe.gov.my/portalv1/en/info-umum/info-kualiti-udara/kronologi-episod-jerebu-di-malaysia/319123

Dimitriou, K., Remoundaki, E., Mantas, E., & Kassomenos, P. (2015). Spatial distribution of source areas of PM2.5 by Concentration Weighted Trajectory (CWT) model applied in PM2.5 concentration and composition data. *Atmospheric Environment, 116*, 138-145. doi:https://doi.org/10.1016/j.atmosenv.2015.06.021

Ding, A., Wang, T., & Fu, C. (2013). Transport characteristics and origins of carbon monoxide and ozone in Hong Kong, South China. *Journal of Geophysical Research: Atmospheres, 118*(16), 9475-9488.

Dirksen, R., Sommer, M., Immler, F., Hurst, D., Kivi, R., & Vömel, H. (2014). Reference quality upper-air measurements: GRUAN data processing for the Vaisala RS92 radiosonde. *Atmospheric Measurement Techniques, 7*(12), 4463-4490.

Dolske, D. A., & Gatz, D. F. (1985). A field intercomparison of methods for the measurement of particle and gas dry deposition. *Journal of Geophysical Research: Atmospheres, 90*(D1), 2076-2084.

Dominick, D., Latif, M. T., Juahir, H., Aris, A. Z., & Zain, S. M. (2012). An assessment of influence of meteorological factors on PM10 and NO2 at selected stations in Malaysia. *Sustainable Environment Research, 22*(5), 305-315.

Dominick, D., Latif, M. T., Juneng, L., Khan, M. F., Amil, N., Mead, M. I., . . . Pyle, J. A. (2015). Characterisation of particle mass and number concentration on the east coast of the Malaysian Peninsula during the northeast monsoon. *Atmospheric Environment, 117*, 187-199. doi:http://dx.doi.org/10.1016/j.atmosenv.2015.07.018

Donets, V., Atlas, E. L., Pan, L., Schauffler, S., Honomichl, S., Hornbrook, R., . . . Ullmann, K. (2018). Wintertime Transport of Reactive Trace Gases From East Asia Into the Deep Tropics. *Journal of Geophysical Research: Atmospheres, 123*(22), 12,877-812,896.

Draxler, R., Stunder, B., Rolph, G., & Taylor, A. (2009). HYSPLIT_4 user's guide. NOAA Air Resources Laboratory: Silver Spring MD.

Draxler, R. R., & Hess, G. (1998). An overview of the HYSPLIT_4 modelling system for trajectories. *Australian meteorological magazine, 47*(4), 295-308.

Elminir, H. K. (2005). Dependence of urban air pollutants on meteorology. *Science of The Total Environment, 350*(1), 225-237.

Emmanuel, S. C. (2000). Impact to lung health of haze from forest fires: the Singapore experience. *Respirology, 5*(2), 175-182.

Etminan, M., Myhre, G., Highwood, E., & Shine, K. (2016). Radiative forcing of carbon dioxide, methane, and nitrous oxide: A significant revision of the methane radiative forcing. *Geophysical Research Letters, 43*(24), 12,614-612,623.

Farren, N. J., Dunmore, R. E., Mead, M. I., Nadzir, M., Shahrul, M., Samah, A. A., . . . Hamilton, J. F. (2019). Chemical characterisation of water-soluble ions in atmospheric particulate matter on the east coast of Peninsular Malaysia. *Atmospheric Chemistry and Physics, 19*(3), 1537-1553.

Fast, J. D., Allan, J., Bahreini, R., Craven, J., Emmons, L., Ferrace, R., . . . Zhang, Q. (2014). Modelling regional aerosol and aerosol precursor variability over California and its sensitivity to emissions and long range transport during the 2010 CalNex and CARES campaigns. *Atmospheric Chemistry and Physic, 14*, 10013-10060.

Feldpausch, T. R., Jirka, S., Passos, C. A. M., Jasper, F., & Riha, S. J. (2005). When big trees fall: Damage and carbon export by reduced impact logging in southern Amazonia. *Forest Ecology and Management, 219*(2), 199-215. doi:https://doi.org/10.1016/j.foreco.2005.09.003

Fitzherbert, E. B., Struebig, M. J., Morel, A., Danielsen, F., Brühl, C. A., Donald, P. F., & Phalan, B. (2008). How will oil palm expansion affect biodiversity? *Trends in ecology & evolution, 23*(10), 538-545.

Fleming, Z. L., Monks, P. S., & Manning, A. J. (2012). Untangling the influence of air-mass history in interpreting observed atmospheric composition. *Atmospheric Research, 104*, 1-39.

Furberg, M., Steyn, D., & Baldi, M. (2002). The climatology of sea breezes on Sardinia. *International Journal of Climatology: A Journal of the Royal Meteorological Society, 22*(8), 917-932.

García-Herrera, R., Díaz, J., Trigo, R. M., Luterbacher, J., & Fischer, E. M. (2010). A review of the European summer heat wave of 2003. *Critical Reviews in Environmental Science and Technology, 40*(4), 267-306.

Giglio, L., Schroeder, W., & Justice, C. O. (2016). The collection 6 MODIS active fire detection algorithm and fire products. *Remote Sensing of Environment, 178*, 31-41.

Gong, D. Y., & Ho, C. H. (2003). Arctic oscillation signals in the East Asian summer monsoon. *Journal of Geophysical Research: Atmospheres, 108*(D2).

Gong, D. Y., Wang, S. W., & Zhu, J. H. (2001). East Asian winter monsoon and Arctic oscillation. *Geophysical Research Letters, 28*(10), 2073-2076.

Grange, S. K., Lewis, A. C., & Carslaw, D. C. (2016). Source apportionment advances using polar plots of bivariate correlation and regression statistics. *Atmospheric Environment, 145*, 128-134.

Grell, G. A., Peckham, S. E., Schmitz, R., McKeen, S. A., Frost, G., Skamarock, W. C., & Eder, B. (2005). Fully coupled "online" chemistry within the WRF model. *Atmospheric Environment, 39*(37), 6957-6975.

GRIMM. (2018). Environ-edm 365 GRIMM Aerosol Technik. Retrieved from https://www.grimm-aerosol.com/products-en/environmental-dust-monitoring/pm-monitoring-station/edm365/

Grimm, H., & Eatough, D. J. (2009). Aerosol measurement: the use of optical light scattering for the determination of particulate size distribution, and particulate mass, including the semi-volatile fraction. *Journal of the Air & Waste Management Association, 59*(1), 101-107.

Hai, O. S., Samah, A. A., Chenoli, S. N., Subramaniam, K., & Ahmad Mazuki, M. Y. (2017). Extreme Rainstorms that Caused Devastating Flooding across the East Coast of Peninsular Malaysia during November and December 2014. *Weather and Forecasting, 32*(3), 849-872.

Han, Y., Holsen, T. M., Hopke, P. K., & Yi, S. (2005). Comparison between back-trajectory based modeling and Lagrangian backward dispersion modeling for locating sources of reactive gaseous mercury. *Environmental Science & Technology, 39*(6), 1715-1723.

Handbook of aviation meteorology. Meteorological office, London (Her Majesty's Stationery Office), 1971 Pp. xvii, 404; 31 Plates; 163 Figures; 12 Tables. £2.10. (1972). *Quarterly Journal of the royal meteorological society, 98*(416), 466-466. doi:10.1002/qj.49709841622

Haurwitz, B. (1965). The diurnal surface-pressure oscillation. *Archiv für Meteorologie, Geophysik und Bioklimatologie, Serie A, 14*(4), 361-379.

Heil, A., & Goldammer, J. (2001). Smoke-haze pollution: a review of the 1997 episode in Southeast Asia. *Regional Environmental Change, 2*(1), 24-37.

Hemond, H. F., & Fechner, E. J. (2014). *Chemical fate and transport in the environment*: Elsevier.

Hersbach, H. (2018). *Operational global reanalysis: progress, future directions and synergies with NWP*: European Centre for Medium Range Weather Forecasts.

Hidemori, T., Nakayama, T., Matsumi, Y., Kinugawa, T., Yabushita, A., Ohashi, M., . . . Kaneyasu, N. (2014). Characteristics of atmospheric aerosols containing heavy metals measured on Fukue Island, Japan. *Atmospheric Environment, 97*, 447-455.

Hoffmann, L., Günther, G., Li, D., Stein, O., Wu, X., Griessbach, S., . . . Vogel, B. (2019). From ERA-Interim to ERA5: the considerable impact of ECMWF's next-generation reanalysis on Lagrangian transport simulations. *Atmospheric Chemistry and Physics, 19*(5), 3097-3124.

Holmes, C. D. (2018). Methane Feedback on Atmospheric Chemistry: Methods, Models, and Mechanisms. *Journal of Advances in Modeling Earth Systems, 10*(4), 1087-1099.

Houghton, J. T., Ding, Y., Griggs, D. J., Noguer, M., van der Linden, P. J., Dai, X., . . . Johnson, C. (2001). Climate change 2001: the scientific basis.

Houghton, R. A. (2005). Aboveground Forest Biomass and the Global Carbon Balance. *Global Change Biology, 11*(6), 945-958. doi:10.1111/j.1365-2486.2005.00955.x

Huffman, G. J., Adler, R. F., Bolvin, D. T., & Nelkin, E. J. (2010). The TRMM multi-satellite precipitation analysis (TMPA) *Satellite rainfall applications for surface hydrology* (pp. 3-22): Springer.

Huffman, G. J., Bolvin, D. T., Nelkin, E. J., Wolff, D. B., Adler, R. F., Gu, G., . . . Stocker, E. F. (2007). The TRMM multisatellite precipitation analysis (TMPA): Quasi-global, multiyear, combined-sensor precipitation estimates at fine scales. *Journal of hydrometeorology, 8*(1), 38-55.

Huijnen, V., Wooster, M., Kaiser, J., Gaveau, D., Flemming, J., Parrington, M., . . . Van Weele, M. (2016). Fire carbon emissions over maritime southeast Asia in 2015 largest since 1997. *Scientific reports, 6*, 26886.

Ichoku, C., Kahn, R., & Chin, M. (2012). Satellite contributions to the quantitative characterization of biomass burning for climate modeling. *Atmospheric Research, 111*, 1-28.

IPCC. (2001). *Climate Change 2001: The Scientific Basis. Contribution of Working Group I to the Third Assessment Report of the*

Intergovernmental Panel on Climate Change. Retrieved from Cambridge University Press, Cambridge, United Kingdom and New York, NY, USA:

IPCC. (2014). *Climate Change 2014: Synthesis Report. Contribution of Working Groups I, II and III to the Fifth Assessment Report of the Intergovernmental Panel on Climate Change* Retrieved from IPCC, Geneva, Switzerland:

Joseph, B., Bhatt, B. C., Koh, T. Y., & Chen, S. (2008). Sea breeze simulation over the Malay Peninsula in an intermonsoon period. *Journal of Geophysical Research: Atmospheres, 113*(D20).

Juneng, L., Latif, M. T., & Tangang, F. (2011). Factors influencing the variations of PM10 aerosol dust in Klang Valley, Malaysia during the summer. *Atmospheric Environment, 45*(26), 4370-4378. doi:http://dx.doi.org/10.1016/j.atmosenv.2011.05.045

Juneng, L., Tangang, F., & Reason, C. (2007). Numerical case study of an extreme rainfall event during 9–11 December 2004 over the east coast of Peninsular Malaysia. *Meteorology and Atmospheric Physics, 98*(1-2), 81-98.

Kaneyasu, N., Takeuchi, K., Hayashi, M., Fujita, S. i., Uno, I., & Sasaki, H. (2000). Outflow patterns of pollutants from East Asia to the North Pacific in the winter monsoon. *Journal of Geophysical Research: Atmospheres, 105*(D13), 17361-17377.

Karaca, F., & Camci, F. (2010). Distant source contributions to PM 10 profile evaluated by SOM based cluster analysis of air mass trajectory sets. *Atmospheric Environment, 44*(7), 892-899.

Kavitha, M., Nair, P. R., Girach, I., Aneesh, S., Sijikumar, S., & Renju, R. (2018). Diurnal and seasonal variations in surface methane at a tropical coastal station: Role of mesoscale meteorology. *Science of The Total Environment, 631*, 1472-1485.

Kellogg, W. W. (2019). *Climate change and society: consequences of increasing atmospheric carbon dioxide*: Routledge.

Khan, M., Latif, M. T., Saw, W., Amil, N., Nadzir, M. S. M., Sahani, M., . . . Chung, J. (2016). Fine particulate matter in the tropical environment: monsoonal effects, source apportionment, and health risk assessment. *Atmospheric Chemistry and Physics, 16*(2), 597-617.

Khan, M. F., Latif, M. T., Amil, N., Juneng, L., Mohamad, N., Nadzir, M. S. M., & Hoque, H. M. S. (2015). Characterization and source apportionment of particle number concentration at a semi-urban tropical environment. *Environmental Science and Pollution Research, 22*(17), 13111-13126.

Khan, M. F., Latif, M. T., Lim, C. H., Amil, N., Jaafar, S. A., Dominick, D., . . . Tahir, N. M. (2015). Seasonal effect and source apportionment of polycyclic aromatic hydrocarbons in PM2. 5. *Atmospheric Environment, 106*, 178-190.

Khatiwala, S., Tanhua, T., Mikaloff Fletcher, S., Gerber, M., Doney, S., Graven, H., . . . Ríos, A. (2013). Global ocean storage of anthropogenic carbon. *Biogeosciences, 10*(4), 2169-2191.

Kim, E., & Hopke, P. K. (2004). Comparison between conditional probability function and nonparametric regression for fine particle source directions. *Atmospheric Environment, 38*(28), 4667-4673.

Koe, L. C., Arellano Jr, A. F., & McGregor, J. L. (2001). Investigating the haze transport from 1997 biomass burning in Southeast Asia: its impact upon Singapore. *Atmospheric Environment, 35*(15), 2723-2734.

Kolb, C. E., & Worsnop, D. R. (2012). Chemistry and Composition of Atmospheric Aerosol Particles. *Annual Review of Physical Chemistry, 63*(1), 471-491. doi:10.1146/annurev-physchem-032511-143706

Krishna Moorthy, K., Pillai, P. S., & Suresh Babu, S. (2003). Influence of Changes in the Prevailing Synoptic Conditions on the Response of Aerosol Characteristics to Land- and Sea-Breeze Circulations at a Coastal Station. *Boundary-layer meteorology, 108*(1), 145-161. doi:10.1023/a:1023073929115

Krzyżanowski, M., Kuna-Dibbert, B., & Schneider, J. (2005). *Health effects of transport-related air pollution*: WHO Regional Office Europe.

Kweku, D. W., Bismark, O., Maxwell, A., Desmond, K. A., Danso, K. B., Oti-Mensah, E. A., . . . Adormaa, B. B. (2017). Greenhouse effect: Greenhouse gases and their impact on global warming. *Journal of Scientific Research and Reports*, 1-9.

Lal, S. (2007). Trace gases over the Indian region. *Indian Journal of Radio and Space Physics, 36*, 556-570.

Langfelder, P., & Horvath, S. (2012). Fast R functions for robust correlations and hierarchical clustering. *Journal of statistical software, 46*(11).

Latif, M. T., Dominick, D., Ahamad, F., Khan, M. F., Juneng, L., Hamzah, F. M., & Nadzir, M. S. M. (2014). Long term assessment of air quality from a background station on the Malaysian Peninsula. *Science of The Total Environment, 482*, 336-348.

Latif, M. T., Dominick, D., Ahmad, F., Khan, M. F., Juneng, L., Hamzah, F. M., & Nadzir, M. S. M. (2014). Long term assessment of air quality from background station on Malaysian Peninsula. *Science of The Total Environment, 482-483*, 336-348.

Latif, M. T., Othman, M., Idris, N., Juneng, L., Abdullah, A. M., Hamzah, W. P., . . . Aghamohammadi, N. (2018). Impact of regional haze towards air quality in Malaysia: a review. *Atmospheric Environment, 177*, 28-44.

Le, T. H., Nguyen, T. N. T., Lasko, K., Ilavajhala, S., Vadrevu, K. P., & Justice, C. (2014). Vegetation fires and air pollution in Vietnam. *Environmental Pollution, 195*, 267-275.

Letcher, T. M. (2019). 1 - Why do we have global warming? In T. M. Letcher (Ed.), *Managing Global Warming* (pp. 3-15): Academic Press.

Lim, J. T., & Samah, A. A. (2004). *Weather and climate of Malaysia*: University of Malaya Press.

Lin, C.-Y., Liu, S. C., Chou, C. C., Liu, T. H., Lee, C.-T., Yuan, C.-S., . . . Young, C.-Y. (2004). Long-range transport of Asian dust and air pollutants to Taiwan. *Terr. Atmos. Ocean. Sci, 15*(5), 759-784.

Lin, C. Y., Zhao, C., Liu, X., Lin, N. H., & Chen, W. N. (2014). Modelling of long-range transport of Southeast Asia biomass-burning aerosols to Taiwan and their radiative forcings over East Asia. *Chemical and Physical Meteorology, 66*, 1-17.

Liu, H., Jacob, D. J., Bey, I., Yantosca, R. M., Duncan, B. N., & Sachse, G. W. (2003). Transport pathways for Asian pollution outflow over the Pacific: Interannual and seasonal variations. *Journal of Geophysical Research: Atmospheres, 108*(D20).

Loo, Y. Y., Billa, L., & Singh, A. (2015). Effect of climate change on seasonal monsoon in Asia and its impact on the variability of monsoon rainfall in Southeast Asia. *Geoscience Frontiers, 6*(6), 817-823.

Mandal, T. K., Khan, A., Ahammed, Y. N., Tanwar, R. S., Parmar, R. S., Zalpuri, K. S., . . . Shepherd, A. J. (2006). Observations of trace gases and aerosols over the Indian Ocean during the monsoon transition period. *Journal of Earth System Science*, 473-484.

Markou, M., & Kassomenos, P. (2010). Cluster analysis of five years of back trajectories arriving in Athens, Greece. *Atmospheric Research, 98*(2), 438-457.

Masson-Delmotte, V., Zhai, P., Pörtner, H.-O., Roberts, D., Skea, J., Shukla, P., . . . Pidcock, R. (2018). *Global Warming of 1.5 OC: An IPCC Special Report on the Impacts of Global Warming of 1.5° C Above Pre-industrial Levels and Related Global Greenhouse Gas Emission Pathways, in the Context of Strengthening the Global Response to the Threat of Climate Change, Sustainable Development, and Efforts to Eradicate Poverty*: World Meteorological Organization Geneva, Switzerland.

McMichael, A. J., Woodruff, R. E., & Hales, S. (2006). Climate change and human health: present and future risks. *The Lancet, 367*(9513), 859-869.

McNeill, V. F. (2017). Atmospheric Aerosols: Clouds, Chemistry, and Climate. *Annual Review of Chemical and Biomolecular Engineering, 8*(1), 427-444. doi:10.1146/annurev-chembioeng-060816-101538

Mead, M. I., Castruccio, S., Latif, M. T., Nadzir, M. S. M., Dominick, D., Thota, A., & Crippa, P. (2018). Impact of the 2015 wildfires on Malaysian air quality and exposure: a comparative study of observed and modeled data. *Environmental Research Letters, 13*(4), 044023.

Michael, M., Yadav, A., Tripathi, S. N., Kanawade, V. P., Gaur, A., Sadavarte, P., & Ventakaraman, C. (2014). Simulation of trace gases and aerosols over the Indian domain: evaluation of the WRF-Chem model. *Geoscientific Model Development, 7*, 431-482.

Michalakes, J., Chen, S., Dudhia, J., Hart, L., Klemp, J., Middlecoff, J., & Skamarock, W. (2001). Development of a next-generation regional weather research and forecast model *Developments in Teracomputing* (pp. 269-276): World Scientific.

Mudelsee, M. (2003). Estimating Pearson's correlation coefficient with bootstrap confidence interval from serially dependent time series. *Mathematical Geology, 35*(6), 651-665.

Munir, S. (2017). Analysing temporal trends in the ratios of PM2. 5/PM10 in the UK. *Aerosol and Air Quality Research, 17*(1), 34-48.

Nadzir, M. S. M., Phang, S. M., Abas, M. R., Abdul Rahman, N., Abu Samah, A., Sturges, W. T., . . . Amiruddin, A. M. (2014). Bromocarbons in the tropical coastal and open ocean atmosphere during the 2009 Prime Expidition Sciencetific Cruise (PESC-09). *Atmospheric Chemistry and Physic, 14*, 8137-8148.

Nair, S. K., Anurose, T., Subrahamanyam, D. B., Kumar, N., Santosh, M., Sijikumar, S., . . . Namboodiri, K. (2011). Characterization of the Vertical Structure of Coastal Atmospheric Boundary Layer over Thumba (*Advances in Meteorology, 2011*.

Nash, J., Oakley, T., Vömel, H., & Wei, L. (2011). WMO intercomparison of high quality radiosonde systems, Yangjiang, China, 12 July–3 August 2010. *World Meteorological Organization, Instruments and Observing methods, report No, 107*.

Nash, J., Smout, R., Oakley, T., Pathack, B., & Kurnosenko, S. (2005). WMO intercomparison of high quality radiosonde systems, Vacoas, Mauritius, 2–25 February 2005. *WMO Report. Available from CIMO*.

NCAR. WRF-CHEM. Retrieved from https://www2.acd.ucar.edu/wrf-chem

Newell, R. E., & Evans, M. J. (2000). Seasonal changes in pollutant transport to the North Pacific: the relative importance of Asian and European sources. *Geophysical Research Letters, 27*(16), 2509-2512.

Nguyen, G. T. H., Shimadera, H., Sekiguchi, A., Matsuo, T., & Kondo, A. (2019). Investigation of aerosol direct effects on meteorology and air quality in East Asia by using an online coupled modeling system. *Atmospheric Environment*.

NOAA. A complete Modelling System for Simulating Dispersion of Harmful Atmospheric Material. Retrieved from http://www.arl.noaa.gov/documents/Summaries/Dispersion_HYSPLIT.pdf

NOAA. Earth System Climate Change. Retrieved from http://sos.noaa.gov/Education/earth_system.html

O'Shea, S., Bauguitte, S.-B., Gallagher, M., Lowry, D., & Percival, C. (2013). Development of a cavity-enhanced absorption spectrometer for airborne measurements of CH 4 and CO 2. *Atmospheric Measurement Techniques, 6*(5), 1095-1109.

OECD. (2019). *Economic Outlook for Southeast Asia, China and India 2019 – Update*.

Ooi, S. H., Samah, A. A., & Braesicke, P. (2011). A case study of the Borneo Vortex genesis and its interactions with the global circulation. *Journal of Geophysical Research: Atmospheres, 116*(D21).

Oram, D. E., Ashfold, M. J., Laube, J. C., Gooch, L. J., Humphrey, S., Sturges, W. T., . . . Mead, M. I. (2017). A growing threat to the ozone layer from short-lived anthropogenic chlorocarbons. *Atmospheric Chemistry and Physics, 17*(19), 11929-11941.

Othman, J., Sahani, M., Mahmud, M., & Ahmad, M. K. S. (2014). Transboundary smoke haze pollution in Malaysia: Inpatient health impacts and economic valuation. *Environmental Pollution, 189*, 194-201.

Owen, R. C. (2009). *Long- Range Pollution Transport: Trans-Atlantic Mechanisms and Lagrangian Modelling Methods* (Doctor of Philosophy (Envieonmental Engineering)), Michigan Technological University.

Palmer, P. I. (2008). Quantifying sources and sinks of trace gases using space-borne measurements: current and future science. *Journal of Geophysical Research*, 1-19.

Park, T. W., Ho, C. H., Jeong, S. J., Choi, Y. S., Park, S. K., & Song, C. K. (2011). Different characteristics of cold day and cold surge frequency over East Asia in a

global warming situation. *Journal of Geophysical Research: Atmospheres, 116*(D12).

Patra, P. K., Takigawa, M., Ishijima, K., Choi, B.-C., Cunnold, D., Dlugokencky, E. J., . . . Kim, J.-S. (2009). Growth rate, seasonal, synoptic, diurnal variations and budget of methane in the lower atmosphere. *Journal of the Meteorological Society of Japan. Ser. II, 87*(4), 635-663.

Pearson, T. R. H., Brown, S., Murray, L., & Sidman, G. (2017). Greenhouse gas emissions from tropical forest degradation: an underestimated source. *Carbon Balance and Management, 12*(1), 3. doi:10.1186/s13021-017-0072-2

Peng, G., Li, J., Chen, Y., Norizan, A. P., & Tay, L. (2006). High-resolution surface relative humidity computation using MODIS image in Peninsular Malaysia. *Chinese Geographical Science, 16*(3), 260-264.

Petit, J.-E., Favez, O., Albinet, A., & Canonaco, F. (2017). A user-friendly tool for comprehensive evaluation of the geographical origins of atmospheric pollution: Wind and trajectory analyses. *Environmental Modelling & Software, 88*, 183-187.

Pierro, M. D., Jaegle, L., & Anderson, T. L. (2011). Satellite observations of aerosol transport from East Asia to the Arctic: three case studies. *Atmospheric Chemistry and Physic, 11*, 2225-2243.

Pochanart, P., Kreasuwun, J., Sukasem, P., Geeratithadaniyom, W., Tabucanon, M. S., Hirokawa, J., . . . Akimoto, H. (2001). Tropical tropospheric ozone observed in Thailand. *Atmospheric Environment, 35*(15), 2657-2668.

Pochanart, P., Wild, O., & Akimoto, H. (2004). Air pollution import to and export from East Asia *Air Pollution* (pp. 99-130): Springer.

Price, O. F., Williamson, G. J., Henderson, S. B., Johnston, F., & Bowman, D. M. (2012). The relationship between particulate pollution levels in Australian cities, meteorology, and landscape fire activity detected from MODIS hotspots. *PloS one, 7*(10), e47327.

Pyle, J. A., Ashfold, M. J., Harris, N. R. P., Robinson, A. D., Warwick, N. J., Carver, G. D., . . . Ong, S. (2011). Bromoform in the tropical boundary layer of the Maritime Continent during OP3. *Atmospheric Chemistry and Physic, 11*, 529-542.

Qian, Y., Gustafson, J. W. I., & Fast, J. D. (2010). An investigation of the sub-grid variability of trace gases and aerosols for global climate modeling. *Atmospheric Chemistry and Physic, 10*, 6917-6946.

Rahman, S. R. A., Ismail, S. N. S., Raml, M. F., Latif, M. T., Abidin, E. Z., & Praveena, S. M. (2015). The assessment of ambient air pollution trend in Klang Valley, Malaysia. *World Environment, 5*(1), 1-11.

Ramanathan, V., & Feng, Y. (2009). Air pollution, greenhouse gases and climate change: Global and regional perspectives. *Atmospheric Environment, 43*(1), 37-50. doi:https://doi.org/10.1016/j.atmosenv.2008.09.063

Ratner, B. (2009). The correlation coefficient: Its values range between+ 1/− 1, or do they? *Journal of targeting, measurement and analysis for marketing, 17*(2), 139-142.

Razali, N. Y. Y., Latif, M. T., Dominick, D., Mohamad, N., Sulaiman, F. R., & Srithawirat, T. (2015). Concentration of particulate matter, CO and CO2 in selected schools in Malaysia. *Building and environment, 87*, 108-116.

Reay, D. (2007). *Greenhouse gas sinks*: CABI.

Reay, D. S., Smith, P., Christensen, T. R., James, R. H., & Clark, H. (2018). Methane and Global Environmental Change. *Annual Review of Environment and Resources, 43*(1), 165-192. doi:10.1146/annurev-environ-102017-030154

Remer, L. A., Chin, M., DeCola, P., Feingold, G., Halthore, R., Kahn, R. A., . . . Yu, H. (2009). *Atmospheric Aerosol Properties and Climate Impacts*. Retrieved from http://irina.eas.gatech.edu/EAS8802_Spring2011/Report2009-aerosol-climate.pdf

Ritchie, H., & Roser, M. (2017). CO_2 and greenhouse gas emissions. *Our world in data*.

Roeloffzen, J. C., Van Den Berg, W., & Oerlemans, J. (1986). Frictional convergence at coastlines. *Tellus A: Dynamic Meteorology and Oceanography, 38*(5), 397-411.

Sahani, M., Zainon, N. A., Mahiyuddin, W. R. W., Latif, M. T., Hod, R., Khan, M. F., . . . Chan, C.-C. (2014). A case-crossover analysis of forest fire haze events and mortality in Malaysia. *Atmospheric Environment, 96*, 257-265.

Samah, A. A., Babu, C., Varikoden, H., Jayakrishnan, P., & Hai, O. S. (2016). Thermodynamic and dynamic structure of atmosphere over the east coast of Peninsular Malaysia during the passage of a cold surge. *Journal of Atmospheric and Solar-Terrestrial Physics, 146*, 58-68.

Saunois, M., Bousquet, P., Poulter, B., Peregon, A., Ciais, P., Canadell, J. G., . . . Houweling, S. (2016). The global methane budget 2000–2012. *Earth System Science Data, 8*(2), 697-751.

Schoot, M. V. v. d., Nahas, A. C., Atsushi, T., Lim, H.-C., Choi, T., Mohamad, M., & Ying, T. Y. (2011). *Asian GAW Greenhouse Gases Newsletter* Retrieved from WMO:

Schroeder, W., Oliva, P., Giglio, L., & Csiszar, I. A. (2014). The New VIIRS 375 m active fire detection data product: Algorithm description and initial assessment. *Remote Sensing of Environment, 143*, 85-96.

See, S., Balasubramanian, R., & Wang, W. (2006). A study of the physical, chemical, and optical properties of ambient aerosol particles in Southeast Asia during hazy and nonhazy days. *Journal of Geophysical Research: Atmospheres, 111*(D10).

Seibert, P., Beyrich, F., Gryning, S.-E., Joffre, S., Rasmussen, A., & Tercier, P. (2000). Review and intercomparison of operational methods for the determination of the mixing height. *Atmospheric Environment, 34*(7), 1001-1027.

Seidel, D. J., Ao, C. O., & Li, K. (2010). Estimating climatological planetary boundary layer heights from radiosonde observations: Comparison of methods and uncertainty analysis. *Journal of Geophysical Research: Atmospheres, 115*(D16).

Semire, F. A., Mohd-Mokhtar, R., Ismail, W., Mohamad, N., & Mandeep, J. (2012). Ground validation of space-borne satellite rainfall products in Malaysia. *Advances in Space Research, 50*(9), 1241-1249.

Shariff, A. R. M., Singh, M. S. J., Chellappan, K., Suparta, W., Tangang, F. T., Salimun, E., . . . Islam, M. T. (2015). A preliminary study of cold surges and precipitation during the northeast monsoon season over Malaysia. *Advanced Science Letters, 21*(2), 185-188.

Sheil, D., Casson, A., Meijaard, E., Van Noordwijk, M., Gaskell, J., Sunderland-Groves, J., . . . Kanninen, M. (2009). *The impacts and opportunities of oil palm in Southeast Asia: What do we know and what do we need to know?* : Center for International Forestry Research Bogor, Indonesia.

Spielvogel, J., Hartstock, S., & Grimm, H. (2009). *New methods and standards for fine dust.* Paper presented at the Journal of physics: conference series.

Stein, A., Draxler, R. R., Rolph, G. D., Stunder, B. J., Cohen, M., & Ngan, F. (2015). NOAA's HYSPLIT atmospheric transport and dispersion modeling system. *Bulletin of the American Meteorological Society, 96*(12), 2059-2077.

Stocker, T. F., Qin, D., Plattner, G.-K., Tignor, M., Allen, S. K., Boschung, J., . . . Midgley, P. M. (2013). Climate change 2013: The physical science basis. *Contribution of working group I to the fifth assessment report of the intergovernmental panel on climate change, 1535*.

Strode, S., & Zhu, Z. (2010). *Report on Consistent MERRA- Atmospheric Trace Gas Distributions*. Retrieved from http://gmao.gsfc.nasa.gov/projects/ARRA/PIESA_Chemistry_FinalReport.pdf

Stull, R. B. (2006). The atmospheric boundary layer. *Atmospheric Science, An Introduction Survey. Elsevier*.

Stull, R. B. (2016). *Practical Meteorology: An Algebra-based Survey of Atmospheric Science.* University of British Columbia.

Su, L., Yuan, Z., Fung, J. C., & Lau, A. K. (2015). A comparison of HYSPLIT backward trajectories generated from two GDAS datasets. *Science of The Total Environment, 506*, 527-537.

Sugimoto, N., Shimizu, A., Matsui, I., & Nishikawa, M. (2016). A method for estimating the fraction of mineral dust in particulate matter using PM2. 5-to-PM10 ratios. *Particuology, 28*, 114-120.

Tajudin, M. A. B. A., Khan, M. F., Mahiyuddin, W. R. W., Hod, R., Latif, M. T., Hamid, A. H., . . . Sahani, M. (2019). Risk of concentrations of major air pollutants on the prevalence of cardiovascular and respiratory diseases in urbanized area of Kuala Lumpur, Malaysia. *Ecotoxicology and environmental safety, 171*, 290-300.

Tan, F., Lim, H., & Abdullah, K. (2013). Effects of Orography on the Tail-End Effects of Typhoon Ketsana. *Open Atmospheric Science Journal, 7*, 14-28.

Tangang, F., Farzanmanesh, R., Mirzaei, A., Supari, Salimun, E., Jamaluddin, A. F., & Juneng, L. (2017). Characteristics of precipitation extremes in Malaysia associated with El Niño and La Niña events. *International Journal of Climatology, 37*(S1), 696-716. doi:10.1002/joc.5032

Tangang, F. T., Juneng, L., Salimun, E., Vinayachandran, P., Seng, Y. K., Reason, C., . . . Yasunari, T. (2008). On the roles of the northeast cold surge, the Borneo vortex, the Madden-Julian Oscillation, and the Indian Ocean Dipole during the extreme 2006/2007 flood in southern Peninsular Malaysia. *Geophysical Research Letters, 35*(14).

Toh, Y. Y., Lim, S. F., & Von Glasow, R. (2013). The influence of meteorological factors and biomass burning on surface ozone concentrations at Tanah Rata, Malaysia. *Atmospheric Environment, 70*, 435-446.

Tong, L., Zhang, J., Xiao, H., Cai, Q., Huang, Z., Zhang, H., . . . Feng, J. (2017). Identification of the potential regions contributing to ozone at a coastal site of eastern China with air mass typology. *Atmospheric Pollution Research, 8*(6), 1044-1057.

Trogler, W. C. (1995). The environmental chemistry of trace atmospheric gases: ACS Publications.

Uria-Tellaetxe, I., & Carslaw, D. C. (2014). Conditional bivariate probability function for source identification. *Environmental Modelling & Software, 59*, 1-9.

Urraca, R., Huld, T., Gracia-Amillo, A., Martinez-de-Pison, F. J., Kaspar, F., & Sanz-Garcia, A. (2018). Evaluation of global horizontal irradiance estimates from ERA5 and COSMO-REA6 reanalyses using ground and satellite-based data. *Solar Energy, 164*, 339-354.

Vardoulakis, S., & Kassomenos, P. (2008). Sources and factors affecting PM10 levels in two European cities: Implications for local air quality management. *Atmospheric Environment, 42*(17), 3949-3963.

Varikoden, H., Preethi, B., Samah, A., & Babu, C. (2011). Seasonal variation of rainfall characteristics in different intensity classes over Peninsular Malaysia. *Journal of hydrology, 404*(1-2), 99-108.

Varikoden, H., Samah, A., & Babu, C. (2010). Spatial and temporal characteristics of rain intensity in the peninsular Malaysia using TRMM rain rate. *Journal of hydrology, 387*(3-4), 312-319.

Vellingiri, K., Kim, K.-H., Lim, J.-M., Lee, J.-H., Ma, C.-J., Jeon, B.-H., . . . Kang, C.-H. (2016). Identification of nitrogen dioxide and ozone source regions for an urban area in Korea using back trajectory analysis. *Atmospheric Research, 176*, 212-221.

Wallace, & Hobbs. (2006). *Atmospheric Science: An Introductory Survey: Second Edition*.

Wang, B. (2006). *The asian monsoon*: Springer Science & Business Media.

Wang, Y., Zhang, X., & Draxler, R. R. (2009). TrajStat: GIS-based software that uses various trajectory statistical analysis methods to identify potential sources from long-term air pollution measurement data. *Environmental Modelling and Software, 24*(8), 938-939.

Wangwongchai, A., Sixiong, Z., & Qingcun, Z. (2005). A case study on a strong tropical disturbance and record heavy rainfall in Hat Yai, Thailand during the winter monsoon. *Advances in Atmospheric Sciences, 22*(3), 436-450.

Wei, J., Tang, G., Zhu, X., Wang, L., Liu, Z., Cheng, M., . . . Wang, Y. (2018). Thermal internal boundary layer and its effects on air pollutants during summer in a coastal city in North China. *Journal of Environmental Sciences, 70*, 37-44.

Wenig, M., Spichtinger, N., Stohl, A., Held, G., Beirle, S., Wagner, T., . . . Platt, U. (2003). Intercontinental transport of nitrogen oxide pollution plumes. *Atmospheric Chemistry and Physics, 3*(2), 387-393.

Westmoreland, E. J., Carslaw, N., Carslaw, D. C., Gillah, A., & Bates, E. (2007). Analysis of air quality within a street canyon using statistical and dispersion modelling techniques. *Atmospheric Environment, 41*(39), 9195-9205.

WHO. (2005). *Air Quality Guidelines: Global Update*. Europe: World Health Organization (WHO) 2006.

Wilcove, D. S., & Koh, L. P. (2010). Addressing the threats to biodiversity from oil-palm agriculture. *Biodiversity and conservation, 19*(4), 999-1007.

Wilks, D. S. (2011). *Statistical methods in the atmospheric sciences* (Vol. 100): Academic press.

WMO. World Meteorological Organization. *Greenhouse gas concentrations surge to new record.* Retrieved from https://public.wmo.int/en/media/press-release/greenhouse-gas-concentrations-surge-new-record

Wooster, M. J., Roberts, G., Perry, G., & Kaufman, Y. (2005). Retrieval of biomass combustion rates and totals from fire radiative power observations: FRP derivation and calibration relationships between biomass consumption and fire radiative energy release. *Journal of Geophysical Research: Atmospheres, 110*(D24).

World Health Organization. (2006). *Air quality guidelines: global update 2005: particulate matter, ozone, nitrogen dioxide, and sulfur dioxide*: World Health Organization.

World Health Organization. (2016). World Health Organization. *Ambient (outdoor) air quality and health.* Retrieved from Ambient (outdoor) air quality and health

World Health Organization. (2018). 9 out of 10 people worldwide breathe polluted air, but more countries are taking action [Press release]. Retrieved from https://www.who.int/news-room/detail/02-05-2018-9-out-of-10-people-worldwide-breathe-polluted-air-but-more-countries-are-taking-action

World Meteorological Organization. (2017). WMO GREENHOUSE GAS BULLETIN-No. 13.

World Meteorological Organization. (2018). WMO GREENHOUSE GAS BULLETIN-No. 14.

Wu, B., & Wang, J. (2002). Winter Arctic oscillation, Siberian high and East Asian winter monsoon. *Geophysical Research Letters, 29*(19), 3-1-3-4.

Wu, Y., Liu, J., Zhai, J., Cong, L., Wang, Y., Ma, W., . . . Li, C. (2018). Comparison of dry and wet deposition of particulate matter in near-surface waters during summer. *PloS one, 13*(6), e0199241.

Wu, Z., Lin, T., Li, Z., Jiang, Y., Li, Y., Yao, X., . . . Guo, Z. (2017). Air–sea exchange and gas–particle partitioning of polycyclic aromatic hydrocarbons over the northwestern Pacific Ocean: Role of East Asian continental outflow. *Environmental Pollution, 230*, 444-452.

Xu, G., Jiao, L., Zhang, B., Zhao, S., Yuan, M., Gu, Y., . . . Tang, X. (2017). Spatial and temporal variability of the PM2. 5/PM10 ratio in Wuhan, Central China. *Aerosol Air Qual. Res, 17*, 741-751.

Xu, M., Chang, C. P., Fu, C., Qi, Y., Robock, A., Robinson, D., & Zhang, H. m. (2006). Steady decline of east Asian monsoon winds, 1969–2000: Evidence from direct ground measurements of wind speed. *Journal of Geophysical Research: Atmospheres, 111*(D24).

Yang, W.-B., Yuan, C.-S., Tong, C., Yang, P., Yang, L., & Huang, B.-Q. (2017). Diurnal variation of CO2, CH4, and N2O emission fluxes continuously monitored in-situ in three environmental habitats in a subtropical estuarine wetland. *Marine Pollution Bulletin, 119*(1), 289-298. doi:https://doi.org/10.1016/j.marpolbul.2017.04.005

Yokoi, S., & Matsumoto, J. (2008). Collaborative effects of cold surge and tropical depression–type disturbance on heavy rainfall in central Vietnam. *Monthly Weather Review, 136*(9), 3275-3287.

Zhou, C., Wei, G., Xiang, J., Zhang, K., Li, C., & Zhang, J. (2018). Effects of synoptic circulation patterns on air quality in Nanjing and its surrounding areas during 2013–2015. *Atmospheric Pollution Research, 9*(4), 723-734.

Zhou, C., Wei, G., Zheng, H., Russo, A., Li, C., Du, H., & Xiang, J. (2019). Effects of potential recirculation on air quality in coastal cities in the Yangtze River Delta. *Science of The Total Environment, 651*, 12-23. doi:https://doi.org/10.1016/j.scitotenv.2018.08.423

Zickfeld, K., Solomon, S., & Gilford, D. M. (2017). Centuries of thermal sea-level rise due to anthropogenic emissions of short-lived greenhouse gases. *Proceedings of the National Academy of Sciences, 114*(4), 657-662.

LIST OF PUBLICATIONS AND PAPERS PRESENTED

PAPERS

Mohyeddin, N., Samah, A. A., Chenoli, S. N., Ashfold, M. J., Mead, M. I., Oram, D., . . . Nor, M. F. F. M. (2020). The effects of synoptic and local meteorological condition on CO2, CH4, PM10 and PM2.5 at Bachok Marine Research Station (BMRS) in Peninsular Malaysia. *Meteorology and Atmospheric Physics*, 1-24. doi:10.1007/s00703-020-00724-7 (APPENDIX D)

PRESENTATIONS

Mohyeddin, N., Samah, A. A., & Chenoli, S. N. (2017a). *The long-range transport of trace gases and aerosols at Bachok Marine Research Station (BMRS)*. Paper presented at the 14th Annual Meeting Asia Oceania Geosciences Society (AOGS), 6-11 Aug 2017, Singapore.

Mohyeddin, N., Samah, A. A., & Chenoli, S. N. (2017b). *The long range transport of trace gases and aerosols at Bachok Marine Research Station (BMRS)*. Poster presented at the IOES HICOE Seminar 2017: Air-Ocean-Land Interactions, 12 Sept 2017, Institute of Graduate Studies, University of Malaya.

Mohyeddin, N., Samah, A. A., & Chenoli, S. N. (2018). *The effects of land-sea breeze on the mixing ratios of CO_2, CH_4, PM_{10} and $PM_{2.5}$ at Bachok Marine Research Station (BMRS) in Peninsular Malaysia*. Poster presented at the 1st International Conference on Tropical Meteorology and Atmospheric Sciences (ICTMAS), September 19-20, 2018, Bandung, West Java, Indonesia.